3-15-2016 12:00 AM

Gold Mineralisation at the FAT Deposit, Courageous Lake Greenstone Belt, Northwest Territories, Canada

Marcus A. Adam
The University of Western Ontario

Supervisor
Robert Linnen
The University of Western Ontario

Graduate Program in Geology
A thesis submitted in partial fulfillment of the requirements for the degree in Master of Science

Abstract

The Courageous Lake Greenstone Belt (CLGB) is hosted in the Yellowknife Supergroup of the Central Slave Province, NWT, Canada: a fertile gold district that includes the former Giant, Con and Lupin orogenic gold mines. The largest deposit in the CLGB is the FAT deposit, which has a proven and probable reserve of 91MT at 2.20gpt gold owned by Seabridge Gold Inc. The FAT deposit differs from other gold deposits in the Yellowknife Supergroup in that deformation and shear textures are intermittent, and where present, deformation does not correlate spatially with mineralisation. The CLGB formed as a volcanic succession that was deposited on a 3218 Ma sodic granitoid gneissic complex. Periodic volcanism commencing at 2660 Ma formed an extrusive cycle of mafic flows to rhyolitic tuffs. The felsic units reach a maximum (post compression) thickness of 1800m proximal to the FAT deposit. Volcanic textures of the rocks hosting the FAT deposit are well preserved sub-aerial lapilli and lesser amounts of ash and bomb tuff. There is periodic intercalation with aqeuously reworked beds. These are overlain by greywacke turbiditic rocks. Three distinct structural/metamorphic events have affected the Courageous Lake Greenstone Belt: 1. compression and vertical tilting of stratigraphy and associated regional dynamothermal metamorphism to mid-greenschist facies commencing at 2592Ma; 2. concurrent discreet thermal metamorphism associated with local granitic intrusions; and 3. late retrograde hydrothermal alteration.

Gold is refractory within acicular and rhombic arsenopyrite. Petrography, SIMS, EMP and LA-ICP-MS analysis have defined three arsenopyrite styles of distinct crystal habit with distinct inclusion abundance, Au enrichment and zoning and trace element zoning. The greatest enrichment is in the earliest type of arsenopyrite, attributed to hydrothermal events associated with volcanism. Later, heterogeneous, less enriched arsenopyrite is a result of metamorphic recrystalisation. A strataform quartz body with arsenopyrite and sulphate in textural equilibrium has sulphur isotopes indicative of an Archean ocean sinter.

Terraspec and EMP analysis identify sericite mineralogy to be dominantly end-member muscovite. Early sericite associated with syn-volcanic arsenopyrite is Mg-rich compared to late, metamorphic Al-rich sericite.

Acknowledgments

I would like to acknowledge Bob Linnen for his assistance and guidance throughout this project. Bob was able to provide insight and ideas into the methods that we used to tackle this problem. His constructive criticism and invaluable understanding of the science enriched my interpretation of the results. Despite his busy schedule he was never short of time to answer my questions or ask me questions I should have been asking myself, Bob's edits significantly improved the quality of this manuscript.

Thank you for financial and logistical support and field season employment to Seabridge Gold and in particular to Bill Threlkeld and Jim Freeman. To be able to learn from Bill so early in my career has been a privilege. It has been invaluable to be able to discuss the geology of Courageous Lake with him (usually over a glass of whisky). He has significantly influenced my understanding of the rocks, the direction of this project and my approach to geology. Amongst countless other skills, Jim taught me how to be an economic geologist. Long discussions about the genesis of FAT existed before this project was proposed and have continued ever since. Thanks to Pete and Tom for further assistance and discussions at Courageous Lake.

Thanks to Marc Beauchamp and Stamen Dimov for assistance with the electron microprobe and SIMS respectively.

I would like to thank Rob Carpenter, Norm Duke, Micha Pazner, Bill Church and Eliseo Gonzalez-Urien for reviewing this thesis and providing helpful edits and considerations.

Thanks to my family (Andrew, Irene and Lucy) for teaching me to be outside exploring and being around when I needed a break.

Thanks to the Western geos: Adam, Randy, Jon, Jess, Mo, Diana, Laura, Nico, Taylor and Connor amongst many others.

Finally, thanks to the distilleries of Islay. Their spirit has been a constant source of guidance, comfort and inspiration that has never been too far away.

Table of Contents

List of Tables

List of Figures

List of Appendices

Chapter 1

1 Introduction

Gold exploration has taken place within the Courageous Lake Greenstone Belt since 1938 (Silke 2009). Multiple gold showings have been discovered and delineated across the belt with two high-grade, low-tonnage historical mines operating between 1964 to 1968 (the Tundra Mine) and 1986 to 1987 (the Salmita mine). Claims at what is now the FAT (Felsic Ash Tuff) deposit were first staked in 1977 by Noranda Exploration. The occurrence of gold in felsic volcanics (Silke 2009) was first recognised in the 1980s following the discovery of the Hemlo deposit in Ontario, that provoked exploration at Courageous Lake.

Exploration at FAT has been carried out regularly since the initial staking. An exploration shaft was sunk in 1988-89 however a declining gold price and refractory metallurgy prevented production of the deposit. The development strategy shifted to an open pit operation and the limit of the possible resource were expanded. Seabridge Gold acquired the whole greenstone belt in 2002 and have drilled over 270 diamond drill holes on the property to date. This exploration included further expansion and delineation of the FAT deposit; it now has a proven and probable reserve of 6.5 Moz (91 million tonnes at 2.20 grams per tonne) is currently defined (Lechner, 2008). Exploration by Seabridge Gold over the entire greenstone belt in order to find analogues of the FAT deposit as well as of the Salmita and Tundra mines has begun. A prefeasibility study published in 2012 indicated that at the current gold price, high grade, near surface deposits are required to make FAT economically viable. As a result, the Walsh Lake deposit (the southern extension of the Tundra mine) has been defined as a resource.

1.1 Thesis Objectives

The principal objective of this study is to define mineralisation styles at the FAT deposit. Previous research focusing on the Courageous Lake Greenstone Belt is minimal and regional studies that may refer to the belt are not contextualised by the current understanding of the deposit. Consequently, this thesis addresses two broad questions:

1. What are the styles of mineralisation at FAT and what are their associated geochemical and mineralogical signatures?

2. Do these styles of mineralisation favour an epithermal or an orogenic model for gold endowment?

A better understanding of these problems will have important consequences. Firstly, as exploration now focuses on the whole greenstone belt, an understanding of the genesis of the belt's only known multi-million-ounce deposit should help define mineralisation footprints and therefore refine exploration strategy. Secondly, the presence of epithermal deposits in Archean rocks is considered rare (Kesler & Wilkinson 2009). If epithermal processes are shown to be responsible for gold mineralisation at FAT, this conclusion will be of interest to exploration geologists working in Archean terranes globally.

A cross section through the central part of the deposit with the most extensive mineralisation was selected in order to evaluate these questions. The study specifically aims to characterise mineralisation and its associated alteration across the three main ore domains in this cross section. The study examines host rock composition and texture, mineralisation types, associated veining and alteration and isotopic signatures.

Chapter 2

2 Regional Geology

The Courageous Lake Greenstone Belt is one of several mineralised greenstone belts within the Slave Craton (figure 2.1) that formed in the late Archean (Padgham & Fyson, 1992). The genesis of the Slave Craton (referred to as the Slave Province in earlier literature) and its metallogenic history is well summarised by Bleeker & Hall (2007). The stratigraphy of the craton accompanies this summary.

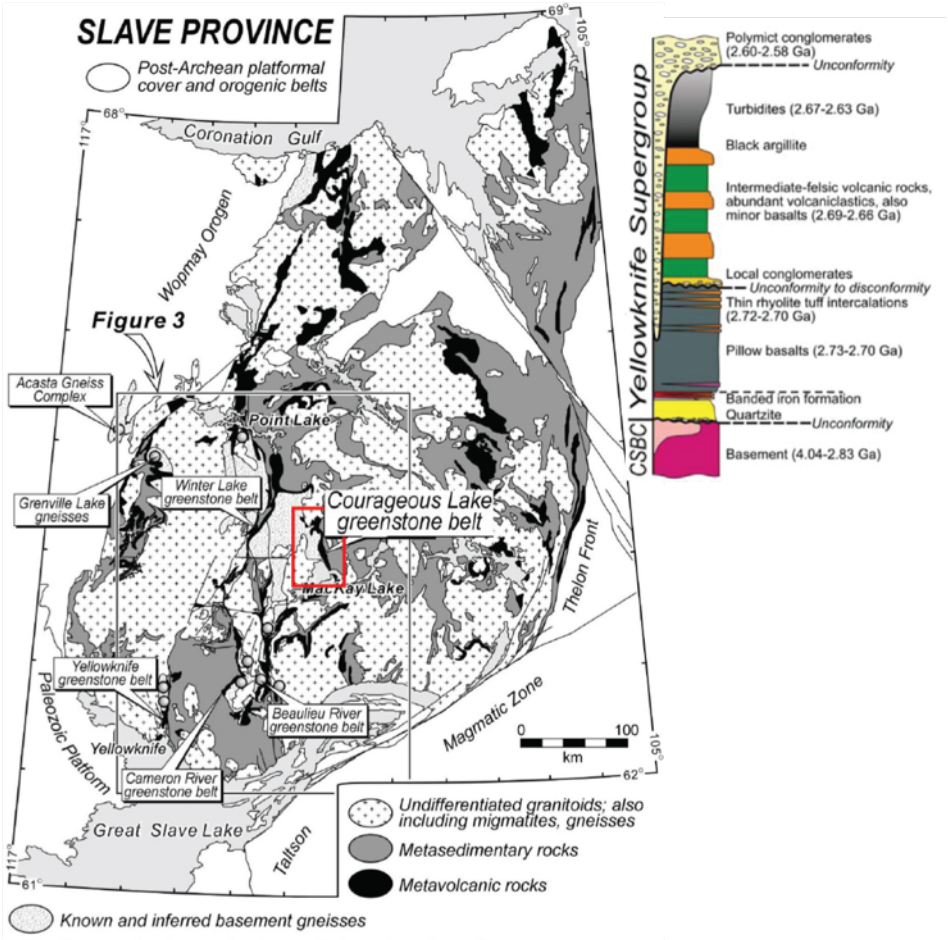

Figure 2.1 Regional scale map of the Slave Craton (modified from Bleeker et al., 1999 after Hoffman, 1993) and stratigraphic column through the Central Slave Craton (after Bleeker et al., 1999). The Courageous Lake Greenstone Belt is highlighted in red and is shown in a more detailed scale in figure 4.1

2.1 The Central Slave Craton

The Central Slave Basement Complex (CSBC) forms the oldest part of the Slave Craton (Baragar & Mcglynn, 1976). It is composed of periodically formed tonalitic gneisses cross cut by mafic dyke swarms. Gneisses across the craton have been dated by U-Pb decay from both detrital and protolith zircons with formational ages between 3400 Ma and 2826 Ma (Davis & Bleeker, 1999) but with rare exceptions of inheritance of up to 4.2 ± .058 Ga in the northeast of the craton (from a zircon within a xenolith in the Acasta gneiss ((Iizuka et al., 2006)).

The CSBC is well exposed in the centre of the Slave Craton close to and underlying the Courageous Lake Greenstone Belt. U-Pb and Pb-Pb dating here records two dates: primary prismatic zircons at 3325 ± 8 Ma and a metamorphic event, interpreted to be related to the dyke swarms at 2723 ± 3 Ma (Bleeker et al. 1999).

Early quartzite and quartz pebble conglomerates known as the Central Slave Cover Group represent a distinct unconformity and usually overly the basement complex. Primary zircons from mafic dykes that cross cut this sequence are dated by Bleeker et al. (1999) to between 2.9 to 2.8 Ga. This unit is not found below the Courageous Lake Greenstone Belt but is exposed below greenstone belts further to the west.

In the centre of the craton, where the Courageous Lake Greenstone Belt is located, the Yellowknife Supergroup overlies the Central Slave Basement Complex and Cover Group (figure 2.1B). The Yellowknife Supergroup is the product of a gradual evolution from episodic volcanism to sedimentary accumulation (Isachesen & Bowring, 1994). Helmstaedt & Padgham (1986) divided the Yellowknife Supergroup into two broad successions: The Kam Group (shown in grey in figure 2.1B) and the Banting Group (in green and orange). The Kam Group is comprised of tholeiitic basalt commonly forming pillowed lavas with minor intercalated rhyolite tuff horizons (Helmstaedt & Padgham, 1986). These are extensive across the craton and represent mantle plume activity and LIP formation associated with rifting during the onset of volcanism (Bleeker & Davis, 1999). These basalts have been dated throughout the craton by (Isachesen & Bowring, 1994)) to between 2722 Ma and 2697 Ma.

The Banting Group is a product of a transition to calc-alkaline volcanism with felsic to intermediate volcanics intercalated with basalt and sedimentary rocks. They have a juvenile arc geochemistry (negative Nb and Ta anomalies) and are interpreted to be derived from the melting of hydrated basalts, possibly the underlying Kam group (Cousens et al., 2002). These rocks are dated at 2690 to 2660 Ma and are interpreted to have been caused by rifting that formed a back arc basin that is filled by the volcanic rocks and later sedimentary rocks (Ketchum et al., 2004).

The Burwash Formation (deposited within the Burwash Basin) encompasses a rapid transition from volcanic rocks to deep-water sediments. Sedimentary rocks are mostly volcanically-derived immature greywacke and mudstone with volcanic intercalations common and persistent throughout the formation (Bleeker & Beaumont-Smith, 1995) Deposition of turbidites was widespread across the craton with the infilling of the Burwash Basin estimated to be at least 400 x 800 km (Helmstaedt & Padgham, 1986). Detrital zircons dated by U-Pb decay by Abraham et al. (1994) indicate that sedimentation began after 2683 ± 3 Ma and lasted until 2661 ± 2 Ma (where primary zircons from intercalated volcanics at the top of the stratigraphy have been dated by U-Pb decay by Bleeker & Beaumont-Smith (1995).

2.2 Deformation and Metamorphism

Two distinct metamorphic (M) events have been outlined in the Slave Craton with three deformation events (D) recognised. A minor (D1) event causing slaty cleavage is sporadically seen throughout the craton (and not observed at the CLGB). Following this M1 occurs with contact metamorphism aureoles around high level TTG plutons. The main regional scale metamorphism (M2) began at 2600 Ma as a distant larger Archean landmass began to grow during the Algoman orogeny (known as the Kenoran orogeny in Canada). M2 is described as low pressure, high temperature with grades ranging from greenschist to upper amphibolite facies (Thompson, 1989; Dillon-Leitch, 1984). Figure 2.2 summarises the main metamorphic processes in the context of the craton formation. Two main generations of folding caused by the M2 event are recorded (D2A and D2B) by Bleeker (1996). These have produced generally steeply plunging northwest-north trending folds and has tilted the CLGB to approximately vertical with 12˚ strike. A suite

of granite plutons formed late in the Algoman orogeny across the Slave, as described and characterised by Davis & Bleeker (1999). Areas of high metamorphic grade are a product of contact metamorphism and are spatially correlated to proximity to these plutons (Bleeker & Davis 1999). The D2 event has a strong temporal correlation with gold mineralisation at the Con-Giant gold deposits in Yellowknife (Ootes et al., 2011) with metamorphic fluid considered the main process responsible for endowment.

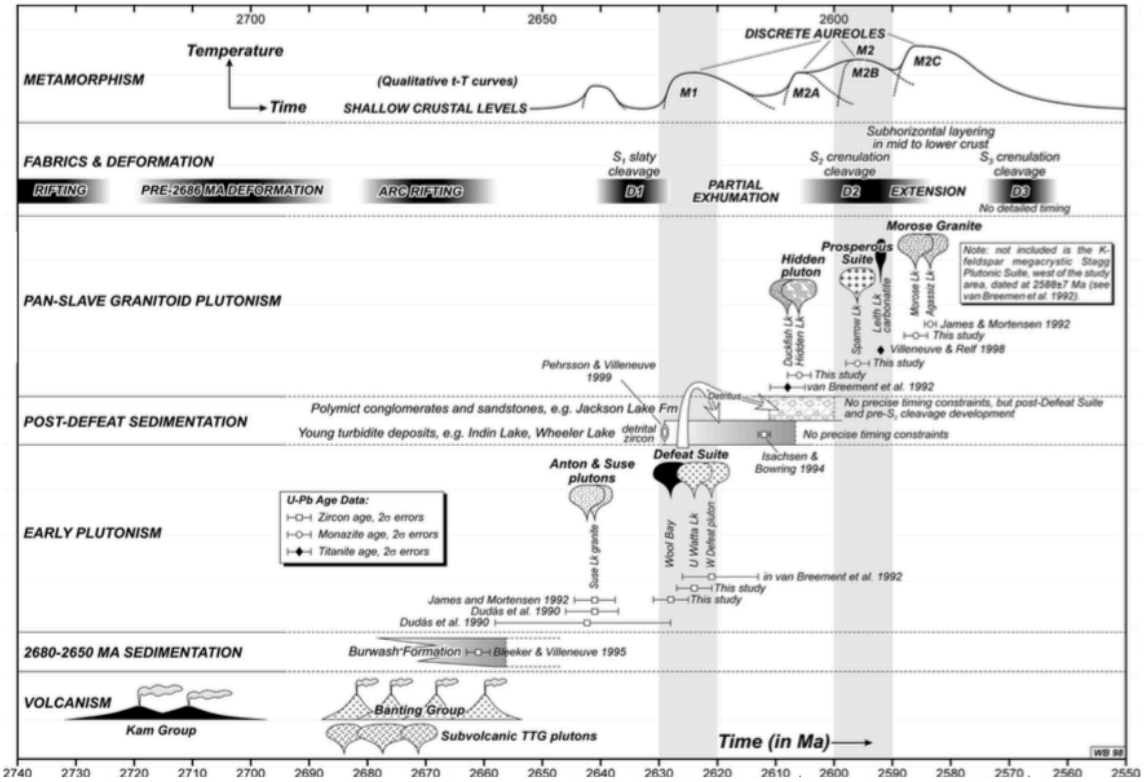

Figure 2.2 Temporal metamorphic evolution of the Slave Craton in the context of stratigraphy (after Ootes et al. (2011)).

2.3 Gold in the Slave Craton

The Slave Craton has been a fairly prolific producer of gold. Most significantly the Giant-Con mines in Yellowknife produced over 15 Moz of gold between them (Silke, 2009). The craton has had a tempered history of production which has remained correlated to fluctuations in the price of gold. Literature comparing and summarising gold formations mostly predates the delineation of the FAT deposit. However, comparisons

with Tundra and Salmita (two past producing mines in the CLGB) exist. Padgham (1992) divides Slave Craton gold deposits into three distinct settings: quartz vein hosted, shear zone hosted and iron formation hosted.

Quartz vein hosted gold occurs in turbidite sequences in bedding-parallel and cross cutting quartz veins (most significantly for example, the Discovery mine and the Ruth property in the Burwash formation (Padgham, 1992)). Although there are some multi-vein stockwork deposits that are spatially associated with quartz-feldspar porphyry intrusives, these are lower grade and rarely economic. Mineralisation at the Discovery and Ruth Deposits is within or immediately adjacent to single veins with gold associated with arsenopyrite. Alteration halos of silica and arsenopyrite flooding rarely extend beyond centimetres from these veins (Abraham et al., 1994). Fluids responsible for mineralisation are meteoric based on fluid inclusions (Abraham et al., 1994). These deposits are generally too small to be significant compared to other mineralisation styles as they lack significant volumes of fluid or suitable trap environments.

The Giant and Con mines are veins in shear-hosted deposits. They are the most important historic deposits in the craton and are the subject of most of the previous research. The Extech III research project (Henderson, 2007) provided a summary of the research assessing the deposits and characterised the greenstone belt in the context of regional paragenesis and metallogenesis. The Giant-Con deposits are located within shear zones within the Yellowknife Greenstone Belt (YGB) that cross cut mafic volcanic lithologies. It is proposed that initial enrichment may have been due to intrusion related gold however this is overprinted by a main orogenic mineralisation event. This has formed ore zones that are hosted by shear zones with less of a spatial association with lithological contacts.

Fluid inclusions and stable isotopes were used by Shelton et al., (2004) to construct a model for fluid flow and gold precipitation. Systematically decreasing oxygen isotopes from fluid inclusions were interpreted to reflect an initially deep $\partial^{18}O$ enriched meteoric fluid that was able to dissolve gold from country metasedimentary rocks and precipitation occurred due to a reaction with high Ti basalts. This occurred at shallow depths with fluid inclusion showing trapping pressure and temperatures of mineralising fluids at 1-2 kbars

and 180 to 360°C. Quartz veins have a large range of $\delta^{18}O$ values interpreted to be a long-lived multiple precipitation event. Ootes et al. (2011) used Re-Os to date pyrite associated with gold mineralisation at 2591 ± 37 Ma relating the mineralisation to crustal anatexis during the Algoman Orogeny.

Iron formation-hosted deposits such as Lupin are orogenic gold deposits with iron formations providing a mechanism for gold precipitation and most recently summarised by Geusebroek & Duke (2005). Gold is generally high grade (≈10 g/t) and thought to have been originally exhalative (to ppb levels) but then remobilised into quartz veins precipitated during metamorphism with iron formations acting as chemical traps. Periodic deformation has created fractures through which fluid was able to pass with multiple stages of precipitation during peak and retrograde D3 metamorphism.

Padgham (1992) spatially divided the Slave Provence into five different zones that define styles of gold deposit in terms of host rock and mineralisation style. These follow a north-easterly trend that cross cuts both regional foliation and bedding. Based on this trend Courageous Lake is correlated with the shear zone-hosted styles of Giant and Con mines in Yellowknife due to lack of banded iron formation traps and similar volcanic greenstone belts.

2.3.1 Gold Mineralisation within the Courageous Lake Greenstone Belt

There have been two historic past producing mines within the Courageous Lake Greenstone Belt (Silke 2009). The Salmita mine and the Tundra mine are lower tonnage, higher-grade and have a different style in both host rock and mineralization style to FAT. Seabridge Gold has defined a 495,000 oz. resource at 2.91 g/t as the Southern extension to the Tundra deposit called the Walsh Lake Deposit (Lechner, 2014) that is referred to in this study. Journal papers on either the Samita or Tundra and information on the geology of these mines is sparse. These deposits both sit on major lithological contacts; the Walsh Lake mineralized zones between both felsic and sedimentary rocks with mafic volcanics. Mineralisation at Walsh Lake is defined by sub 10mm rhombic arsenopyrite often composing over 5% of intervals with occasional flecks of visible gold particularly

abundant bordering blue-grey meter-scale quartz veins and a chloritic alteration assemblage. Grades are higher than FAT however mineralised intervals are discreet with considerably lower tonnage and contained ounces. These deposits are currently envisioned as smaller satellite deposits that may be amalgamated into the mine plan and contribute to the economics of the property. The Salmita deposit was mostly a single north-striking blue-grey quartz vein (the B) vein between Banting Group mafic volcanics and Burwash formation argillite. Mineralisation is mostly native gold with minor arsenopyrite and pyrite (www.nwtgeoscience.ca).

Gold showings that have not been defined as resources are common throughout the belt. These usually occur on the contacts of the felsic tuff lithology. Drilling has occurred on mineralised surface showings with the intention of finding analogues to the Salmita and Tundra deposits. Since the discovery of FAT there has been little systematic exploration of the greenstone belt as a whole.

Chapter 3

3 Methods

Various analytic processes were carried out during the project and the methods and operating procedures that were used are outlined here. These are mostly listed in the order that they appear in this thesis however some are grouped for simplicity.

3.1 Sampling Strategy

Sampling was carried out by the author at the Courageous Lake property during the summers of 2013 and 2014. A single cross section through the deposit was selected in order to constrain the project into a manageable and definable size. This was mine section 4800N (its location and context is shown in Chapter 4) and was picked as it had a broad range of mineralisation styles across the three principal ore domains (domains 3, 4 and 5). The project was restricted to these domains as they contain 86% of the resource. Seabridge Gold has previously sampled and assayed all of their drilling. These samples were typically taken over 1.5m intervals. They were analysed by ACME labs (now BV Upstream Minerals). Samples were crushed to 150 mesh pulp and then digested by aqua-regia. Samples were analysed by fire assay for Au and ICP-ES for a standard 34 element package (economic metal and gangue elements used for exploration). Standard operating and analytical procedures were carried out as required for a National Instrument 43-101 compliant resource. A full description of these produces can be found in the Courageous Lake National Instrument 43-101 (www.seabridgegold.net). The pulp rejects for the cross section were retained and some were used in this project for XRD and whole rock geochemistry.

Eight drill holes along 4800N were relogged for this project. Detailed logs that included host rock, alteration and mineralisation were described and where possible quantified. A representative sample was taken from each lithology. Sixty polished thin sections were made from selected samples that represented a range of host rock, alteration and mineralisation. Thin sections were prepared by Vancouver Petrographics and at the University of Western Ontario Sample Prep Lab.

3.2 Whole Rock Geochemistry

Twenty-four pulps were re-assayed for a complete whole rock suite that was used to geochemically define primary lithology and compare alteration geochemistry. Pulps were already crushed to 150 mesh and sent to ALS minerals for analysis. These methods are taken from ALS Minerals methods descriptions (www.alsglobal.com) A whole rock major oxide package was analysed by ICP-AES (ALS method code ME-ICP-06). The sample is added to lithium metaborate/tetraborate flux and fused in a furnace at 1000°C. The resulting melt is then cooled and dissolved in 4% nitric acid and 2% hydrochloric acid. This solution is then analysed by ICP-AES. Lower detection limits are 0.01% and errors within 0.01 %. Oxide concentration is calculated from the determined elemental concentration. Trace elements were analysed by lithium borate fusion then ICP-MS (ALS method code ME-MS81). Lower detection limits range from 0.01 to 1 ppm (dependant on element). Full details can be found at www.alsglobal.com. Errors are within 0.1ppm. The sample is added to a lithium metaborate flux and fused in a furnace at 1000°C. The resulting melt is then cooled and dissolved in 4% HNO_3 and 2% HCl_3 solution. This solution is then analysed by ICP-MS. Total sulphur was calculated by leco analysis (ALS method code S-IR08). The lower detection limit is 0.01% and errors are within 0.01%. The sample is heated to approximately 1350 °C in an induction furnace while passing a stream of oxygen through the sample. Sulphur dioxide released from the sample is measured by an IR detection system to calculate total sulphur. Base metals were analysed by ICP-MS following a 4 acid digest. Gold values were taken from the assay results for the same samples that were previously analysed by fire assay by Seabridge Gold. Detection limits are between 0.01 and 100 ppm and errors are within 0.05 ppm.

3.2.1 Comparison of Whole Rock and Seabridge Gold's ICP Data

Since Seabridge Gold's ICP data for K, Mg and Al is used to infer geochemical trends in alteration (Chapter 6) a comparison aqua regia with lithium borate digestion whole rock data is necessary to understand how the analytical methods affect whole rock data. Figure 3.1 shows a very good correlation between whole rock aqua regia and lithium borate digestions for Mg (where above detection limit) but not for K or Al. The very good correlation indicates that Mg can be used to assess alteration (Chapter 6).

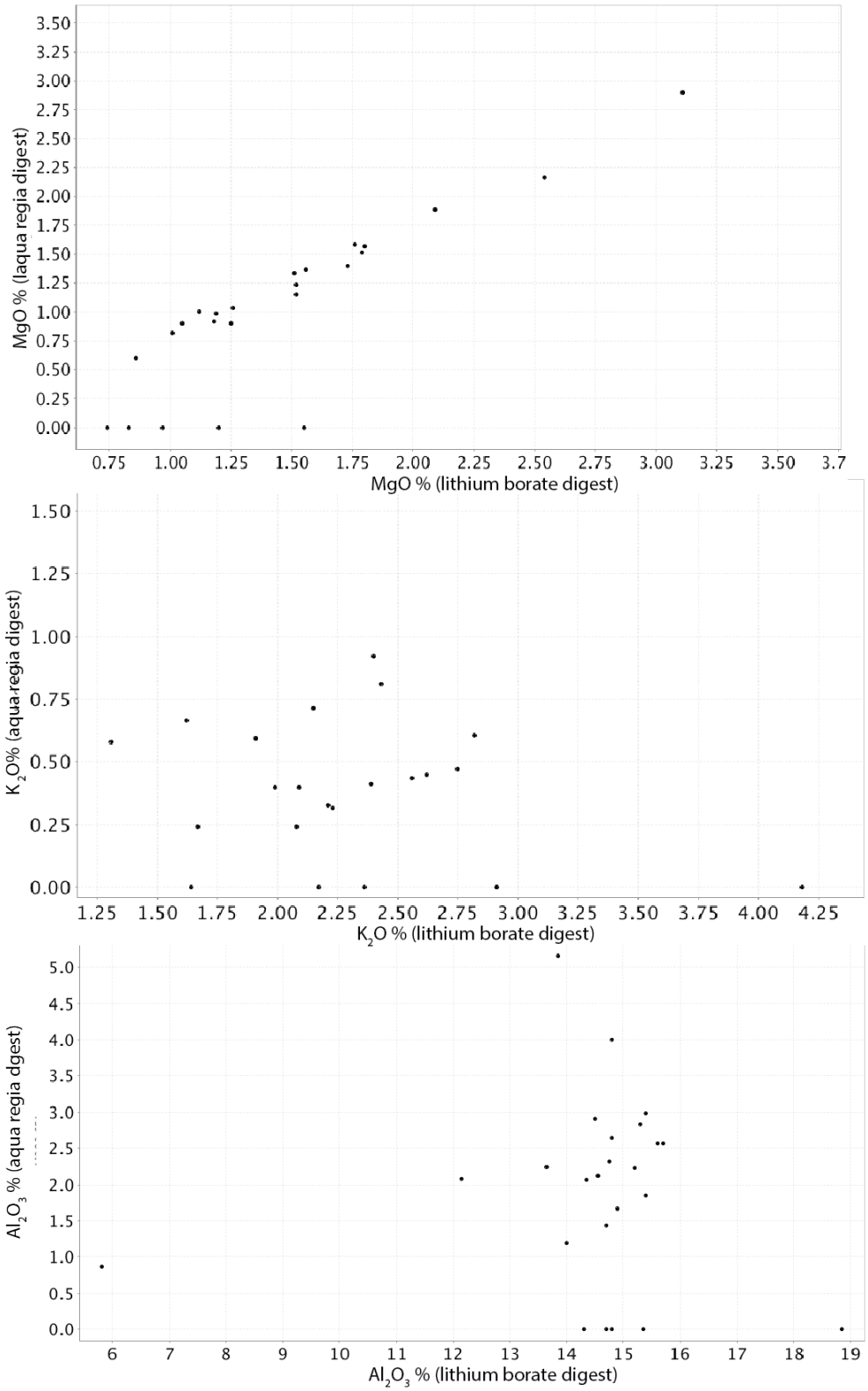

Figure 3.1 Comparison between whole rock and assay data. There is a strong correlation for Mg but not for K and Al.

3.3 X-ray Diffraction (XRD)

Two styles of X-ray diffraction were carried out at the X-Ray Diffraction and Microdiffraction Laboratory at The University of Western Ontario. Whole rock XRD was performed on pulps and powdered quartz veins. Powders were mounted on a glass slip and the surface smoothed to ensure the random orientation of crystals. Analysis was carried out on a Rigaku rotating-anode X-Ray diffractometer. The instrument operated at 45 kV and 160 mA with a scan rate of 10º 2 θ per minute. Scans were collected from 5º to 82º.

A micro-XRD (μXRD) was used in order to help identify the sulphate species. Analysis was performed on a Bruker AXS D8 Discover Diffractometer. This uses Cu Kα radiation generated at 40 kV and 40 mA. A pinhole collimator snout is able to focus this bean diameter to 500μm on the sample. Diffraction rays are collected using a general area diffraction system (GADS). Full specifications and capabilities of this machine are discussed by Flemming (2007). The sample is targeted using a digital video camera system and laser sight. Scans were carried out from 5º to 82º at a scan rate of 10º 2 θ per minute.

Peaks were identified using Bruker AXS EVA software package that uses the International Centre for Diffraction Data PDF4 database.

3.4 Leapfrog Interpolations

Interpolations used ICP data from Seabridge Gold's database using ARANZ Leapfrog Geo (version 3.0.0). Interpolations were run over the whole deposit though the only cross section is displayed. For gold, downhole compositing was used over 10m with a minimum coverage of 50%. Pre transform clipping with a lower bound of 0.1 and upper bound of 24.6 g/t was applied. The interpolant was applied with a trend that was defined by using the orientation of the domains. A spherical interpolant (with a variance of 1.82) was then applied. For magnesium and aluminium, the same composting was used. Pre transform clipping (between 0.05 and 4.99 for magnesium and between 0.11 and 4.78 for aluminium) was applied. The interpolant used the same global trend that was used for gold. A spheroidal interpolant (with a variance of 0.146 for magnesium and 0.247 for

aluminium) was used. Various isosurfaces were generated and the shapes that best reflected apparent trends were selected and sliced along the cross section.

3.5 Secondary Ion Mass Spectrometry (SIMS)

Two separate studies used SIMS analysis. Firstly, a study of gold enrichment and distribution was carried out at Surface Science Western. In situ sulphur isotopes were quantified by SIMS at Memorial University, St Johns, Newfoundland.

3.5.1 Gold

Dynamic SIMS (D-SIMS) analysis was carried out using a Cameca IMS 3/4s at Surface Science Western. A review of the technique and the application of the instrument used was given by Dimov & Hart (2011). Selected areas from thin sections and arsenopyrite separates were analysed by D-SIMS. Individual spots from the thin sections can be analysed and quantified for gold content by SIMS analysis, however a silicate matrix makes image analysis of the arsenopyrite not possible due to charging effects. Epoxy mounts containing arsenopyrite and graphitic carbon to prevent charging effects were created in order to image the gold distribution. For that purpose, samples were crushed and then arsenopyrite was separated by gravity separation using a superpanner. The resulting arsenopyrite was set in the mount which was then polished and individual crystals were selected for analysis. Analysis was completed in two sessions, firstly spot analysis in order to quantify gold enrichment on both thin sections and mounts and secondly image analysis to view gold distribution across individual crystals on the mounts.

The Dynamic SIMS uses a primary ion beam which ablates the crystal surface. Particles are ejected as secondary ions and fed into a magnetic sector mass spectrometer where they were analysed for As, S, Au and Sb. These are quantified against a custom arsenopyrite standard made at *Physics Western* in order to eliminate matrix effects. A detection limit of 0.2 ppm and errors of ± 10 % are reported. For the imaging application the primary ion beam is rastered across the crystal. The spatial resolution in imaging mode is 1 μm. and it is defined by the secondary optics of the mass spectrometer.

3.5.2 Sulphur Isotopes

Thin sections containing Au bearing arsenopyrite were sent to Memorial University for sulphur 34 isotope analysis. Targets as close as possible to the pits created by gold analysis were selected. Samples were coated with 300 Å of Au to prevent charging. A 600-800 pA Cs ion microbeam was focused into a 5-15 μm spot. Negatively charged ions from this bean were accelerated into a mass spectrometer at a potential of 4.5 keV and analysed for isotopes of sulphur. Errors are reported to be within 0.5 per mil.

3.6 Laser Ablation Inductively Coupled Plasma Mass Spectrometry (LA-ICP-MS)

LA-ICP-MS analysis was carried out in order to analyse major and trace elements across transects of arsenopyrite crystals. Analysis was conducted at the Great Lakes Institute for Environmental Research, University of Windsor. The laser ablation was carried out using a Photon Machines Excite. This produced a 193nm ultra short pulse Excimer Laser (generated via an ArF matrix). Ablated material was analysed by an Agilent 7900 ICP-MS for Au, Ag, Fe, As, Sb, Th, Te, Hg, Se, Pb (208 and 206), Co and Ni. An operating current of 20 Hz was used to produce a 20 μm spot with a stage speed of 5μm per second. Results were calibrated against a NST 610 standard to account for matrix affect. Statistical analysis was performed on some of the results to calculate precise concentration of elements. This was done over the whole crystal before variations in concentrations were defined and understood in different arsenopyrite species. As a result, counts are used in this study. Concentrations are not given but can be calculated from the analysis in the future if required.

3.7 Electron Microprobe (EMP)

Spot analysis for the arsenopyrite was carried out by wavelength dispersal spectroscopy (WDS) analysis. Analyses were collected using a 20 kV accelerating voltage, 100 nA beam current, spot size beam. Iron, sulphur, and arsenic were analysed using the EDS detector, using an arsenopyrite from Yaogangxian Mine, Hunan Province, China as the standard. Counting times for each of these elements was 60 seconds. Antimony (Lα) and Silver (Lα) were analysed using the PETJ analysing crystal, using pure antimony and

pure silver as standards. Counting times of 30 seconds on the peak and 15 seconds on both background positions were used for each of these elements. Gold (Mα), tellurium (Lα), and lead (Mα) were analysed using the PETH crystal, using pure gold, tellurium, and lead respectively. Counting times of 30 seconds on the peak and 15 seconds on both background positions were used for each of these elements. Copper (Kα), nickel (Kα), and zinc (Kα) were analysed using the LIFL crystal, using pure copper, nickel, and zinc respectively. Counting times of 30 seconds on the peak and 15 seconds on both background positions were used for each of these elements. Errors are reported to be within 1% and lower detection limits are defined as 3σ of the background levels for the trace elements. These are Sb=31ppm, Ag=28 ppm, Au=32 ppm, Te=17 ppm, Pb=32 ppm, Cu=19 ppm, Ni=17 ppm, Zn= 23ppm. Since major elements were analysed by EDS there are no lower detection limits.

3.8 Terraspec

A Terraspec 4 Hi-Res Mineral Spectrometer was used to attempt to define the crystallographic properties of mica species. The hardware was loaned to the author by ASD Inc. (a subsidiary company of PANalytical) as part of their 'Students in Mining' program. Whole core samples were cleaned and then dried prior to scanning. An ASD contact probe with a spot size of 10 mm was placed against the mica species visually identified in the sample. The light source in this probe is a halogen bulb with a colour temperature of 2901 ± 10 º% K. Reflected light was transported back to the Terraspec unit with a fibre optic cable. The machine was calibrated against a white blank every minute and against a muscovite sample from the DANA collection every 10 samples. Three detectors within the unit give a total wavelength range of 350-2500 nm (a VNIR detector from 350-1000 nm, a SWIR 1 detector from 1001-1800 nm and a SWIR 2 detector from 1801-2500 nm). Scanning time was 100 milliseconds and machine wavelength reproducibility is reported to be 0.1 nm and wavelength accuracy 0.5 nm (www.asdi.com).

Results were collated and analysed with The Spectral Geologist Pro 4 (TSG) software. TSG matched spectra against an internal database to give a generalised mineral

composition. Wavelength peak shifts at 1900 nm and 2210 nm were extracted and exported for all samples by this software.

3.9 Benchtop SEM

A JEOL JMC-600 NeoScope equipped with a JEOL JED-2300 energy dispersive X-ray analyser benchtop SEM was used to assist with petrography and to quantify magnesium, potassium and aluminium by EDS analysis. A review of the specification and capabilities of this machine in the mining industry is provided by Cao et al. (submitted). Samples were carbon coated in order to mitigate charging and analysis was conducted with a probe current of 15 kV, high beam current mode and high vacuum mode. Beam size is 30-40 μm. Elements totals were quantified using the Kα peaks of each element and comparing this with the Kα oxygen peak with an oxygen number of 12.

3.10 Sulphur Isotopes

Sulphur isotopes of sulphate minerals were analysed at McGill University, Montreal, Quebec. The sulphate minerals were separated manually with a micro dermal. From this a solution was created by dissolving it in zinc acetate to avoid oxidation. Zinc sulphide precipitates were separated from filtration and then rinsed with Milli-Q water. This was then converted to silver sulphide by the addition of silver nitrate. This was rinsed with ammonium hydroxide and Milli-Q water and dried overnight. The silver sulphide was then weighed and cleaned and reacted at 250ºC in the presence of F_2 in order to produce SF_6. This was purified and then analysed in a Thermo Finnigan MAT 253 dual-inlet gas-source mass spectrometer for $^{32}SF^{5+}$, $^{33}SF^{5+}$, $^{34}SF^{5+}$ and $^{36}SF^{5+}$ and analysed against an in-house standard (MSS-1). Errors are within 0.01 ‰.

Chapter 4

4 Local Geology

Gold was discovered at Courageous Lake in 1938 (Moore, 1956). Since then exploration along the CLGB has occurred sporadically, resulting in two past producing mines (the Salmita mine and the Tundra mine), the delineation of the FAT deposit and the Walsh Lake deposit as well as the discovery multiple further gold prospects (figure 4.1). The geology and Au endowment of the Salmita and Tundra deposits are briefly described in the NORMIN database (www.nwtgeoscience.ca). Free milling, Au-rich quartz veins occurred at the contacts between felsic volcanics and Burwash Formation sedimentary rocks and mafic volcanics and Burwash Formation sedimentary rocks, respectively. Salmita had a resource of 80,000T of 29.20 g/t Au and Tundra had 200,000T of 27.43 g/t Au (Silke., 2009). Literature that specifically addresses the geology of the CLGB is sparse, however it is frequently referred to in regional studies. An MSc thesis by Dillon-Leitch (1986) mapped the greenstone belt and classified metamorphism and the structural history of the belt. The FAT deposit is hosted in Banting Formation volcanics roughly in the centre of the greenstone belt and is underlain by a granitoid gneissic complex and overlain by Burwash formation turbidites (figure 4.2). Stratigraphy has been tilted to roughly vertical during the regional D2 event (Dillon-Leitch, 1984).This study focuses on a 200m thick central portion of the felsic volcanics that encompasses most of the mineral reserves along the studied cross section.

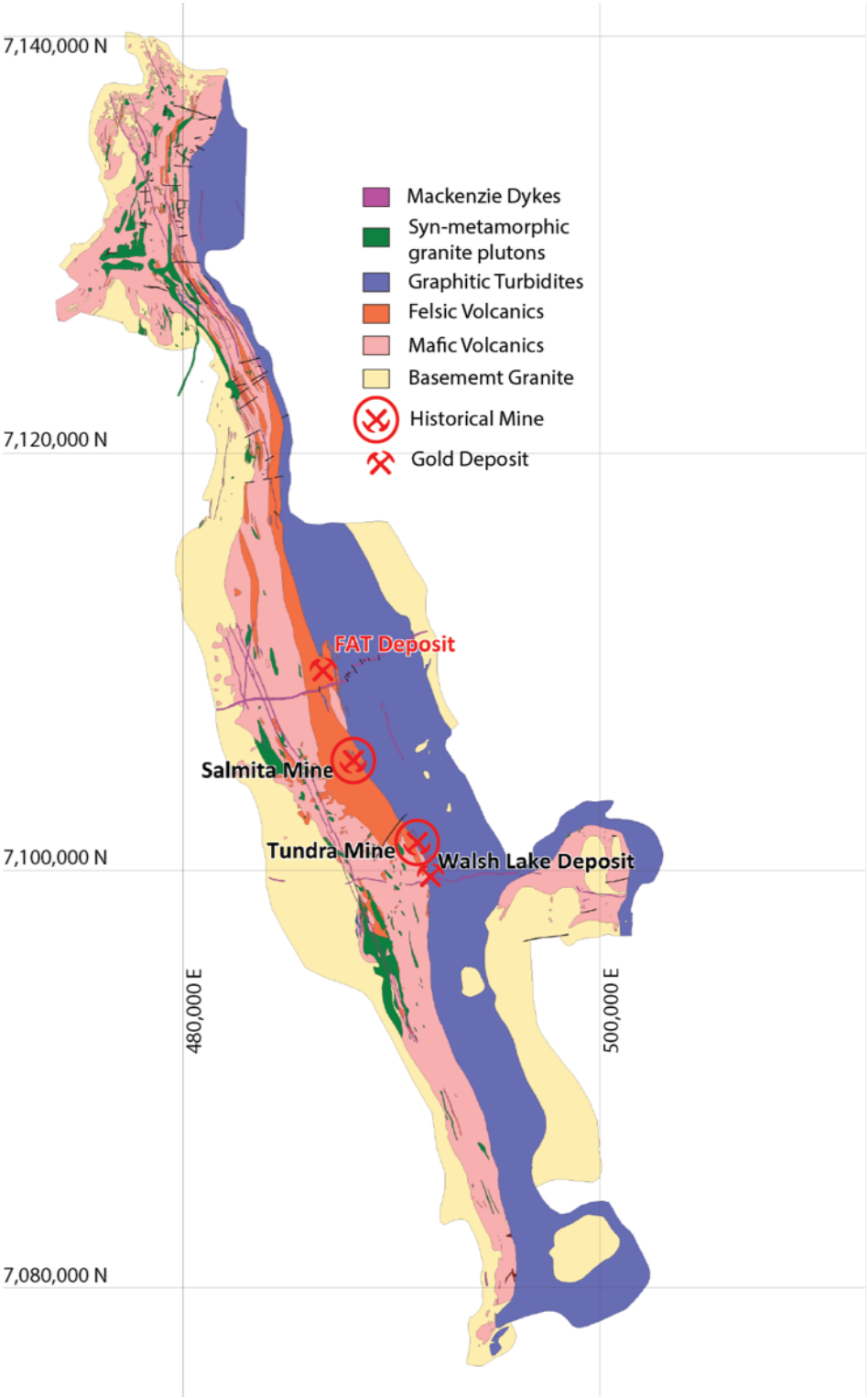

Figure 4.1 The Courageous Lake Greenstone Belt (after Dillon-Leitch, 1984). The FAT deposit is centred within the volcanics whereas the Salmita and Tundra mines (and Walsh Lake deposit) lie on contacts with Burwash Formation turbidites.

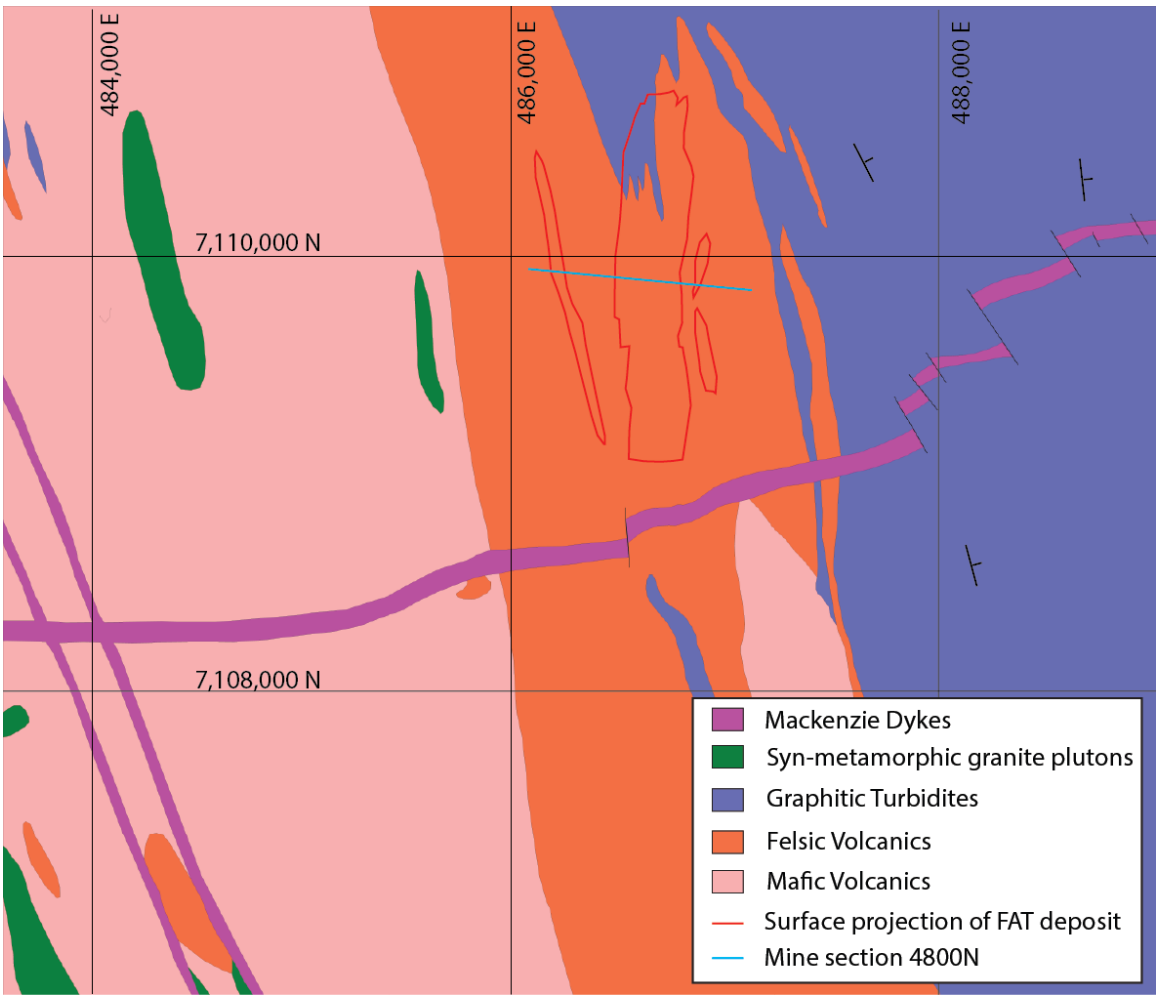

Figure 4.2 The FAT deposit (modified from Dillon-Leitch, 1984). This map shows the position of the FAT deposit in the centre of the felsic volcanic unit and mine section 4800N on which this study focuses. The contact between the felsic volcanic unit and the turbidites at the North of the resource is believed to represent a gradational intercalation of sediments but folding cannot be excluded.

4.1 Central Slave Basement Complex

Biotite-hornblende tonalite granitoids are the oldest rocks on the property and outcrop west of Courageous Lake (figure 4.1). They are part of the Central Slave Basement Complex and described as a heterogeneous dioritic-tonalite gneisses which are cross cut with mafic dyke swarms (Bleeker et al., 1999). They are composed dominantly of hornblende and plagioclase with trace pyroxene. Feldspars are commonly completely

altered to sericite, epidote or clinozoisite with hornblende locally altered to chlorite and epidote (Bleeker & Davis, 1999). As referred to in Chapter 2, a sample 'within eyesight' of the CLGB was dated by U-Pb decay by Bleeker et al. (1999). Primary zircons yielded an age of 3325 ± 8 Ma whereas another distinct group record a metamorphic event at 2723 ± 3 Ma believed to be related to the emplacement of the mafic dyke swarms. The granitoid rocks at Courageous Lake are thought to be the youngest of the CSBC (Bleeker et al., 1999). Initial deformation that predated the Yellowknife Supergroup is widely recorded in these rocks (Davis & Bleeker, 1999) with folding commonly seen in outcrop.

4.2 Yellowknife Supergroup

4.2.1 Mafic Volcanics

As described in Chapter 2, granitic gneisses of the CSBC are unconformably overlain by a volcanic succession that is part of the Yellowknife Supergroup. Mafic lavas are locally metamorphosed primarily to hornblende schist amphibolite. They range in texture and occurrence with pillowed lavas, amygdaloidal lavas and porphyritic lavas all visible across the property. Primary zircons from a rhyolite bed in between mafic volcanic rocks are dated at 2729+8/-7 Ma and are the oldest reported date for the Yellowknife Supergroup at the CLGB (Villeneuve, 1993). This age date is interpreted to show that these volcanics are fed by the mafic dykes within the Central Slave Basement Complex but this relationship has not been demonstrated by any other means.

4.2.2 Felsic Volcanics

4.2.2.1 Composition

The felsic volcanic rocks that conformably overlie mafic lavas host the FAT deposit. They are calc-alkaline lapilli agglomerates to ash tuff with a rhyodacite composition (figure 4.3) (Bleeker & Davis 1999). Powdered XRD analysis indicate that their composition is primarily quartz and alkali feldspar (figure 4.4). Thin sections of unaltered felsic tuff (figure 4.5) exhibits feldspars with both lamellar albite twinning and simple Carlsbad twinning. Whole rock rare earth and Zr/TiO_2 vs Nb/Y patterns and XRD of

pulps within the studied cross section indicate that primary composition does not vary systematically or significantly with stratigraphy (figures 4.3, 4.6).

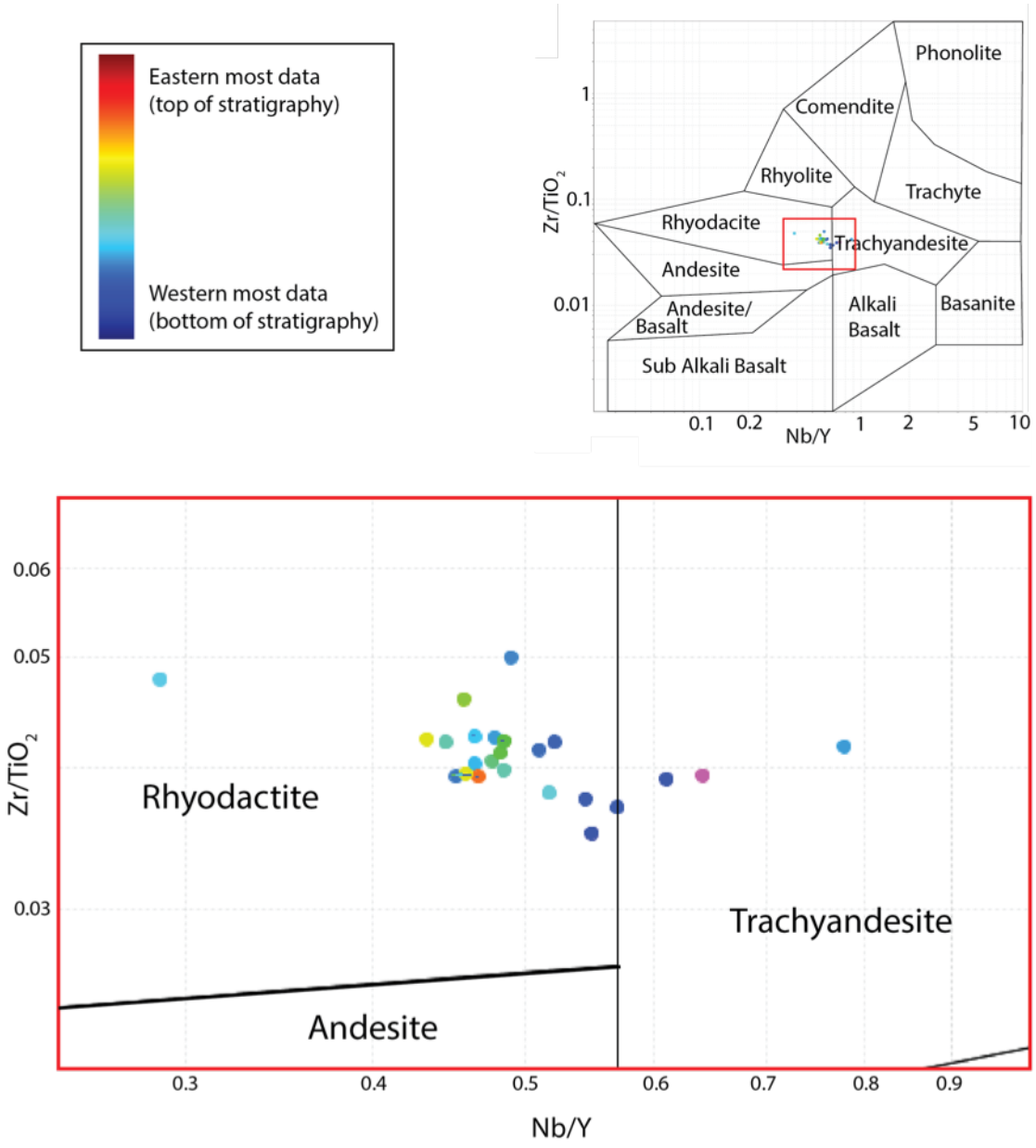

Figure 4.3 Rare earth element ratios indicate composition is mostly rhyodacite. There does not seem to be a strong stratigraphic control on composition (after Winchester and Floyd, 1977)

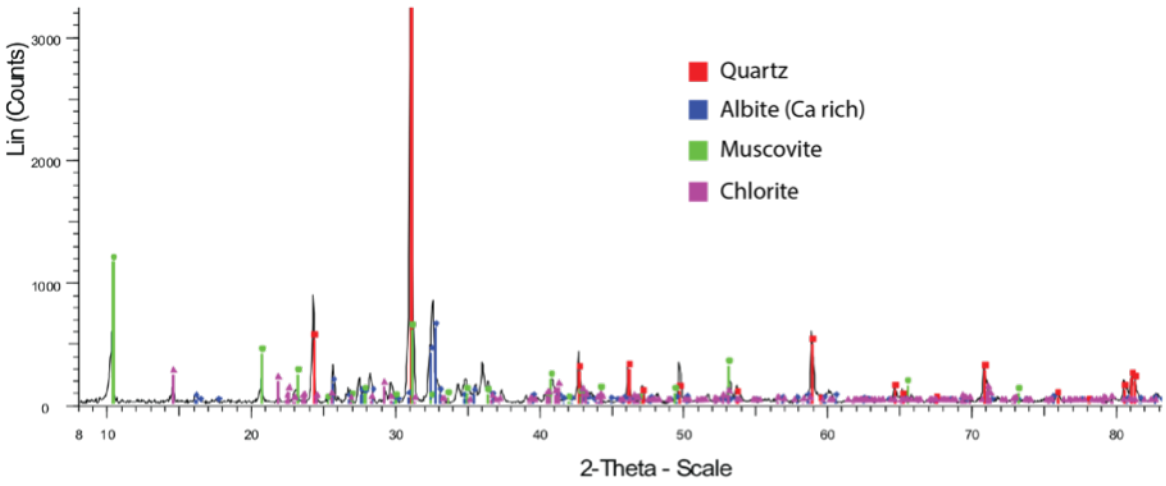

Figure 4.4 XRD pattern for felsic volcanic rock. Multiple analyses were carried out throughout the stratigraphy and whilst peak height varied composition was consistent. This indicates that protolith is mainly composed of quartz and albite with muscovite and biotite

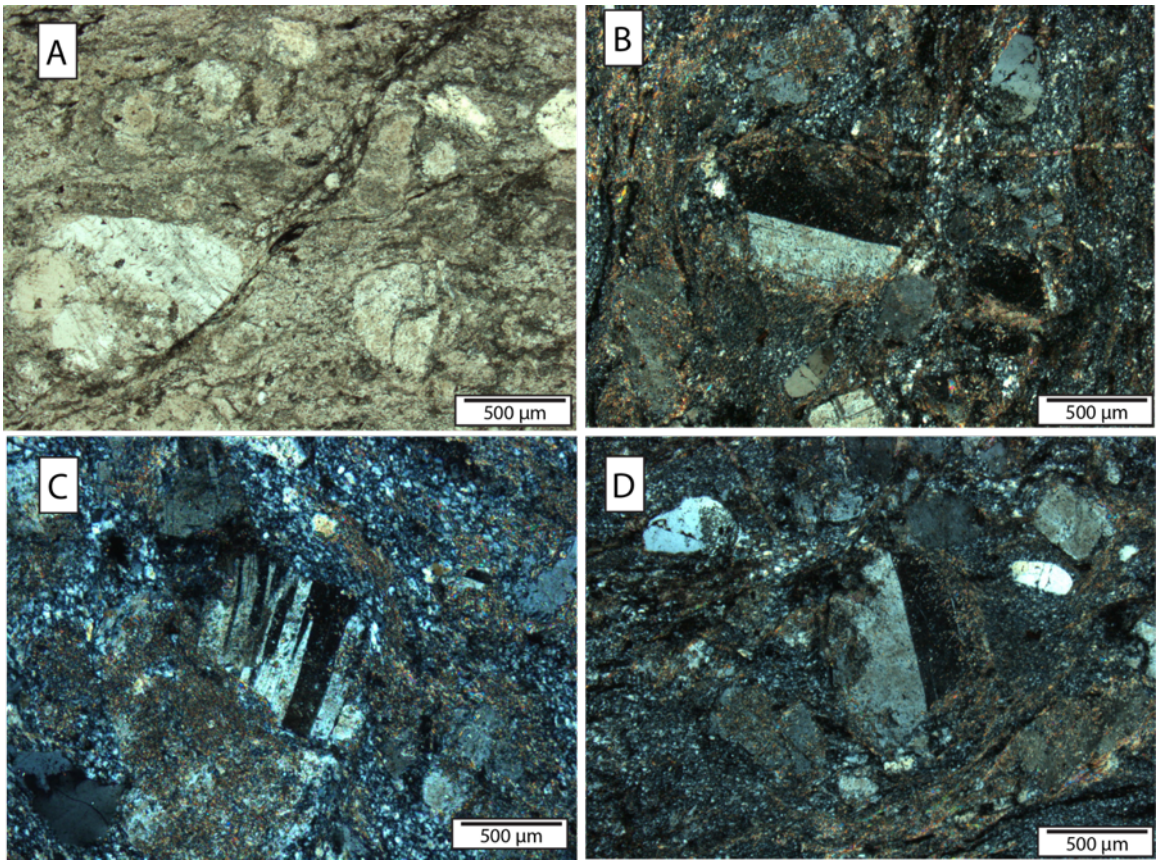

Figure 4.5 Unaltered felsic volcanic rock composition. A: Ejectors in fine grained ash (PPL). B: Simple carlsbad twinning of feldspar surrounded by fine grained ash matrix. (XPL) C: Lamellar twinning of feldspar in fine grained quartz ash (XPL). D: Carlsbad twinning and quartz ejectors in fine grained ash matrix (XPL)

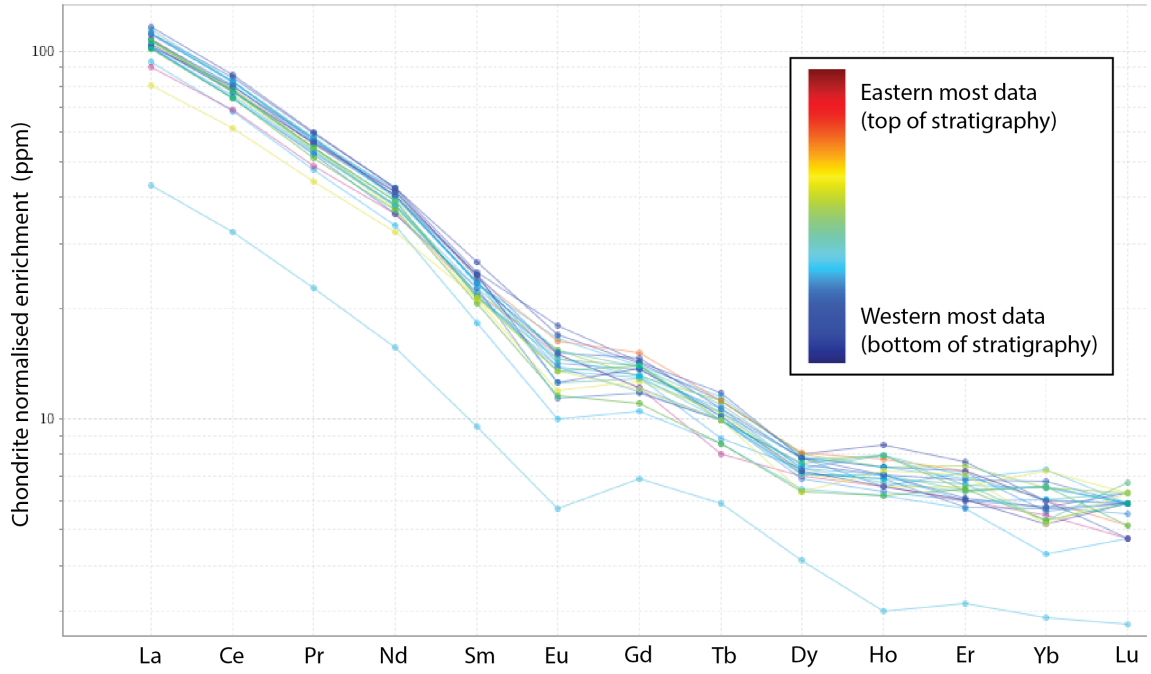

Figure 4.6 Chondrite normalised REE spider diagram. With one exception, there is a fairly tight REE pattern indicating no large change in composition. As with figure 4.3, this shows that there is no stratigraphic control on composition

4.2.2.2 Texture

Although composition remains constant, texture varies substantially within the study area (figure 4.7). Lithologies are defined by ejecta abundance and size and can be connected as strata from drill hole intercepts. The deposit youngs to the East. This is inferred by Freeman (2004) and based on sedimentary bedding structures visible in outcrop towards the top of the felsic volcanics (shown in figure 4.15).

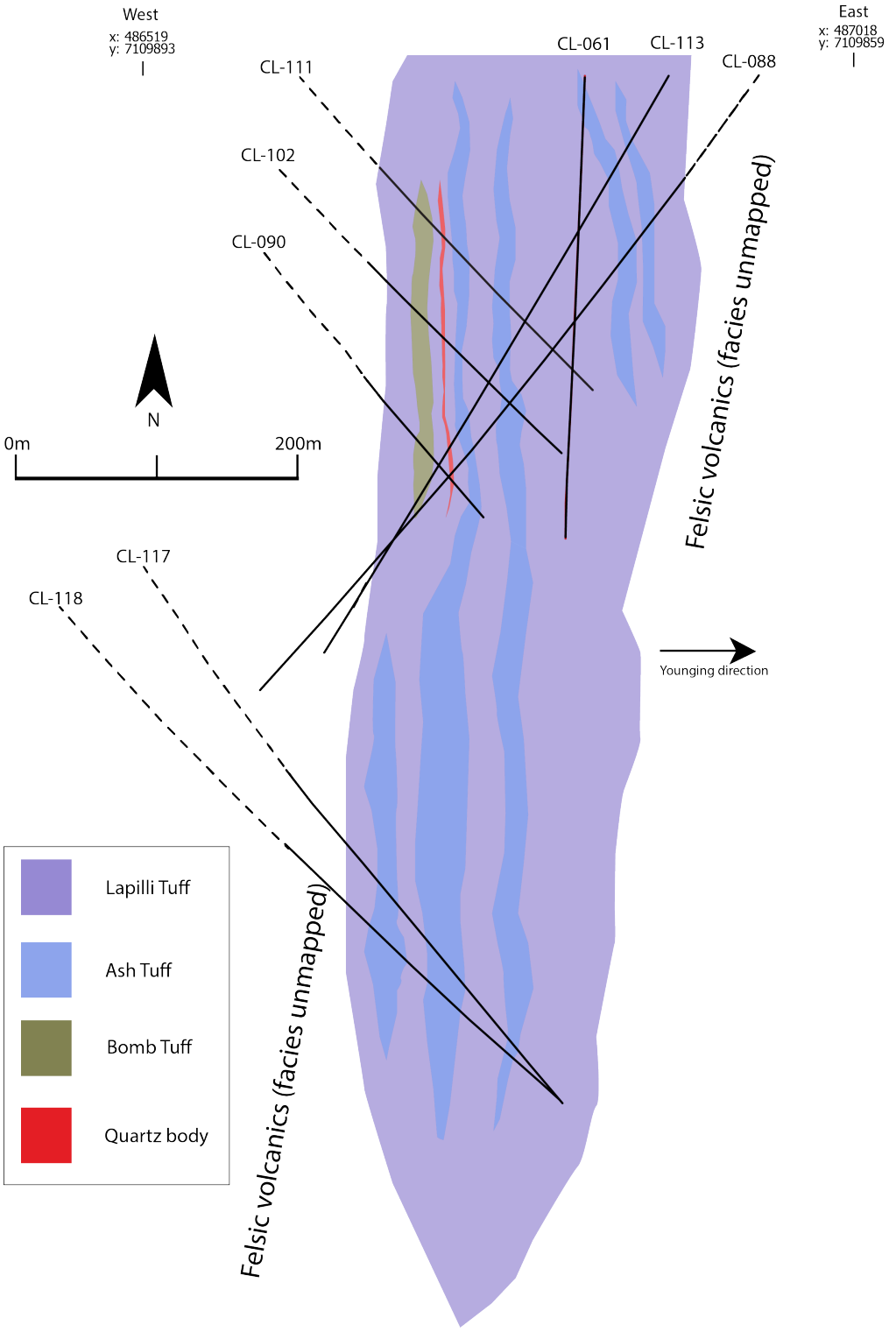

Figure 4.7 Facies map of mine section 4800N. Stratigraphy is tilted to approximately vertical. Felsic volcanics are mostly lapilli tuff with intercalated ash and bomb tuff horizons. A single stratabound quartz body is intersected in 5 drill holes.

4.2.2.2.1 Ash Tuff

Ash tuff is dominated by fine grained ash that is >95% of its composition. Ejectors are rare but when present tend to be <5mm. The unit is therefore extremely well sorted. Ash tuff is usually homogenous and massive in appearance with little primary volcanic or sedimentary structure however towards the top of the stratigraphy it is more commonly aqeuously reworked and bedding and cross bedding is more common. It is rare to find pristine samples of this lithology since it is prone to exhibit foliation caused by deformational metamorphism (figure 4.8).

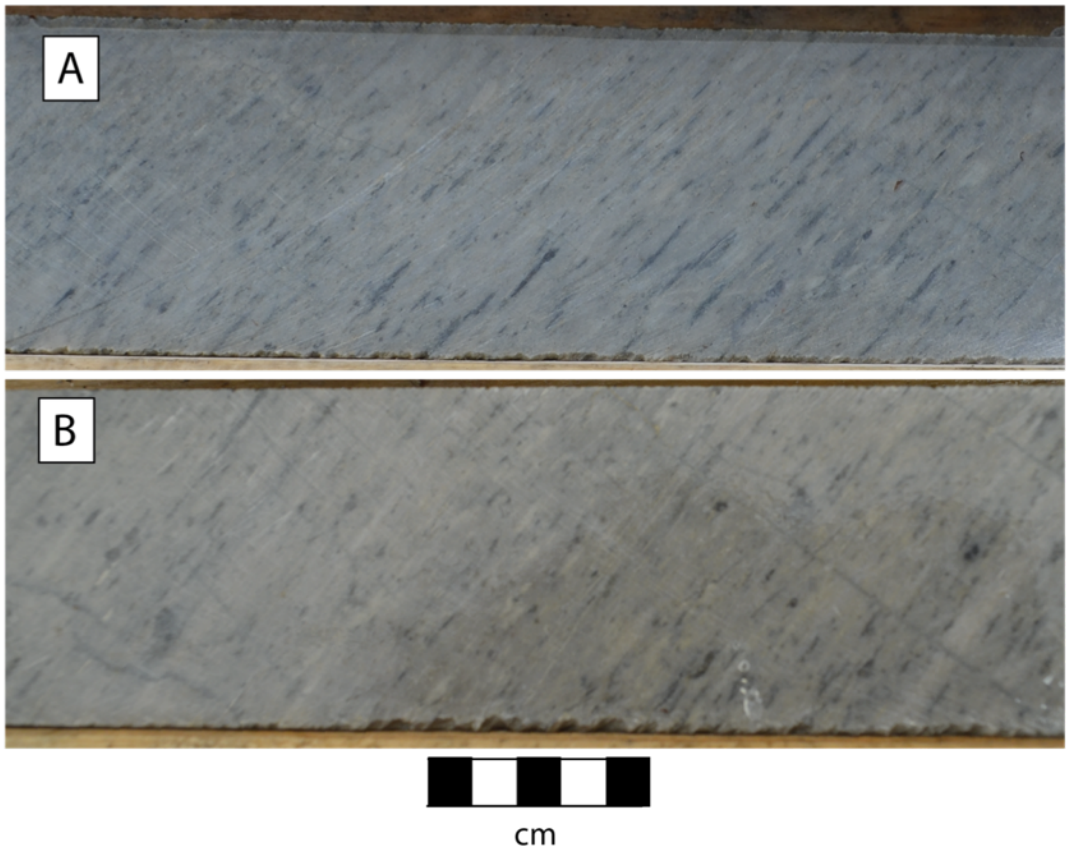

Figure 4.8 Ash tuff from drill core. There is a homogenous, consistent appearance with >5% sub 5mm ejectors (elongated with foliation).

These properties are also clear in thin section (figure 4.9). It is homogenous in appearance and is dominated by fine grained quartz ash that is consistently very well

sorted and grain size is typically 30-50 µm. Small ejectors are common and are quartz or alkali feldspar in composition.

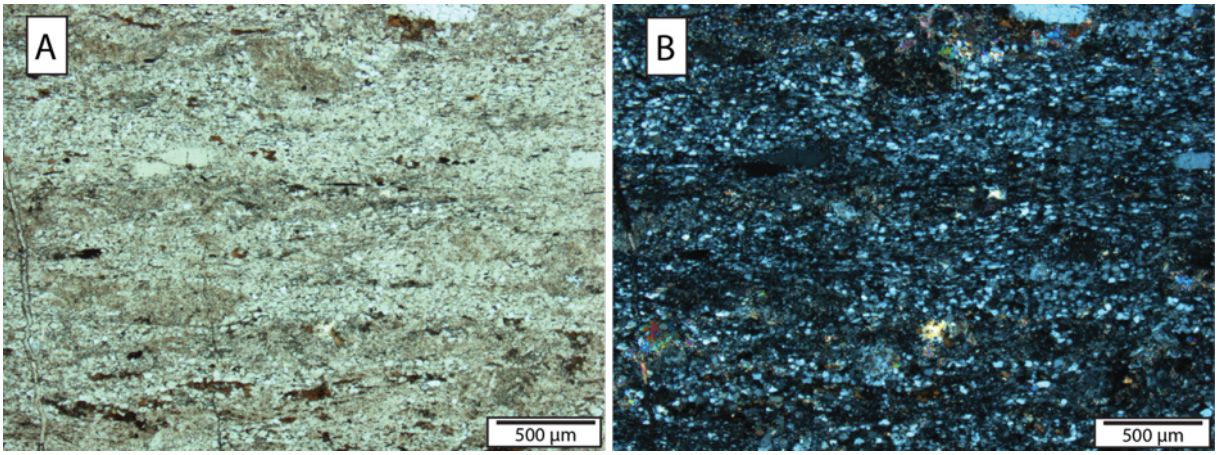

Figure 4.9 Ash tuff in thin section (A: PPL and B: XPL). Homogenous texture with well sorted, fine grained quartz

4.2.2.2.2 Lapilli Tuff

Lapilli tuff is seen extensively throughout the section. Clast size and sorting range considerably. Clasts are 2 to 64 mm in diameter and are typically rounded to sub-rounded with extensive variation in texture both laterally and stratigraphically (figure 4.10). Clasts are present in a fine grained ash matrix that composes 20-60 % of the unit. Locations where the facies becomes more juvenile are common (figure 4.10A); here sorting becomes poorer, modal clast size increases and clasts become sub angular to angular. Welded textures with flattening of clasts are locally present (figure 4.10B). This is a primary depositional texture in some areas as opposed to a product of deformation due to the lack of prominent local foliation fabric. Correlating differing lapilli tuff textures along sections is not possible with the current drilling density.

In thin section textural differences between the clasts and the matrix can be recognised. Clasts have a very fine crystalline (<10µm) groundmass that is dominated by quartz with feldspar phenocrysts up to 500µm in diameter (figures 4.11A and 4.11B). The quartz groundmass is homogenous whilst feldspars have an intermittent distribution and vary in size from 40 to 500 µm (figure 4.11B). The matrix has a similar appearance to the ash

tuff with fine crystalline quartz and smaller ejectors (figures 4.11 C and 4.11D). The matrix is thought to have a greater porosity than the clasts due to be more preferentially exploited by alteration as seen in figure 4.11A.

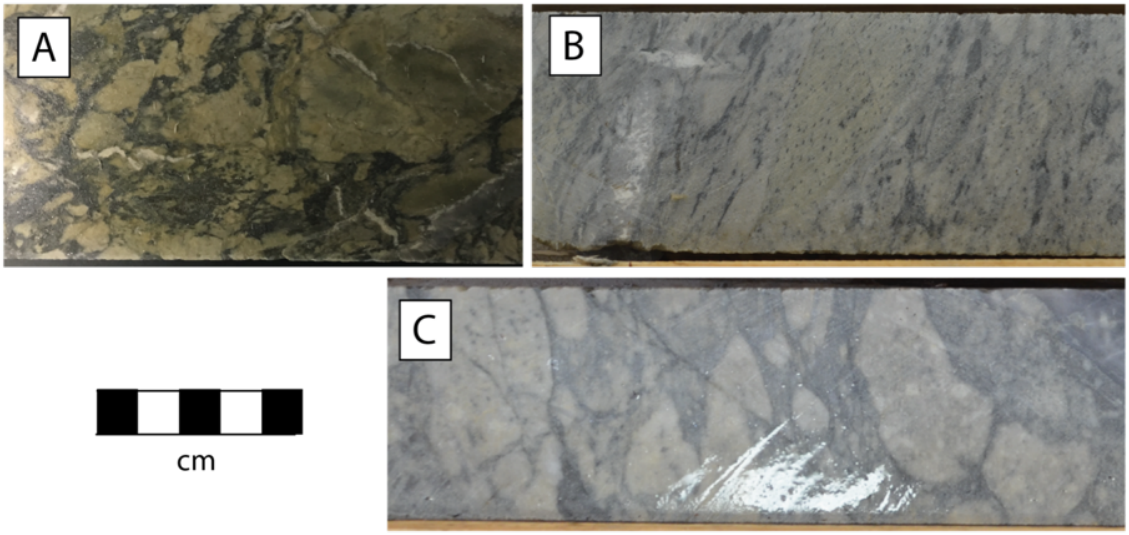

Figure 4.10 Lapilli tuff from drill core. A: Juvenile, poorly sorted sub-angular to angular clasts. B: Welded clasts with variation in clast size. C: Moderately well sorted lapilli tuff with greater ash component.

4.2.2.2.1 Bomb Tuff

A bomb tuff occurs where clast size exceeds 64 mm. Since FAT has almost exclusively been drilled with NQ core (47.6mm diameter) it is difficult to differentiate this facies from the lapilli tuff. Bomb tuffs are identified in outcrop south of the deposit in stratigraphy that are analogous to FAT (figure 4.12C). In drill core, where clasts are obviously larger (greater than 64mm) and more juvenile (sub angular to sub rounded boundaries and poorly sorted) as seen in figures 4.12A and 4.12B. The composition and textural changes within these clasts are similar to lapilli tuffs; the only difference is that the clasts are larger.

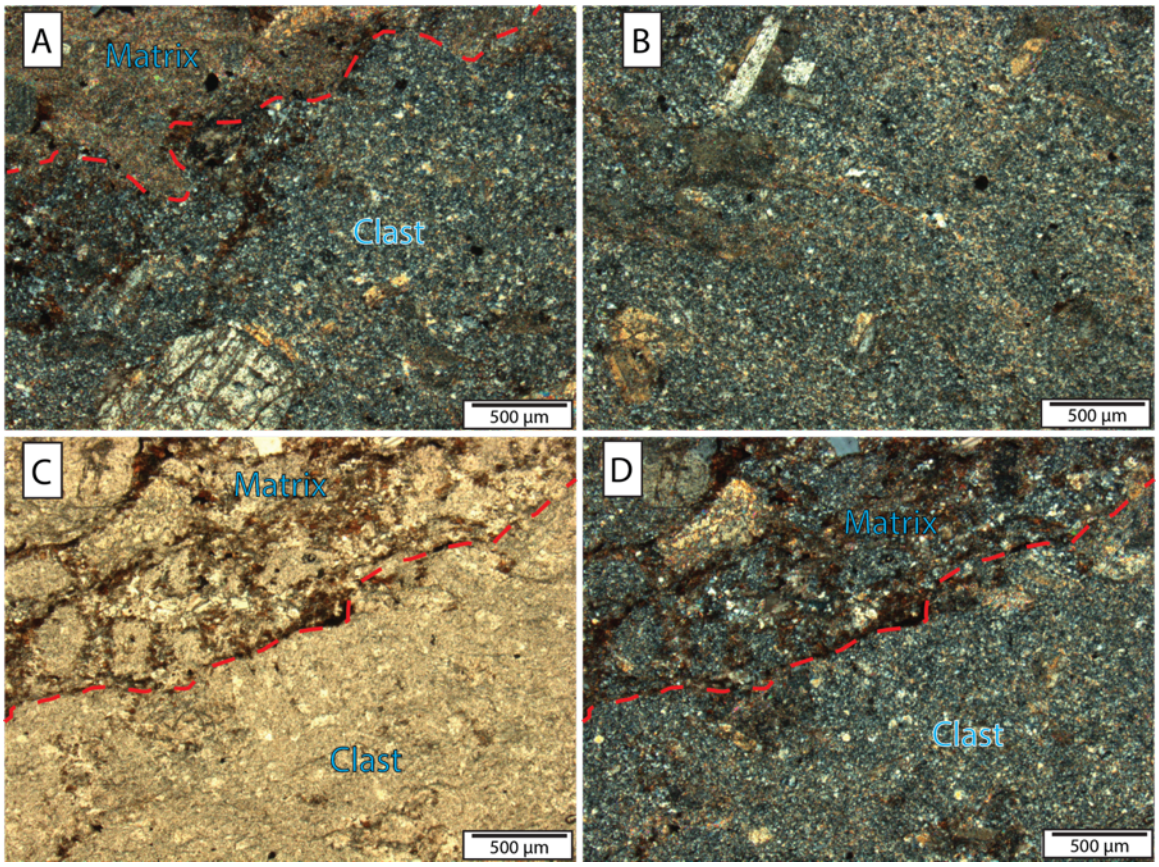

Figure 4.11 Thin section of lapilli tuff. Red line shows clast boundaries. A: Cross polarised light image showing the difference between matrix and the clast. Clasts are generally very fine crystalline (<10µm diameter) quartz with feldspar phenocrysts (seen in bottom of image) up to 1000µm. In this example the matrix has a biotite alteration overprint B: Cross polarised light image of a lapilli clast with fine crystalline quartz groundmass and feldspar phenocrysts. C: Plane polarised light image showing contrast between lapilli clast and matrix. Clast has a homogenous appearance with small phenocrysts visible whereas matrix has similar textures to ash tuff with small sub 500µm clasts throughout. D: Cross polarised light image of C showing similarity of composition between matrix and clast.

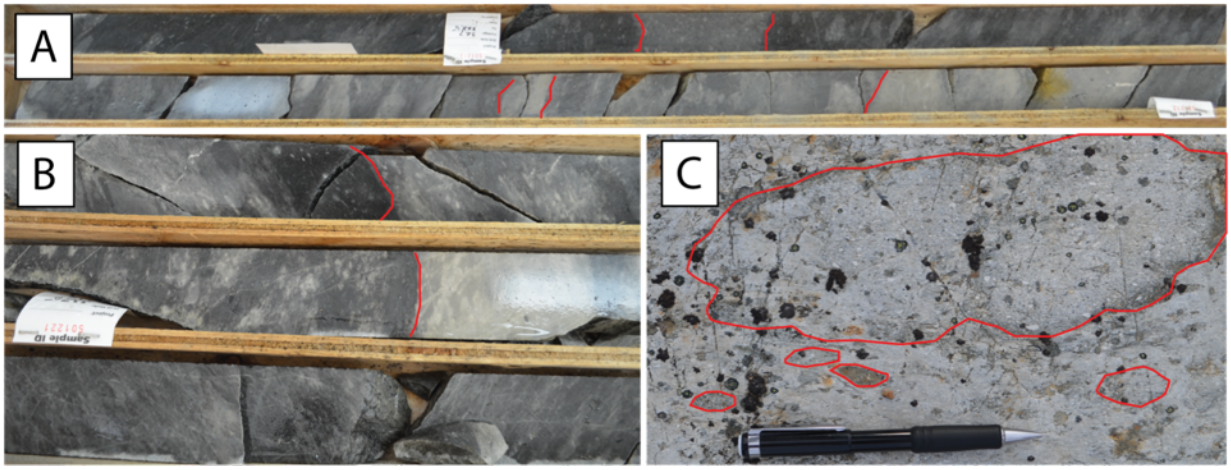

Figure 4.12 Bomb tuff in drill core and outcrop. Examples of clast boundaries are highlighted in red. Core diameter is ~47mm. A: Bomb tuff in drill core. Clasts exceed the aperture the core and so shape and size is impossible to infer but can be distinguished by clast boundaries and differences in colour. B: Close up of clast boundaries with distinct textural changes from homogenous ash to porphyritic clasts. C: Bomb tuff in outcrop with 35cm angular ellipsoid bomb in ash matrix with lapilli clasts. The bomb and lapilli clasts have a porphyritic texture with inclusions common whilst the ash is fine grained and homogenous.

4.2.2.2.2 Quartz Body

A single quartz body is intersected in five drill holes. It is stratabound and is parallel to the other lithologies (figure 4.7). This unit is 1.5-2.5m in width and has sharp contacts with neighbouring tuff (figures 4.13A and 4.13B). The contact overprints the tuff (figure 4.13B). Quartz has a consistently mottled texture with plain white quartz interwoven with dark intercalations (figure 4.13). The quartz is interwoven with an unknown orange mineral (discussed in Chapter 7) that is more abundant at the contacts (figures 4.13B and 4.13C). In thin section (figure 4.14), the intercalated quartz and host rock is visible with replacement textures of the quartz visible. This is therefore believed to be a product of alteration that occurred after the formation of the host rock. The mechanisms for the genesis of this quartz body are discussed in Chapter 6.

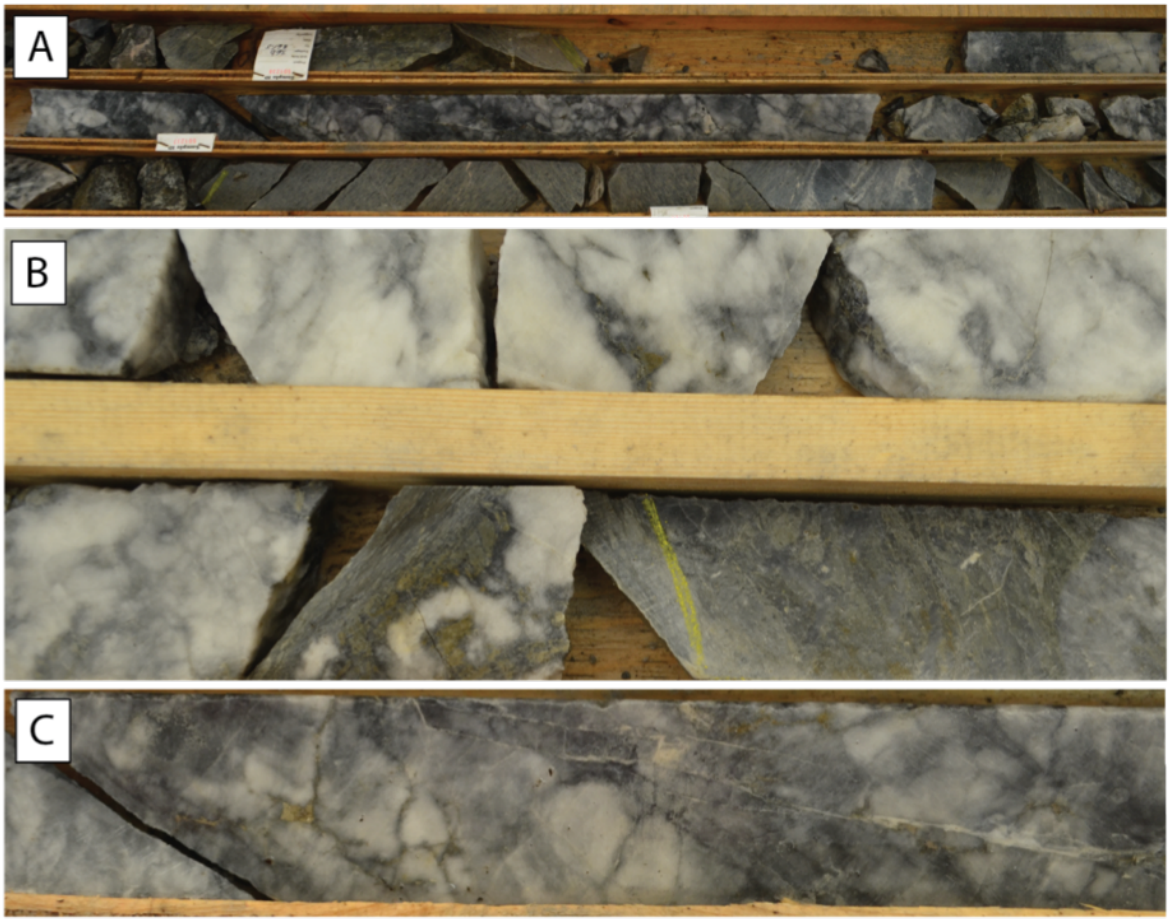

Figure 4.13 Quartz body in drill core. Core diameter is ~47mm (and core box is 1.1m length in image A). A: Approximately 1.5m of quartz vein with sharp contacts with surrounding lapilli tuff. B: Mottled quartz vein. Quartz is mostly plain white with darker interwoven zones of unidentified orange mineral (discussed in Chapter 6). Contact with lapilli tuff (marked by yellow line) is sharp with quartz overprinting the tuff. C: Mottled texture within quartz. Intercalations of orange mineral in left third of image.

4.2.2.1 Volcanic Environment

Since the ejecta is dominantly lapilli clasts with occasional ash and bombs, eruption activity is inferred to be moderate to violent and have a vulcanian to sub-plinian eruption type based on Easton & Johns' (1986) classification.

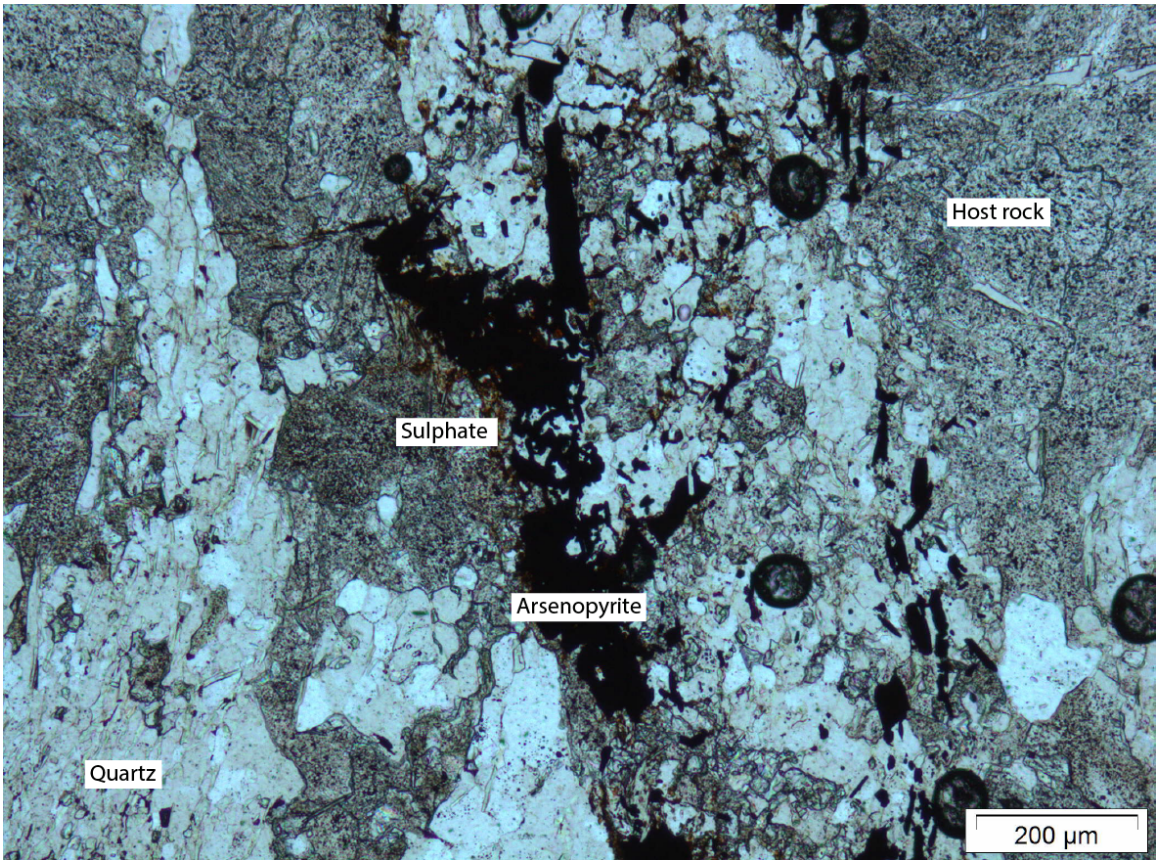

Figure 4.14 Quartz body in thin section. Quartz with intercalated host rock with replacement textures. Arsenopyrite rimmed with sulphate on the margins of the quartz.

During volcanism there is a gradual transition from a sub aerial to sub aqueous environment indicated by the gradually intercalated and overlying Burwash Formation sediments. Initially, primary sub aerial facies have poorly sorted, angular ejecta, no sedimentary intercalations and are generally not welded. As a sub aqueous environment prevails, sedimentary intercalations are more common, ejecta can become well sorted and rounded (thought to be a product of aqueous reworking) and welded textures become common (figure 4.15). Figures in section 4.2.2.2 are all thought to represent sub aerial facies (with the exception of figure 4.10B which shows welding).

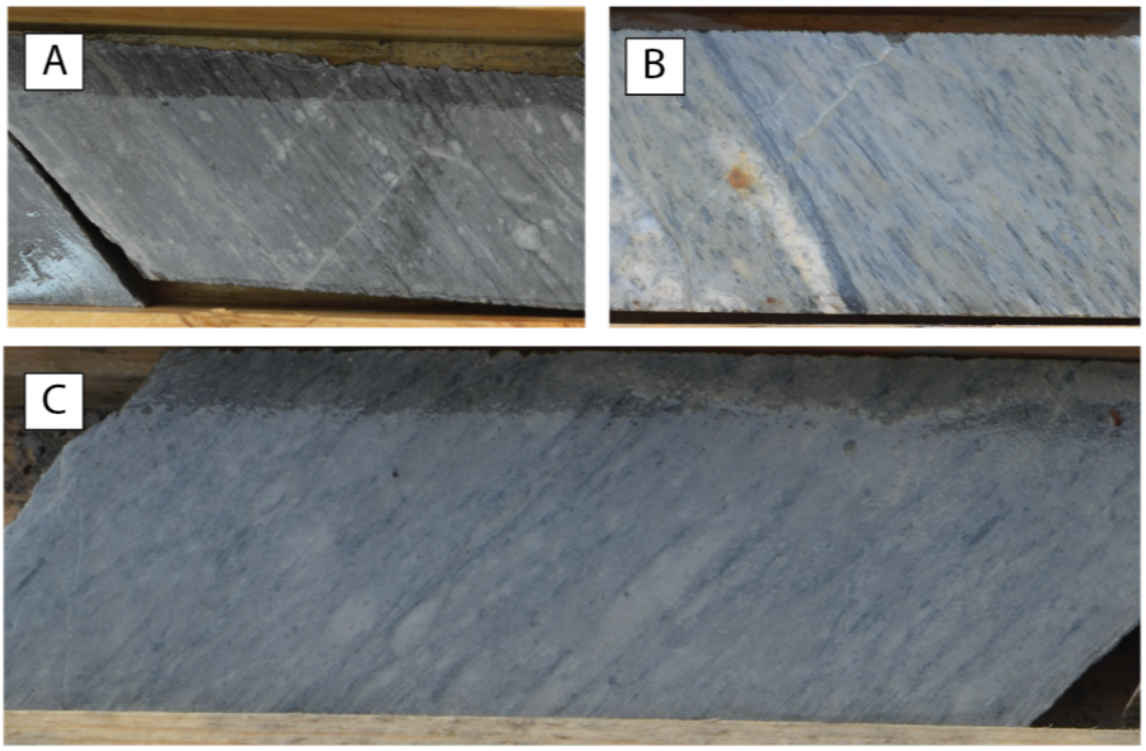

Figure 4.15 Sub aqueous textures. Core diameter is ~47mm. A and B: Intercalated sedimentary beds. C: Rounded and welded eject

4.2.3 Burwash Formation Sedimentary Rocks

A greywacke sedimentary sequence (the Burwash Formation) conformably overlies the felsic volcanics (figures 2.1 and 3.1) At the top of the felsic volcanics, intercalations of sedimentary rocks become gradually more common towards the East as the contact is approached (figure 4.16). Sedimentary rocks are initially derived from volcanic tuffs with intercalated mudstone deposited in periods of volcanic quiescence (Moore 1956; Dillon-Leitch 1984). Sediments are dominated by greywacke-arkose beds with graded sandstone beds typically 1-2cm (but up to 1m) thick overlain by 1-10cm thick pelitic beds (Dillon-Leitch, 1984). These are interpreted to be bouma A and E beds and are turbidite facies typical of a proximal basin facies (Dillon-Leitch, 1984; Moore, 1956). A gradational contact with the underlying volcanics is visible in the drill core. There are rare discreet, locally occurring volcanic conglomerate packages with clasts up to 10mm in size in the initial 100m of the sedimentary rocks.

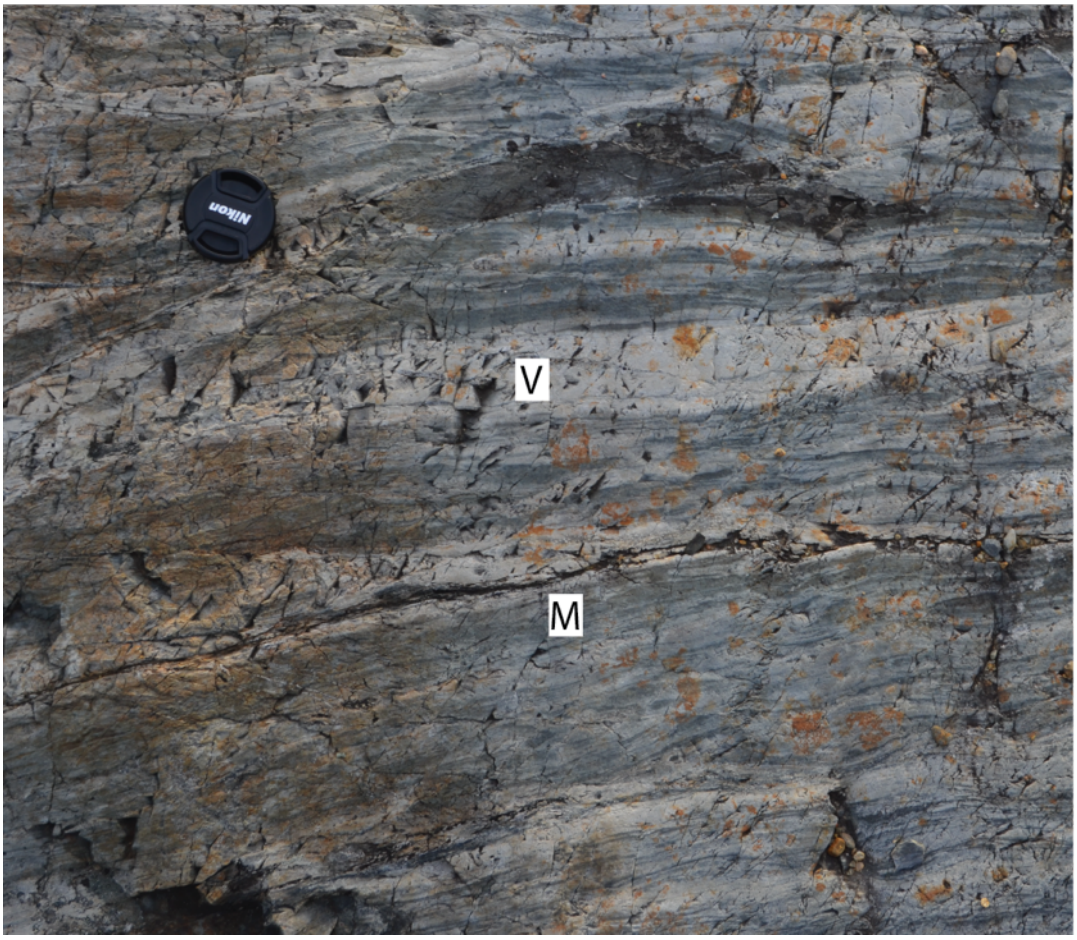

Figure 4.16 Intercalated volcanically derived sedimentary rocks (lighter colour and marked with a 'V') and mudstone (darker colour and marked with an 'M').

Chapter 5

5 Mineralisation

Mineralisation at FAT is observed at a variety of scales. On a cross section scale, the shape of grade shells and their position within the resource model broadly indicates strataform mineralisation. In hand samples the abundance of quartz veins and style and abundance of arsenopyrite mineralisation correlates with Au enrichment. In thin section, three distinct arsenopyrite type (termed A-type, B-type and C-type) with different levels of Au enrichment are identified by SIMS analysis. These type can be further defined geochemically with EMP analysis and LA-ICP-MS indicating distinct geochemical signatures.

5.1 Cross Section Trends

Seabridge Gold has split the deposit into 15 sub parallel strataform domains that define the resource model (figure 5.1). These domains were based on host rock facies, mineralisation style and gold grade. Due to the size of the deposit only the most enriched domains (3, 4 and 5 containing 86% of the resource) were examined in this study. Detailed faces descriptions of the domains not investigated in this project can be found at seabridgegold.net (Freeman, 2004). Figure 5.1 shows the location of these three strataform domains and their relationship with Au. The overlaid leapfrog interpolation shows that individual zones of mineralisation and particularly high grade gold are strataform, some zones of mineralisation cross cuts the domains. Each domain has been interpreted to be formed by distinct volcanic events because of their strataform distribution and broad lithological similarities (Freeman, 2004).

Since each domain is defined by a change in volcanic facies and texture as well as mineralisation style, the lithology and then mineralisation characteristics of each domain are described here. Domains 3, 4 and 5 define the study area however their unique geological characteristics are not thought to have a significant effect on the mineralisation interpretation. This is addressed in the discussion (Chapter 8).

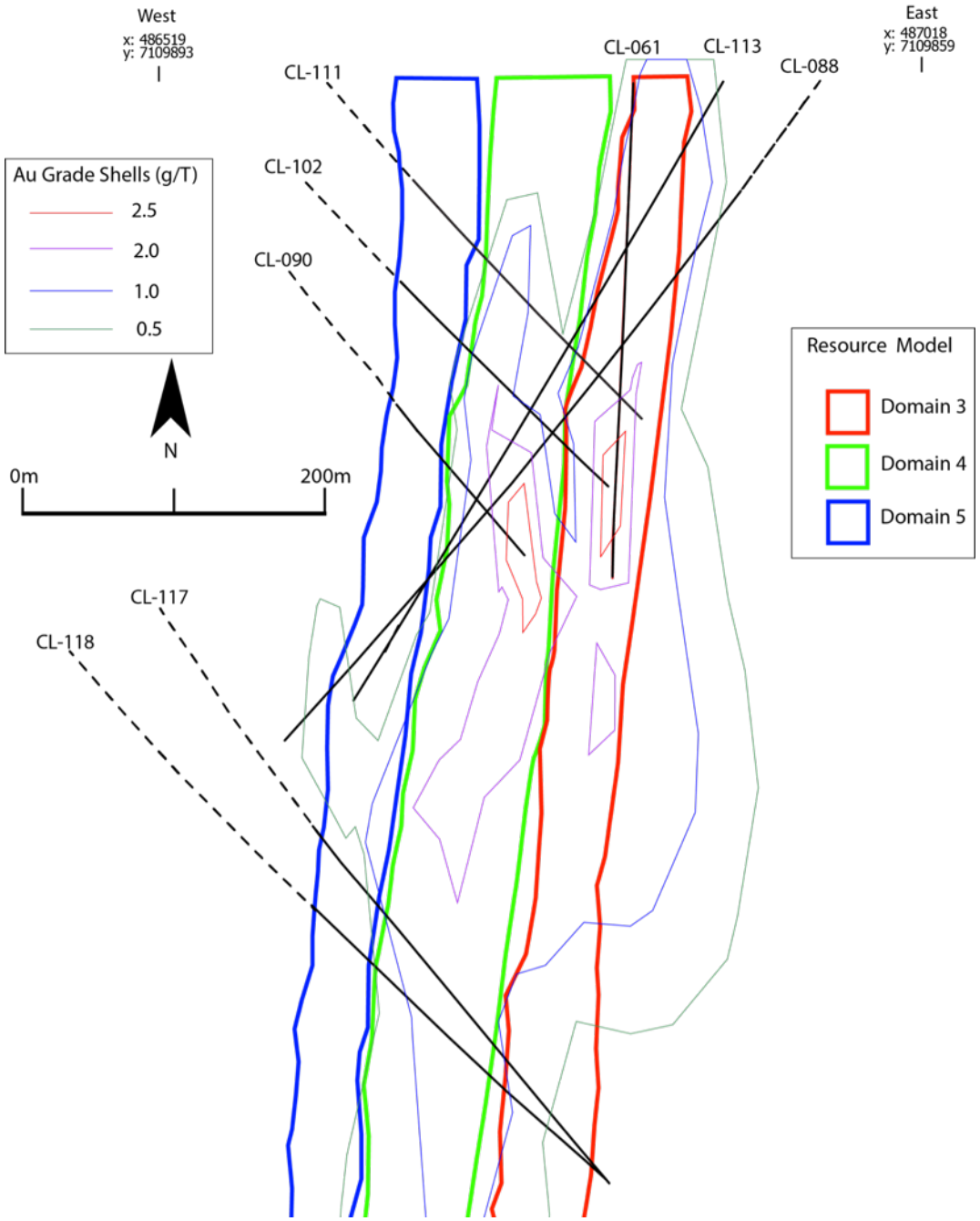

Figure 5.1 Cross section looking north at mine section 4800N. Resource model showing domains 3,4 and 5. at the FAT deposit. Grade shells are defined from leapfrog interpolations. Drill holes used in this study shown by black lines (and outside the study area by dashed lines). Cross section is at the same position as figure 4.7 for a comparison with facies.

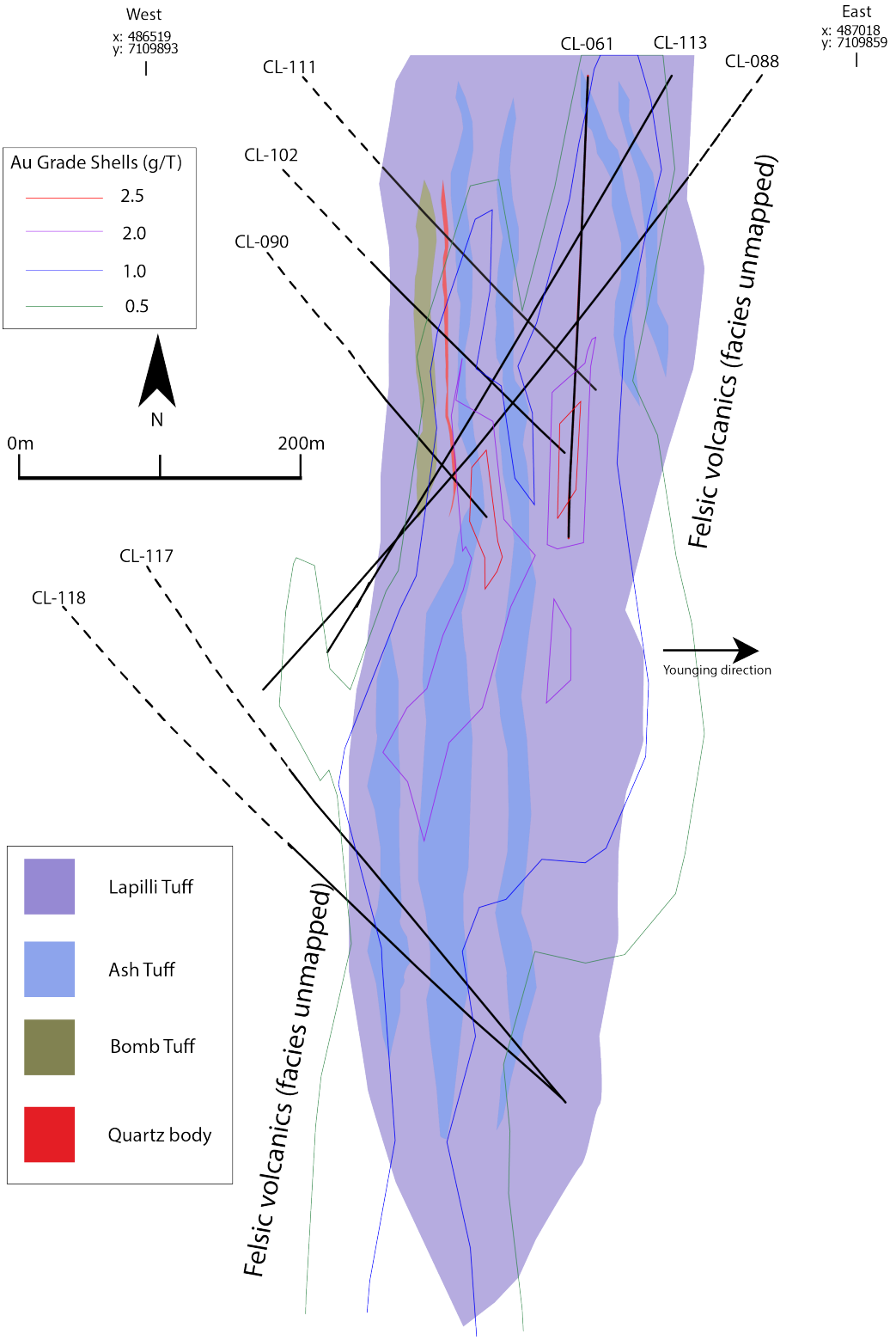

Figure 5.2 Cross section 4800N showing stratigraphy with grade shells overlain. This shows mineralisation to be strataform.

5.1.1 Domain 5

Domain 5 is the most westerly and oldest (based on the stratigraphy of the of CLGB) of the three domains principally studied. It is dominated by lapilli tuffs that contain 5-10mm sized fragments that range from rounded to lenticular in shape. Variance in clast size is low. There are discreet, intercalated greywacke lenses throughout the domain. Rounded to sub rounded lithic clasts (that are interpreted represent aqueous reworking of ejector) are common but not ubiquitous. Juvenile, sub angular clasts also frequently occur. Sub 10mm clast size that is indicative of a relatively distal volcanic environment is consistently observed over the 500m of depth of drill holes. Deformation of the clasts is rare with apparent pre metamorphism morphology generally preserved.

Mineralisation is present as acicular very-fine crystalline arsenopyrite blades that occur mostly within the matrix of the tuff. Arsenopyrite is usually randomly oriented and fine crystalline. It is generally in a lower abundance compared to domains 3 and 4 (<1 modal % over 2m intervals). Domain 5 mineralisation is found within centimetres of and on the margins of thin, commonly deformed quartz veins. It is classified as mostly A-type arsenopyrite and phase 1 quartz (as described and defined below).

5.1.2 Domain 4

Domain 4 is the central and thickest of the studied domains. Volcanic clasts sizes and abundances are variable. They range from less than 5mm to 100's mm in diameter with common sub-meter thick beds of ash tuff. Clasts are usually sub-rounded and lenticular in shape, indicative of a fairly proximal sub-aerial environments (Easton & Johns 1986). There is minimal evidence of sub-aqueous textures. Large clasts tend to be rich in plagioclase feldspar and quartz crystals. Deformation is common and is manifested by clast elongation parallel to foliation. Parallel mica bands that vary in intensity define this foliation.

Arsenopyrite is much more abundant than domains 3 and 5 (up to 5 modal % over 2m intervals). It occurs in the host rock usually within 5 to 10 centimetres of quartz veins. It generally conforms to an orientation that is defined by foliation. It typically overprints

both the clasts and matrix of the tuff. Arsenopyrite of all types defined in this chapter are observed.

5.1.3 Domain 3

Domain 3 is the youngest (due to being higher up in the stratigraphy) and most easterly of the three principally studied domains. Clasts range in size from 5mm to 20mm across and are much more angular than domains 4 and 5. This suggests a sub-aerial environment with the reduction in clast size indicating either a waning in volcanic activity or a more vent-distal environment. There are common, thin greywacke intercalations indicating intermittent flooding events. Mica does not appear to form in bands as seen in domain 4 however isolated crystals aligned to form a bedding parallel foliation are fairly common. Carbonate content within the matrix is more abundant than domains 3 and 4.

5.1.4 Geochemical Trends

The lithogeochemical As content from samples typically taken over 1.5m intervals correlates with Au. Since all of Seabridge Gold's drill holes have been analysed by ICP and fire assay for Au, trends can be spatially correlated across the whole of the cross section and used as an exploration vector. Figure 5.2 shows the highest Au values correspond to high As to S ratios. This is a trend that is also observed from the EMP analysis of individual crystals (discussed in section 5.3.4). The increase in the As to S ratio seen in whole rock ICP is a function of the arsenopyrite increasing in abundance with respect to pyrite. This is because the largest changes in S and arsenic content are due to the respective abundances of arsenopyrite and pyrite rather than As content of arsenopyrite. Domains 3, 4 and 5 do not seem to have distinctly different grades or As/S content.

5.2 Quartz Veins

There is a spatial correlation of Au and quartz veins at FAT observed on a hand sample scale (for example figure 5.4A shows a mineralised quartz vein with arsenopyrite rich rims). Two styles of quartz veins can be recognised (figure 5.4). Early 'phase 1' veins are thin (2-15mm). They are commonly but not consistently contorted and broken

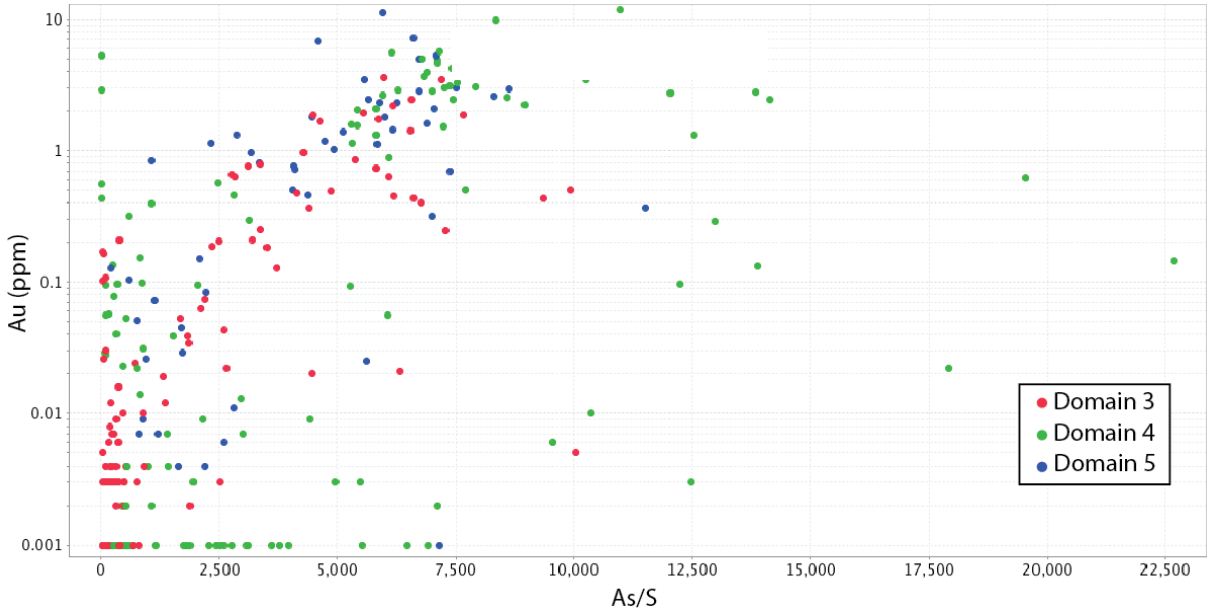

Figure 5.3 ICP data for intervals with<0.25% S. Shows As/S vs Au vs domain for the three domains investigated. There is an increase in Au when the As increases relative to S. There does not seem to be a difference in degree of mineralisation or in As/S with respect to domain.

(discontinuous). These frequently have a blue-grey colour that is commonly more apparent towards the rims. They are typically folded and foliation is usually parallel to the fold axial trace of these folds. The foliation and its relationship with veining and mineralisation is addressed in Chapter 6 (alteration) and Chapter 8 (discussion).

Phase 2 quartz is more abundant and cross cuts phase 1 veins (figure 5.4). They are typically parallel to foliation and have a cloudy, brighter white colour. They can be boudinaged and discontinuous with surrounding host rock appearing bleached. Veins typically range from 1cm to 30cm thick. Carbonate is variably present as a constituent.

Arsenopyrite mineralisation (and therefore Au enrichment) occurs within centimetres of these quartz veins and is described in section 5.3.1 as individual type are addressed.

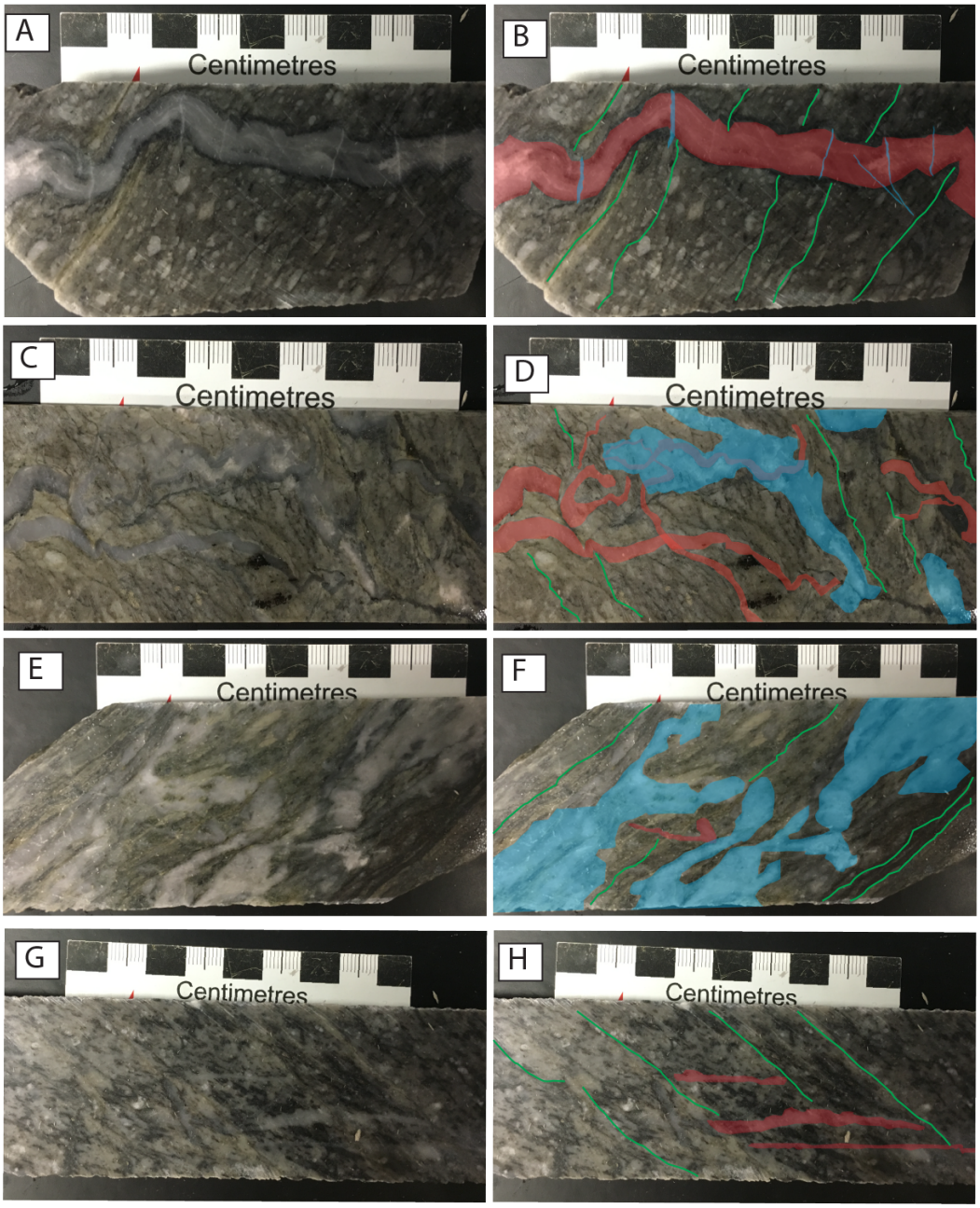

Figure 5.4 Vein styles at FAT as recognised in drill core. Image on the left is a photograph of the rock. Image on the right is annotated to show different vein generations. Red overlay is phase 1 veins, blue overlay is phase 2 veins whilst the green lines represent foliation.

5.2.1 Phase 1 Quartz Veins

Phase 1 quartz veins can be recognised in thin section by their thin width (sub 15mm), multiple generations as they cross cut each other, cockade texture and their degree of deformation (figure 5.5). They tend to be finer crystalline than phase 2 veins. Figures 5.5 A and C shows multiple generations of phase 1 veins that are contorted and deformed. Figure 5.5D shows a broken raft of phase 1 quartz within ash tuff. White mica that defines foliation truncates and cross cut quartz veins and is parallel to fold axial traces (figure 5.5B). This relationship is also shown in figure 5.3. Therefore, the veins seem to be syn-metamorphic with sericite developed as an axial planar foliation.

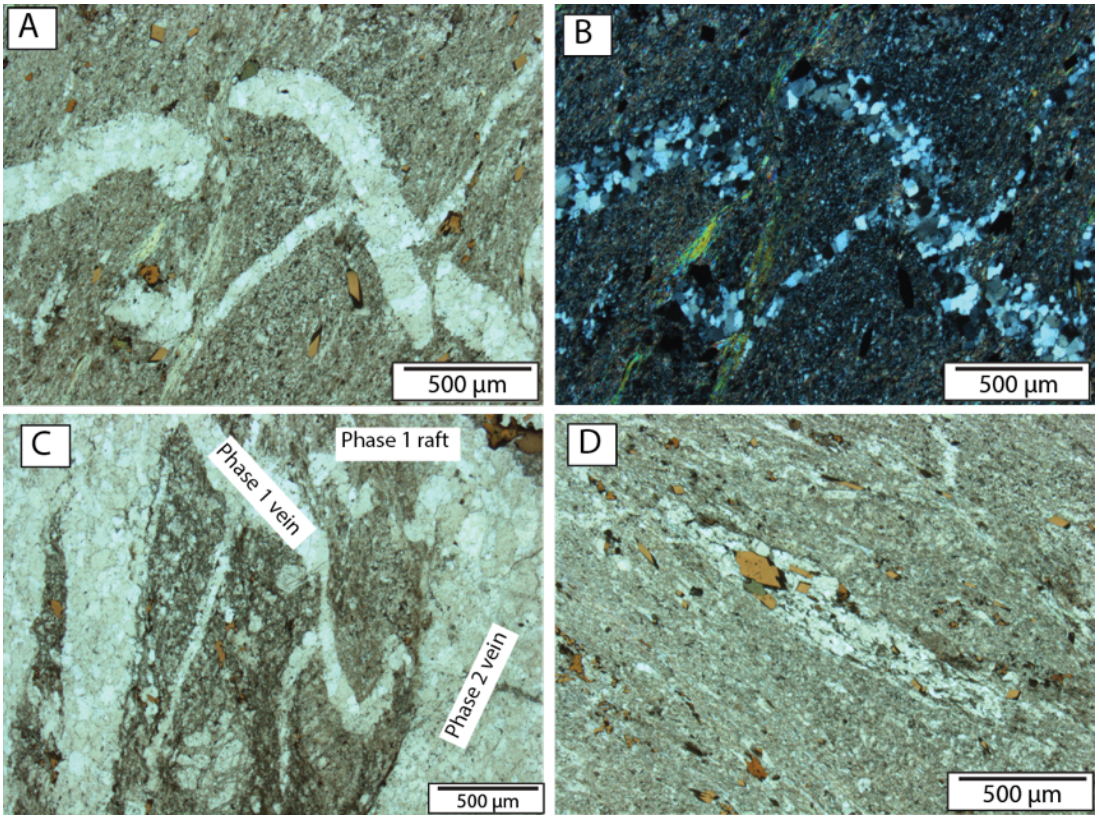

Figure 5.5 Phase 1 quartz vein in thin section. A: Deformed and broken quartz vein (partial reflected and plane polarised light). B: Image A in cross polarised light showing quartz crystals. C: Multiple phases of cross cutting phase 1 quartz veins. Phase 2 quartz vein (thicker and overprinting) cross cuts phase 1 in the right of the image (partial reflected and plane polarised light) D: Boudinaged phase 1 quartz vein containing mineralisation (partial reflected and plane polarised light)

5.2.2 Phase 2 Quartz Veins

Phase 2 quartz veins cross cut phase 1 quartz veins (figure 5.4 and 5.6A). They are thicker, are typically coarser crystalline (figure 5.6B, F) and sometimes have a carbonate component (figure 5.6F). They are usually parallel to foliation defined by sericite (figure 5.6B, D, F). Mineralisation is not always proximal to these veins. Arsenopyrite and pyrite is present on the vein margins and proximal (as halos within 10 centimetres) of these veins (figure 5.6A, C, E).

5.3 Sulphide Mineralogy

The sulphide minerals that are identified within the studied section are (in order of decreasing abundance) pyrite, arsenopyrite, and rarely chalcopyrite. The element most strongly correlated with Au at FAT is As (figure 5.3) and the abundance of acicular arsenopyrite has been traditionally used as a pre-assay proxy for gold mineralisation (Freeman, 2004). Au is usually invisible at the sub-micron scale. Depth profiles for SIMS analysis shows very consistent Au values that indicate it is refractory. Gold is very rarely observed as micron scale inclusions within arsenopyrite by SEM and as visible gold adjacent to quartz veins visually in drill core.

Arsenopyrite at FAT is divided into three distinct types (A-type, B-type and C-type). Crystal type can be identified in thin section by geological environment, aspect ratio, inclusion abundance and relationship with foliation. These types have different levels of Au enrichment shown by SIMS analysis (decreasing from A to C) and distinct geochemical signatures shown by EMP analysis and LA-ICP-MS.

5.3.1 Arsenopyrite Classification

5.3.1.1 A-type

A-type arsenopyrite is inclusion free and rarely fractured (figure 5.7 B). Crystal habit ranges from equant to acicular (and measured aspect ratios range from 1 to 17). Acicular, elongate crystals are considerably more common and the rhombic crystal habit may be a product of orientation of thin sections. Crystals range in size from 10 to 2000 μm.

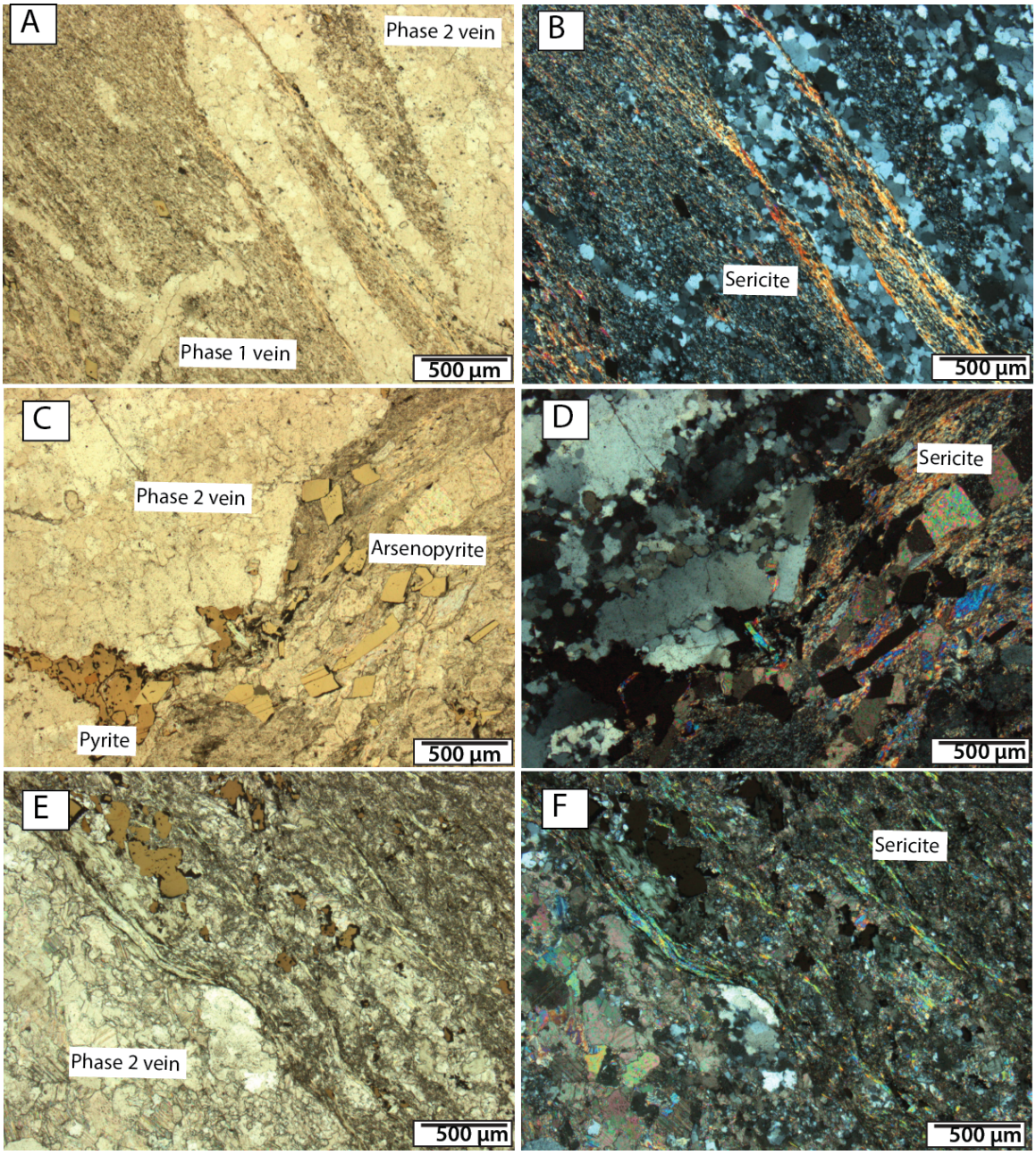

Figure 5.6 Phase 2 quartz veins. A (partial reflected and plane polarised light) and B (cross polarised light) shows a phase 2 vein sub parallel to sericite foliation cross cutting a phase 1 folded quartz vein in the left of the image. C (partial reflected and plane polarised light) and D (cross polarised light) Shows a phase 2 quartz vein with pyrite and B-type asp on the vein margin. E (partial reflected and plane polarised light) and F (cross polarised light) shows a phase 2 quartz vein with carbonate parallel to foliation and C-type arsenopyrite.

A-type arsenopyrite is more commonly found in domains 3 and 5. Crystals are found in all lithologies of felsic volcanics (ash tuff in figure 5.7 B-C and lapilli tuff in 5.7 A, D-G). In lapilli tuff it is most commonly found in the ash matrix between clasts (figure 5.6 A-C, F, G) but finer-crystalline examples can also be found in the clasts (figure 5.7D-E). This is probably a result of primary porosity with fluid preferentially migrating through the matrix as a result of porosity contrast. Crystals are commonly randomly oriented and form rosettes (figure 5.7 C, D, G) however when large quartz veins are present are often found in a consistent orientation parallel to these (figure 5.7 B). Where crystals are observed in clasts they are very commonly randomly oriented (figures 5.7 D-E). Rosettes are usually found where arsenopyrite density increases; they are commonly surrounded by single arsenopyrite crystals (figure 5.7 G). A-type arsenopyrite is also frequently observed in thin sections where B-type and (to a lesser extent) C-type arsenopyrite is present (for example figure 5.7 C). In these cases, it commonly has a specific orientation parallel to foliation.

5.3.1.1 B-Type

B-type arsenopyrite can be differentiated from A-type arsenopyrite by inclusion and fracture abundances. They have rounded inclusions commonly found towards the centre of the crystal although uniform distribution of these is rare (figure 5.8 B). Crystals are commonly fractured or show corrosion of their boundaries. Crystals are commonly elongate however range in aspect ratio to a lesser extent than A-type. They rarely exhibit the long aspect ratio seen in the A-type asbestiform crystals.

B-type arsenopyrite is found in all domains. It is commonly found within the matrix of lapilli tuff (figure 5.8A). Within the matrix crystals are usually sub parallel to each other defining a foliation (figure 5.8 C, E, F) however random orientation and rosette patterns similar to A-type arsenopyrite are frequently observed (figure 5.8 C, D). B-type arsenopyrite can also be found within the clasts of the lapilli tuff however these crystals are usually isolated and less abundant.

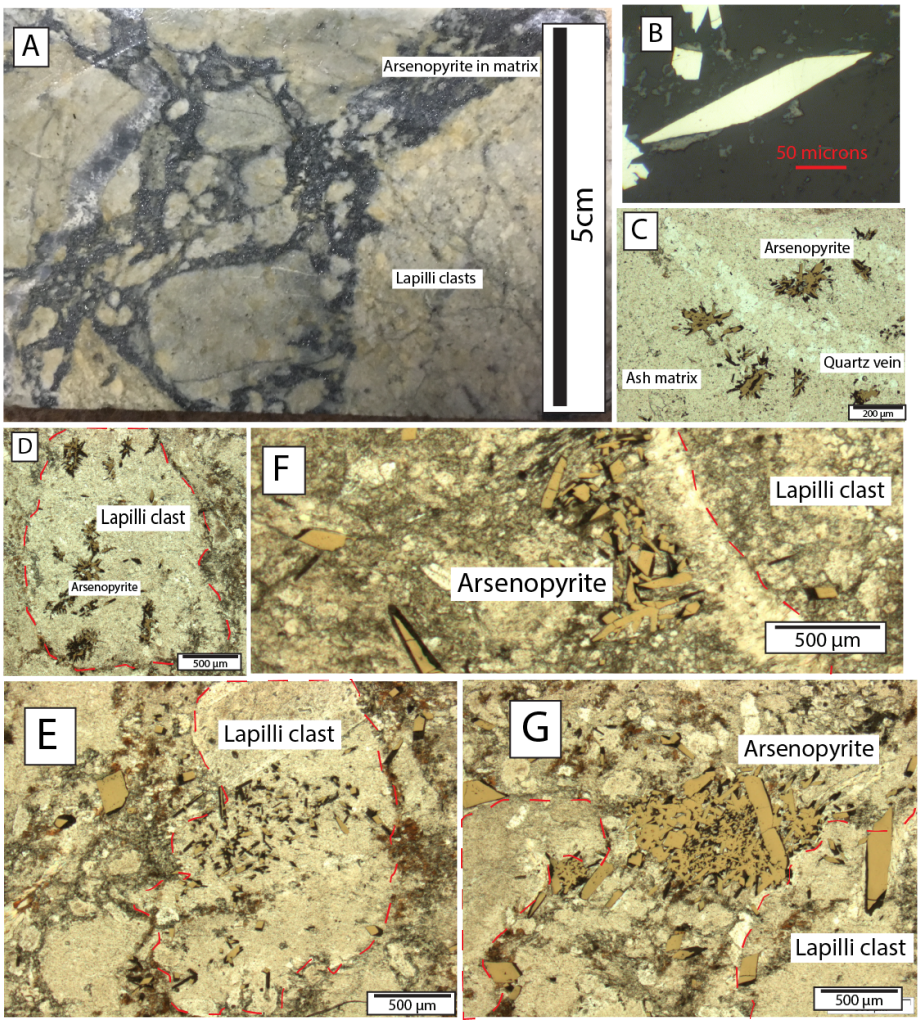

Figure 5.7 Occurrence of A-type arsenopyrite. Red lines represent clast boundaries. A: Photograph of core. Arsenopyrite in matrix surrounding lapilli clasts. B An example of an A-type arsenopyrite crystal (reflected light). C: Rosettes of arsenopyrite proximal to phase 1 quartz vein (partial plane polarised and reflected light photomicrograph). D: Rosettes of arsenopyrite within a clast (partial plane polarised and reflected light photomicrograph). E: Two styles and sizes of arsenopyrite (finer crystalline within clasts and coarser, more equant crystals within the matrix). Partial plane polarised and reflected light photomicrograph. F: Arsenopyrite within the matrix of the lapilli tuff (partial plane polarised and reflected light photomicrograph). G: Randomly orientated arsenopyrite within the matrix of the lapilli tuff (partial plane polarised and reflected light photomicrograph).

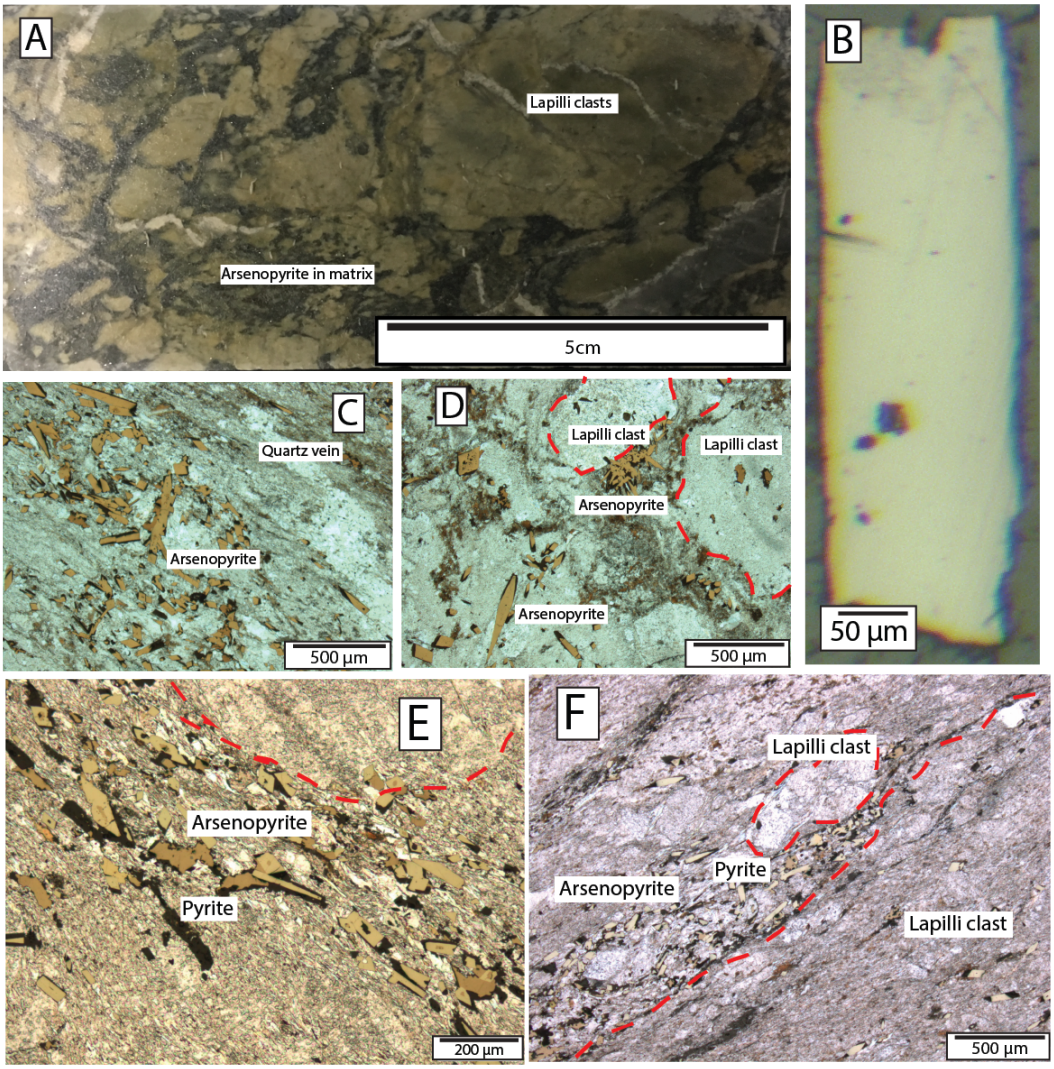

Figure 5.8 Occurrence of B-type arsenopyrite (photograph of drill core). A: Lapilli tuff with B-type arsenopyrite in ash matrix surrounding clasts. B: Example of B-type arsenopyrite (reflected light) C: B-type arsenopyrite within ash tuff matrix. The more elongate arsenopyrite are typically orientated parallel to foliation (approx. 150° in this image). Partial plane polarised and reflected light photomicrograph. D: B-type arsenopyrite in similar setting to A-type (within the matrix of lapilli tuff). Partial plane polarised and reflected light photomicrograph. E: B-type arsenopyrite within matrix of lapilli tuff with pyrite and parallel to foliation (partial plane polarised and reflected light photomicrograph). F: B-type arsenopyrite and pyrite at greater density but present in both the matrix and clasts of lapilli tuff (partial plane polarised and reflected light photomicrograph).

5.3.1.2 C-Type

C-type arsenopyrite crystals range in morphology and habit from rhombic to elongate. They are gradational textural transition from B-type arsenopyrite with a greater abundance of fractures and inclusions and larger inclusions. The arsenopyrite is heavily fractured and has either large or numerous inclusions (figure 5.9 C). Inclusions are either minerals from the matrix that also surrounds the crystal or are pyrite. The inclusion abundance and proximal location of anhedral arsenopyrite and pyrite with respect to C-type arsenopyrite (figure 5.9 E) suggests these are also cogenetic type.

C-type arsenopyrite tends to occur in more foliated rock and does not seem to be confined to any particular lithological facies. It is still commonly found in the matrix of lapilli tuff (figure 5.9 A, D) however is more abundant overprinting clasts than A and B-type arsenopyrite (figure 5.9 G). C-type arsenopyrite crystals tend to be sub parallel to each other and a preferred orientation can be recognised in all images in figure 5.9.

5.3.2 Arsenopyrite Relationship with Quartz Veins

Phase 1 quartz veins and the degree of deformation that they have undergone have a definable relationship with arsenopyrite type. An increase in deformation leads to a progressive increase from A-type to B-type to C-type arsenopyrite. A-type arsenopyrite mineralisation occurs within 1-2 centimetres and on the margins of undeformed phase 1 quartz veins (figure 5.10 A and B). A-type arsenopyrite rosettes occur in close proximity to these quartz veins with a greater abundance proximal to the larger vein. Arsenopyrite found where these veins are undeformed is usually randomly oriented. Figure 5.10 C and D show a more deformed phase 1 vein. Mineralisation is still present however now conforms to an orientation (roughly 130º). A, B and C type arsenopyrite are now all present. Where phase 1 veins exhibit the most deformation (for example figure 5.10 E and F) they have C-type (and rarely B-type) mineralisation that is parallel to the sericite that defines foliation. This is addressed in Chapter 8.

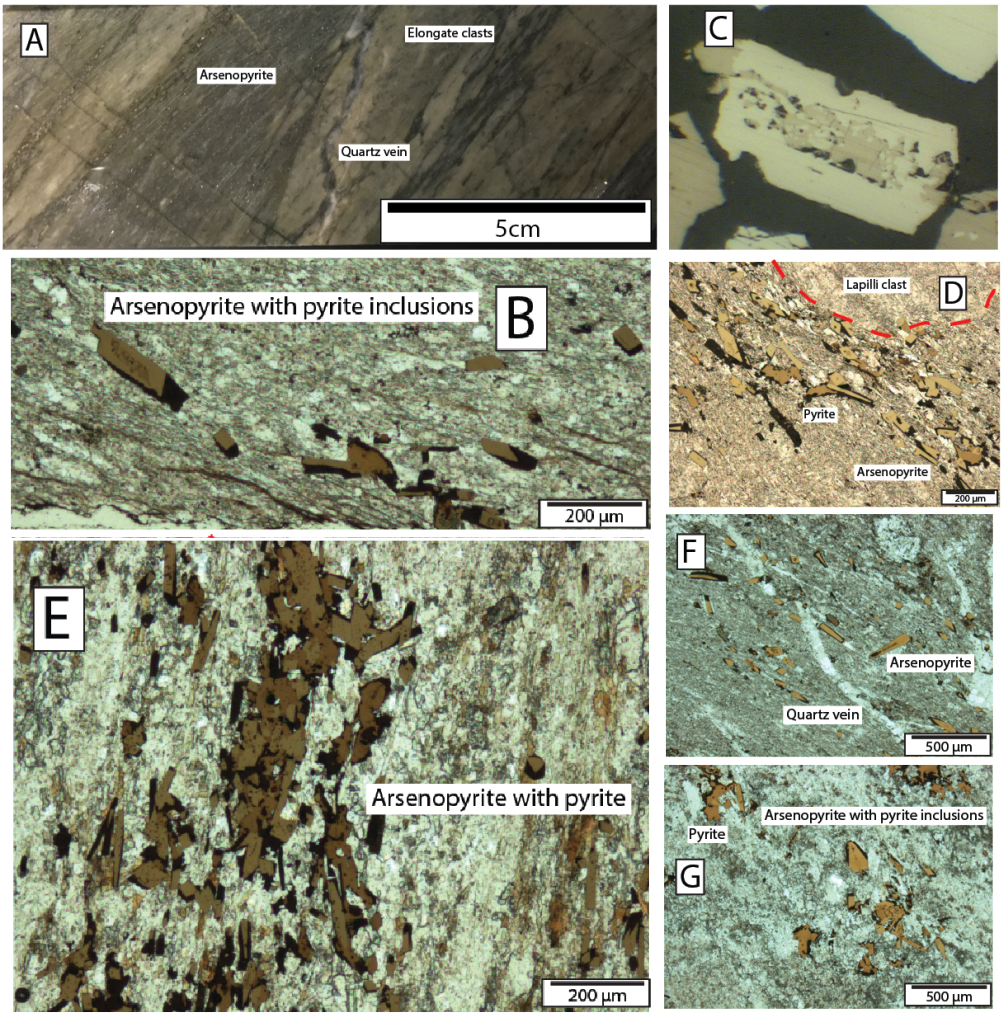

Figure 5.9 Occurrence of C-type arsenopyrite. A: Core sample with C-type arsenopyrite elongated parallel to foliation. B: C-type arsenopyrite showing with crystal alignment (partial plane polarised and reflected light photomicrograph). C: Example of a C-type arsenopyrite (reflected light). D: C-type arsenopyrite surrounding a clast (shown by red line). Partial plane polarised and reflected light photomicrograph. E: Inclusion rich C-type arsenopyrite mostly conforming to foliation (roughly vertical in this image) however there is still some variance to this orientation. Anhedral arsenopyrite can be seen in this image (partial plane polarised and reflected light photomicrograph). F:C-type arsenopyrite with A and B-type in ash tuff (partial plane polarised and reflected light photomicrograph). G: C-type arsenopyrite within a clast in lapilli tuff (partial plane polarised and reflected light photomicrograph).

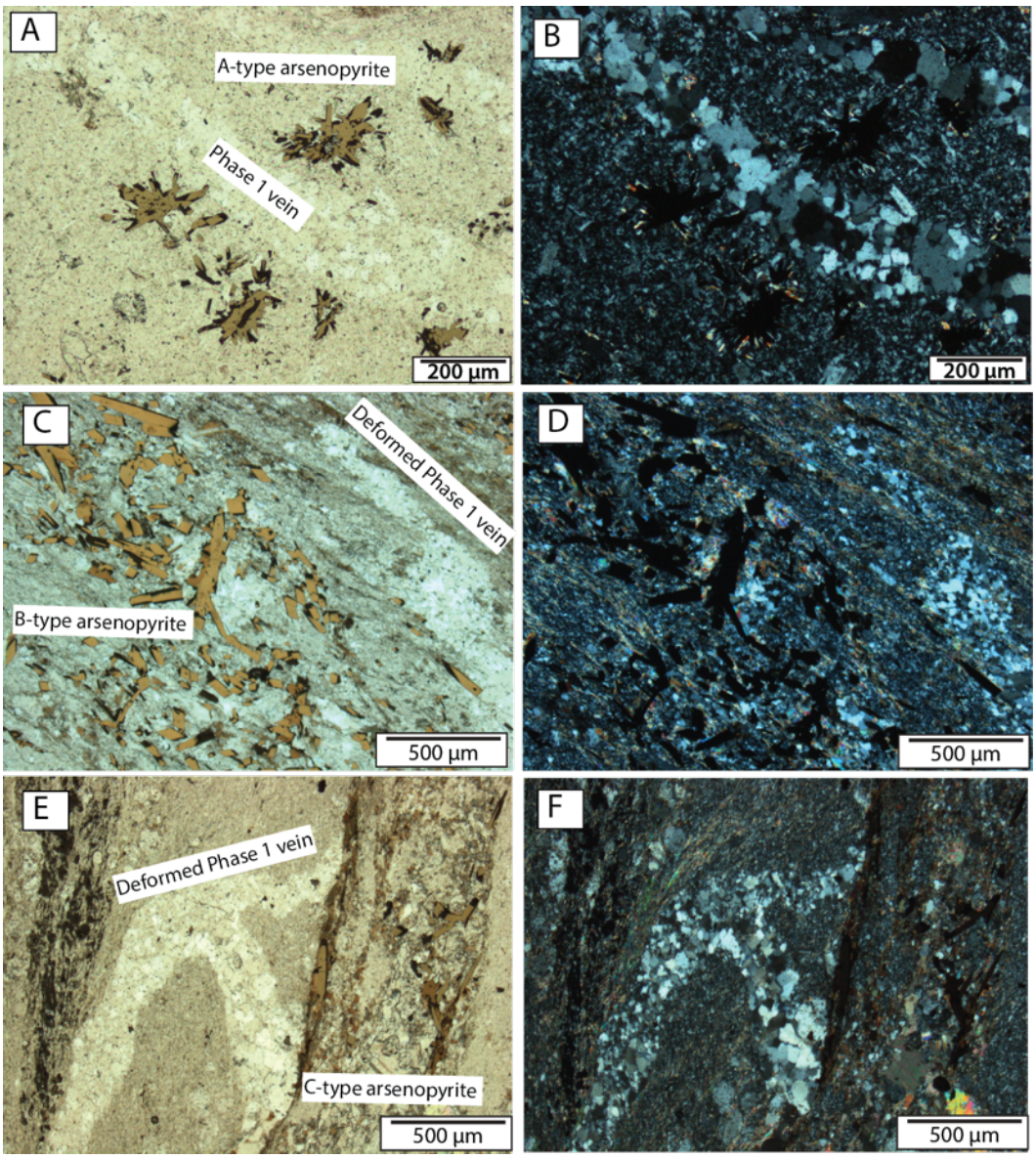

Figure 5.10 Arsenopyrite mineralization with phase 1 quartz veins. Plane polarised light images show mineralisation style whilst cross polarised light images show quartz style. A (partial plane polarised and reflected light) and B (cross polarised light) show a relatively undeformed quartz vein. Rosettes of A-type arsenopyrite are present proximal to this vein. C (partial plane polarised and reflected light) and D (cross polarised light) show a moderately deformed quartz vein with A and B type mineralisation with a preferred orientation parallel to deformation. E (partial plane polarised and reflected light) and F (cross polarised light) show a highly deformed phase 1 quartz vein with C-type and B-type mineralisation sub parallel to fold axis.

5.3.3 Arsenopyrite Relationship with Sericite

The cross section scale distribution sericite alteration trends and the composition of specific sericite types are described in Chapter 6. Each type of arsenopyrite however has a distinct textural relationship with white mica that can be seen in thin section and so are discussed here. A-type arsenopyrite has two distinct relationships with sericite. Where it is the only type present (figure 5.11) the samples generally lack white mica. Crystals form in in lineated sub parallel orientations (figure 5.11A, B) randomly oriented rosettes (figure 5.11C, D) Abundant mica was not observed in these thin sections and there is no distinct foliation as a result of this. Where observed in areas where B-type and C-type arsenopyrite is also found (figure 5.11E) a white mica foliation has developed. This is sub parallel to the preferred orientation of the arsenopyrite clasts.

White mica is always found with B-type and C-type arsenopyrite. Arsenopyrite is found in lineations that is always sub parallel to white mica foliations. When viewed in XPL (figure 5.12) the orientation of the sulphides are always consistent with the foliation defined by the white mica. There is also a relationship between the abundance of mica and the abundance of C-type mica relative to A-type and B-type. In figure 5.12A, the sulphide type is mostly B-type and there is a low mica abundance (figure 5.12B). Figure 5.12E and figure 5.12C have progressively more C-type arsenopyrite and pyrite (relative to A-type and B-type) and there is a greater abundance of mica (figure 5.12F, D).

5.3.4 Gold Abundance and Distribution

Thin sections that had a range of each type of mineralisation were selected for SIMS analysis. The following section uses data from five thin sections (two from domain 3 and 4 and one from domain 5) and seven mounts (two from domain 4 and 5 and three from domain 5). SIMS spot analysis for Au can be carried out on thin sections however in order to image Au distribution arsenopyrite separates were mounted in graphitic pucks. In total 106 spots were analysed (27 A-type, 54 B-type, 25 C-type and 7 pyrite). 12 crystals were imaged for Au distribution (4 A-type, 4-B type and 4 C-type).

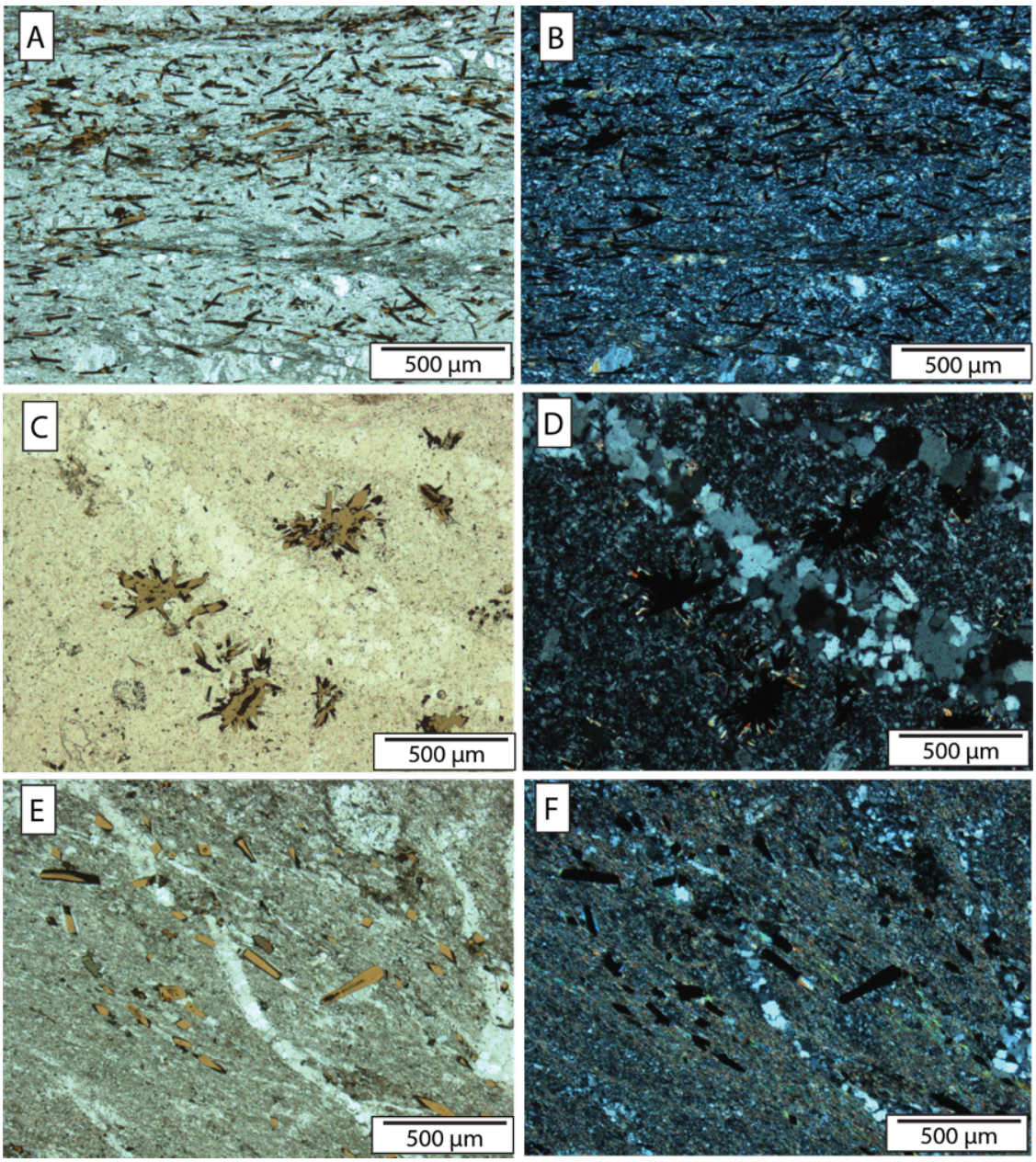

Figure 5.11 A type arsenopyrite relationship with white mica foliation. A: A-type arsenopyrite proximal to phase 1 quartz vein (partial plane polarised and reflected light). B: Image A in cross polarised light showing low of white mica but the absence of foliation bands. C: Randomly oriented A-type arsenopyrite rosette (partial plane polarised light and reflected light). D: Image C in cross polarised light showing absence of white mica. E: Sub parallel A-type arsenopyrite with B-type and C-type (partial plane polarised light and reflected light). F: Image E in cross polarised light showing white mica defining foliation that the arsenopyrite is parallel with.

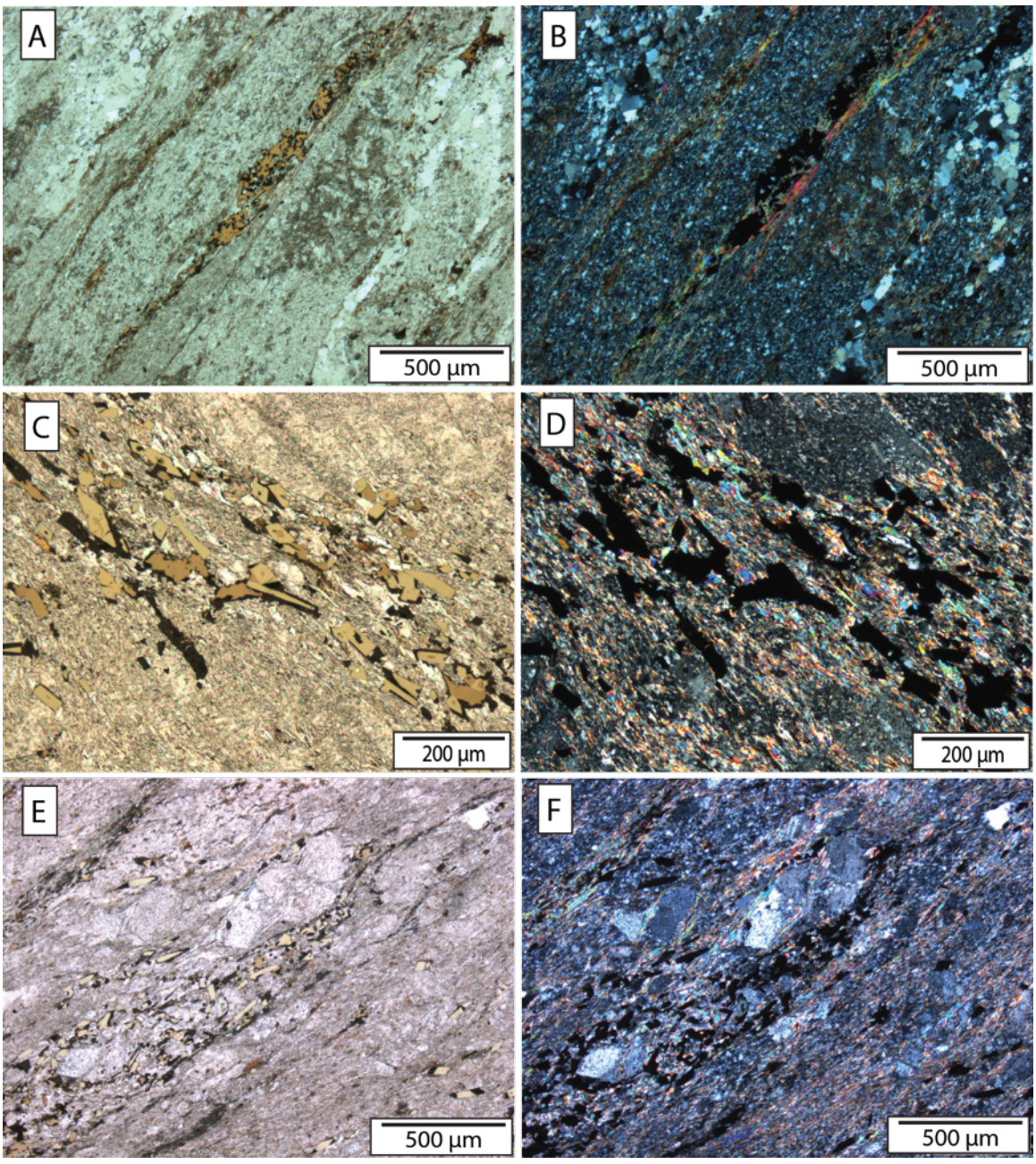

Figure 5.12 B-type and C-type arsenopyrite and their relationship with white mica. A: Thin vein of A-type and B-type arsenopyrite (partial plane polarised light and reflected light). B: Image A in cross polarised light showing vein is surrounded by white mica. C: Mostly C-type arsenopyrite with B-type arsenopyrite and pyrite parallel to foliation (partial plane polarised light and reflected light). D: Image C in cross polarised light showing mica habit. Abundant white mica forming the same foliation as seen with the sulphide minerals. E: A-type, B-type, C-type arsenopyrite

and pyrite sub parallel and aligned (partial plane polarised light and reflected light). F: Image E in cross polarised light. Abundant white mica forming foliation parallel to the sulphide minerals seen in image F.

5.3.4.1 A-Type

Gold enrichment is generally high in A-type arsenopyrite (figure 5.13). SIMS spot analysis on these crystals yield values up to 2460ppm Au. The mean of all samples tested was 446ppm Au. Changes in size, width and aspect ratio within this type do not appear to affect the level of Au enrichment. These values are given in appendix B.

Gold distribution was analysed by SIMS imaging (figure 5.14). In A-type arsenopyrite there are two types of Au distribution. Figures 5.14 A and 5.14 B show a fairly homogenous distribution and the core is slightly more enriched than the rim (termed type Ai). In Figure 5.14 C Au is enriched in the rims with a barren core (termed type-Aii). There do not seem to be any visible difference in crystal habit or form between these two types of crystal however geochemical differences are discussed in section 5.3.5.

5.3.4.1 B-Type

SIMS spot analysis of B-type arsenopyrite shows a large range in gold concentration (figure 5.15). The crystals with the greatest density of inclusions seem to have less Au whereas crystals with fewer inclusions have higher Au concentration. Overall Au is consistently less than A-type arsenopyrite (measured up to 1650 ppm Au). The mean Au concentration from spot analysis on B-type crystals was 188ppm.

Gold distribution in the crystal was analysed by SIMS imaging (figure 5.16). In all B-type crystals there is a heterogeneous, blotchy distribution of Au. This seems to vary in intensity. For example, in figure 5.16B would seem to have the greatest variance of gold within the crystal followed by figure 5.16A and then 5.16C.

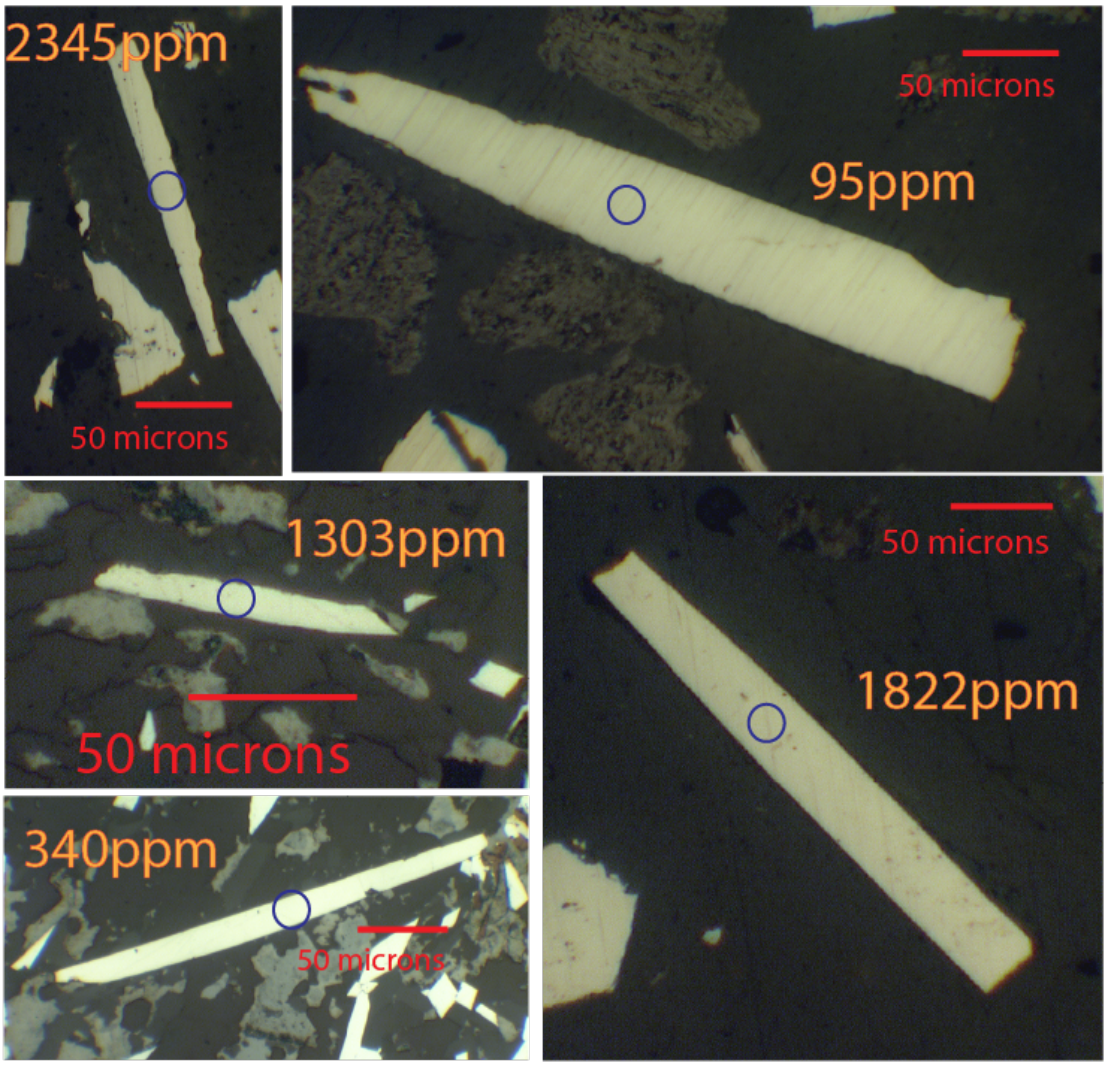

Figure 5.13 Reflected light images of A-type arsenopyrite crystals. SIMS targets for spot analysis for Au are shown with a blue circle with results shown in orange. Crystals have no inclusions and are commonly acicular. Although all crystals shown here have the same habit, size does not seem to affect Au enrichment.

5.3.4.1 C-Type

SIMS spot analyses indicate that gold is consistently much lower than the previously described arsenopyrite type. Measured Au concentration was up to 315ppm (figure 5.17). The mean Au concentration from spot analysis for C-type arsenopyrite is 97ppm. This is considerably less than both A-type and B-type arsenopyrite.

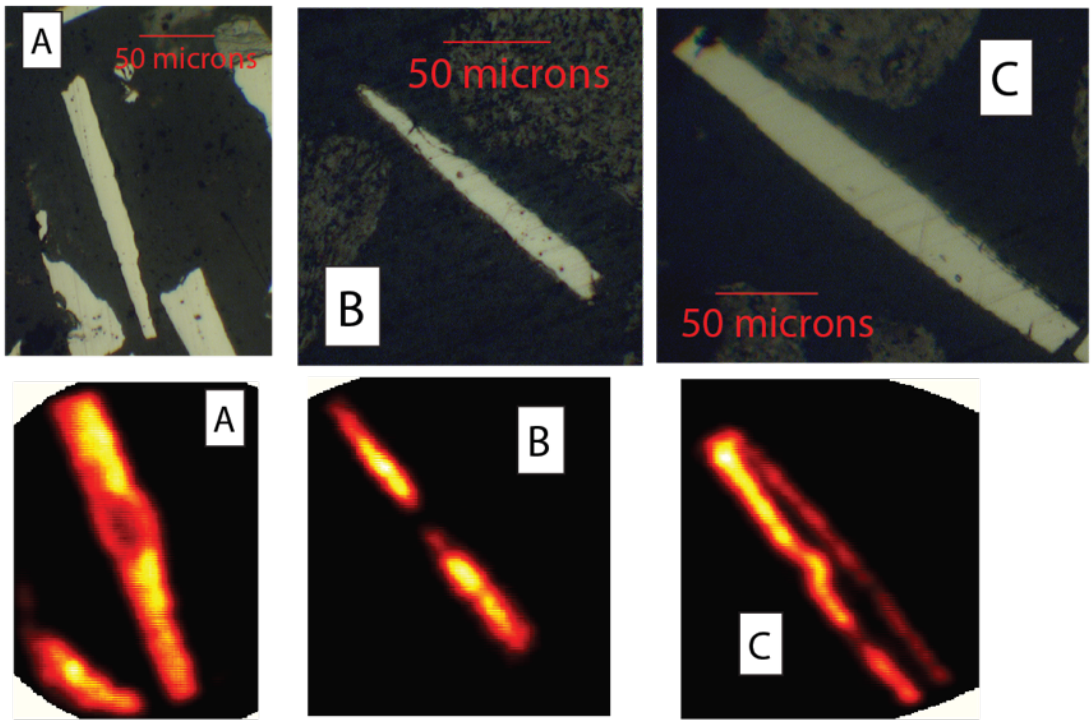

Figure 5.14 SIMS images of Au distribution in A-type arsenopyrite crystals. Photomicrographs at top show scale and crystal habit with SIMS images at the bottom. Warm colours indicate increased Au contents. A and B (type-Ai) have slight enrichment in the core whilst C shows the inverse relationship with enrichment in the rim and a barren core (type A-ii). Depletion in the centre of A and B is due to a SIMS spot destroying the crystal in previous quantitative analysis.

Gold distribution in C-type arsenopyrite is usually bladed (figure 5.18 A, B and D). Blades are enriched areas of Au that usually occur towards the edge of the crystal and are parallel to the C axis.

5.3.5 Geochemical Associations

Once the Au concentration was quantified and the distribution characterised, LA-ICP-MS and EMP analysis was carried out in order to evaluate whether there are specific geochemical associations. Each type would seem to have a unique relationship with other elements that can help differentiate and further define these type.

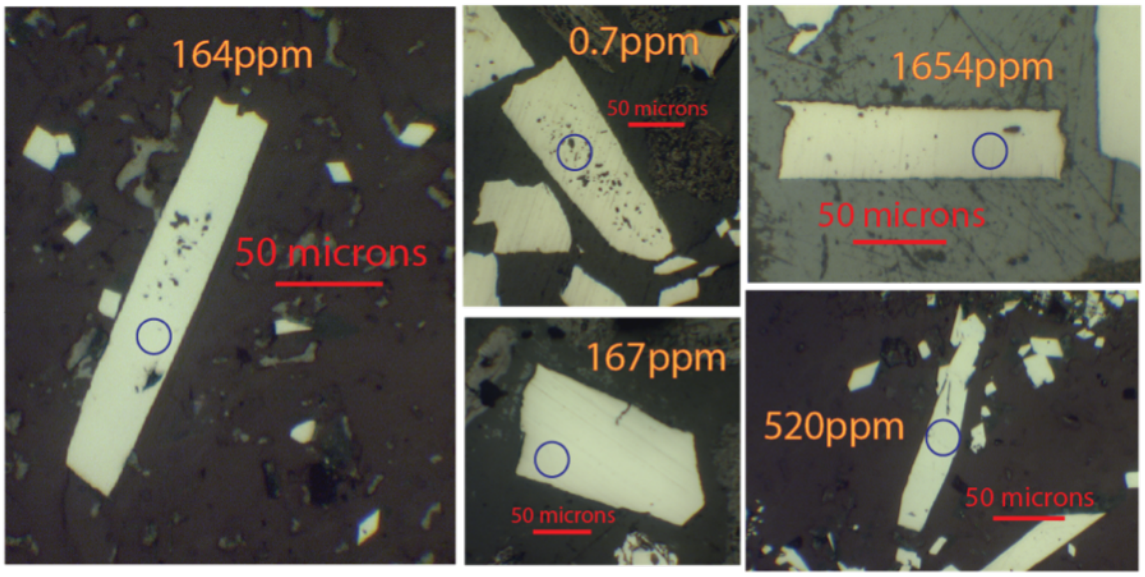

Figure 5.15 Reflected light images of B-type arsenopyrite crystals. SIMS targets for spot analysis for Au is shown with a blue circle with results shown in orange. Crystals are commonly elongate but range in aspect ratio. Inclusions and fractures are common but vary in abundance. These are commonly, but not exclusively, found in the centre of the crystal.

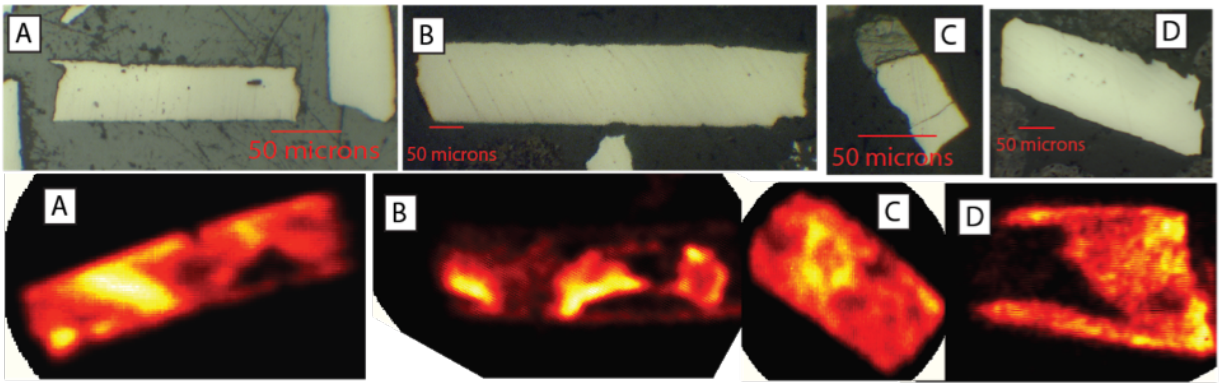

Figure 5.16 SIMS images of Au distribution in B-type arsenopyrite crystals. Photomicrographs at top show scale and crystal habit with SIMS images at the bottom. All images show a blotchy heterogeneous distribution of Au throughout the crystal. In image D, the barren Au core is matches an Sb high.

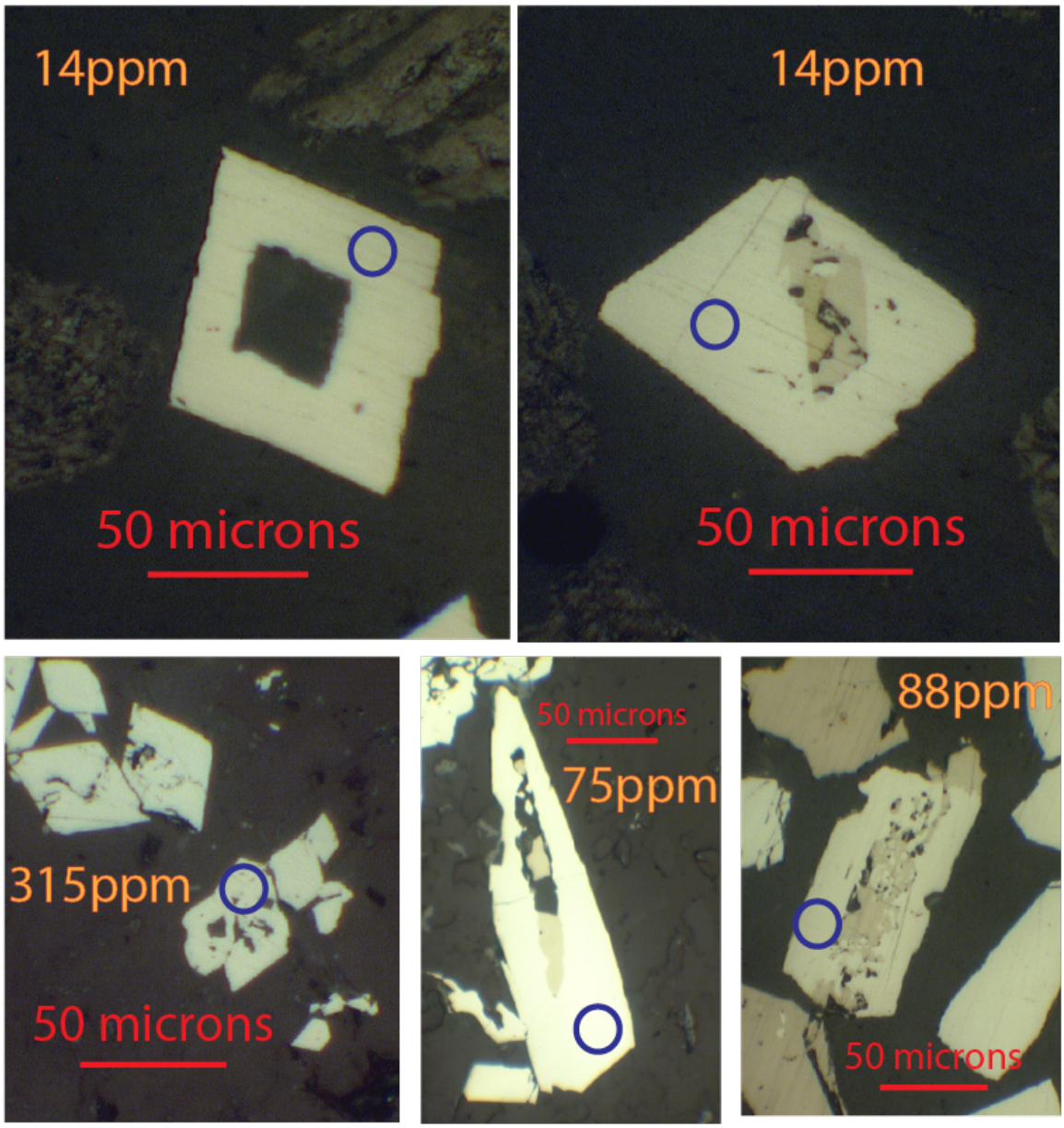

Figure 5.17 Reflected light images of C-type arsenopyrite crystals. SIMS targets for spot analysis for Au is shown with a blue circle with results shown in orange. Inclusions and fractures are common with both host rock matrix and pyrite infilling inclusions. Crystal boundaries are commonly ragged and corroded. Crystal morphology ranges from rhombic to elongate with no common aspect ratio.

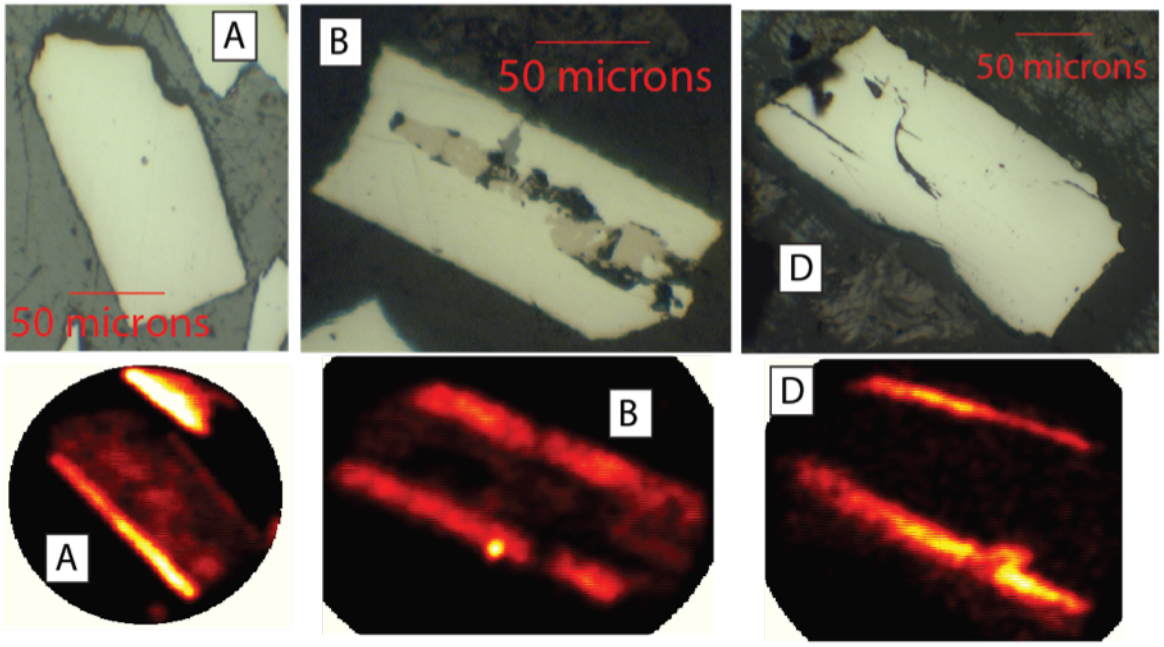

Figure 5.18 SIMS images of Au distribution in C-type arsenopyrite crystals. Photomicrographs at top show scale and crystal habit with SIMS images at the bottom. Au has a bladed distribution that are parallel to the C-axis and close to the crystal rims.

5.3.5.1 A-Type

This distribution can be seen with LA-ICP-MS with transects across A-type crystals. The two Au distributions (type-Ai with more homogenous distribution and type-Aii with Au rich rims) can be seen clearly. Whilst there is no apparent physical difference that distinguishes these two types of A-type arsenopyrite, there are subtle chemical changes and these have an apparent relationship with gold enrichment and distribution. In figure 5.19 (a type-Ai arsenopyrite), the core is Au rich with a slight decrease of Au towards the rim. This is also seen in figure 5.20 transect 1 (red section) and transect 2 (blue section). Element distribution seems to be similar across the whole crystal indicated by similar profiles in both transects in figure 5.20. In figure 5.20 (transect 1 blue and green sections and transect 2 red sections) Au is enriched in arsenopyrite rims in type-Aii arsenopyrite. Here, the magnitude in difference between the core and rim is much greater and the cores are frequently barren. The greatest gold counts are consistently found in the rims of the

rim rich arsenopyrite (figure 5.20 transect 1 (green section) and transect 2 (red section) are good examples of this). However, Au over the whole crystal (the area underneath the gold curve) is greater in the core rich arsenopyrite as peaks are significantly wider and there is a larger volume of gold mineralisation.

The Au relationship with other elements can also be identified. For the type-Ai arsenopyrite, there is a strong correlation with As and Sb and a weak correlation with Pb (figure 5.19, figure 5.20 transect 1 red). Peaks and troughs occur simultaneously with high As in the core being an especially good proxy for Au.

In type-Aii arsenopyrite the Au peaks occur near the edge of the crystal as As is lower. None of the other elements analysed mimic this relationship. Relative to type-Ai arsenopyrite, there is more enriched Sb and As (figure 5.20 transect 1 blue and green, transect 2). The As counts in the rim rich arsenopyrite crystals are significantly higher than the core rich arsenopyrite with lower Au. The Au peaks are high and thin and are therefore thought to be micro nuggets that are not in the arsenopyrite structure.

5.3.5.1 B-Type

LA-ICP-MS of B-type crystals (figures 5.21 and 5.22) also show a heterogeneous and generally lower distribution of Au. There is a strong positive correlation of Au with As there is a very similar profile with peaks and troughs occurring simultaneously. Sb, Ni and Co have variable concentrations that appear to more enriched than A-type crystals. Although there is not a consistent correlation between these elements and Au over the whole crystal, the highest concentrations of Au occur at these peaks. EMP maps in figure 5.21 show identify small Ni and Sb highs in the crystal that occur in similar areas to the Au highs in figure 5.15A.

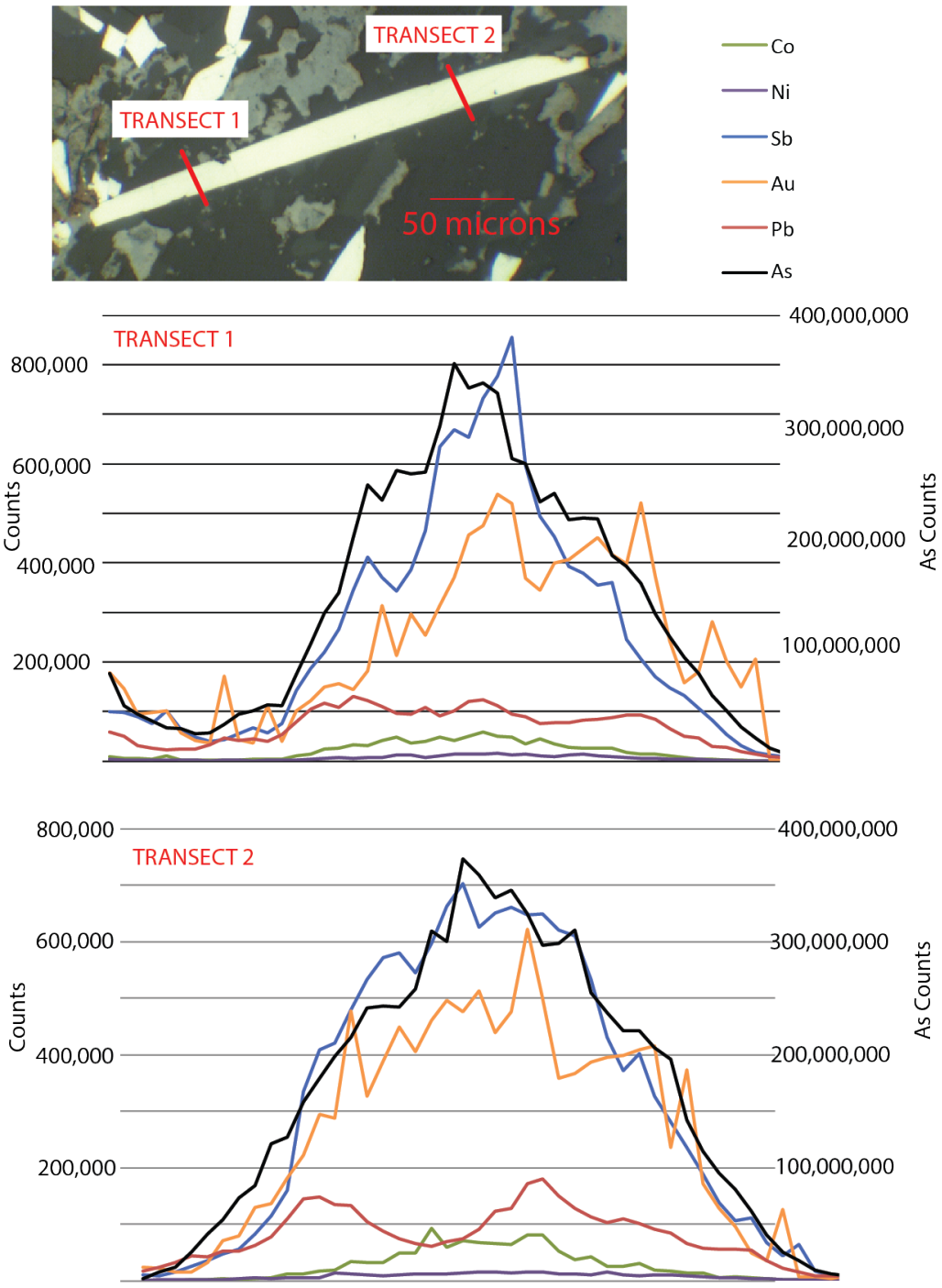

Figure 5.19 LA-ICP-MS showing two transects across an A-type crystal. As is on the Y axis to the right whereas other elements are shown on the left Y axis. The crystal was previously analysed by SIMS spot analysis (figure 5.3 bottom left image). Au is fairly homogenous in both transects and Sb is relatively high compared to Au.

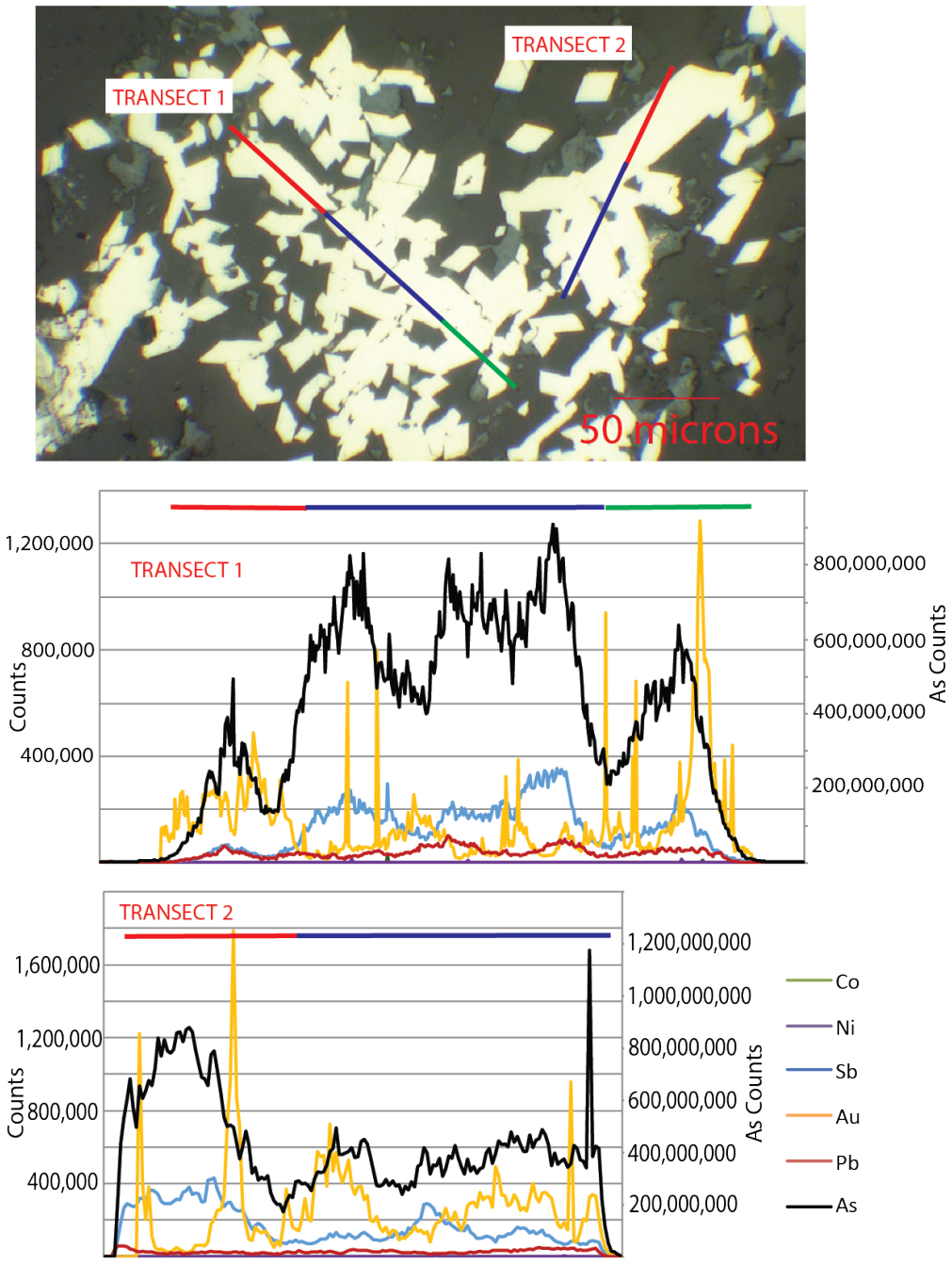

Figure 5.20 LA-ICP-MS showing two transects across A-type arsenopyrite crystals. In transect 1 three distinct sections are broken out: The red section has a Au rich core and the blue and green sections have similar enrichment in the core but significant Au enrichment in the rims. In transect 2 two distinct sections are broken out. The red section has Au enrichment in the rims while the blue section has Au enrichment in the core.

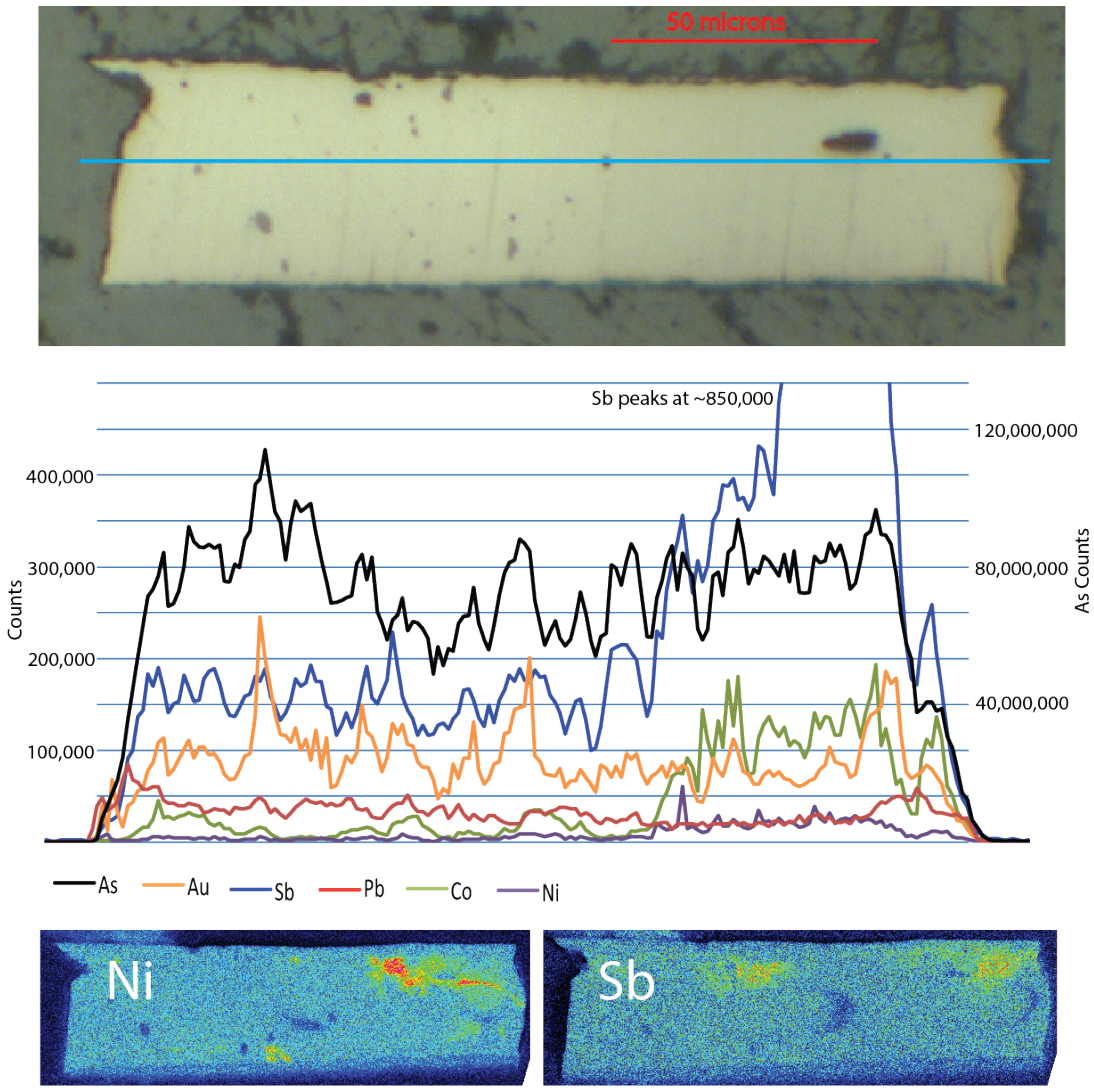

Figure 5.21 LA-ICP-MS transect (from left to right) of a B-type arsenopyrite crystal with X-ray maps from EMP analysis of the same crystal for Ni and Sb. Blue line in the top image represents the transect. Au correlates well with As peaks and locally correlates with Sb and Ni.

5.3.5.1 C-type

The bladed distribution of Au is clear in LA-ICP-MS transects of the arsenopyrite crystal (figure 5.23). Au peaks occur at different magnitudes in two peaks across each transect. The crystal is barren otherwise. Au enrichment is inconsistent with varying peak heights in terms of counts. Correlations with other elements are also not as consistent. At each Au peak there is an As peak however all As peaks are not associated with Au. Au

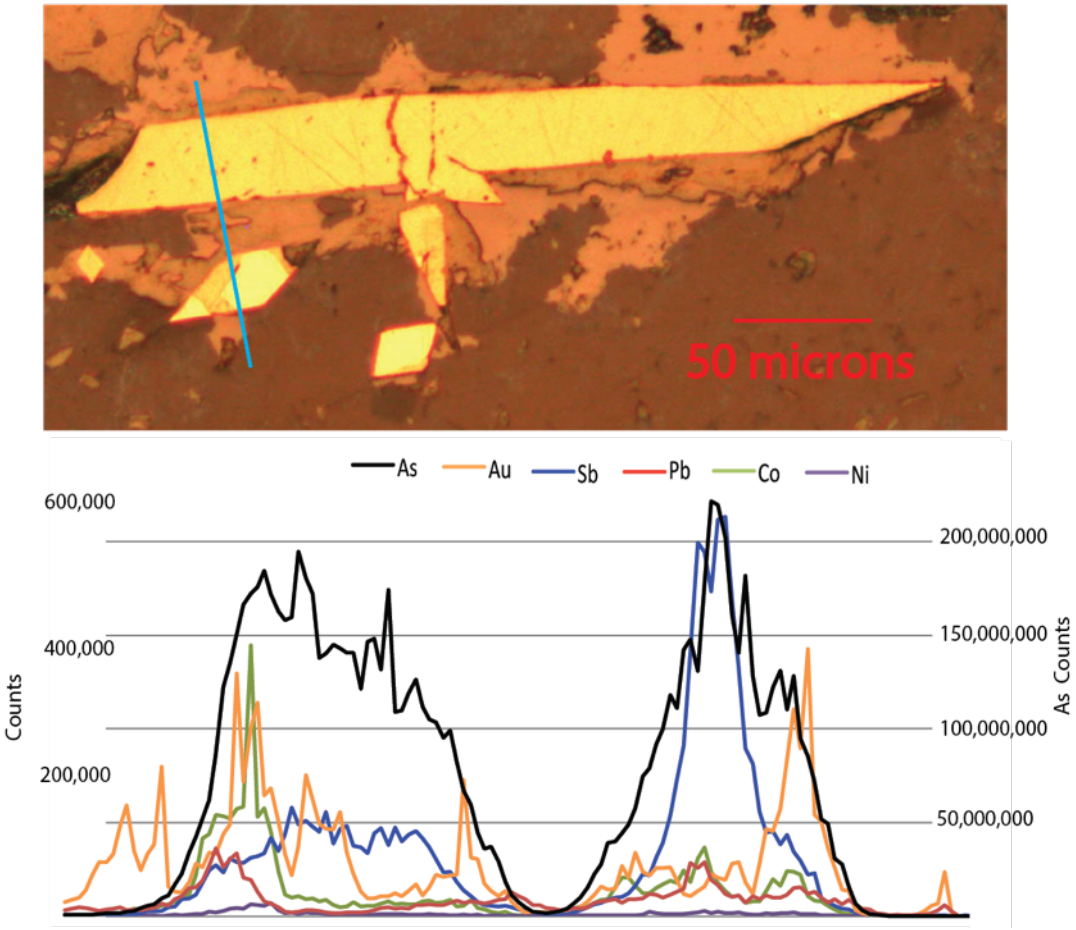

Figure 5.22 LA-ICP-MS showing a different B-type crystal. Blue line shows transect across the crystal and direction of transect is from top to bottom. The first crystal has similar element distribution and correlations as described in figure 5.10. Gold correlates well with As peaks and locally but not consistently with Sb and Ni. The second crystal may be an A-type crystal (no inclusions or fractures, high Sb and gold rich rims).

variation with other elements is not consistent. In transect 1, the Au peak occurs with a Pb peak. In transect 2 the Au peak occurs with a Pb and Sb peak. In transect 3 the Au peak occurs with an Sb peak which has a greater abundance across the whole crystal compared with the previous two transects. The crystal clearly has a heterogeneous geochemistry and it is not possible to correlate chemical changes across it.

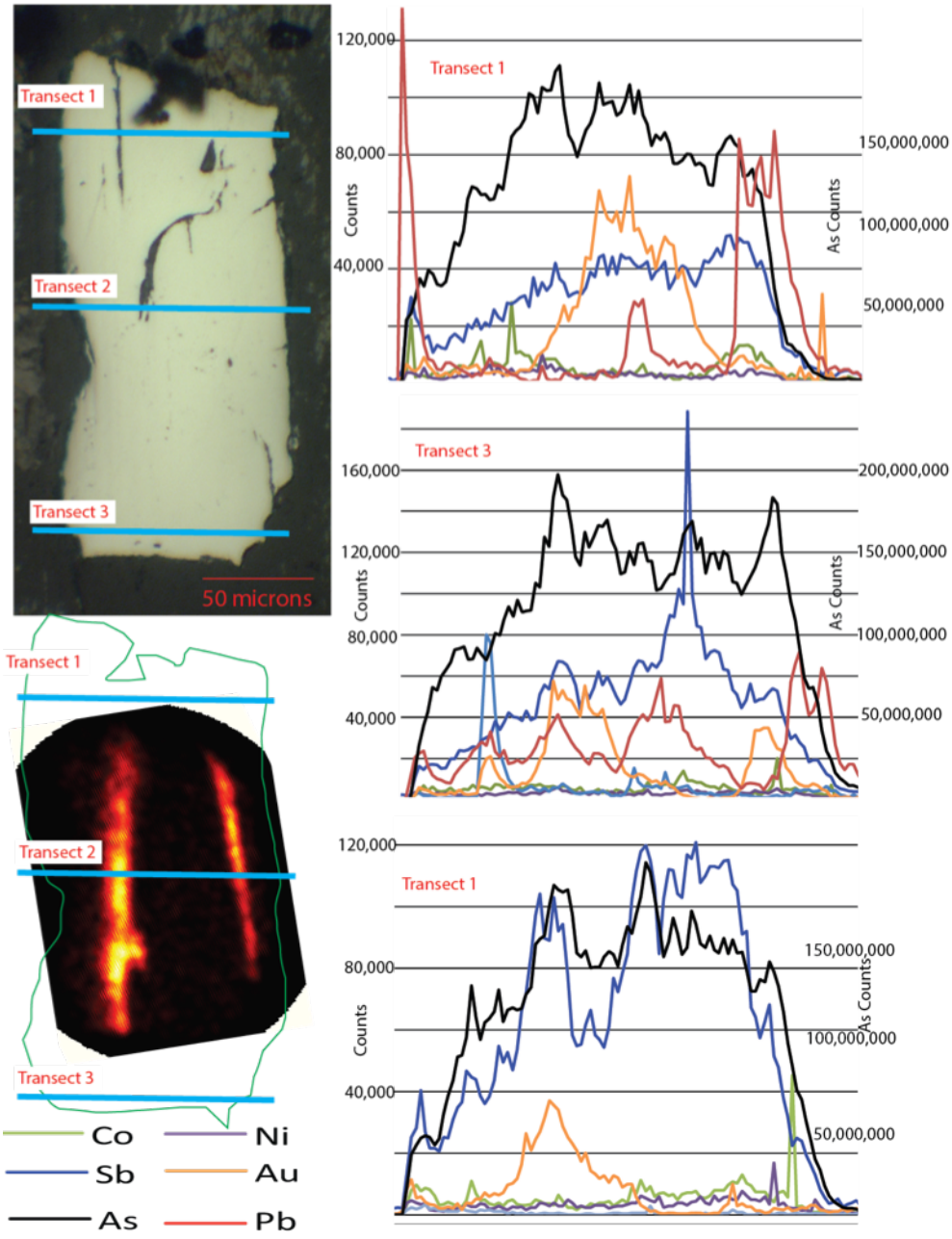

Figure 5.23 LA-ICP-MS of a C-type arsenopyrite crystal. Shows a reflected light image, SIMS map (with crystal outlined in green) for Au and three LA transects (from left to right) across the crystal. The blades shown in the SIMS image are visible as high concentrations in the transects. These seem to correlate with As peaks, a Sb peak in transect 2 and 3 and a Pb peak in transect 1.

5.3.6 Pyrite and Chalcopyrite

Pyrite and chalcopyrite are present in all domains. Up to 5% pyrite occurs at FAT whilst chalcopyrite is rare (mostly only observed in thin section) and is always in textural equilibrium with pyrite. Pyrite rarely occurs with A-type arsenopyrite, and commonly with B-type and with C-type arsenopyrite. It is therefore most commonly found in environments where arsenopyrite has inclusions and defines a foliation. Pyrite is always anhedral and generally is found in lineations parallel to foliation. Probe analysis has shown an absence of As and Au in the pyrite.

Pyrite is commonly on its own however when observed with arsenopyrite it is commonly surrounding arsenopyrite (figure 5.24) and as inclusions within C-type arsenopyrite (figure 5.24 C, D). Chalcopyrite when found in thin section is in equilibrium with the pyrite as it shares a crystal boundary (figure 5.24A).

Whilst pyrite commonly shares a crystal boundary and therefore occurs in equilibrium with arsenopyrite, the abundance of pyrite does not seem to have a good correlation with Au. Pyrite commonly occurs in areas with no Au mineralisation and there are multiple areas with an absence of pyrite and good mineralisation (generally where A-type arsenopyrite is present).

5.4 Geochemical Trends

Due to the heterogeneity and geochemical variability within individual crystal types it is difficult to use point data to construct geochemical trends. It has therefore not been possible to use spot analysis to define A-type, B-type and C-type arsenopyrite chemically. They have more definable ∂S^{34} signatures that are outlined in Chapter 7. Enrichment of As and Sb relative to Au can be quantified by WDS analysis with an EMP. As explained in section 5.3.5, correlations with Au, Sb and As are observed (although not always consistently) in all crystal types and across crystal transects.

Figure 5.25 illustrates the Au distribution defined by the SIMS analysis. Many of the points had low Au enrichment however A-type arsenopyrite is noticed to have the highest Au concentrations. This figure shows that B and C type are more skewed towards lower

Au concentrations. For As, A-type has the most consistent distribution. B-type and C-type have a similar distribution but lower As values are also present.

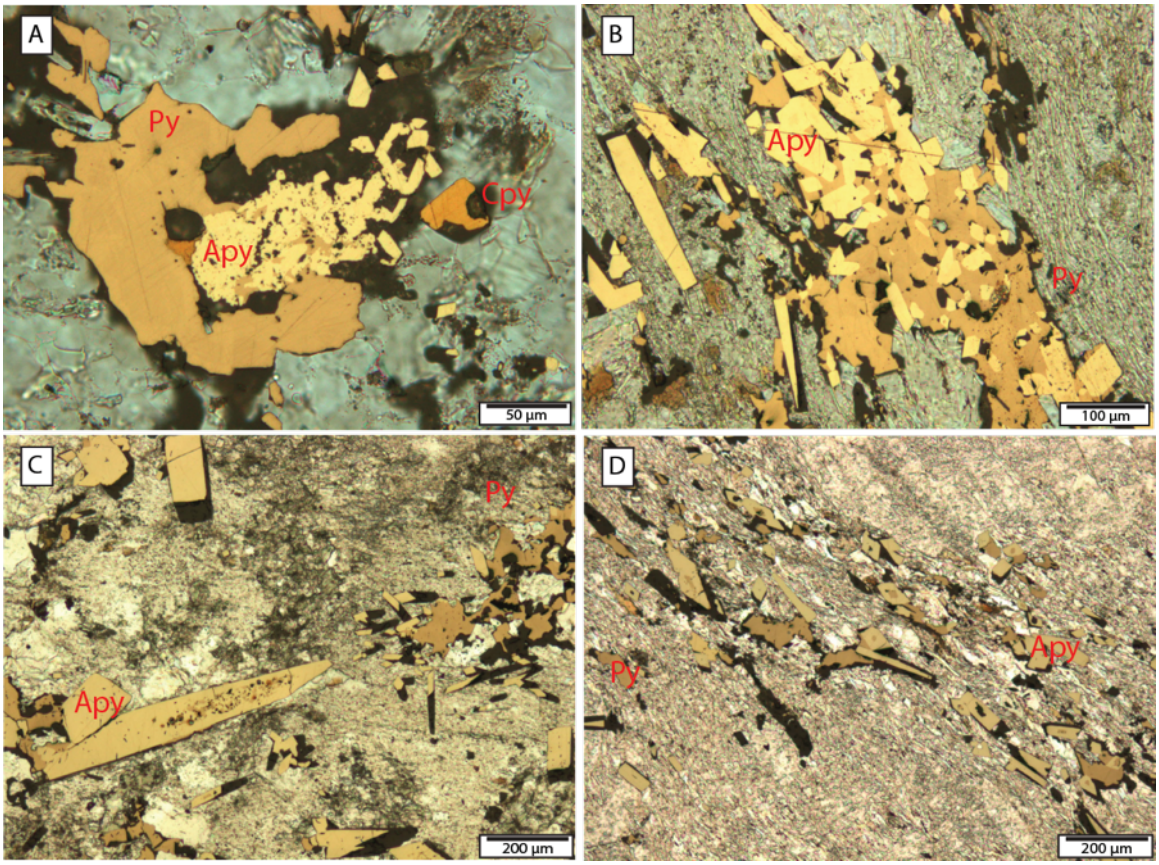

Figure 5.24 Partial reflected and plane polarised light photomicrographs of pyrite. A: Pyrite and chalcopyrite overprint on C-type arsenopyrite inclusions. B: Pyrite surrounding A-type and B-type arsenopyrite. C: Pyrite overprint on arsenopyrite and as inclusions within arsenopyrite in elongate crystal. D: Typical relationship with C-type arsenopyrite. It is aligned parallel to foliation and overprints and forms the inclusions within the arsenopyrite.

The complex and variable trace element geochemistry demonstrated for each crystal type makes spot analysis challenging. It is not known whether the spot occurred in a high or low within each crystal without an EMP map. It has therefore not been possible to assign geochemical definitions to each crystal type however broad geochemical trends are recognised.

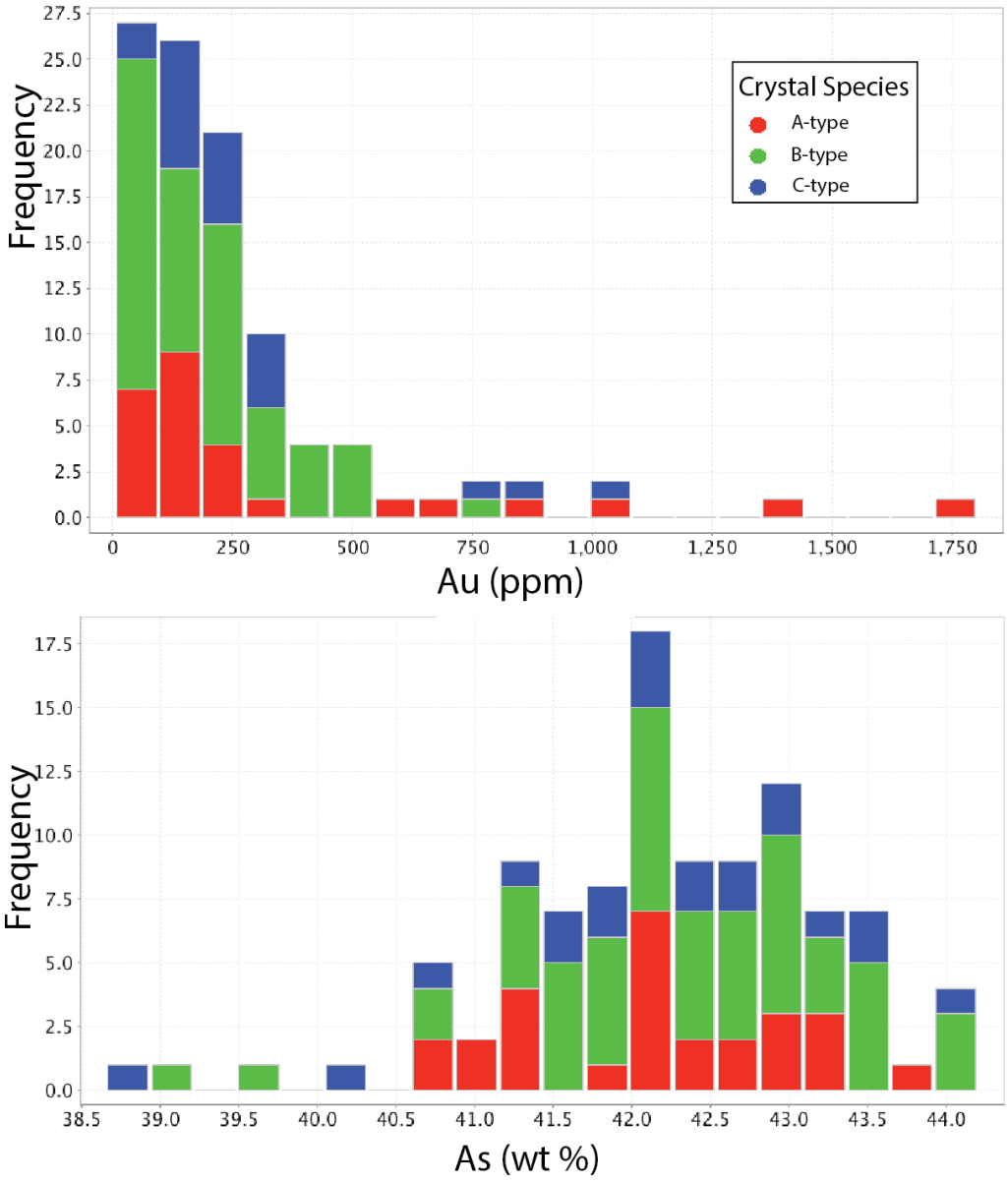

Figure 5.25 Histograms showing Au and As content as a function of arsenopyrite type. Au data is from SIMS spots. As data is from EMP analysis

Figures 5.26 and 5.27 shows how As vs S vs Fe co-vary. Enrichment in As is accompanied by a slight depletion of S and Fe. This is also where the highest concentrations of Au are found. In figure 5.26, there is a high Au anomaly to the left of the diagram. This is a C-type arsenopyrite and so is likely to be a Au-enriched blade of arsenopyrite. Sb shows the opposite relationship to this and it is most enriched in low As areas where Au is depleted (figure 5.27).

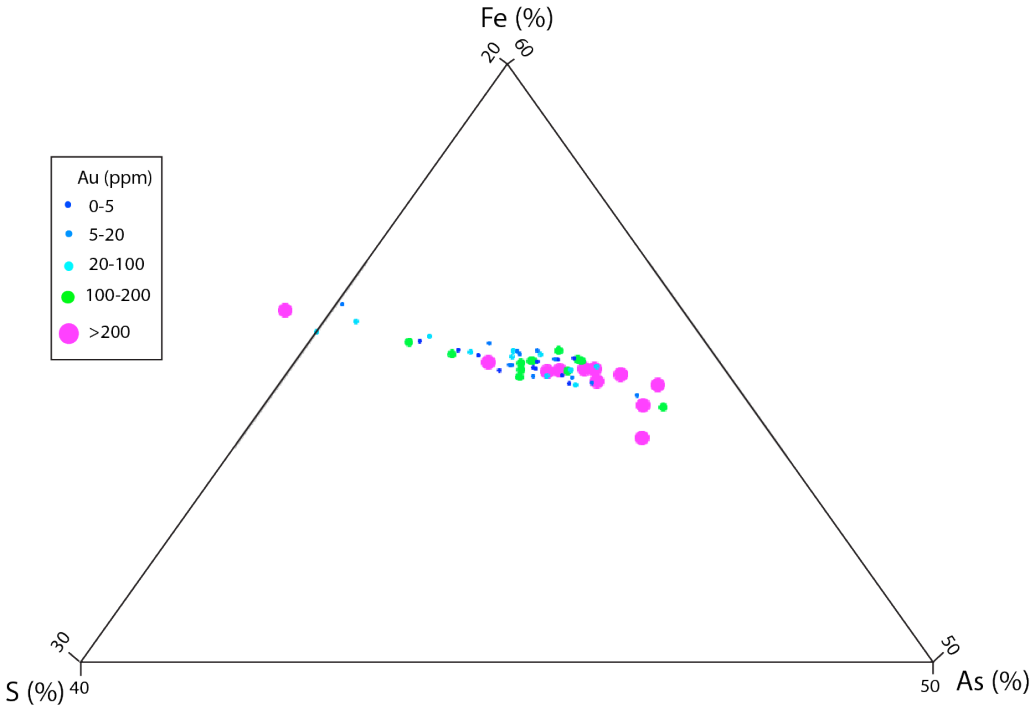

Figure 5.26 Ternary diagram showing wt% S vs Fe vs As vs Au from proximal SIMS spots. All spots conform to a single trend with an increase in As associated with a slight decrease in Fe and S. The high Au occurs where As is enriched and occurs in a fairly tight distribution. The anomalous Au high to the left of the diagram is a C-type arsenopyrite and is likely where the SIMS spot hit an enriched blade of Au.

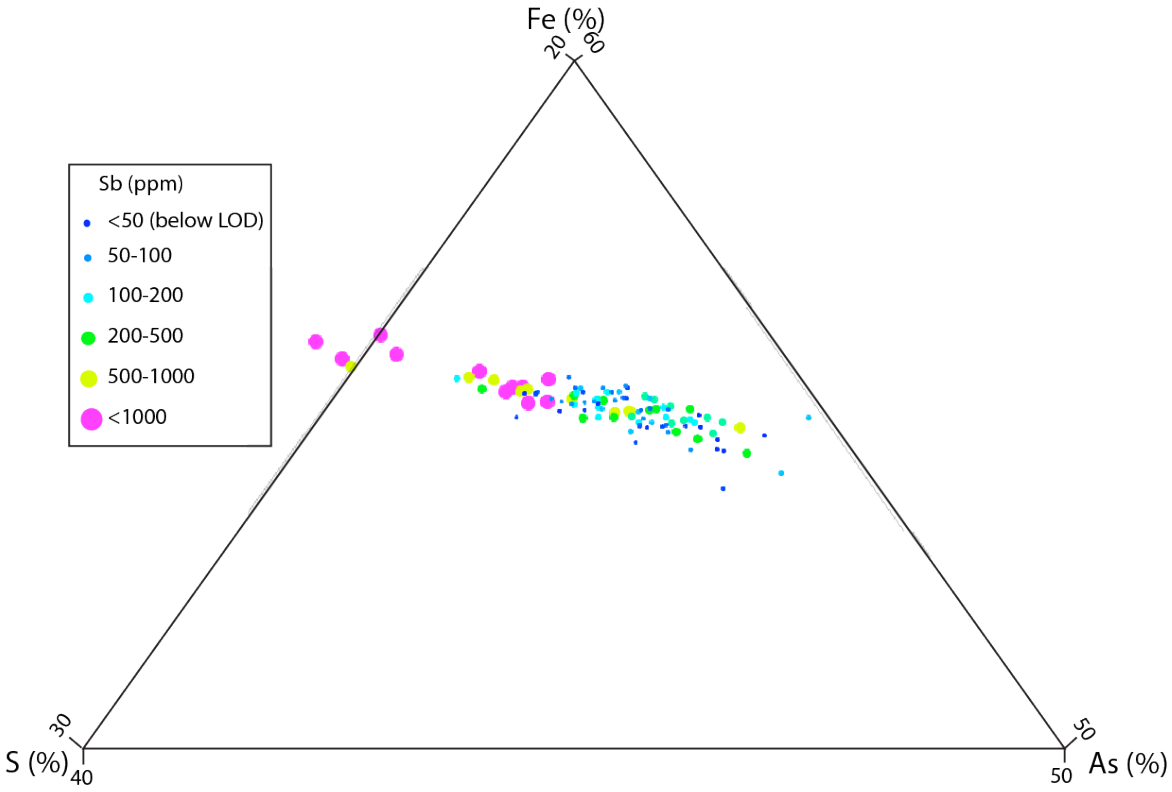

Figure 5.27 Ternary diagram showing wt% S vs Fe vs As vs Sb from EMP WDS spots. Sb is enriched in the low As areas.

Chapter 6

6 Alteration

Four types of alteration are recognised at FAT: sericite, silica, carbonate and biotite alteration (table 6.1). Differentiating between pre and syn metamorphic alteration is attempted however primary characteristics of pre-metamorphic alteration are typically challenging to identify. Mineralised intervals have a broad macro scale association with silica and sericite alteration and therefore are examined in more detail. Silica flooding of the matrix has a proximity to mineralised quartz veins. Sericite occurs in random orientation, associated with A type arsenopyrite in undeformed rocks, but sericite and biotite typically also define a foliation that is occurred during the M2 metamorphic event. Sericitic alteration locally shows a strong spatial association with mineralization, but this association is not consistent and the intensity of sericitic alteration throughout the deposit. Sericitised areas are commonly barren however for mineralisation to occur, sericite must be present. Arsenopyrite species defined in Chapter 5 can each be attributed to distinct events. Since A and B type arsenopyrite have the closest relationship with Au, understanding alteration footprints associated with these enrichment events (its chemical and spectral signatures) can be helpful in providing vectors towards Au mineralisation both within the FAT deposit and throughout the CLGB.

6.1 Silica Alteration

The quartz veins described in section 5.2 have associated silica alteration. The clearest manifestation of this silica alteration at FAT is bleached wall rock proximal to these veins (figure 6.1). Mineralisation is hosted by arsenopyrite is that are commonly at the margins of, or are proximal to these veins (as illustrated by arsenopyrite occurring on the edge of phase 1 veins in figure 5.9). Due to the felsic nature of the host rock, recognising silica alteration in thin section and in geochemical trends is difficult. Mineralised quartz veins have only been observed in drill core (rather than outcrop) at FAT.

Type	Style	Relationship with Au
Silica	• Two styles of quartz veins • Silica flooding of matrix proximal to quartz veins	Highly correlative to Au. Mineralisation is usually within centimetres of blue-grey quartz veins
Sericite	• Mostly muscovite in composition • Found throughout the deposit, intensity is variable on a m to 10's m scale • Commonly defines a foliation conformable to regional metamorphism	Present with Au but intensity does not correlate with grade
Carbonate	• Generally occurs higher in the stratigraphy floods the matrix confined to certain ore domains outside this study • Also found as late extensional calcite and ankerite veins that cross cut mineralisation and metamorphism.	No correlation although domain 8 is a distinct zone of carbonate alteration
Biotite	• Related to metamorphism (defining foliation) and occurs throughout the deposit and belt • Biotite seen frequently in drill core	Unrelated to gold mineralisation

Table 6.1 Summary of alteration styles seen at FAT and their relationship with Au

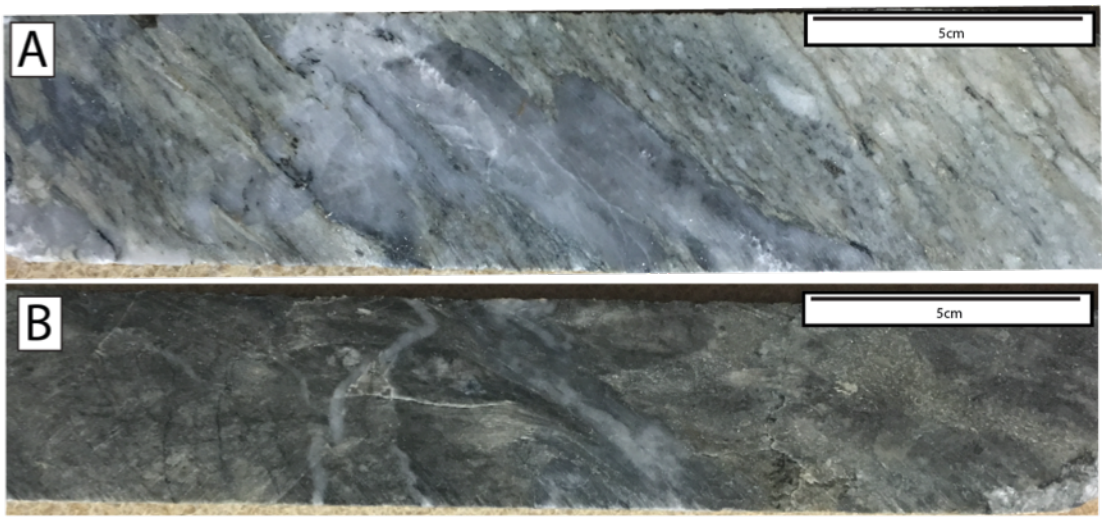

Figure 6.1 Silica flooding of host rock proximal to quartz veins. A: Thick phase 2 vein with bleached host rock beside vein. B: Phase 2 vein with bleached proximal host rock.

6.2 Sericite Alteration

Mineralisation occurred in conjunction with hydrothermal alteration that will have caused sericite to form. The earliest, A-type arsenopyrite mineralising event is responsible for the most consistent gold enrichment (Chapter 5) and so residual spectral and geochemical signatures of this event are examined. Greenschist metamorphism will have recrystalised sericite; if Au endowment is pre metamorphism, recognising and differentiating between two sericite generations is crucial. Broad alteration patterns are assessed through a range in scales. The term ‘sericite’ has been used as a logging term but is here identified as most commonly muscovite with rare phengite.

6.2.1 Cross Section Geochemical Trends

Figure 6.2 shows a ternary diagram showing whole rock Mg-K-Al from Seabridge Gold’s assay database change with respect to Au enrichment. Since the major element composition of the host rock does not change significantly with stratigraphy though the deposit (Chapter 4), these changes reflect a change in mica (and possibly carbonate) composition from to Al-rich muscovite ($KAl_2(AlSi_3O_{10})(F,OH)_2$) to Mg-rich phengite ($K(AlMg)_2((SiAl)_4O_{10})(OH)_2$). Analysis of the mica species is addressed in section 6.2.3.

Au increases along this trend; then highest Au values are generally found with greater than 50% Mg on figure 6.2. Where Al increases relative to Mg, the less enriched samples are found and there is less of a correlation with Au. Since this data is taken from over the whole section where most samples are unmineralised, it clearly reflects a broad change in composition from barren to enriched however does not have the resolution to indicate any correlation in the Mg-Al ratio in samples with over 1 g/t Au.

The decrease of K values with an increase in Mg and Au is curious. It could reflect carbonate alteration, however carbonate concentrations are low (<1% modal) and Ca does not vary with and Au. The K-Mg variation could be related to sericite/phengite alteration, however, further lithium metaborate fusion digestion whole rock analyses are needed to resolve this problem.

Reassessing the data on a more discreet scale by removing samples below 0.2 g/t Au (figure 6.3) shows the same overall trend. Samples on figure 6.3 with over 30% Mg has the highest Au values whereas below 30% Mg (and higher Al) have no apparent correlation with Au. Samples with Au enrichment of between 0.5 and 1.5 g/t occur over a broad range of Mg-Al ranges and do not have a clear relationship. This would indicate that whilst on a wide spatial scale, this ratio may reflect areas where Au mineralisation may occur this trend is not strongly retained within mineralised areas.

In order to assess how the trends identified in figures 6.2 and 6.3 correspond to mineralisation these can be assessed spatially over the studied cross section (figure 6.4). Considering the scale of the deposit, broad Mg highs and Al lows can be seen proximal to the Au grade shell. These clearly have a wider footprint than the Au or As shells and so can help indicate the locations of the correct sericite species may serve as a vector for mineralisation.

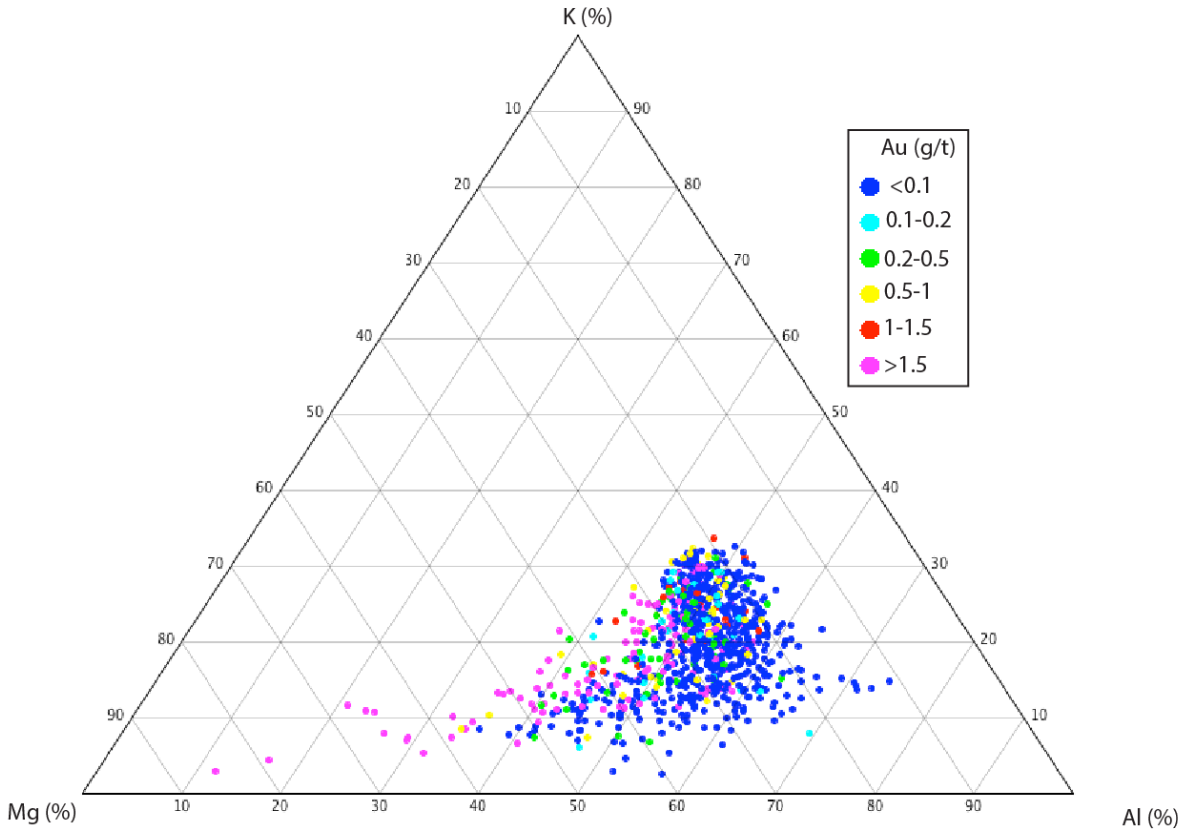

Figure 6.2 Whole rock Mg-K-Al molar cation % ternary diagram also showing Au concentrations. Au is more enriched in areas with higher Mg and lower Al. From Seabridge Gold's database of aqua regia whole rock digestion followed by ICP analysis. The samples are all from section 4800N and there are 3534 data points.

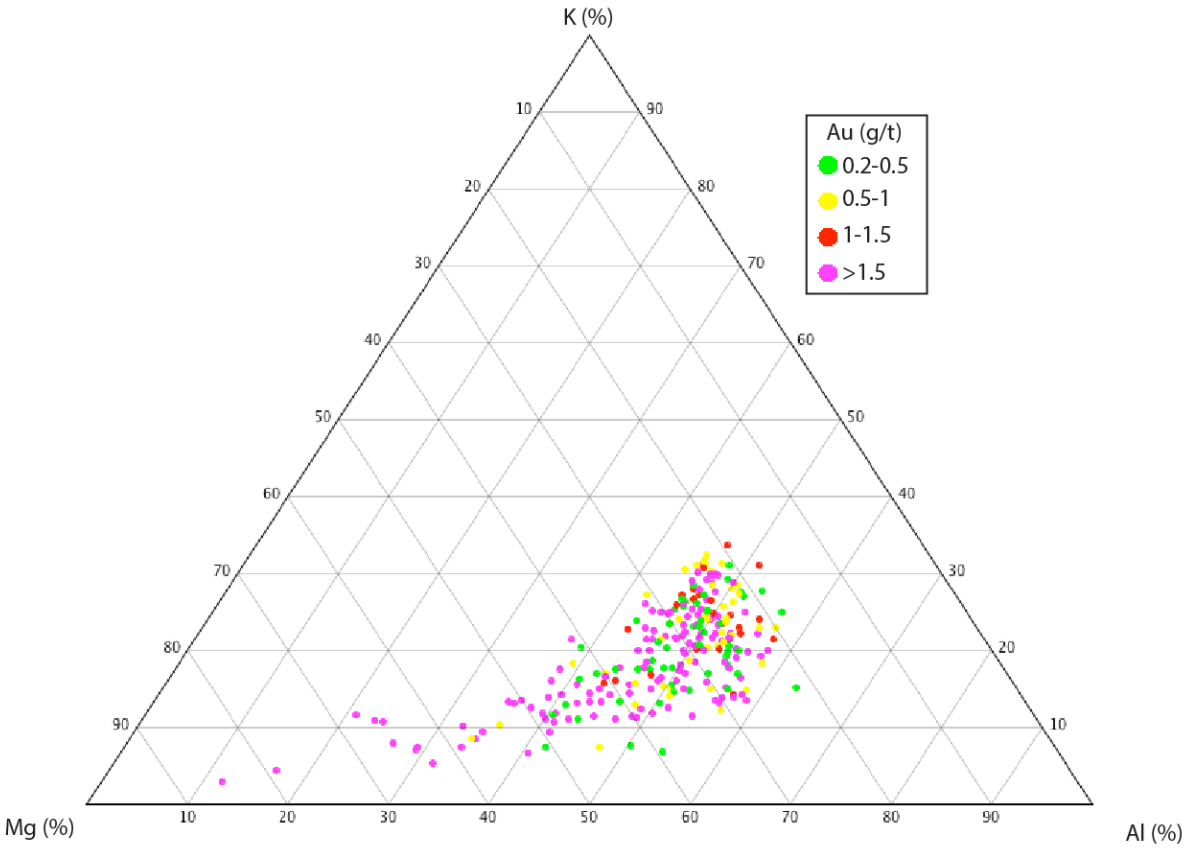

Figure 6.3 Whole rock Mg-K-Al molar cation % ternary diagram also showing Au concentrations. Similar to figure 6.2 but only showing samples with over 0.2 g/t Au (797 data points). The most Au enriched samples still occur with high Mg-Al ratio and the least enriched with low Mg-Al ratio.

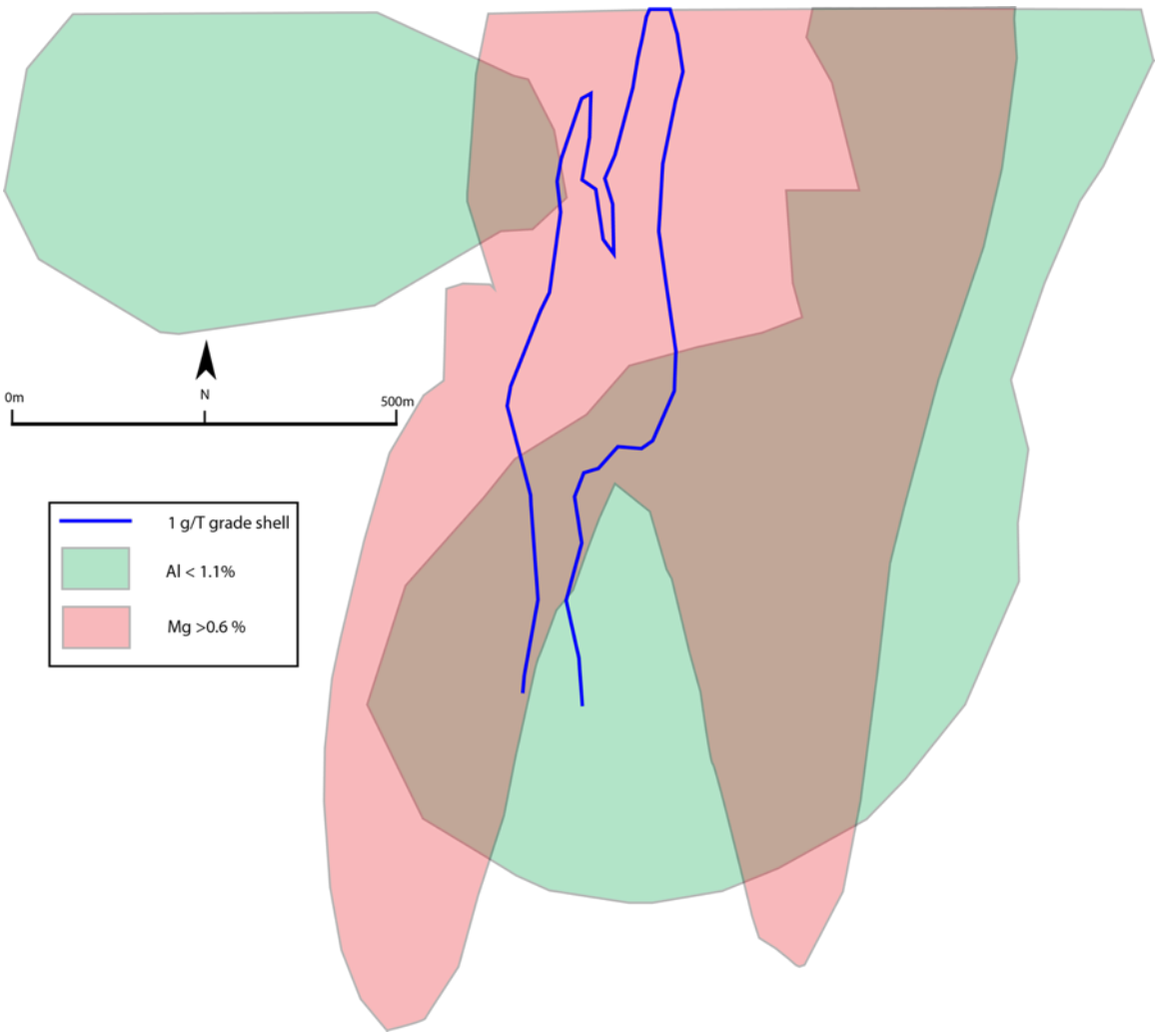

Figure 6.4 Spatial relationships between Al, Mg and Au. The blue line represents the 1 g/t grade shell outlined in Chapter 5. Overlain are leapfrog interpolations showing a broad Mg high and Al low in proximity to the 1 g/T grade shell.

6.2.2 Hyperspectral Signature

The changes in the whole rock Mg-Al ratio may be recognisable by hyperspectral signatures. As described by Yang et al. (2011), the composition of mica can be identified by the Al-OH peak occurring at the 2210 nm wavelength. This is a function of the substitution of octahedral Al cations for tetrahedral cations (Mg or Fe). This can be translated into composition (Duke, 1994). Where the Al-OH peak is below 2210 nm, muscovite crystal structures are present. If the Al-OH peak exceeds 2210 nm, then phengite crystal structures are present.

Figure 6.5A and B shows that (with one exception) there are no points where the Al-OH peak occurs above the 2210 nm wavelength and therefore each of the samples have a muscovite composition when assessed by hyper spectral composition. This suggests that while geochemical composition varies with Mg-Al ratio increasing with grade (thought to indicate a change in mica composition) the composition does not change significantly and the mica species is dominantly muscovite. There does not appear to be a correlation of wavelength and geochemical composition in terms of Mg, Al or Au. The Al-OH peaks occur over a wide range of wavelengths. This variation may be caused by contamination of a mostly muscovitic composition with small quantities of phengite causing small increases and hence variation in wavelength. Since the Terraspec sampling window is 1cm in diameter it is not possible to sample crystals individually. Samples from within the mineralised area were only analysed so the cross section scale trend indicated by figure 6.4 could not be assessed.

As demonstrated in section 6.2.3, probe analysis of the mica yields low Mg and high Al values from WDS analysis of mica. This would indicate that the mica is muscovitic in composition with slight variations in Mg but not enough to cause a compositional variation that can be identified by hyperspectral analysis.

6.2.3 Sericite Habit and Composition

The geochemical trends identified in section 6.2.2 can attributed to mica identified in thin sections. White mica is common but not ubiquitous on a hand sample and thin section scale. Intensity and abundance does not appear to be correlative across the cross section and fluctuates on a meter scale through drill holes. In hand samples, white mica forms a fabric that defines the foliation. In the heavily sericitised areas, the volcanic clasts are elongate (figure 6.6A) with lineations parallel to this elongation (figure 6.6B) are common. In thin section muscovite defines a foliation (figure 6.6 C, D). This foliation is commonly bent and locally wraps around clasts (figure 6.6D). This white mica fabric appears to be related to the main (D2) deformation event as it is not crenulated. As described in section 6.1, muscovite cross cuts and is parallel to the fold axial traces of phase 1 quartz veins and is parallel to phase 2 quartz veins.

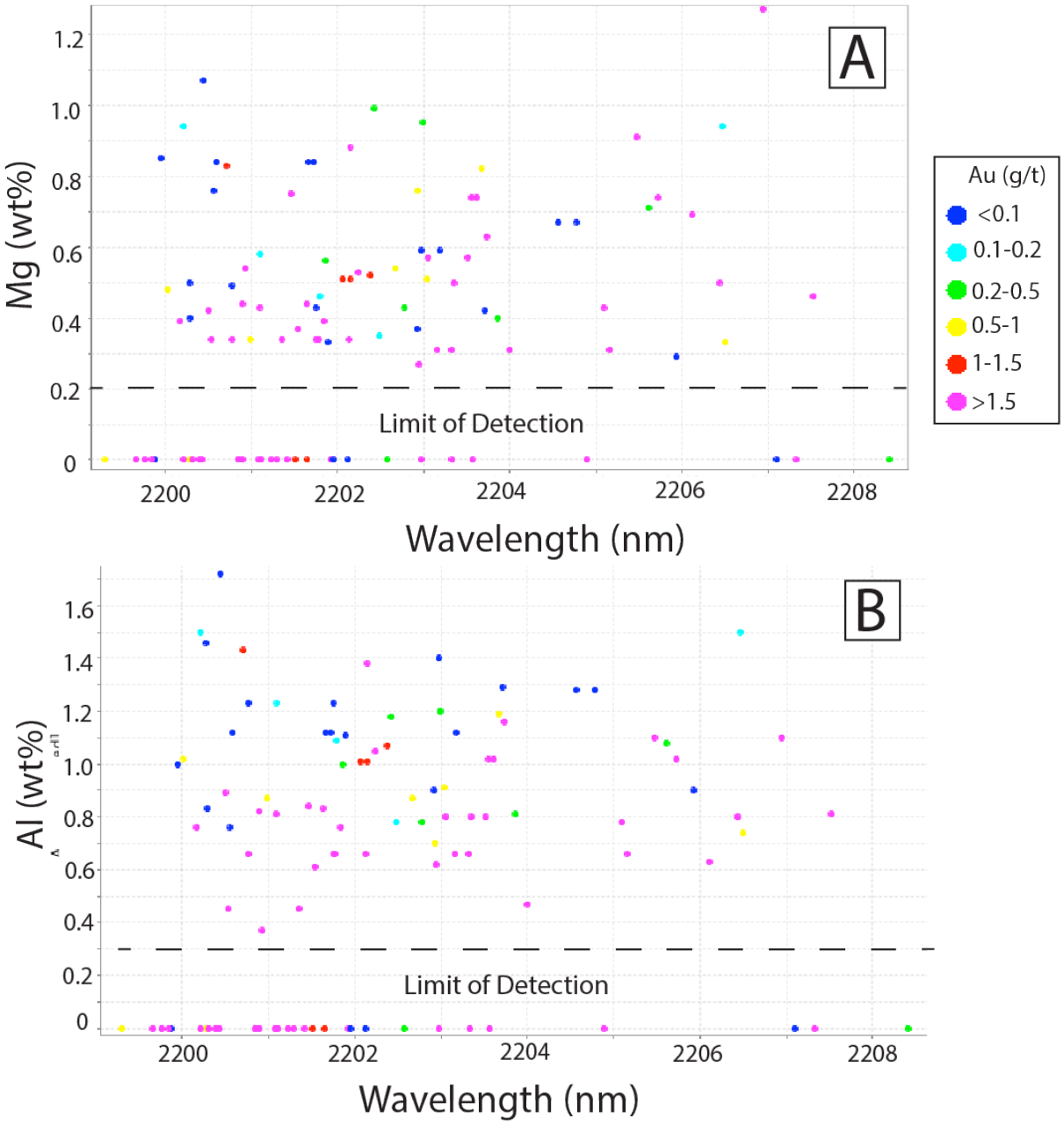

Figure 6.5 Al-OH hyperspectral peak with compared to assay data for Mg, Al and Au. A and B shows the 2210 nm peak vs Mg and Al respectively. There is only one sample exceeding the 2210 nm wavelength (indicative of phengite crystallinity) and therefore most samples have a muscovite crystal structure. Samples are all taken from within domains 3,4 and 5. There does not appear to be a relationship on this scale between Al-OH peak, Mg, Al and Au.

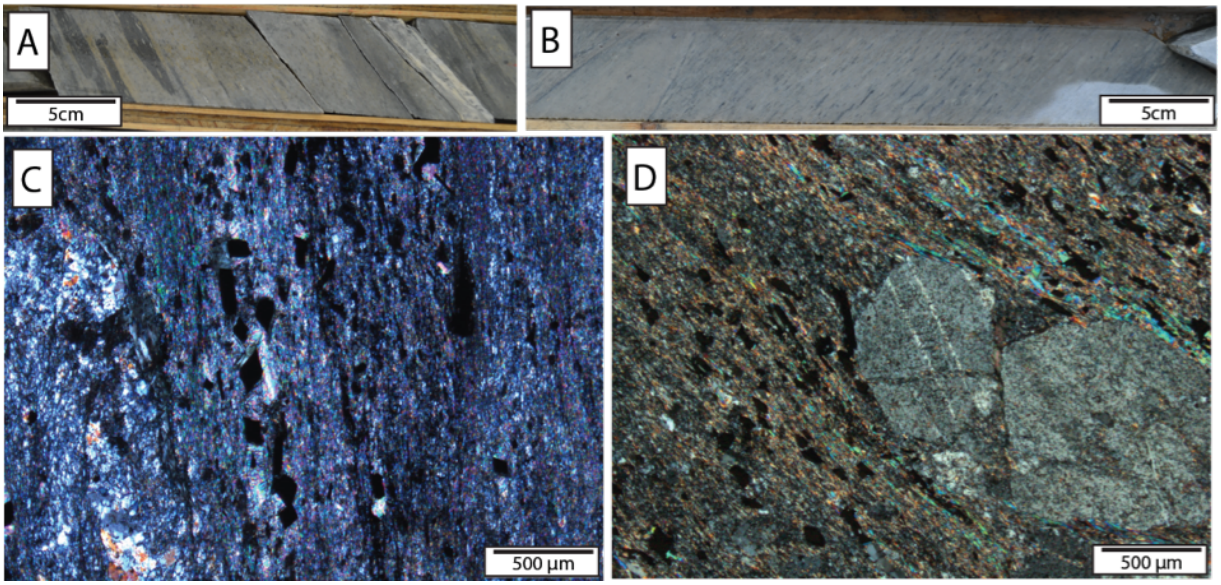

Figure 6.6 White mica in core samples and thin sections. A: Drill core showing elongate clasts. B: Lineations caused by sericite. C: Foliation fabric defined by white mica in thin section (XPL). D: Foliation fabric wrapping around a clast in thin section (XPL).

The composition of the mica was analysed by EDS analysis on a benchtop SEM. Six thin sections were analysed that had a variety of gold grades, from a range in locations across in the cross section and had a different degrees of mica abundance. As shown by figure 6.7 the same Mg-K-Al trend that was identified in figure 6.2 and 6.3 is still visible, however the correlation of this trend with Au is poor. Although not a perfect correlation, what remains consistent is that the most enriched samples have a higher Mg-Al ratio whereas the least enriched samples have lower Mg-Al ratios. Although the hyperspectral composition does not appear to have differed (section 6.2.2) this shows that the difference in the whole rock geochemistry trend appears to have been a function of mica composition change.

Further to this, the Mg-Al ratio was further investigated using WDS analysis on an electron microprobe (figure 6.8). This examined mica in a further eight thin sections that showed a variety of levels of mineralisation from a wider variety of locations. This included each of the three principally studied domains as well as unmineralised felsic tuff from Bulldog Lake along the CLGB.

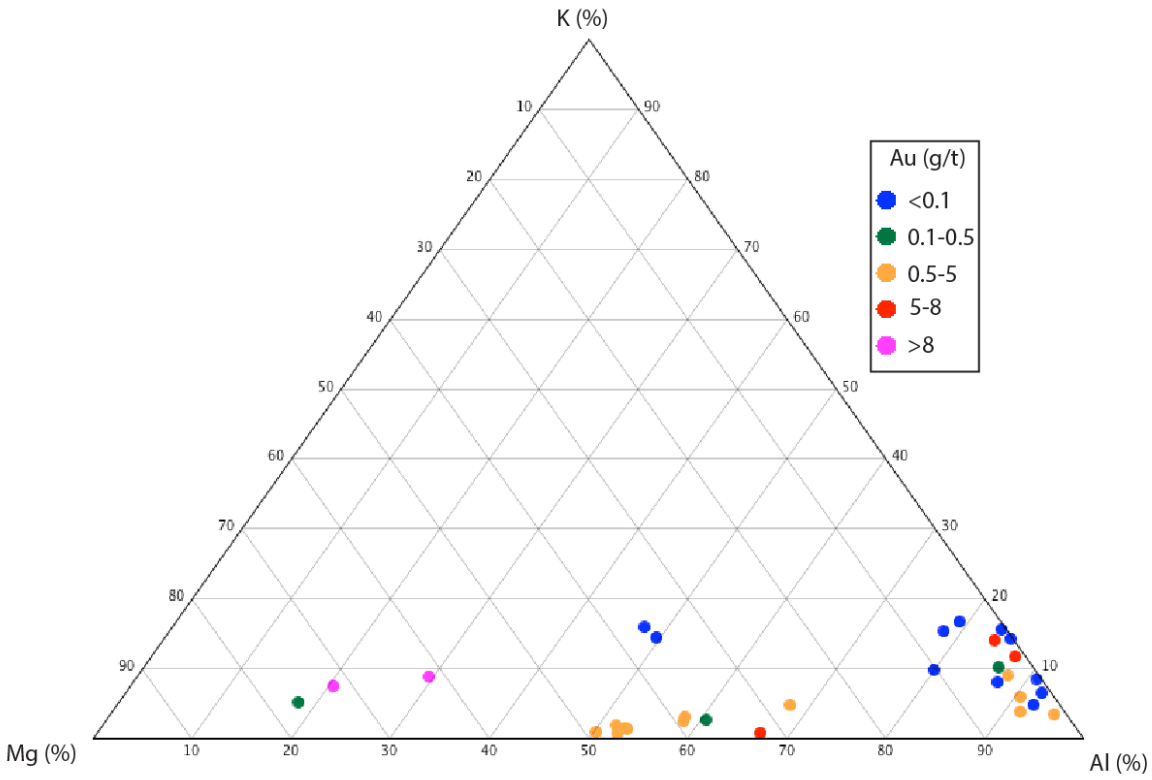

Figure 6.7 Spot analysis of mica in thin sections with a variety of Au grades and locations through the cross section. Mica had different levels of abundance in each thin section.

The Mg-Al ratio can be seen clearly but there is the inverse relationship with Au that was previously observed. The highest levels of Au occur where Al is enriched with respect to Mg. There would also appear to be strong spatial control on Mg-Al ratio. Higher Mg tends to occur in domain 3 and Bulldog Lake (which have less textural evidence of metamorphism). Domain 4 and 5 have a lower Mg but higher gold. In these thin sections strong foliation is observed and the mica is therefore thought to be metamorphic.

The correlation with Au may represent differing volumes of arsenopyrite in each thin section and the relationship with individual mica species is unclear. This could show that

although the Mg-Al ratio is inconsistent as a gold vector at this scale, the spatial control could be useful for belt-scale exploration target generation.

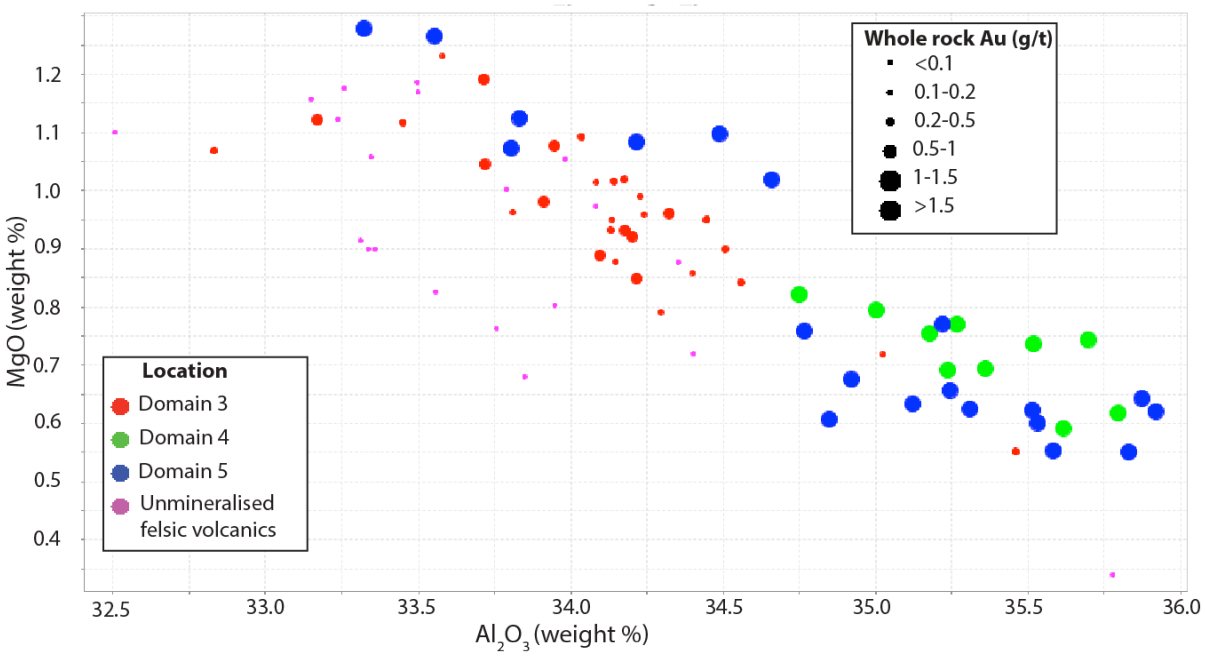

Figure 6.8 WDS EMP analysis of MgO vs Al2O3 in mica. Plotted against whole rock Au for 2m interval and location. Mg substitution correlates well with Al. Au here is correlated with higher Al. Higher Al areas are typical of domain 4 and 5 and higher Mg in domain 3 and Bulldog lake.

6.2.4 Relationship with Gold Enrichment

On a broad scale, the degree of foliation intensity (and therefore mica abundance) does not correlate with grade. The holes that were logged throughout the cross section were visually categorised for foliation with 0 representing an absence of foliation and 5 representing the best defined foliation observed. Figure 6.9 shows that both the most and least foliated areas are the most enriched in Au. There does not seem to be a correlation between Au grade and foliation intensity. Chapter 5 has addressed the relationship with arsenopyrite species and Au on a thin section scale; there appears to be two phases of sericite that can be attributed to mineralisation events. A-type arsenopyrite is related to an early sericite (here defined as more Mg rich in composition) whereas B-type and C-type

arsenopyrite is related to the later foliation defining sericite (now identified as Al-rich muscovite).

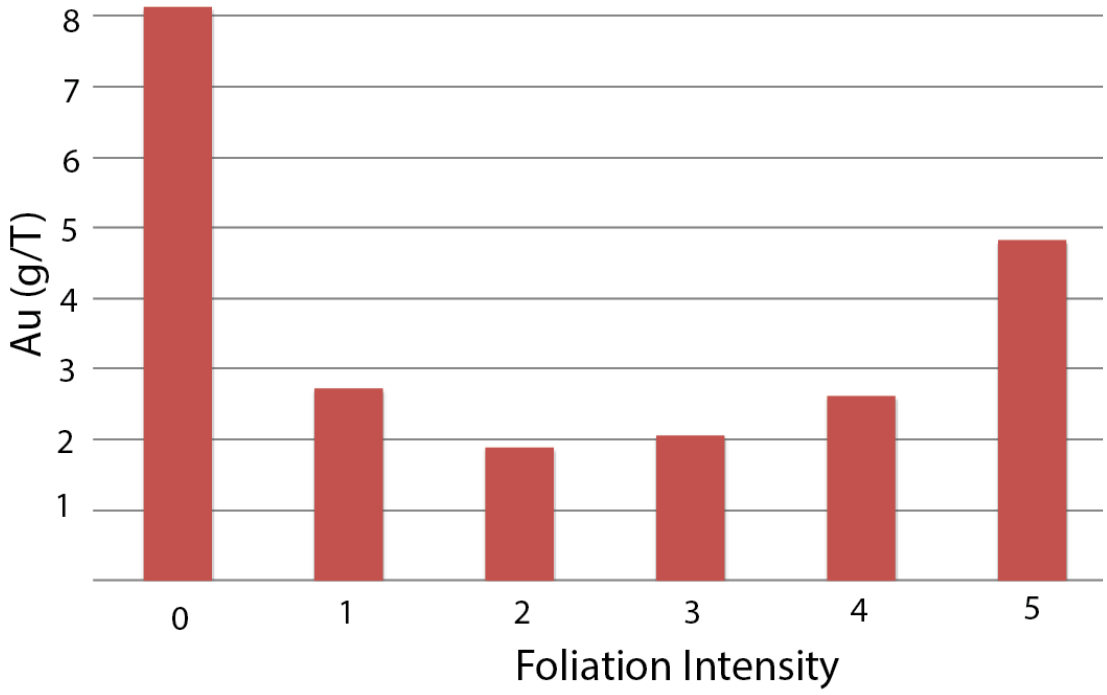

Figure 6.9 Visual degree of foliation versus Au grade throughout the cross section. The greatest levels of Au enrichment occur in the least and the most foliated areas. There does not seem to be a correlation with intensity and grade.

6.3 Composition of the Quartz Body

The quartz body described in Chapter 4 has unique alteration assemblage, not recognised elsewhere in the deposit. It has more complex mineralogy than quartz veins seen throughout the deposit (figure 6.10A). µXRD Peaks indicate a mineralogy that has a significant host rock component. This quartz is thought to be replacement of the host rock rather than a vein with XRD results and petrography indicating a simpler mineralogy with only quartz present as seen in the veins (figure 6.10B). Petrography addressed in Chapter 4 has recognised intercalation of host rock and replacement textures of this by the quartz body and is therefore interpreted to be a sinter.

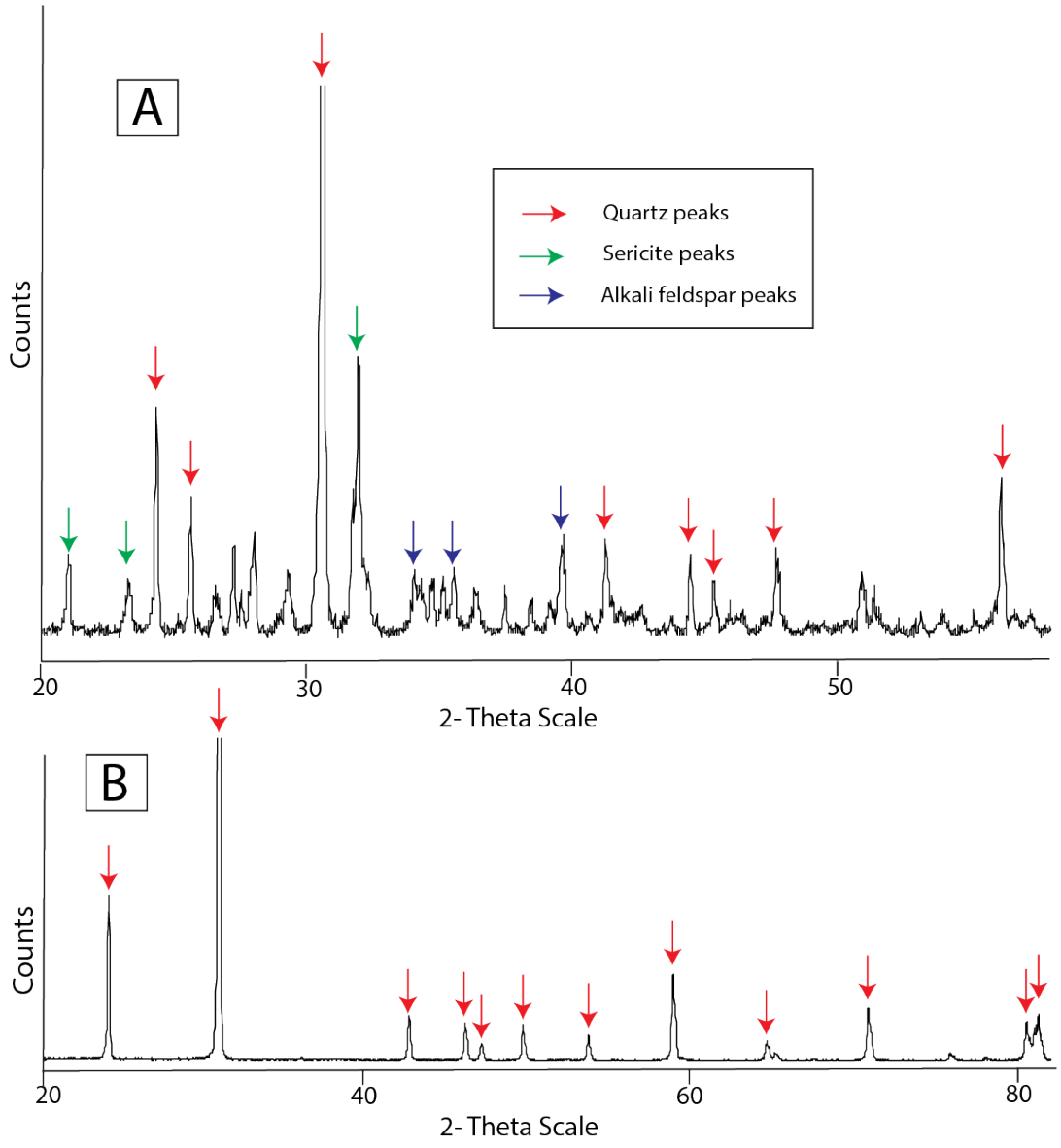

Figure 6.10 Powder XRD peaks from a sample of the quartz body (A) compared with a phase 2 quartz vein (B). In A, mineralogy is more complex than other quartz veins (B) in the deposit with alkali feldspar and sericite peaks.

A sulphate mineral was identified as having an arcanite-like (K_2SO_4) structure in figure 6.12 (hereafter referred to as 'arcanite'). It occurs within and proximal to the quartz body that is shown in figure 6.11, particularly on the margin of the quartz body (figure 6.11A). It also occurs as very fine crystalline and disseminated within the host rock (figure 6.11B). Here it is on the margins of A-type arsenopyrite.

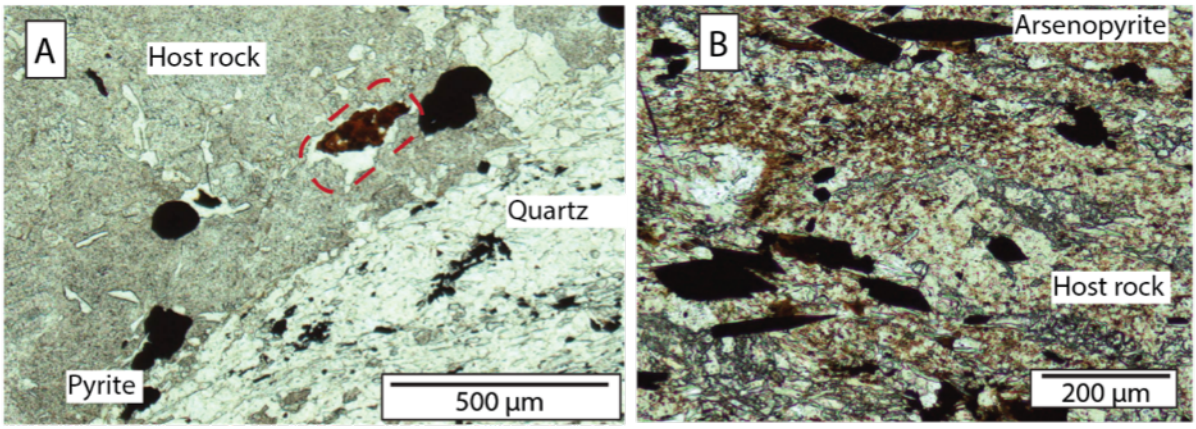

Figure 6.11 Transmitted PPL images of 'arcanite' mineral (identified in figure 6.11). A: Example of a large crystal (circled in red) in the host rock. Quartz body can be seen towards the bottom of the image. B: 'Arcanite' disseminated within the host rock. A-type arsenopyrite is overgrown by 'arcanite'.

The crystal in figure 6.11A was analysed by EMP and micro XRD (figure 6.12). EMP BSE and EDS analysis indicates that it is a micron-scale heterogeneous mixture of minerals that overall have an iron sulphate mineral composition (figure 6.12A). The micro XRD analysis that targeted this crystal (figure 6.12C) and identified as having the same crystal structure as arcanite (figure 6.12D). Thus the exact mineral remains unknown, but nevertheless it is a sulphate mineral. The GADS image indicates that the crystal has undergone deformation as diffraction peaks are visible in multiple orientations (figure 6.12B) and therefore not a result of Quaternary alteration as it is pre metamorphic.

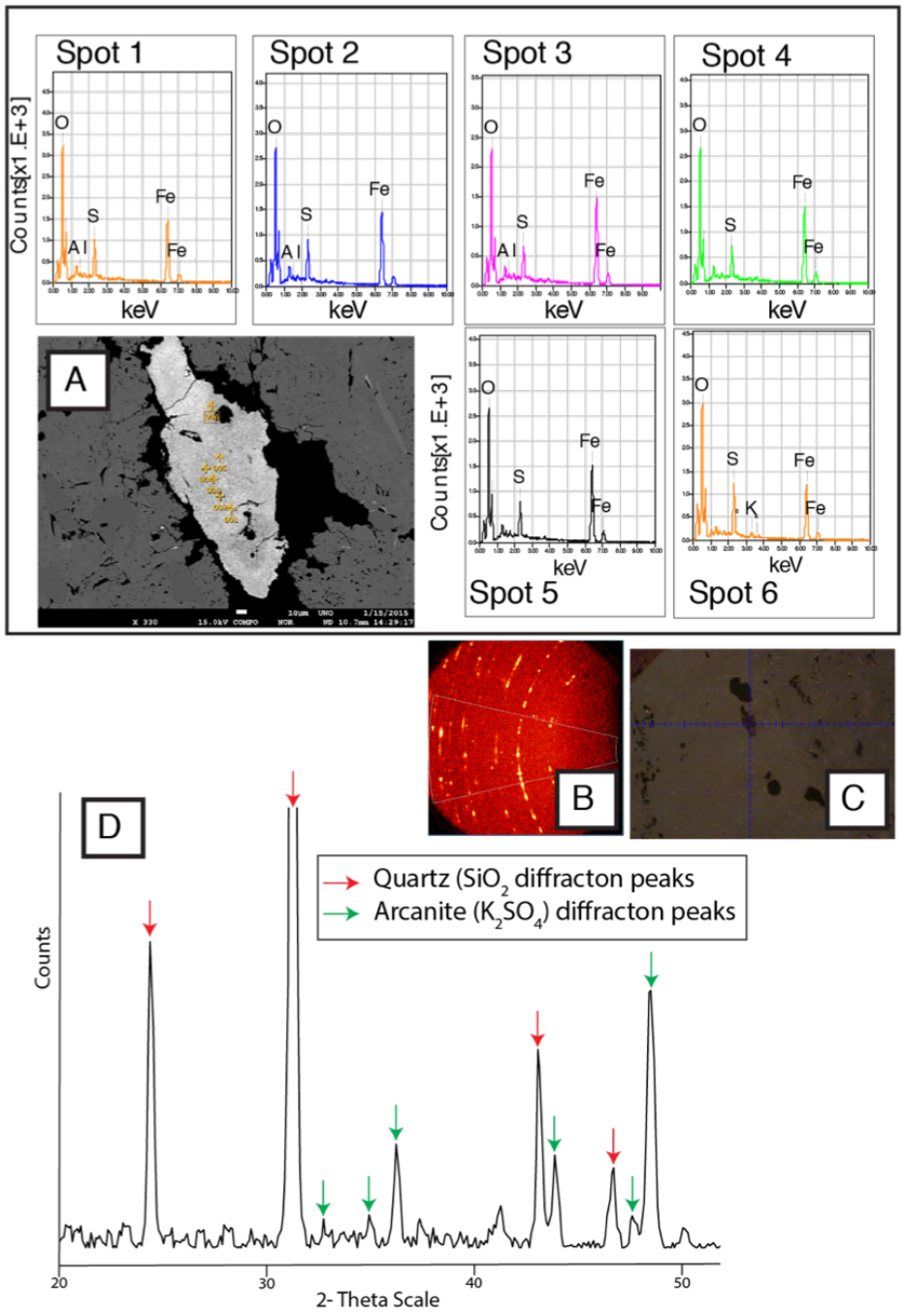

Figure 6.12 EMP EDS and micro XRD analysis the crystal circled in figure 6.15A. A: EMP EDS analysis showing image of spot and consistent sulphate peaks (although cation composition is unclear) B: GADS image showing XRD spot. The rounded trail indicates deformation of the primary crystal structure. C: Reflected light image of the spot targeted by micro XRD. D: XRD peaks showing arcanite (K_2SO_4) in quartz host rock.

6.4 Biotite

Biotite occurs parallel to the foliation that is defined by the sericite (for example figure 6.13A). Where A-type arsenopyrite is present and B-type and C-type arsenopyrite are absence, biotite is rarely present. These areas are the least deformed areas of the deposit. Biotite can occur surrounding B-type and C-type arsenopyrite. Biotite is formed during the D2 deformation and M2 metamorphism event that has tilted the stratigraphy (Dillon-Leitch, 1984) and therefore interpreted to have formed after the A-type mineralisation event. The assertion that A-type arsenopyrite is recrystalised into B-type and C-type with metamorphism (manifested by sericite foliation) would also seem to be indicated by biotite.

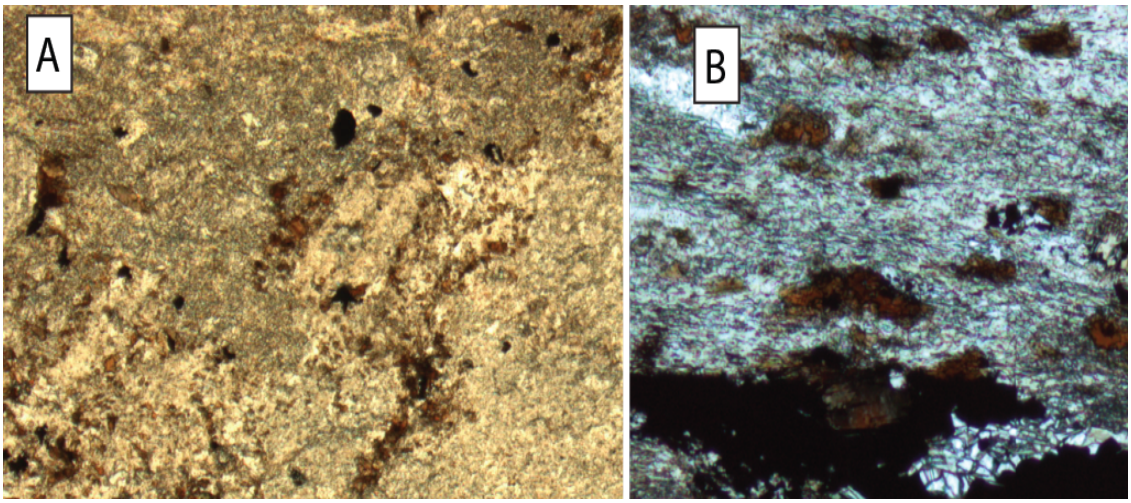

Figure 6.13 Biotite in thin section. A: PPL image showing example of biotite (brown mineral) within the host rock. B: PPL image of biotite conforming to foliation and surrounding sulphides.

Chapter 7

7 Isotopes

Two isotope studies were undertaken. Firstly, SIMS in situ spot analysis of the sulphur isotopic compositions of arsenopyrite was undertaken to establish whether the different types of arsenopyrite are isotopically homogenous. Spots were analysed as close as possible to the Au SIMS spots in order to correlate S isotopic composition with gold content. Secondly, whole rock $\partial^{34}S$ and $\Delta^{33}S$ values were determined from separates of the 'arcanite' sulphate within the quartz body. This was carried out to evaluate if the oxidation to form the sulphates had been caused by modern or Archean fluids. A brief description of the likely causes of these isotope fractions and comparison with similar results from other studies are presented to provide a framework from which the current work can be interpreted. The implications for the genesis of the deposit in the context of Au enrichment is subsequently addressed in Chapter 8.

7.1 Arsenopyrite In Situ ∂S^{34} Isotopes

Figure 7.1 shows that each of the arsenopyrite types have broadly similar ∂S^{34} values: A-type has high values ranging from ∂S^{34} 1.7 to 4.1 ‰, B-type has ∂S^{34} ranging from 0.5 to 2.9 ‰ and B-type has lower ∂S^{34} values ranging from -1.8 to 2.2 ‰ (with one higher outlier). The error on the SIMS analyses is 0.5 ‰, but nevertheless the differences of isotopic values between the different arsenopyrite types are significant due to a low fractionation factor in sulphide minerals (Wagner et al., 2004). Pyrite has a very tight, distinct range of ∂S^{34} compositions, from 2.0 to 3.0 ‰. Further to this, overall there is a wide range of ∂S^{34} values throughout all of the data (from -0.8 to 5.1 ‰).

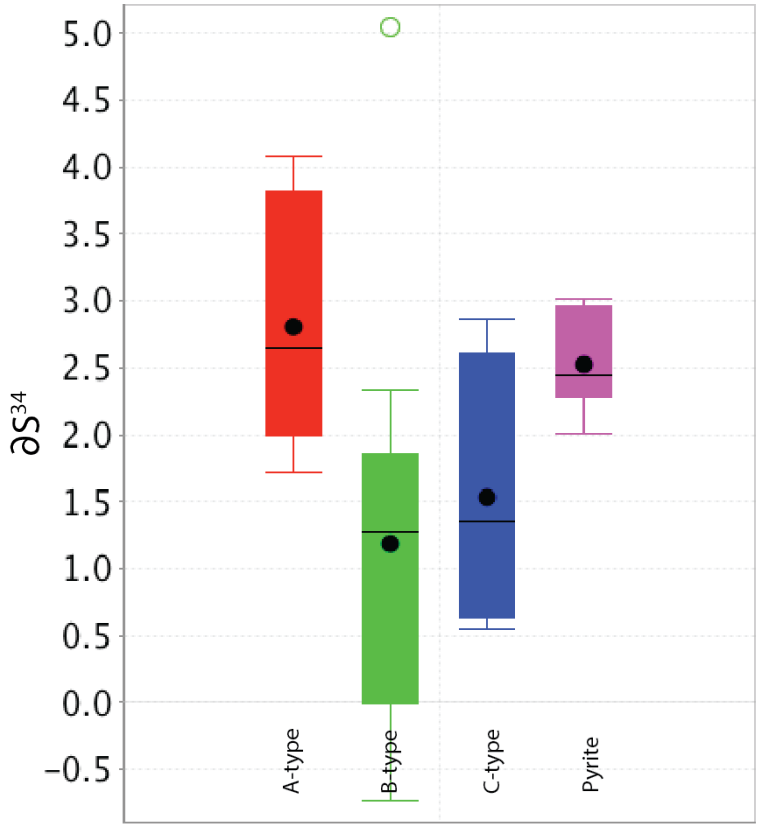

Figure 7.1 Box plot showing range of ∂S^{34} (‰) for arsenopyrite species and pyrite. Black spot shows mean, black line is the median, box shows middle 50% of data whiskers show maximum and minimum (excluding an outlier shown by the circle).

These ∂S^{34} values are plotted against SIMS spot analysis for Au in proximal locations of the same crystal on figure 7.2. The spots with significantly higher Au (greater than 500 ppm) tend to have a broadly similar isotopic signature (∂S^{34} 2.5-3.5 ‰) although there are too few points to be conclusive. High gold content can be observed over the whole range of ∂S^{34} isotopes.

This would suggest each arsenopyrite type reflects a distinct fluid event. Although there is some overlap shown by figure 7.1, the fluid (which is assumed to be the source of the S) would appear to belong to fairly constant for the crystallisation of each species. For example, A-type arsenopyrite has relatively high ∂S^{34} values compared to B-type and C-type. This suggests at least two hydrothermal stage were responsible for A-type, and B- and C-type, respectively.

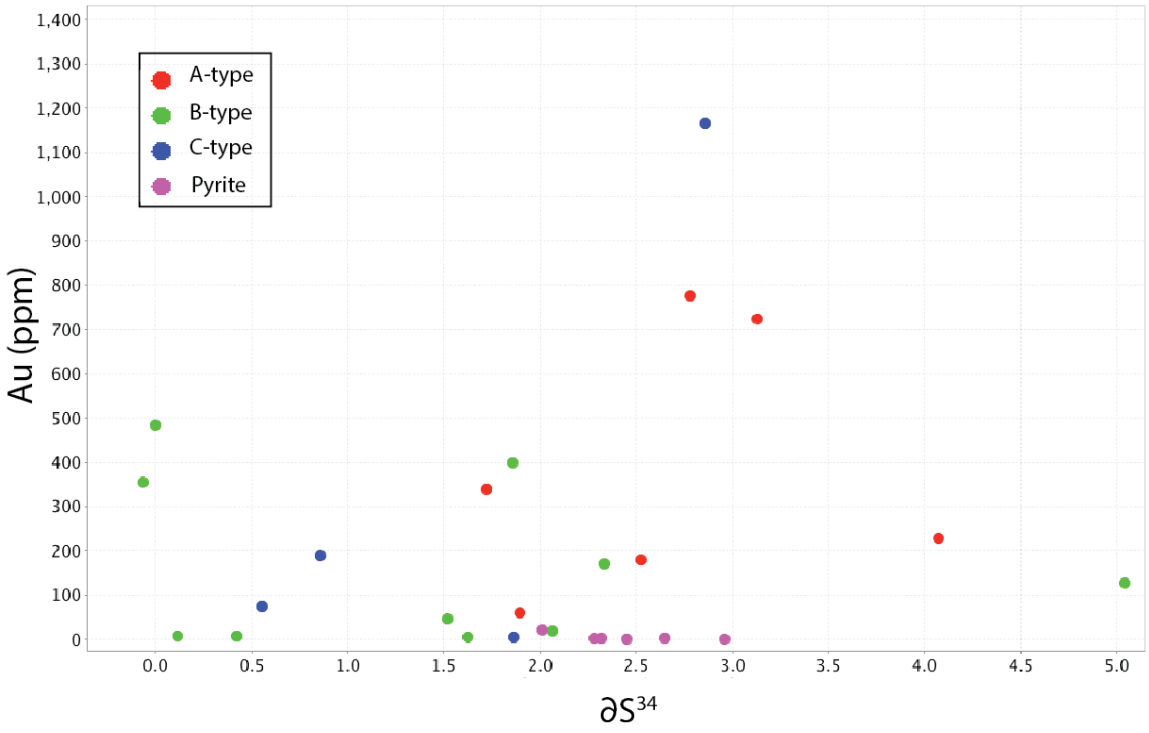

Figure 7.2 ∂S^{34} data from figure 7.1 plotted against adjacent Au analysis by SIMS. This shows that crystals with a greater ∂S^{34} are more likely to be A-type arsenopyrite and to be enriched in Au (however some C-type and B type have higher ∂S^{34} and Au values.

7.2 Sulphate Minerals

The sulphur isotopic composition of the sulphate minerals (tentatively arcanite) from the stratiform quartz body were also analysed. Samples were taken from three different holes that intersected the quartz body on the same stratigraphic horizon. The results of these analyses are reported in table 7.1 and $\Delta^{33}S$ and $\Delta^{36}S$ are displayed graphically in figure 7.3. The $\Delta^{33}S$ values are the most significant for assessing Archean deposits. These fall in two distinct populations, one with slightly negative values (-0.072 and -0.054 ‰) and another with slightly positive values (0.003 to 0.014).

Sample	$\delta^{33}S$ (‰)	$\delta^{34}S$ (‰)	$\delta^{36}S$ (‰)	$\Delta^{33}S$ (‰)	$\Delta^{36}S$ (‰)
111-03D	0.093	0.320	0.70	-0.072	0.09
11-04A	-0.050	-0.108	-0.38	0.006	-0.17
111-02	1.855	3.580	6.64	0.013	-0.17
88-151	0.840	1.625	2.64	0.003	-0.45
111-04W	1.129	2.186	4.07	0.004	-0.08
111-03A	1.293	2.485	4.59	0.014	-0.14
111-03B	1.361	2.750	5.09	-0.054	-0.14

Table 7.1 Sulphate isotope results.

The values that are slightly negative and close to zero ‰ for $\Delta^{33}S$ indicate that the sulphate minerals were deposited from a fluid that was dominantly magmatic in origin and has undergone mixing with a highly oxidised Archean fluid. Jamieson et al. (2006) reported similar values from the Kidd Creek mine (an Archean VMS deposit) and interpreted to the values to be indicative of "a homogenous, well-mixed sulphur source probably from deep hydrothermal fluids". This is because a magmatic $\Delta^{33}S$ values are zero whereas Archean seawater $\Delta^{33}S$ is consistently reported to be negative (Farquhar & Wing, 2003). In order to create a negative $\Delta^{33}S$ isotope, the fluid that formed the arcanite would have had to have mixed with Archean ocean sulphates.

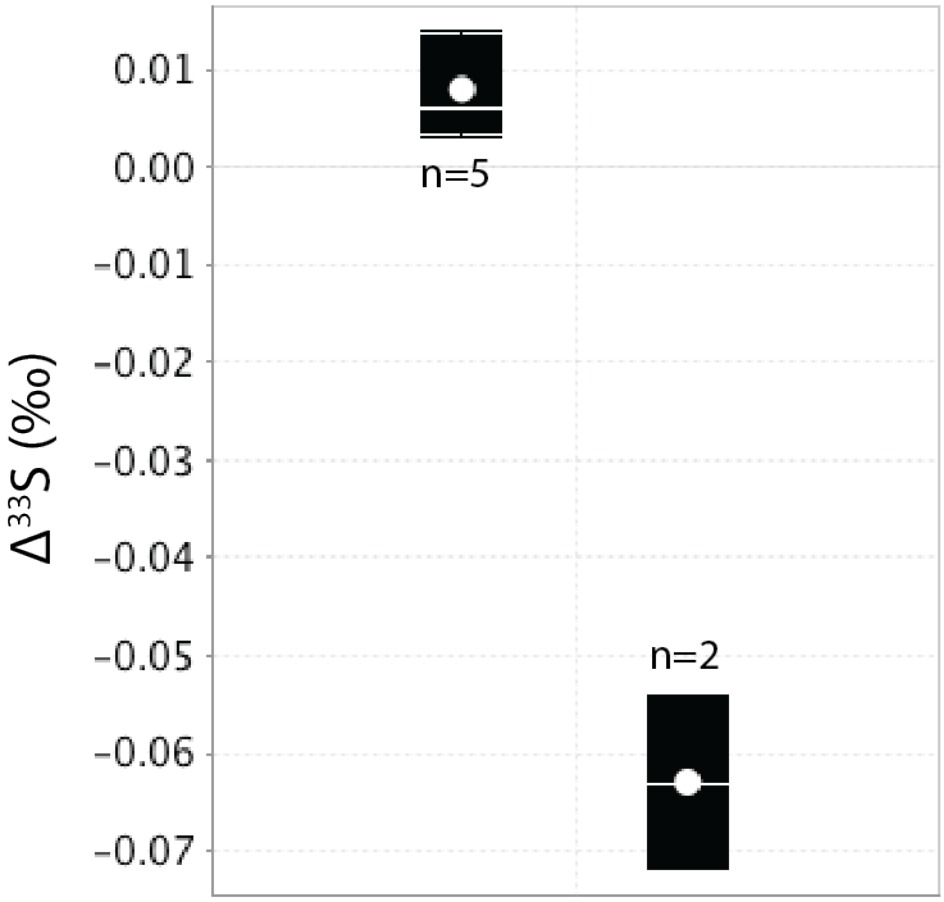

Figure 7.3 Box plots of $\Delta^{33}S$ values. Two distinct populations are shown. Most results have low positive values however a separate population have low negative results.

The second population with low positive $\Delta^{33}S$ values are also similar to values at Kidd Creek reported by Jamieson et al. (2013). They interpret these low positive values to have been caused by interaction between another distinct hydrothermal fluid (that is now evolved to be metal rich and sulphur limited) that scavenged local sulphide precipitates creating a sinter. This would suggest that reduced sulphur (in the case of FAT, arsenopyrite) was initially precipitated and then later amalgamated by a separate oxidising fluid. This would have occurred as a multi-stage, epithermal system enabled post-mineralising oxidised fluids to interact with the sinter.

Chapter 8

8 Discussion

This chapter summarises the observations in order to construct a model for gold mineralisation at the FAT deposit. This model can be used to evaluate the spatial and geochemical signatures that are associated with Au enrichment at FAT and provide an explanation for the genesis of the deposit. The original hypotheses were to characterise the mineralisation styles at FAT and their associated geochemical and mineralogical characteristics and to establish the genesis of the FAT deposit. For the latter, epithermal and orogenic origins have been proposed and a comparison of FAT with other Archean deposits of a similar style is therefore warranted. The genesis has implications for exploration along the CLGB and similar terranes globally.

8.1 Deposit Genesis

The main objective of this thesis is to understand the styles of arsenopyrite mineralisation and the significance of each of these with respect to Au enrichment. Arsenopyrite types are interpreted to be the product of distinct mineralising events. This is because of their differing crystal habit, Au content and distribution and its associated trace element chemistry and sulphur isotope ratios. In order to crystallise a certain type of arsenopyrite distinct mineralising events are required. Since each type is found in all of the studied domains, the spatial distribution of arsenopyrite would indicate that these events affected the whole of the studied area. Therefore, each domain does not necessarily represent a distinct mineralising event, rather a change in host rock facies that may be more or less susceptible to mineralisation or display different degrees of metamorphic sericite. The consequence of this is that there are at least two, distinct and definable events that affected mineralisation at FAT. The large, positive range in ∂S^{34} values indicates that mineralisation occurred in a variably oxidising environment.

Differing veining, alteration and isotopic implications can be attributed to each of these events. Since alteration and veining can provide an important temporal correlation with

metamorphism, the gold enrichment event at FAT can be evaluated as pre-, syn- or post-orogenenic at the CLGB.

8.1.1 Timing of A-type Arsenopyrite

The interpretation of the cause of the main gold enrichment event at FAT is reliant on understanding the timing of A-type arsenopyrite and whether it is pre- or syn-metamorphic. The pristine, inclusion-free crystal texture of A-type arsenopyrite could be interpreted as having formed during a retrograde metamorphic or other fluid event. In this scenario A-type crystals are post-deformation, would not have been overprinted by subsequent fluids and would represent the youngest arsenopyrite type.

There are however, numerous arguments for A-type arsenopyrite to be pre-metamorphic. It is consistently found in the least deformed rocks that do not seem to have undergone pervasive, strong metamorphism. Lapilli clasts in areas where A-type arsenopyrite is present rarely exhibit elongation, deformation or metamorphic foliation typically manifested by sericite. The distribution of A-type arsenopyrite in these tuffs would seem to be controlled by primary permeability in the host rock (as mineralisation occurs preferentially in the tuff matrix. A-type arsenopyrite is associated with phase 1 veins that have since been deformed during the metamorphic event. Since the volcanic stratigraphy indicate multiple eruption events (many transitions from ash to lapilli to bomb tuff) there is likely be consistent and extensive fluid circulation through the tuff. It thought that this epithermal fluid that is responsible for A-type arsenopyrite mineralisation. The FAT deposit sits in the thickest part of the felsic volcanics in the CLGB which therefore allows for extensive hydrothermal activity due to a long-lasting volcanic system. Finally, there is a lack of evidence for a retrograde metamorphic event at FAT, e.g., biotite is rarely altered to chlorite.

A possible resolution of this problem could be through age dating. The Re-Os method was attempted on arsenopyrite however the Re concentrations were insufficient for ages to be obtained. A summary of the arguments for arsenopyrite being pre or syn metamorphic is given as table 8.1. This thesis argues that A-type arsenopyrite is early and is pre-metamorphic.

	Pre Metamorphic	Syn-Metamorphic
Crystal Habit	Randomly oriented crystals forming in rosettes do not have metamorphic orientations or textures	Inclusion-free crystals are likely to be the youngest as inclusions often indicate multiple fluidising events
Crystal geochemistry		Simple geochemistry indicative of few fluidising events
Host Rock	Occurs in the least deformed environments and therefore may have survived the metamorphic event without recrystalisation	
Veining	Occurs proximal to the earliest style of veining which themselves have been deformed by the metamorphic event	
Sericite	Is not found in areas with a strong sericite metamorphic overprint	

Table 8.1 Summary of arguments for pre-metamorphic arsenopyrite vs syn-metamorphic arsenopyrite

8.1.2 Stage One

A-type arsenopyrite is consistently found in the most undeformed environments and is frequently randomly orientated. It is usually found in the matrix of undeformed lapilli tuff. In some instance in domain 5 it occurs in rosettes that replace clasts. This is interpreted to be a consequence of a low lithostatic pressure with mineralisation exploiting the lowest porosity pathways. Many of the crystals are acicular and this is interpreted to be a product of rapid crystal growth (Puel et al. 2008).

The greatest concentrations of A-type arsenopyrite occur in areas proximal to undeformed phase 1 quartz veins. It is therefore thought to a product of this veining event. Mg-rich Phengite is locally present although it does not necessarily define a foliation.

A-type arsenopyrite has relatively simple geochemistry. Au distribution is usually relatively homogenous although a similar morphology but with Au concentrated in the rims is also observed. Sb is variably present and this is dependent on whether the Au content is homogenous or concentrated in the rims. This simple geochemistry is indicative of a simple mineralising fluid composition. The range of ∂S^{34} compositions of A-type arsenopyrite has the highest values and therefore the fluid is the most evolved due to oxygenation. The mineralising fluid would have undergone a high level of sulphur fractionation that could concentrate the metal content. This contributes to the simple geochemistry and high Au content.

A-type arsenopyrite is therefore interpreted to be the earliest species of arsenopyrite at FAT. This is due to its relationship with host rock, veining and white mica, its crystal orientation, and its simple geochemistry. A schematic representation of this is shown in figure 8.1.

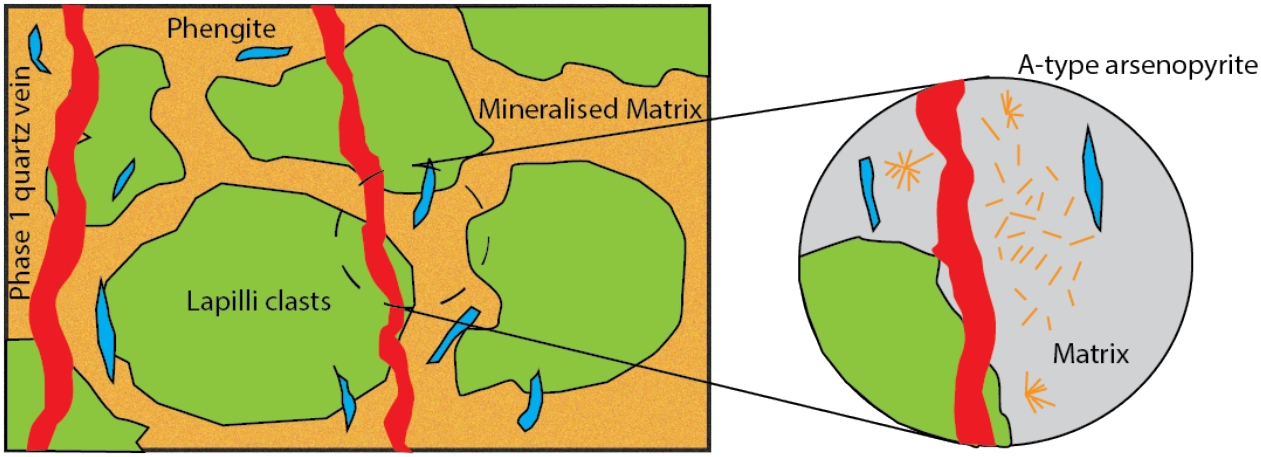

Figure 8.1 Simplified schematic representation of A-type arsenopyrite mineralisation.

8.1.3 Stage 2

In B-type arsenopyrite there is a heterogeneous Au distribution. Au is no longer consistent and within the crystal. Ni, Sb and Co are now present (also with a heterogeneous distribution). This would suggest that the fluid that is responsible for the crystallisation is different to the fluid responsible for A-type arsenopyrite. The distinct ∂S^{34} values support this. Inclusions and fractures within the crystal would indicate that the crystal has undergone multiple fluid events.

When phase 1 veining occurs proximal to B-type arsenopyrite, they are folded. Phase 2 veining is generally but not consistently present. There is always a foliation fabric defined by muscovite (Al-rich) mica. Phengite is still thought to present however geochemically is hard to identify as muscovite dominates the bulk composition. Crystals are typically orientated sub parallel to the muscovite-defined foliation.

B-type arsenopyrite is therefore interpreted to have formed as a separate mineralising event. This distinct mineralising event is interpreted due to a more complex geochemistry and Au distribution within the arsenopyrite and a different, lower ∂S^{34} signature. B-type arsenopyrite is found in a different geological environment with elongation of lapilli clasts and foliation typically present. The crystal orientation (sub parallel to metamorphic

white mica) and deformed phase 1 quartz veins indicates crystallisation to be syn-metamorphic. This relationship is shown schematically in figure 8.2.

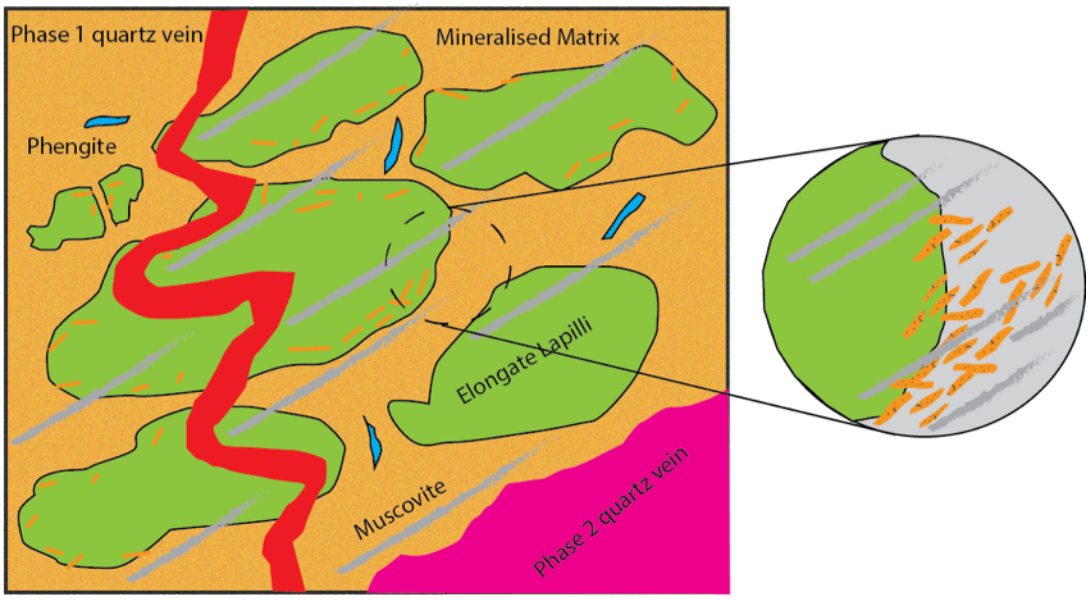

Figure 8.2 Simplified schematic representation of B-type mineralisation

The geochemical composition and distribution in C-type arsenopyrite is the most complex. Au enrichment is low and its distribution usually bladed. There is a significant enrichment of Sb and sporadic enrichment of Pb that is not seen in A-type and B-type arsenopyrite. The crystals are aggressively fractured with abundant inclusions that are often filled with pyrite. This would indicate that the crystals have had a complex history with multiple phases of fluid processes.

Where phase 1 veining is observed it is highly deformed and often broken. Phase 2 veining is common and cross cuts phase 1 veins. Metamorphic, Al-rich muscovite mica defines the foliation and is parallel to the fold axis of the phase 1 veins and parallel to phase 2 veining.

C-type mineralisation is interpreted to be an evolution of the event that caused B-type mineralisation. It occurs in more intense metamorphic environments and the original volcanic texture of the host rock is often hard to distinguish due to an aggressive sericite overprint. These are areas where muscovite foliation is ubiquitous and the clasts are most

elongate C-type arsenopyrite and associated pyrite is always parallel with this foliation. It has a broadly similar (but slightly greater) ∂S^{34} value and is therefore interpreted to be formed by a similar but slightly more oxidised fluid. A schematic representation of this is shown in figure 8.3.

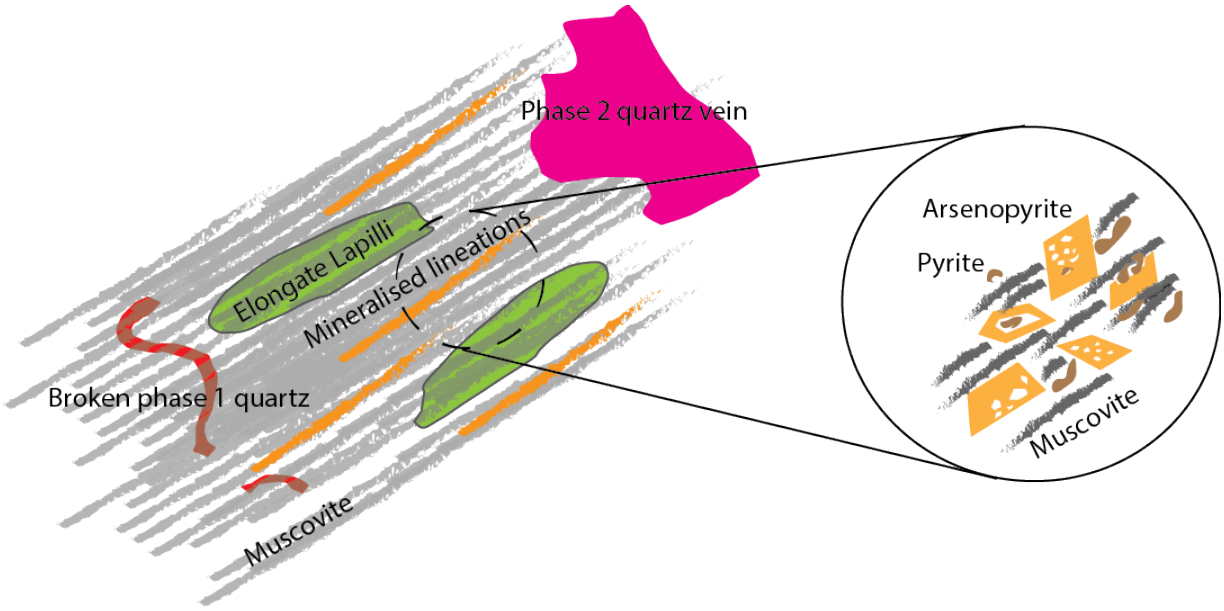

Figure 8.3 Simplified schematic representation of C-type mineralisation

8.1.4 An epithermal model with a metamorphic overprint

The timing of the arsenopyrite indicates early, pre-metamorphic crystalisation. Fluids are believed to have been originally magmatic in origin due to sulphur isotope results. A multi-stage, long-lasting volcanic environment that created the felsic volcanic unit at FAT would have allowed for geothermal volcanic fluids to circulate depositing gold in strataform domains (figure 8.4A). The geothermal fluid could have either been magmatic- or meteoric-dominant as they are in modern systems but determining the origin of this fluid is beyond the scope of the current work.

The quartz body is a sinter that formed as a result of this epithermal fluid (figure 8.4B). This quartz vein has intercalated sulphate that has been in contact with an Archean ocean. Consequently, this must have formed prior to metamorphism. The sulphate also has a

μXRD GADS pattern that is indicative of deformation (and is therefore pre metamorphism).

B-type and C-type arsenopyrite are interpreted to be formed as A type arsenopyrite has recrystalised as a result of metamorphic fluid (figure 8.4C). This accounts for their inclusion abundance, more complex geochemistry and heterogeneous Au distribution. There is also a significant pyrite mineralisation event associated with this. This metamorphic event forms Al-rich muscovite mica and is associated with the deformation event that folded phase 1 quartz veins and formed phase 2 quartz veins. It has tilted the stratigraphy to roughly vertical. This is linked to the main deformational event in the Slave province (D2).

8.2 Implications for Exploration

The characteristics associated with mineralisation and the resulting model has implications for exploration along the CLGB. This model argues that mineralisation of A-type arsenopyrite occurs concurrently with volcanism and represents the introduction of Au to the deposit. This would imply that where felsic volcanism has occurred in conjunction with epithermal fluid circulation, gold enrichment is viable. Felsic volcanics are found throughout the CLGB and so this lithology remains a feasible exploration target. Near surface Au showings throughout the belt have been drilled but mineralisation in areas with poor outcrop and the discovery of subsurface mineralisation remain targets.

Since mineralisation within felsic volcanics is not ubiquitous, recognising and isolating a Au mineralisation event within the felsic volcanics and any geological associations is required. The characteristics associated with this event are listed in order of size of footprint are listed:

- High Mg to Al ratio indicative of mica species
- Phase 1 quartz veins
- Acicular, inclusion free arsenopyrite

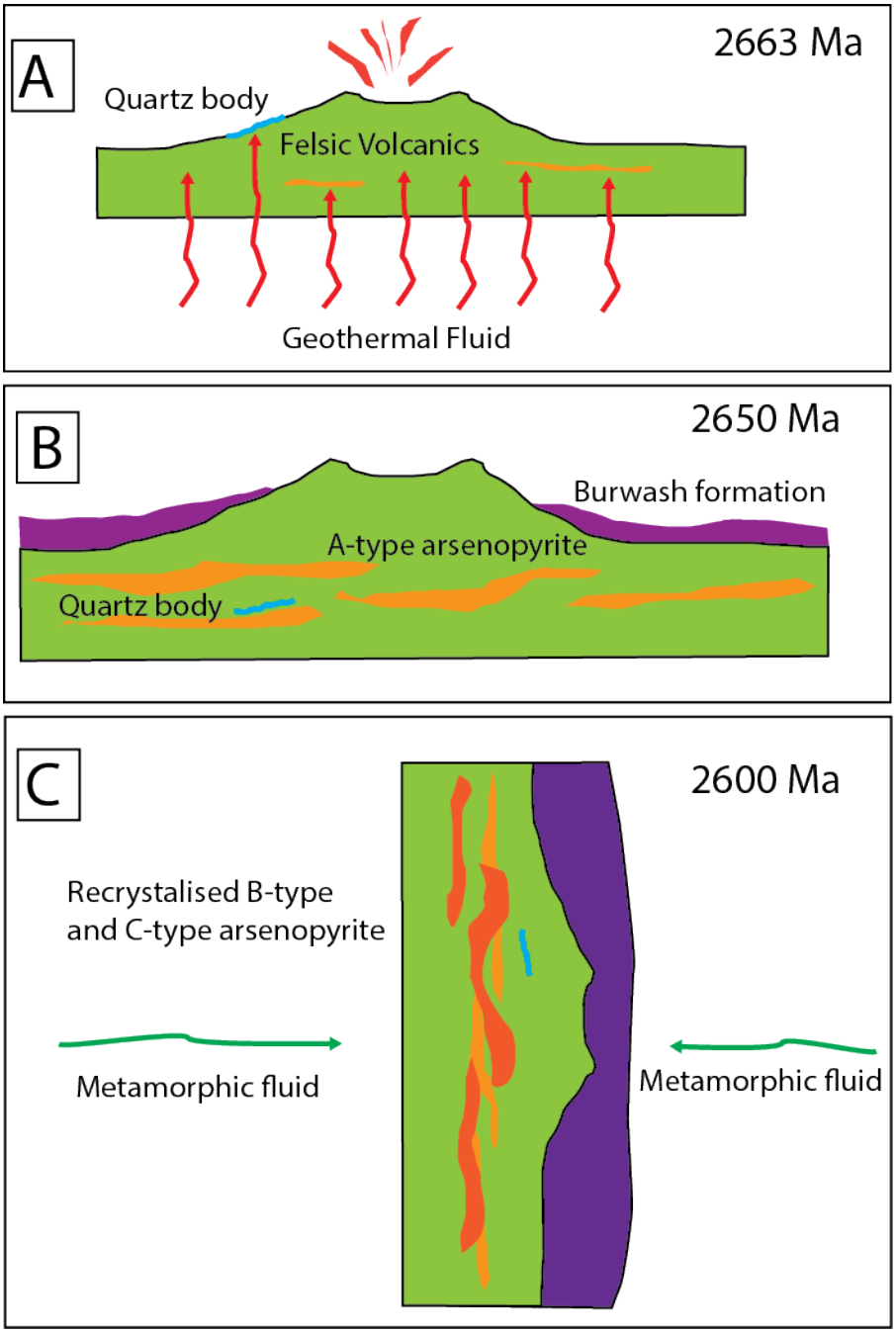

Figure 8.4 Representation of the processes that have caused gold mineralisation at FAT. A shows epithermal fluid creating stratiform A-type arsenopyrite mineralised lenses. This eventually forms B as volcanism wanes and Burwash formation

sediments are overlain. During metamorphism (C) A-type arsenopyrite lenses recrystalise into B-type and then C-type arsenopyrite.

Because of poor outcrop, soil sampling using As and Au has recently been used to assess whether areas along the CLGB are viable drilling targets. A belt scale review of the Mg to Al ratio of these soil samples can focus further drilling campaigns. A high Mg to Al ratio (not necessarily with the presence of As and Au) could be indicative of the mica species associated with mineralisation. This could identify blind deposits that do not daylight. A benchtop SEM has been demonstrated to be able to identify this trend in drill core and along with ICP data it can be used to evaluate a drilling campaign as drilling is underway. It still remains curious that this compositional change is not reflected in the hyperspectral results. Expanding this dataset across the whole cross section (and not just domains 3, 4 and 5) would thoroughly evaluate a Terraspec as an exploration tool at Courageous Lake.

The recognition of phase 1 quartz veins would also be useful. This study has been unable to find geochemical differences in the vein species. Recognition of these veins can be achieved in drill core by colour and texture and in thin section by crystal size. Understanding the spatial distribution of these and capturing their abundance and habit during core logging would be useful.

Finally, the recognition of A-type arsenopyrite during core logging is important. Once the shape of the A-type arsenopyrite ore body is properly defined the trends of the deposit can be better understood. B-type and C-type mineralisation occur later and so may have an oblique trend. As a result of this, Au and As trends do not necessarily correspond to primary mineralisation shape. Distinguishing a Au trend with A-type arsenopyrite geochemical characteristics has not been possible using the ICP data. It would be interesting to see if geochemical characteristics visible on a smaller scale (for example via point data from a pXRF) can be translated across the cross section and deposit.

8.3 Evaluation of FAT as Epithermal Archean Gold Deposit

Since the concept of epithermal gold in Archean rocks is rare and controversial it is worth considering other Archean global deposits with a proposed epithermal endowment event for comparison. Investigations into these deposits include two themes, whether the Archean tectonics can cause epithermal mineralisation and if these deposits can survive metamorphism and deformation. As outlined by Kessler and Wilkinson (2009), epithermal deposits older than 60 Ma are rare and must have undergone exceptional preservation.

FAT can be compared to modern epithermal deposit models. Simmons et al. (2005) provide a summary of the models for epithermal deposits and overview of the methods for transportation and precipitation of gold. The distinction should be made between epithermal and magmatic hydrothermal systems. The chemistry of ore hosting minerals and the shape of the ore body at FAT would suggest an epithermal low sulphidation system. There is likely to be a deeper intrusion related heat source that has driven magmatic fluids to cause mineralisation as mixing with meteoric fluids in lower temperature and pressure environments near the surface. These deposits are often found in arcs undergoing extension and eventually rifting. The tectonic setting of the Slave basin has been proposed to be a product of a rifting event that caused the formation of the Yellowknife Supergroup (Helmstaedt & Padgham, 1986). Following this subsidence seems to be important in the preservation of epithermal assemblages in order to prevent erosion. FAT is immediately overlain by turbidites and the inferred shallow orogenic processes inferred to have occurred at the Yellowknife greenstone belt (Shelton et al., 2004) may have allowed for preservation.

Metamorphism of epithermal mineral assemblages are seen globally in deposits through a broad range in geological time. There are a number of examples of proposed low sulphidation epithermal systems discussed here and these have undergone a range of metamorphic overprints. Gangue mineral assemblages are one of the few characteristics common to all unmetamorphosed epithermal deposits. Typical minerals coeval with mineralisation are quartz, calcite, adularia and illite (sericite).

Mallery Lake, Nunuvut provides a good analogue for how low sulphidation epithermal gold may have occurred in Precambrian environments (Turner et al. 2001). This seems to be a very well preserved environment with little later stage alteration and a low grade metamorphic overprint that is similar to FAT. They hypothesise that the abundance of Precambrian epithermal gold is controlled by preservation rather than magmatic processes and note that ancient deposits have immediate burial and limited structural deformation. Following this exhumation must occur in order to expose these deposits; Kesler & Wilkinson (2009) propose that whilst formation is consistent there are specific exhumation rates required to expose an economic deposit.

Garde et al., (2012) discusses the preservation of late Archean epithermal systems in metamorphic terranes with specific reference to the Qussuk region, Greenland. They suggest that metamorphic processes quickly destroy porosity and permeability of epithermal environments once a certain pressure-temperature threshold is achieved. This creates limited possibilities for fluid migration and so whilst recrystalisation of minerals is common, redistribution of metals will be very localised and the geochemical characteristics of the epithermal system will be preserved. This is demonstrated at Qussuk with: spatial association of gold with andesitc and felsic host rocks, hydrothermal alteration and volcanic textures. The preservation of hydrothermal passageways and trace element geochemistry is attributed to intense multistage hydrothermal alteration deemed too severe for orogenic processes.

The Challenger deposit in South Australia would also seem to be Archean epithermal with a strong orogenic overprint. Mcfarlane et al. (2007) attempted to recognise the hydrothermal assemblage and epithermal characteristic of the deposit by attempting to define the changes to sericite-adularia mineralisation through high grade metamorphosis. This deposit has undergone much higher grade metamorphosis (granulite facies) than FAT however seeing how the deposit responds to these changes is still useful. It is concluded that elemental depletions and enrichments that were originally caused by the epithermal processes were spatially preserved during metamorphosis and correlate to grade. The authors conclude that Au, Ag, As, S, Bi and Be are all pathfinders for gold.

Penczak & Mason (1999) identify epithermal characteristics that may have caused gold endowment at Campbell-Red Lake, Ontario. Its geological setting would have allowed for post depositional and pre orogenic gold endowment due to felsic plutons producing multi-stage epithermal gold. Metal ratio differences with modern systems are analogous with Courageous Lake (high Au to Ag ratio), however, they do not recognise metamorphosed epithermal gangue minerals (for example the absence of adularia).

Chapter 9

9 Conclusions

Three main types of arsenopyrite are identified at FAT and these have differing levels of Au enrichment. The habit of arsenopyrite and their mineralogical associations favours an initial epithermal endowment event with a metamorphic overprint. They are put in the context of a temporal evolution of the deposit:

- Banting Group felsic volcanics (ash, lapilli and bomb tuff) form the host rock for FAT

- Early, A-type arsenopyrite is the most enriched in Au and this has a homogenous or a rim-rich distribution. A-type arsenopyrite is associated with ‘phase 1’ cockade veins and Mg-rich mica. These are interpreted to be syn-volcanic and with epithermal processes responsible for this mineralisation event.

- A sinter vein intersected multiple times across a single horizon has intercalated oxidised sulphur that has isotopic signatures indicative of interaction with Archean meteoric fluid.

- An evolution to a sub aqueous environment occurred. Greywacke intercalations are intersected and then followed by deposition of graphitic turbidites.

- Metamorphism occurred during the Algoman orogeny. This caused the dissolution of A-type arsenopyrite and precipitation of less enriched, more heterogeneously distributed Au in B-type and C-type arsenopyrite. Pyrite, Al-rich mica and ‘phase 2’ bull veins are associated.

References

Abraham, A., Davis, D.,Kamo, S. & Spooner, E.. 1994., Archean magmatism deformation and gold-quartz vein mineralization in the northwestern Anialik River greenstone belt and igneous complex, Slave Province, NWT. *Canadian Journal of Earth Sciences*, 31, pp 1365-1383.

Baragar, W.R.A. & Mcglynn, J.C., 1976. Early Archean basement in the Canadian Shield: A review of the evidence. *Geol. Surv. Can*, 76(14), p.20.

Bleeker, W., Ketchum, J., Jackson, V., 1999. The Central Slave Basement Complex, Part I: its structural topology and autochthonous cover. *Canadian Journal of Earth Sciences*, 36(7), pp.1083–1109.

Bleeker, W., 1996. Thematic structural studies in the Slave Province, Northwest Territories: the Sleepy Dragon Complex. *Current Research 1996-C; Geological Survey o f Canada*, pp.37–48.

Bleeker, W. & Beaumont-Smith, C., 1995. Thematic structural studies in the Slave Province: preliminary results and implications for the Yellowknife Domain, Northwest Territories. *Current Research 1995-C; Geological Survey of Canada*, pp.87–96.

Bleeker, W. & Davis, W.J., 1999. The 1991 – 1996 NATMAP Slave Province Project : Introduction, *Canadian Journal of Earth Science,* 36, pp.1033–1042.

Bleeker, W. & Hall, B., 2007. The Slave Craton: Geology and metallogenic evolution. In Mineral Deposits of Canada: A Synthesis of Major Deposit-Types, District Metallogeny, the Evolution of Geological Provinces, and Exploration Methods. *Edited by W.D. Goodfellow. Geological Association of Canada, Mineral Deposits Division, Special Publication*, 5, pp.849–879.

Cao, Y., Linnen, R., Good, D., Samson, I., Epstein, R., The Application of pXRF and benchtop SEM to Cu-Pd exploration in the Coldwell Alkaline Complex, Ontario,

Canada, Submitted to *Geocehmistry: Exploration, Environment, Analysis, 2015*

Cousens, B., Facey, K. & Falck, H., 2002. Geochemistry of the late Archean Banting Group, Yellowknife greenstone belt, Slave Province, Canada: simultaneous melting of the upper mantle and juvenile mafic crust. *Canadian Journal of Earth Sciences*, 39, pp.1635–1656.

Davis, W.J. & Bleeker, W., 1999. Timing of plutonism, deformation, and metamorphism in the Yellowknife Domain, Slave Province, Canada. *Canadian Journal of Earth Sciences*, 36(7), pp.1169–1187

Dillon-Leitch, 1984. Volcanic stratigraphy, structure and metamorphism in the Courageous-Mackay Lake Greenstone Belt. *Unpublished Thesis, University of Ottowa.*

Dimov, S. & Hart, B., 2011. Quantitative analysis of sub-microscopic and surface preg-robbed gold in gold deportment studies. In *50th Annual Conference of Mettalurgists of CIM*. pp. 1–12.

Duke, E.F., 1994. Near Infra red spectra of muscovite, Tschemak substitution and metamorphic reaction progress: implication for remote sensing. *Geology*, 22(1992), pp.621–624.

Easton, R.M. & Johns, G.W., 1986. Volcanology and Mineral Exploration: The Application of Physical Volcanology and Facies Studies, *Ontario Geological Survey miscilanious paper 129,* pp 2-40

Farquhar, J. & Wing, B. a., 2003. Multiple sulfur isotopes and the evolution of the atmosphere. *Earth and Planetary Science Letters*, 213(1-2), pp.1–13.

Flemming, R.L., 2007. Micro X-ray diffraction (μXRD): a versatile technique for characterization of Earth and planetary materials. *Canadian Journal of Earth Sciences*, 44, pp.1333–1346.

Freeman, J., 2004, Courageous Lake internal company technical report. Availible online

at www.seabridgegold.net

Garde, A., Whitehouse, M., & Christensen, R., 2012. Mesoarchean Epithermal Gold Mineralization Preserved at upper amphibolite-facies grade, Qussuk, Southern West Greenland. *Economic Geology*, 107, pp.881–908.

Geusebroek, P.A. & Duke, N.A., 2005. An Update on the Geology of the Lupin Gold Mine, Nunavut, Canada., *Exploration Mining Geology,* 13, pp.1–13.

Helmstaedt, H. & Padgham, W., 1986. A new look at the stratigraphy of the Yellowknife Supergroup at Yellowknife, NWT-implications for the age of gold-bearing shear zones and Archean basin evolution. *Canadian Journal of Earth Sciences,* 23, pp 454-475.

Henderson, J.F., 2007. Gold in the Yellowstone Greenstone Belt, Northwest Territories: Results of the EXTECH III Multidisciplinary Research Project, *Economic Geology,* 102, pp.159–162.

Hoffman, P.F. (Compiler). 1993. Geology, Slave craton and envi- rons, District of Mackenzie, Northwest Territories. Geological Survey of Canada, Open File 2559.

Iizuka, T., Horie, K., Komiya, T., Windley, B., 2006. 4.2 Ga zircon xenocryst in an Acasta gneiss from northwestern Canada: Evidence for early continental crust. *Geology*, 34(4), pp.245–248.

Isachesen, C.E. & Bowring, S.A., 1994. Evolution of the Slave craton. *Geology*, 22(October), pp.917–920.

Jamieson, J., Wing, B., Hannington, M., Farquhar., J., 2006. Evaluating isotopic equilibrium among sulfide mineral pairs in Archean ore deposits: Case study from the Kidd Creek VMS deposit, Ontario, Canada. *Economic Geology*, 101(5), pp.1055–1061.

Jamieson, J., Wing, B., Farquhar., J., Hannington, M., 2013. Neoarchaean seawater sulphate concentrations from sulphur isotopes in massive sulphide ore. *Nature*

Geoscience, 6(1), pp.61–64.

Kesler, S. & Wilkinson, B., 2009. Resources of gold in Phanerozoic epithermal deposits. *Economic Geology*, pp.623–633. Available at: http://gsecongeo.highwire.org/content/104/5/623.short [Accessed December 13, 2013].

Ketchum, J.W.F., Bleeker, W. & Stern, R., 2004. Evolution of an Archean basement complex and its autochthonous cover, southern Slave Province, Canada. *Precambrian Research*, 135(3), pp.149–176. Available at: http://linkinghub.elsevier.com/retrieve/pii/S0301926804002050 [Accessed September 17, 2013].

Lechner, 2008, National Instument 43-101 on FAT deposit, www.sedar.com

Lechner, 2014, National Intsrument 43-101 on Walsh Lake deposit, www.sedar.com

Mcfarlane, C., Mavrogenes, J. & Tomkins, A., 2007. Recognizing hydrothermal alteration through a granulite facies metamorphic overprint at the challenger Au deposit, South Australia. *Chemical Geology*, 243(1-2), pp.64–89.

Moore, J.C.G., 1956. Courageous-Matthews Lakes Area, District of Mackenzie, Northwest Territoires. *Geological Survey of Canada, Department of Mines and Technical Surveys*, 283.

Ootes, L., Morelli, R. & Creaser, R., 2011. The Timing Of Yellowknife Gold Mineralization: A Temporal Relationship With Crustal Anatexis? *Economi Geology*, 106, pp.713–720.

Padgham, W. a. & Fyson, W.K., 1992. The Slave Province: a distinct Archean craton. *Canadian Journal of Earth Sciences*, 29, pp 2072–2086.

Helmstaedt, H. & Padgham, W.A., 1986. A New Look At The Stratigraphy Of The Yellowknife Supergroup At Yellowknife, N.W.T. Implications For The Age Of Gold-Bearing Shear Zones And Archean Basin Evolution., *Canadian Journal of*

Earth Sciences, 23, pp 454- 475.

Padgham, W.A., 1992. Mineral deposits in the Archean Slave Structural Province ; lithological and tectonic setting. *Precambrian Research*, 58(i), pp.1–24.

Penczak, R.S. & Mason, R., 1999. Characteristics and Origin of Archcan Premetamorphic Hydrothermal Alteration at the Campbell Gold Mine, Northwestern Ontario, Canada, *Economic Geology,* 94, pp 507- 528

Puel, F. et al., 2008. Crystallization mechanisms of acicular crystals. *Journal of Crystal Growth*, 310(1), pp.110–115.

Shelton, K., McMenamy, T., van Hees, E., Falk., H, 2004. The complex fluid history of a Greenstone-hosted gold deposit: fluid inclusion and stable isotope studies of the Giant mine, Yellowknife, northwest Territories, Canada. *Economic Geology,* 99, pp.1643–1663.

Silke, R., 2009. The Operational History of Mines in the Northwest Territories , Canada. *Northwest Terretories Geoscience Office.*

Simmons, S., White, N. & John, D., 2005. Geological characteristics of epithermal precious and base metal deposits., *Economic Geology 100th Aniversary Volume*, pp 485–522.

Thompson, P., 1989. Moderate overthickening of thinned sialic crust and the origin of granitic magmatism and regional metamorphism in low-P-high-T terranes. *Geology*, (17), pp. 520–523.

Turner, W., Richards, J., Nesbitt, B., Muehlenbachs, K., Biczok, J., 2001. Proterozoic low-sulfidation epithermal Au-Ag mineralization in the Mallery Lake area, Nunavut, Canada. *Mineralium Deposita*, 36(5), pp.442–457.

Villeneuve, M., 1993, Preliminary geochronological results from the Winter Lake- Lac de Gras Slave Province NATMAP project, Northwest Territories, Geological Survey of Canada Paper 93-2, pp 29- 38.

Wagner, T. et al., 2004. Laser microprobe sulphur isotope analysis of arsenopyrite: Experimental calibration and application to the Boliden Au-Cu-As massive sulphide deposit. *Ore Geology Reviews*, 25(3-4), pp.311–325.

Winchester J., Floyd, P., 1977, Geochemical discrimination of different magma series and their differentiation products using immobile elements, *Chemical Geology,* 20, pp 325- 343

Yang, K., Huntington J., Gemmell J., Scott K., 2011, Variations in composition and abundance of white mica in the hydrothermal alteration system at Hellyer, Tasmania, as revealed by infrared reflectance spectroscopy, *Journal of Geochemical Exploration,* 108, pp 143-156.

Appendices

Appendix A: Drill Logs.

Hole	From	To	Sample taken	Rock name	Description	Modal Clast size (mm)	Well sorted (1-5)	Foliation Intensity (0-5)	Sericite Alteration (0-5)	Silica Alteration (0-5)	Calcite Alteration (0-5)	Arsenite Alteration (0-5)	Chlorite Alteration (0-5)	Py (%)	Po (%)	Asp (%)
CL-061	0	11.72	114 and 115	Ash Tuff	Fine grained ash with limited evidence of foliation. The unit has a moderate sericite bleaching throughout which would seem to very consistent in occurance. Small ejector quartz fragments are common throughout the unit and do not seem to be restricted to one particular area of bedding plane. Wormy quartz veins that do not seem to conform to foliation are common throughout the unit. Fine rhombahedral crystals are scattered uniformly throughout the unit. Areas close to these quartz veins would seem to have a strong silica bleaching. Surrounding these quartz veins acicular arsenopyrite is common.	<1	4	1	4	2	1	1	0	0.1	0.1	0.3
CL-061	11.72	23.51	116	Ash Tuff	Similar unit to previous with the consistent sericite bleaching still occuring. There is a greater density and intensity in terms of silica veins. This correlates to patches of greater arsenopyrite intensity with very fine, acicular arsenopyrite crystals common. These are randomly orientated. Fragile lithoclastic textures are visible and well preserved throughout the unit.	1	4	1	4	3	1	1	0	0.1	0.1	0.4
CL-061	23.51	32.85		Ash Tuff	Rounded lithic clasts generally replaced with fine crystaline sulphides are held within a bleached ash matrix. Unit as a whole remains similar to previous lithologies. Quartz-carbonate veins gradually become more abundant throughout the unit with thicker veins surrounded by sulphide arsenopyrite veins.	<1	4	1	4	3	3	3	0	0.1	0.1	0.5
CL-061	32.85	47.9	117 and 118	Ash Tuff	Increase in silica alteration throughout the unit. Large (5-10cm) quartz veins are more common and overprint the unit. Surrounding this are dense arsenopyrite veins. Unit has moe oxidation that is thought to be post mineralisation and due to quarternary fluids. This potentially marks a change towards a coarser unit with bomb size ejector clasts spordacially preserevered (sample 118). These show poor levels of deformation.	<1	4	2	4	4	2	2	0	0.1	0.1	0.6
CL-061	47.9	72.39	119, 120, 121 and 122	Lapilli Tuff	Much more complete silica flooding accompanied by whispy bendy sulphide veins. Silica largely overprints the matrix with a moderate oxidation marking any palaeo textures. Quartz veins are generally planar but do not nessecarily conform to foliation. In some instances they are noticed to bend around the lithic ejector clasts.	3	4	1	4	5	3	3	0	0.1	0.1	1.5
CL-061	72.39	95.1	123, 124, 125 and 126	Lapilli Tuff	Loss of silica alteration but continuation of sericite bleaching. The unit seems to be primarily an ash tuff with 2mm ejector beta quartz crystals common. Lithic clasts are generally replaced with fine crystaline sulphides and these show low intensity alteration. There is a gradual coarsening of the unit. As the unit coarsens the sytle of mineralisation changes; initially sulphides replace whole small (sub 5mm) clasts before forming thin sulphide veins enveloping bombs. Randomly orientated acicular arsenopyrite is frequently seen in the matrix throughout.	2	2	1	4	3	2	2	0	0.1	0.1	1
CL-113	51.3	62.39	127	Ash Tuff	Ash tuff with small (sub 5mm) lithic clasts replaced with fine crystaline sulphides.. These clasts are elongate but the unit as a whole does not seem to show overall levels of deformation or intense foliation. Sulphides are concentrated in these clasts but still present within the matrix of the unit. There is a strong and consistent sericite bleaching throughout the unit. There is minor silica alteration and quartz veining throughout but the unit does not seem to have shown an intense silica flooding. Very consitent throughout.	<1	4	1	4	2	1	1	0	0.1	0.1	0.4

Hole	From	To	Sample taken	Rock name	Description	Modal Clast size (mm)	Well sorted (1-5)	Foliation Intensity (0-5)	Sericite Alteration (0-5)	Silica Alteration (0-5)	Calcite Alteration (0-5)	Ankerite Alteration (0-5)	Chlorite Alteration (0-5)	Py (%)	Po (%)	Asp (%)
CL-113	62.39	71.59	128, 129 and 130	Lapilli Tuff	Ejector fragments have coarsened. As this has occurred the habit of mineralisation has changed with sulphide veins now forming around the larger clasts. These are typically elongate and have shown good examples of deformation in a consistent foliation plane. Protolith chemistry and alteration suites would seem to remain consistent with previous.	4	2	3	4	2	1	1	0	0.1	0.1	0.8
CL-113	71.59	88.08	131	Ash Tuff	Loss of mineralisation as protolith suddenly tightens with well sorted consistent felsic ash now dominating the unit. Intially oxidisation is fairly abundant but this soon drops off as ash content slowly increases. Alteration is very poor throughout. There is markedly less quartz veining and the unit now has a medium grey colour rather then the pale green sericite bleach. There is moderate foliation with occasional elongate clasts throughout the unit. Thought to represent aqueous processes.	<1	4	4	1	1	2	1	0	0.1	0.1	0.1
CL-113	88.08	97.76	132, 133 and 134	Conglomerate	Rounded clasts do not seem to show any alignement or imbrication. Occur in very small discreet package and are thought to represent erosion of palaeo tuff bed and re amalgamation of clats in channel fill conglomerate. Mineralisation appears to be largely absent but may be present and examined as a palaeoplacer occurance within the clasts.Unit has weak to moderate shear fabric towards the begining however this quickly turns to a well presearved conglomerate (sample 133). The whole unit has very poor alteration. Occsional minor silica veins.	5	1	2	1	1	1	1	0	0.1	0.1	0.1
CL-113	97.76	113.2	135 and 136	Lapilli Tuff	Change in unit towards more ash dominated tuff. Occssional lapilli sized clasts are often elongate. There is a minor sericite bleaching however this does not seem to be associated with mineralisation which remains minor throughout. Crosscutting ankerite veins are common as are smll patches of chlorite. Ejector fragments are common throughout and these range from beta quartz crystals to lapilli clasts and do not seem particularly consistent in their occurance	2	1	3	1	1	2	3	2	0.1	0.1	0.1
CL-118W1	113.2	900.79	137 and 138	Lapilli Tuff	Ash tuff with small lapilli sized clats sporadically present throughout. There is poor overall alteration with occasional quartz carbonate veins. There is occasional very fine crystalline disseminated arsenopyrite clasts and these tend to correlate with the patches of coarse lapilli tuff. Calcite veins are common however these seem to cross cut foliation. These do not accompany significant mineralisation but very fine crystaline arsenopyrite clasts are seen within the surrounding matrix. Foliation is moderate with elongate lapilli clasts best defining this.	1	4	1	2	1	3	2	1	0.1	0.1	0.3
CL-118W1	900.79	909.5	139	Lapilli Tuff	Much greater silica flooding and prevassive alteration. The unit has patchy bleaching. This creates banding concordant with elongation of small (sub 5mm) clasts. Small, thin carbonate veins parallel to foliation are common. There are very fine acicular arsenopyrite crystals throughout the unit that conform to foliation.	2	2	4	2	2	4	2	3	0.1	0.1	0.3
CL-118W1	889.91	884.38	140	Lapilli Tuff	Increase in carbonate alteration. Thick carbonate veins cross cut the unit and often show minor levels of post genetic deformation. These seem to generally exploit areas with greater sericite bleaching and fine crystaline acicular arsenopyrite can be generally seen within the matrix.	2	2	4	3	3	4	3	2	0.1	0.1	0.5

Hole	From	To	Sample taken	Rock name	Description	Modal Clast size (mm)	Well sorted (1-5)	Foliation intensity (0-5)	Sericite Alteration (0-5)	Silica Alteration (0-5)	Calcite Alteration (0-5)	Ankerite Alteration (0-5)	Chlorite Alteration (0-5)	Py (%)	Po (%)	Asp (%)
CL-117	844.66	838.81	161, 162 and 163	Ash Tuff	Much more prevelant banding. Sericite alteration now seems totally confined to follow paleo ash beds. Sericite alteration is now more patchy. Sericite alteration is not as intense or continuous which seems to have prevented the formation of previously seen sulphide veins. Silica alteration is now more prevelant with flooding of the matrix. This has allowed for the largest randomly orientated arsenopyrite crystals. Unclear whether foliation is a product of deformation or change in composition of protolith. Thick ankerite blebs common but not ubiquitous.	2	4	5	4	4	3	3	1	0.5	0.5	0.7
CL-117	838.81	825.37	164 and 165	Lapilli Tuff	Loss of alteration. Much fresher unit with poor foliation. 2-3mm clasts are common and held within ash tuff matrix. These usually appear fairly angular. Much less mineralisation and alteration which seems to remain very consistently poor. Ankerite and associated chlorite patches are fairly common. These would appear to be discordant and do not seem to be correlative with any mineralisation. Occasionally there is background fine crystaline arsenopyrite.	2	3	1	1	2	3	3	3	0.2	0.2	0.1
CL-117	825.37	813.07	166	Ash Tuff	Protolith remains similar however slightly greater sericite and carbonate alteration. Density of ejecor clasts seems to have decreased with ash matrix dominating the unit. Carbonate impregnation is now much stronger then previous and there are cross cutting calcite and carbonate veins. Clasts that are present have minor elongation and there is a slight banded texture. Mineralisation would seem to be poor	1	3	2	2	2	4	3	2	0.2	0.2	0.1
CL-117	813.07	800.19	167, 168, 169 and 170	Lapilli Tuff	Increase in size and abundance of ejector clasts although alteration and foliation remain similar. Clasts gradually largen towards bomb sized. These are well presearved and seem angular and usaully fairly undeformed. Weak to moderate sericite and carbonate alteration with common calcite veinletts throughout. There seems to be consistent fine arsenopyrite crystals thoughout the whole unit. These tend to correlate with the areas with elongate ejector clasts, a trait common in the unit shown by saimple 167 and 168.	3	2	3	2	1	3	3	2	0.1	0.1	0.3
CL-111	238.1	233.28		Lapilli Tuff	Dark grey tuff with lapilli sized (sub 5mm) ejector clasts. Clasts are typically angular and do not appear to show relationship with foliation. Occasionally foliation is stronger (small up to 20cm packages) and in these areas clasts become elongate. These areas typically have greater serectite alteration. Weak carbonate impregnation throughout. Grade and mineralisation is absent throughout	4	2	3	1	0	3	0	0	0	0	0
CL-111	233.28	228.74	1	Lapilli Tuff	Slightly more poorly sorted with lower density of lapilli sized fragments. Serecite bleaching is more common throughout the unit but preferentially stronger surrounding areas of greater sized lapilli fragments. These areas have later stage overprinted ankerite tension gashes. Foliation is not well developed however clasts usually show deformatio and have consistent orientation. There are discreet 10cm unfoliated packages correlative with poor serecite. Moderate carbonate alteration consistent throughout whole unit. No mineralisation	2	3	1	2	0	3	1	0	0	0	0
CL-111	228.74	218.92		Lapilli Tuff	Finer lapilli tuff with clasts of a consistent 3mm size held in a fine grained matrix. Clasts have consistent and more intense deformation and foliation throughout whole unit. Serecite alteration is much less intense. Ankerite veins at a consistent orientation overprint andf are oblique to orientation. These occur where foliation is at its weakest.	2	3	3	1	0	2	1	0	0	0	0

Hole	From	To	Sample taken	Rock name	Description	Modal Clast size (mm)	Well sorted (1-5)	Foliation intensity (0-5)	Sericite Alteration (0-5)	Silica Alteration (0-5)	Calcite Alteration (0-5)	Ankerite Alteration (0-5)	Chlorite Alteration (0-5)	Py (%)	Po (%)	Asp (%)
cl-111	218.92	215.65	2	Ash Tuff	Unit becomes finer grained with better sorting. Deformation is consistent. Possibly more distal system? Serecite bleacheing more uniform. There is now stronger overall serecite bleaching that is much more consistent. Within this there are stringers of fine crystaline pyrite. These are consistently parallel to foliation and would seem to be preferentially occur surronding individual beds of coarser detritus often containing ejector fragments. Small beta quartz crystals are visible throughout held within a fine grained felsic ash matrix. Two stages of carbonate veins pre and post deformation are visible. Post deformation cross cutting veins seem to have more of an ankerite composition.	1	4	4	3.5	0	3	3	0	0.1	0	0
cl-111	215.65	213.1	3 and 4	Jerocite Ash Tuff	As previous but with much greater carbonate and jerocite content. Moderate foliation stays consistent throughout the whole unit however carbonate abundance and jerocite content increases with younging. Stringer foliation parellel arsenopyrite crystals noticed preferentially occuring with the elevated carbonate. Interfingered silica veins begin to creep in towards the top of the unit.	1	4	4	2	1	3	5	0	0.2	0	0.1
cl-111	213.1	209.55	5 and 6	Quartz vein	Thick, mottled quartz vein. Milky white cores with dark grey blebs. More intense blebs dark grey areas have cores of jerrocite with potential rip up texture from previous unit. Contact is broken core throught to be more intese oxide layer below the quartz.	-1	-1	0	0	5	0	3	0	0	0	0
cl-111	209.55	202.59	7	Ash Tuff	Sharp transition out of quartz. One small instance of similar looking quartz vein 30cm into unit (sample 7). Fine grained felsic ash with small quartz ejector fragments common. Small ejector fragments (sub mm) common throughout. Foliation is consistent but fairly minor with and quartz crystals generally not showing elongation. Rounded quartz clasts indicative of ageous texture. Minor serecite bleaching common throughout. Very fine grained acicular aresenopyrite crystals are common. Occasional cross cutting pinkish carbonate vein	<1	5	2	3	1	1	1	0	0.1	0	0.2
cl-111	202.59	198.24	8 and 9	Lapilli Tuff	Increase in size of clasts with small ejector fragments much more common. Acicular arsenopyrite common and found in matrix of rock to a much greater extent then previous occuring preferentially in coarser, more poorly sorted packages. Would seem to be aligned parallel to foliation which is minor. Sub parallel quartz veins would seem to cross cut foliation(?) and seem correlative with the greatest grade. Blebs of pyrite common surrounding this. Ejector clasts do not seem elongate. Gradual evolution throughout the unit with coarser ejector clasts becoming more common	2	3	2	3	2	1	1	0	0.2	0	0.3
cl-111	198.24	182.21	10, 11, 12, 13	Lapilli Tuff	Serecite bleached unit very similar in protolith to previous. Foliation is well developed with potential ejector fragments showing deformation. Degree of alteration would seem variable. Small quartz veins (1cm) parallel to foliation accompany more altered areas are associated with acicular arsenopyrite and pyrite blebs (sample 10). These do not nessecarily seem to be the areas showing the strongest deformation (sample 11 shows good bleaching. common arsenopyrite) with clasts here seeming fairly rounded.	3	2	2	4	2	1	1	0	0.2	0	0.4

Hole	From	To	Sample taken	Rock name	Description	Modal Clast size (mm)	Well sorted (1-5)	Foliation Intensity (0-5)	Sericite Alteration (0-5)	Silica Alteration (0-5)	Calcite Alteration (0-5)	Ankerite Alteration (0-5)	Chlorite Alteration (0-5)	Py (%)	Po (%)	Asp (%)
CL-111	182.21	178.6	14 and 15	Lapilli Tuff	Similar in terms of composition to previous however large grey-white mottled quartz veins now are common. They seem to cross cut foliation. There look to be multiple generations of sulphides with pyrite embayed within and rimming the quartz. Arsenopyrite usually in its acicular form is found adjacent to this. In greater quantities then previous suggesting the quartz bears some responsibility for mineralisation. Quartz seems to be oblique to foliation but smaller veins seem broken by deformation. In one instance a deformed cross cutting ankerite vein has small pyrite inclusions.	2	4	3	4	4	1	1	0	2	0	0.6
CL-111	178.6	172.91		Ash Tuff	Greater developed foliation with less sericite bleaching and now with less quartz veining. Less mineralisation with sulphides not common. Some instances of small, cross cutting quartz veins. System seems more distal with smaller less common ejector clasts. Some small packages of larger angular ejector fragments occur in areas of slightly more intense sericitie bleaching.	1	4	4	3	2	1	0	0	0.1	0	0.1
CL-111	172.91	168.27	16	Bomb tuff	Conglomerate looking rock with sericitie bleaching. Foliation seems fairly poorly developed with clasts retaining a rounded perspective. Clasts seem to be meta-porphyry with occasional feldspar crystals still visible but largely overprinted with sericitie. Does not seem to be any mineralisation.	4	1	2	4	1	1	0	0	0.1	0	0
CL-111	168.27	160.7	17	Ash Tuff	Gradual transition to finer grained system. Unit is much more well sorted and more consistent. There small 5-10cm bands of oxidation (potentially sub arial system shut off). Foliation is well developed with elongate lapilli clasts common. Very limited mineralisation with occasional concordant quartz veins.	1	4	4	2	1	2	3	0	0	0	0
CL-111	238.1	233.28		Lapilli Tuff	Dark grey tuff with lapilli sized (sub 5mm) ejector clasts. Clasts are typically angular and do not appear to show relationship with foliation. Occasionally foliation is stronger (small up to 20cm packages) and in these areas clasts become elongate. These areas typically have greater sericitie alteration. Weak carbonate impregnation throughout. Grade and mineralisation is absent throughout	4	2	3	1	0	3	0	0	0	0	0
CL-111	233.28	228.74	1	Lapilli Tuff	Slightly more poorly sorted with lower density of lapilli sized fragments. Sericite bleaching is more common throughout the unit but preferentially stronger surrounding areas of greater sized lapilli fragments. These areas have later stage overprinted ankerite tension gashes. Foliation is not well developed however clasts usually show deformatio and have consistent orientation. There are discreet 10cm unfoliated packages correlative with poor sericite. Moderate carbonate alteration consistent throughout whole unit. No mineralisation	2	3	1	2	0	3	1	0	0	0	0
CL-111	228.74	218.92		Lapilli Tuff	Finer lapilli tuff with clasts of a consistent 3mm size held in a fine grained matrix. Clasts have consistent and more intense deformation and foliation throughout whole unit. Sericite alteration is much less intense. Ankerite veins at a consistent orientation overprint andf are oblique to orientation. These occur where foliation is at its weakest.	2	3	3	1	0	2	1	0	0	0	0
CL-111	218.92	215.65	2	Ash Tuff	Unit becomes finer grained with better sorting. Deformation is consistent. Possibly more distal system? Sericite bleacheing more uniform. There is now stronger overall sericite bleaching that is much more consistent. Within this there are stringers of fine crystaline pyrite. These are consistently parallel to foliation and would seem to be preferentially occur surronding individual beds of coarser detritus often containing ejector fragments. Small beta quartz crystals are visible throughout held within a fine grained felsic ash matrix. Two stages of carbonate veins pre and post deformation are visible. Post deformation cross cutting veins seem to have more of an ankerite composition.	1	4	4	3.5	0	3	3	0	0.1	0	0

Hole	From	To	Sample taken	Rock name	Description	Modal Clast size (mm)	Well sorted (1-5)	Foliation Intensity (0-5)	Sericite Alteration (0-5)	Silica Alteration (0-5)	Calcite Alteration (0-5)	Ankerite Alteration (0-5)	Chlorite Alteration (0-5)	Py (%)	Po (%)	Asp (%)
CL-111	215.65	213.1	3 and 4	Jerocite Ash Tuff	As previous but with much greater carbonate and jerocite content. Moderate foliation stays consistent throughout the whole unit however carbonate abundance and jerocite content increases with younging. Stringer foliation parellel arsenopyrite crystals noticed preferentially occuring with the elevated carbonate. Interflingered silica veins begin to creep in towards the top of the unit.	1	4	4	2	1	3	5	0	0.2	0	0.1
CL-111	213.1	209.55	5 and 6	Quartz vein	Thick, mottled quartz vein. Milky white cores with dark grey blebs. More intense blebs dark grey areas have cores of jerrocite with potential rip up texture from previous unit. Contact is broken core throught to be more intese oxide layer below the quartz.	-1	-1	0	0	5	0	3	0	0	0	0
CL-111	209.55	202.59	7	Ash Tuff	Sharp transition out of quartz. One small instance of similar looking quartz vein 30cm into unit (sample 7). Fine grained felsic ash with small quartz ejector fragments common. Small ejector fragments (sub mm) common throughout. Foliation is consistent but fairly minor with and quartz crystals generally not showing elongation. Rounded quartz clasts indicative of aqeous texture. Minor serecite bleaching common throughout. Very fine grained acicular aresenopyrite crystals are common. Occasional cross cutting pinkish carbonate vein	<1	5	2	3	1	1	1	1	0.1	0	0.2
CL-111	202.59	198.24	8 and 5	Lapilli Tuff	Increase in size of clasts with small ejector fragments much more common. Accicular arsenopyrite common and found in matrix of rock to a much greater extent then previous occuring preferentially in coarser, more poorly sorted packages. Would seem to be aligned parallel to foliation which is minor. Sub parallel quartz veins would seem to cross cut foliation(?) and seem correlative with the greatest grade. Blebs of pyrite common surrounding this. Ejector clasts do not seem elongate. Gradual evolution throughout the unit with coarser ejector clasts becoming more common Serecite bleached unit very similar in protolith to previous. Foliation is well developed with potential ejector fragments showing deformation. Degree of alteration would seem variable. Small quartz veins (1cm) parallel to foliation accompany more altered areas are associated with acicular arsenopyrite and pyrite blebs (sample 10). These do not nesscecarily seem to be the areas showing the strongest deformation (sample 11 shows good bleaching, common arsenopyrite) with clasts here seeming fairly rounded.	2	3	2	3	2	1	1	0	0.2	0	0.3
CL-111	198.24	182.21	10, 11, 12, 13	Lapilli Tuff	Similar in terms of composition to previous however large grey-white mottled quartz veins now are common. They seem to cross cut foliation. There look to be multiple generations of sulphides with pyrite embayed within and rimming the quartz. Arsenopyrite usually in its acicular form is found adjacent to this. In greater quantities then previous suggesting the quartz bears some responsibility for mineralisation. Quartz seems to be oblique to foliation but smaller veins seem broken by deformation. In one instance a deformed cross cutting ankerite vein has small pyrite inclusions.	3	2	2	4	2	1	1	0	0.2	0	0.4
CL-111	182.21	178.6	14 and 15	Lapilli Tuff	Greater developed foliation with less serecite bleaching and now with less quartz veining. Less mineralisation with sulphides not common. Some instances of small, cross cutting quartz veins. System seems more distal with smaller less common ejector clasts. Some small packages of larger angular ejector fragments occur in areas of slightly more intense serectite bleaching.	2	4	3	4	4	1	1	0	2	0	0.6
CL-111	178.6	172.91		Ash Tuff		1	4	4	3	2	1	0	0	0.1	0	0.1

Hole	From	To	Sample taken	Rock name	Description	Modal Clast size (mm)	Well sorted (1-5)	Foliation intensity (0-5)	Sericite Alteration (0-5)	Silica Alteration (0-5)	Calcite Alteration (0-5)	Ankerite Alteration (0-5)	Chlorite Alteration (0-5)	Py (%)	Po (%)	Asp (%)
CL-111	172.91	168.27	16	Bomb tuff	Conglomerate looking rock with serectie bleaching. Foliation seems fairly poorly developed with clasts retaining a rounded perspective. Clasts seem to be meta-porphyry with occasional feldspar crystals still visible but largely overprinted with serectie. Does not seem to be any mineralisation.	4	1	2	4	1	1	0	0	0.1	0	0
CL-111	168.27	160.7	17	Ash Tuff	Gradual transition to finer grained system. Unit is much more well sorted and more consistent. There small 5-10cm bands of oxidation (potentially sub arial system shut off). Foliation is well developed with elongate lapilli clasts common. Very limited mineralisation with occasional concordant quartz veins.	1	4	4	2	1	2	3	0	0	0	0
CL-118W	819.8	809.7		Ash Tuff	Fine grained, homogenous, very well sorted ash tuff. Potentially from distal or low energy system. Unit has poor foliation. Appears to have an aqeous texture with small rounded quartz fragments common throughout. Alteration is poor and there is no mineralisation. Small calcite veins cross cut foliation	<1	5	1	0	0	2	0	0	0	0	0
CL-118W	809.7	797.55		Ash Tuff	Similar protolith to previous unit- potentially slightly coarser then previous. Unit has undergone a very minor serecite bleaching that would appear to conform to foliation. This weak but slightly more evident then previous. Mineralisation is still poor. Slightly greater abundance of cross cutting calcite veins	<1	5	2	1	0	3	0	0	0	0	0
CL-118W	797.55	792.19	18	Ash Tuff	Serecite alteration now more common exploiting foliation in the unit. These often accompany concordant quartz veins and small instances of non acicular arsenopyrite. These tend to flank quartz veins. Gradually there is an increase in quartz veins and serectie alteration which becomes more and more consistent. Protolith remains fine grained ash however ejector fragments are now more common. Concordant and discordant ankerite veins are common throughout the unit.	1	4	3	3	3	3	1	0	0.2	0	0.3
CL-118W	792.19	785.76	19 and 20	Lapilli Tuff	Volcanic texture seems to mature towards slighty coarser more vent-proximal system. Enlongate clasts common with strong foliation. Fine grained sulphides replacing small (plagioclase?) phenocrysts within elongate ejector clasts. Accompanied by high levels of foliation with strong pervassive serecite alteration. Blocky quartz veins up to 5cm in width are fairly common. Smaller quartz veins are noticed to be parallel to foliation. Fairly consistent acicular arsenopyrite throughout the whole unit elevated abundance proximal to quartz veins. There are greater levels of stringer pyrite close to these quartz veins. Gradual evolution throughout the unit with an increase in serecite alteration and mineralisation throughout. Illustrated by samples 19 (start of the unit) and 20 (towards the end).	3	3	4	4	4	2	1	0	1	0.2	0.3
CL-118W	785.76	783.53	21	Lapilli Tuff	Alteration intensity and protolith composition remains similar however there is an increase in grade which seems to occur in areas of higher ankerite alteration. This cross cuts the previous lithology. Sample 21 shows a typical area of this. Mineralisation becomes more patchy and intense in these ankerite proximal areas	3	3	4	4	4	2	3	0	1	0.2	0.4
CL-118W	783.53	780.71	22	Lapilli Tuff	Foliation becomes narrower and straighter. Mineralisation is now fairly consistent as is serecite alteration. Ankerite altertion is less obvious however cross cutting calcite veins have curious relationship and may correlate with the greatest grade (sample 22). Similar protolith to previous and system does not seem to have evolved. Less quartz veins and silica alteration to previous.	3	3	4	4	3	3	3	0	2	0.5	0.5

Hole	From	To	Sample taken	Rock name	Description	Modal Clast size (mm)	Well sorted (1-5)	Foliation Intensity (0-5)	Sericite Alteration (0-5)	Silica Alteration (0-5)	Calcite Alteration (0-5)	Ankerite Alteration (0-5)	Chlorite Alteration (0-5)	Py (%)	Po (%)	Asp (%)
CL-118W	780.71	773.31	23	Lapilli Tuff	Abrupt change to very bleached unit. Whole but boudinaged quartz veins become much more abundant. Cross cutting ankerite veins are common. Flattened sub cm sized clasts would seem to be replaced by sulphides. Small quartz ejector fragments common within the whole unit. Flattened pyrite stringers are common in patches of less intense sericite bleaching. Variation in levels of deformation (sample 23 to test the concentration of gold related to texture). Towards the bottom of the unit mineralisation increases with acicular arsenopyrite very common and seemingly randomly orientated. There is an increase in deformation with broken core with pyrite coating fracture surfaces.	3	3	3	5	4	2	3	0	3	1	1
CL-118W	773.31	763.97	24	Lapilli Tuff	Sudden decrease in deformation. Rock now has a spotty, poorly sorted characteristic. Clasts are around 5mm in size and seem angular. Quartz crystals are common throughout and angular in appearance. Within the matrix arsenopyrite crystals are common and seem randomly orientated. Quartz calcite veins often cross cut foliation. Although quartz clast seems undeformed surrounding, softer clasts are flattened indicating deformation has occured but possibly less intense.	2	1	2	4	3	3	1	0	1	0.5	1
CL-118W	763.97	757.1		Ash Tuff	Loss of proximal vent facies. Well sorted fine grained ash. There still is consistent and strong sericite bleaching however mineralisation seems much less abundant with limited sulphides. This decreases as the unit youngs. Occsionall cross cutting quartz calcite vein.	<1	4	2	4	2	2	1	0	0.5	0.1	0.4
CL-118W	757.1	753.24	25 and 26	Quartz-Lapilli Tuff	Reactivation of system. Sudden appearance of ejector fragments appearing angular and poorly sorted. Quartz veins are very common and strong throughout the unit. Increasing in abundance and eventually forming an apron overlying and including (possible rip up clasts) underlying felsic ash. Between these quartz veins are fine grained arsenopyrite veins appearing wavy and deformed.	1	2	4	3	5	1	1	0	2	1	3
CL-118W	753.24	739.5	27	Ash Tuff	Fine ash tuff. Unit has imideiatly lost its foliation and sericite bleaching. There is a loss of the coarse ejector fragments with a much finer well sorted unit. Mineralisation is now absent. A cyclical pattern can often been seen with a gradual evolution and fining of the facies however mineralised pathways are absent. There are occasional cross cutting calcite veins usually boudinaged. End of domain 4.	<1	5	3	2	1	1	1	0	0.1	0	0.1
CL-090	400	395.45		Quartz-Conglomerate	Heavily bleached sericite with clasts. Strict foliation seems to be absent with an altered breccia common. Slow bleed into quartz rich zones with small quartz veins with sharp boundaries cross woven between clasts. Transition from ash to violence into large quartz veins.	6	1	2	4	5	1	1	0	0.1	0.1	2
CL-090	395.5	393	28 and 29	Ash Tuff	Similar but without strong quartz alteration. Dominated by fine grained ash without rounded brecciation. Cognate lithic fragments are still common and hjave intense sericite bleaching. Small quartz veins seem to have fine grained arsenopyrite rims and appear folded (sample 29). Quickly develops into broken core presumed fault related	2	2	0	4	2	2	1	0	1	0.5	1

Hole	From	To	Sample taken	Rock name	Description	Modal Dast size (mm)	Well sorted (1-5)	Foliation Intensity (0-5)	Sericite Alteration (0-5)	Silica Alteration (0-5)	Calcite Alteration (0-5)	Ankerite Alteration (0-5)	Chlorite Alteration (0-5)	Py (%)	Po (%)	Asp (%)
CL-090	393	389.2		Fault	Broken core. Similar composition to previous however broken core	2	2	0	4	2	2	1	0	1	0.5	1
CL-090	389.2	384	30	Ash Tuff	Ash tuff with pervassive serecite alteration and strong silica alteration. Begins with white-black, very mottled quartz vein before a dark grey silica alteration overprints the whole unit. Foliation is largely absent rather a hydrothermal brecciated texture would seem to dominate. Patchy consistency with breaks in breciation replaced by foliation and stronger serecite alteration. Within these areas there would seem to be more concordant ankerite veins.	1	2	2	3	5	1	2	0	1	0	0.5
CL-090	384	381.21	31	Lapilli Tuff	Poorly sorted cognate lithic tuff. Foliation is now much more obvious and the unit has lost its strong silica overprint. Serecite alteration remains prevelent. Foliation is apparent with concordant ankerite veining. These tend to rim concordant quartz veins (31) and only occur proximal to silica veins. There is limited mineralisation with pyrite and pyrrhotite but small levels of arsenopyrite.	2	2	4	3	3	1	3	0	0.2	0.1	0
CL-090	381.21	371.61		Lapilli Tuff	Change towards a moderatley silica altered unit. Dark grey silica alteration seems to impregnate and overprint most of the unit. Serecite alteration and mineralisation is much weaker then previous. Unit conitnues as this and is patchy in its consistency throughout. Elongate ejector fragments are coommon.	3	1	2	2	3	2	2	0	0.2	0.1	0
CL-090	371.61	359.69	32	Lapilli Tuff	Foliation is now more visible and the unit has a bleached serecite appearance. Fluid pathways show movement along foliation with quartz veins common. Occasional bomb size ejectors also show serecite bleaching. Angular ejector fragments are common and although there is a good degree of serecite bleaching they do not seem to have shown much compression. Occasional small ankerite veinletts cross cut the foliation. Very consistent in appearance and grade throughout	2	2	4	3	1	1	2	0	1	0.1	0
CL-090	359.69	358.4	33	Quartz vein	Quartz blanket. Mottled and grey-bright white in appearnace similar to the other veins seen to overlie domain 4. Does not seem to have any lithic inclusions. Coarse pyrite can be seen within the sample (33)				0	5	0	0	0	2	1	1
CL-090	358.4	344.7	34 and 35	Ash Tuff	Moderatly serecite altered foliated ash tuff. Mineralisation is much less apparent. There is a decrease in mineralisation with the quartz vein seemingly indicative of gold genesis shuf off. Cross cutting ankerite veins are common and in one instance (sample 35) a 2cm thick arsenopyrite vein	1	4	4	2	1	2	2	0	0.1	0.1	0
CL-090	344.7	339.27		Bomb tuff	Change to more vent-proximal or more violent lithofacies. Bleached and altered 5cm sized ejector clasts are common with a whole-bleached serecite matrix. Foliation is not as intense as previous. There is poor mineralisation throughout.	4	1	2	3	1	1	2	0	0.5	0.1	0
CL-090	339.27	325.01	37	Bomb tuff	Sudden increase in silica impregnation. Black quartz is common throughout and mineralisation is notably higher. Thick 10cm diameter bombs are common and usually heavily bleached. Occasionally small felsic phenocrysts are apparent. Unit has a moderate to strong serecite alteration. The most intensely deformed areas show very limited arsenopyrite mineralisation. Clasts are all elongate in a consistent direction. Sample 37 shows the best example of mineralisation within this unit	5	1	3	4	4	2	1	0	1	0.5	0.1

Hole	From	To	Sample taken	Rock name	Description	Modal Clast size (mm)	Well sorted (1-5)	Foliation intensity (0-5)	Sericite Alteration (0-5)	Silica Alteration (0-5)	Calcite Alteration (0-5)	Ankerite Alteration (0-5)	Chlorite Alteration (0-5)	Py (%)	Po (%)	Asp (%)
CL-088	344.12	348.2	90 and 91	Silica tuff	Flooding of matrix with silica. This appears within the foliation however is broken. Sericite alteration remains constant and there is good mineralisation throughout. Acicular pyrite is common and, in areas of intense silica wavy arsenopyrite veins are common (sample 90). There seems to be a faint outline of foliation which is obvious in patches of weaker silica where sericite ash appears similar to previous lithology. Where protolith does appear it seems to be elongate and heavily deformed. Silica flooding appears to gradually decrease through the unit.	1	3	2	4	5	1	1	0	1	1	3
CL-088	348.2	357.09	92	Lapilli Tuff	Decrease in silica flooding. Sericite alteration still remains stong with the rock inccuring a pale green bleached look. Small lithic clasts are common throughout the unit. There are thin, very fine crystaline sulphide replaced clasts common throughout the unit. These cause a foliated fabric. Quartz and ankerite veins commonly cross cut foliation.	2	3	3	4	2	3	3	0	0.5	0.5	0.3
CL-088	357.09	363.19	93	Ash Tuff	Gradual decrease in alteration intensity and composition and texture of protolith becomes more obvious.There are occasional thick (up to 5cm ejector fragments) shown by sample 93. Phenocrysts within these clasts often seem replaced by fine crystaline sulphides. Small later stage liquid textures of chlorite are occasionally visible. There are small stringers of fine crystaline pyrite throughout the unit.	<1	4	3	2	2	2	2	1	1	1	0.1
CL-088	363.19	368	94 and 95	Lapilli Tuff	Similar unit with notable increase in carbonate alteration. These generally conform with foliation. The protolith imidiatly coarsens to a sub cm size lapilli tuff. These clasts seem elongate but do not seem to show a high degree of elongation.A single area here has the coarsest clasts and is surrounded by acicular arsenopyrite that seem randomly orientated even though there is a prevelant foliation direction from the clast elongation (sample 94).	<1	4	2	4	1	4	4	1	1	1	1.5
CL-088	368	370.68	96 and 97	Bomb tuff	Much larger 10cm bomb tuff. These are largely altered with an aggressive sericite overprinting. Angular quartz clasts are preserarved within this unit. Well foliated planer ash beds underlie these clasts however overlying these are more contorted beds (potentially syn-deposition). These preferntially have greater levels of ankerite alteration and small acicular arsenopyrite crystals (sample 96). Seicite bleaching is patchy throughout the whole unit but usually fairly intense. Pyrite in small stringers foliation parallel are common in the ash rich layers (sample 97).	<1	1	2	4	1	2	3	0	1	1	1
CL-088	370.68	395.3	98 and 99	Lapilli Tuff	Unit becomes very patchy in appearnace and lacks consitency. 10cm scale changes from well sorted fine grained ash to large bomb clasts with small quartz phenocrysts are common. A moderate foliation overprints the whole unit and causes distinct styles of mineralisation. Fine grained ash is commonly associated with small blebs of pyrite and pyrrhotite. When coarser ejector clasts are found, acicular arsenopyrite clasts can be found (sample 99). Alteration would seem to vary throughout the unit with original clasts occasionally well presearved. This is illustrated by sample 98.	<1	1	3	3	2	2	2	0	1	1	0.1
CL-102	315.06	324	100 and 101	Lapilli Tuff	Lapilli tuff with well preserarved angular clasts. Bleaching and mineralisation is very poor throughout (illustrated by sample 100). Small bands of sericite exist and these tend to exhibit the areas with the coarsest beds and (5cm size). These bands conform with foliation with fine crystaline acicular arsenopyrite clasts (sample 101).	4	2	1	2	1	0	0	0	0.1	0.1	0.1
CL-102	309.47	315.06	102 and 103	Lapilli Tuff	Sudden increase in sericite bleaching. This does not seem to exploit a sudden change in protolith. Lapilli clasts show minor deformation. Whereas sericite alteration would seem to be consistent the degree of deformation would seem to change throughout. There is poor mineralisation. Even though there is a greater degree of deformation then previous units there is little evidence of mineralisation suggesting they may not be correlative.	3	2	2	3	1	1	1	0	0.1	0.1	0.1

Hole	From	To	Sample taken	Rock name	Description	Modal Clast size (mm)	Well sorted (1-5)	Foliation intensity (0-5)	Sericite Alteration (0-5)	Silica Alteration (0-5)	Calcite Alteration (0-5)	Ankerite Alteration (0-5)	Chlorite Alteration (0-5)	Py (%)	Po (%)	Asp (%)
CL-088	293.66	302.95	80	Lapilli Tuff	Greater bleaching- rock is a paler colour. There is a transition into a broken more brecciated texture. Mostly composed of elongate sub cm lithic clasts. There is poor alteration and there does not seem to be a large extent of sulphide replacement or mineralisation. Cross cutting ankerite veins are common.	2	3	2	2	2	2	4	0	0.1	0.1	0.1
CL-088	302.95	311.41		Ash Tuff	Similar to initial unit. There is there a drop in sericite alteration as fine grained ash now dominates the unit. There are occasional silica clasts. Small clasts are usually flattened consistent with minor foliation. There is poor mineralisation with small isolated examples of pyrite.	<1	5	2	2	1	2	2	0	0.1	0	0
CL-088	311.41	322.5	81	Lapilli Tuff	Coarser and more obvious ejector fragments abundant. These all show deformation in one consistent plane. There is a much heavier sericite bleaching throughout the unit. Silica alteration does not seem to impregnate the rock with poor silica veins. Small clasts of arsenopyrite are visible throughout the whole rock and do not seem to show any orientation. There does not seem to be any other visible mineralisation. Small patches of chlorite are occasionally visible. There is an overall carbonate bleaching.	<1	2	2	4	2	2	2	1	0	0	0.1
CL-088	322.5	327.88	82 and 83	Lapilli Tuff	Gradual increase in alteration. A silica alteration gradually becomes apparent. There is a slow change in protolith with larger lithic clasts becoming more abundant and ejector quartz frequent. A sericite bleaching gradually overprints the unit. Clasts are not overly elongate but do show deformation texture contributing to a moderate foliation. Very fine crystaline arsenopyrite is abundant within the unit in a similar mineralisation style to previous unit. Mineralisation density is thought to gradually increase in density thoughout the unit.	2	2	3	4	3	3	2	0	0	0	0.2
CL-088	327.88	333.07	84 and 85	Quartz-Lapilli Tuff	Sudden increase in silica alteration as quartz veins become prevelant within the unit. Aggressive grey/white quartz veins dominate the unit. These are interupted by 10cm patches of intensly sericitcally altered rock (sample 84). These areas have intense foliation that would seem to be overprinted by hydrothermal brecciation. Mineralisation seems to preferentially occur on the younger side of the quartz vein. There does not appear to be obvious intense mineralisation however localised areas have acicular arsenopyrite aligned with foliation. Protolith would have appeared to be of a similar composition to previous. Ankerite veins become very common towards the bottom of the unit.	2	2	4	4	5	2	3	2	0.1	0.1	0.2
CL-088	333.07	344.12	86, 87, 88 and 89	Ash Tuff	Largre silica and carbonate veining diminish however sericite alteration remains stong and prevelant. The unit has a high foliation intensity. Thin 5mm quartz veins parallel to foliation are common throughout. There is good mineralisation with acicular arsenopyrite common throughout. Occasionally these appear wormy usually accompanied by the strongest mineralisation. This would appear to correlate with the areas of coarser (up to 2cm lithic fragments (sample 86)). Small sub 0.5cm ejector fragments are common throughout the unit. Lithic fragments (corresponding with good grade) to not appear to show very intense deformation. Acicular arsenopyrite accompanies areas of greater clasts size whereas fine hollocrystaline rhomoheadral arsenopyrite is generally found throughout the unit.	1	3	5	5	4	2	2	0	0.5	0.5	1

Hole	From	To	Sample taken	Rock name	Description	Modal Clast size (mm)	Well sorted (1-5)	Foliation Intensity (0-5)	Sericite Alteration (0-5)	Silica Alteration (0-5)	Calcite Alteration (0-5)	Ankerite Alteration (0-5)	Chlorite Alteration (0-5)	Py (%)	Po (%)	Asp (%)
C565-082	260.32	251.82	67, 68 and 65	Ash Tuff	Spotty rock with ankerite spots common throughout the unit. There appears to be a complete flooding of the matrix with iron carbonate. These appear to be compressed along the axis of deformation (sample 67). Where this is the case acicular arsenopyrite parallel to this foliation is often visible (sample 69). Protolith appears to be fine grained ash with palaeo lithic clasts accompanying the areas of greater mineralisation. Isolated areas of more intense ankerite altartion are flanked by silica veins and then the most intense arsenopyrite seen within this interval (sample 68).	<1	4	4	2	3	3	4	0	1	1	1.5
C565-082	251.82	234.18	70	Ash Tuff	Similar unit to previous however with sericite alteration more apparent. Foliation is more pronounced and ankerite veins more common. Mineralisation is not as intense as previous but is consistent throughout the unit. Sample 70 shows typical style.	<1	4	4	3	3	3	4	0	0.5	0.5	0.8
C565-082	234.18	228.48	71, 72 and 73	Ash Tuff	Unit looses its intense carbonate alteration and instead has much greater silica and sericite alteration. Concordant silica veins are common and often replaced with arsenopyrite (sample 71). There is consistent intense mineralisation throughout the whole unit with all of the veins concordant with foliation. Unit cumulates in patch of more intense carbonate alteration although this does not seem to correlate to grade (sample 73)	<1	5	4	5	4	2	3	0	0.2	0.2	5
C565-082	228.48	218.39	74, 75 and 76	Quartz-Lapilli Tuff	Gradual decrease in carbonate alteration while sericite alteration and silica alteration intensifies. In its most intense quartz veins become saturated and wormy within totally altered sericite rock (similar to 271-265) illustrated by sample 75. Leading into this foliation becomes defined by concordant quartz and sulphide veins (sample 74). 1-2cm ejector clasts are common but usually overprinted by sericite alteration.	5	1	4	5	4	2	3	0	1	1	4
C565-082	218.39	215.32	77	Quartz vein		N/A	N/A	0	0	5	0	0	0	0	0	0
C565-082	215.32	206.97	78	Lapilli Tuff	Black, mottled quartz vein that typically overlies domain 4. Seen previously. Sampled 77 should test continuity. Abrupt switch on of system above quartz vein. Mineralisation would still seem to be abundant however gradually diminishes as the system fines. Mineralisation style changes from sulphide veins surrounding clasts, to gnerally foliation parallel acicular arsenopyrite. This corresponds to dimishing sericite alteration. Ankerite alteration is present with foliation parallel thin veinletts throughout the unit.	2	2	4	3	3	3	3	0	1	1	1.5
C565-082	206.97	199.22		Ash Tuff	Slow loss in mineralisation. Unit gradually dominated by fine grained ash. Mineralisation, sericite, silica alteration gradually diminish. Carbonate alteration would seem to remain throughout. Similar relationship to that seen in previous drill holes along section.	1	5	3	2	2	2	2	0	0.2	0.2	0.1
CL-088	283	293.66	79	Ash Tuff	Felsic ash tuff. Very continuous in appearance. Poor alteration and mineralisation. Composition varies throughout with small patches of coarser ejector fragments although this does not seem to alter mineralisation or alteration. These often appear elongate however there is no prominent foliation texture. Cross cutting calcite-ankerite veins are common and occur in greater magnitudes and densities surrounding patches of slight bleaching. Minor silica flooding.	2	3	2	1	2	2	2	0	0.1	0.1	0.1

Hole	From	To	Sample taken	Rock name	Description	Modal Clast size (mm)	Well sorted (1-5)	Foliation intensity (0-5)	Sericite Alteration (0-5)	Silica Alteration (0-5)	Calcite Alteration (0-5)	Ankerite Alteration (0-5)	Chlorite Alteration (0-5)	Py (%)	Po (%)	Asp (%)
C565-050 (Part 1)	137.15	129.96	S3	Ash Tuff	Most of the core consumed by Seabridge for HPGR tests. Assumed to be patches of more intense silica alteration corresponding to grade. Remaining rock appears very similar to previous unit with a slight increase in frequency of small quartz veins and small areas of alteration visible.	<1	5	3	3	3	2	3	0	0.1	0.1	0
C565-050 (Part 1)	129.26	114.78	S4, S5, S6 and S7	Quartz-Ash Tuff	Large blocky quartz veins intrude into ash tuff. Quartz is mottled and dark grey with liquid-texture arsenopyrite rich inlcusions (sample 55). Quartz veins domianate the unit but in there absence foliated ash tuff is visible with strong sereicite bleaching with acicular arsenopyrite and small sulphide-replaced clasts (sample 54). Quartz veins seem to cross cut folation and are associated with spots of broken ankerite.	<1	5	3	4	5	3	3	0	1	0.5	2
C565-082	279.81	274.56		Ash Tuff	Fine grained ash. Foliation is apparent exposing paleo bedding planes. There are occasional rounded quartz crystals which would indicate aqueous reworking processes. There is poor alteration throughout and very occasionally and mainly towards the bottom of the unit, small arsenopyrite crystals are visible. Pyrite and pyrrhotite are commonly seen in association.	<1	5	3	2	1	1	1	0	0.2	0.2	0.2
C565-082	274.56	271.57	58, S9 and 60	Ash Tuff	Foliation becomes more obvious. The unit has a sericite bleaching throughout and a silica flooding. There is much better mineralisation with acicular arsenopyrite conforming to foliation. Broken quartz veins are seen throughout. Sericite alteration gradually increases throughout the unit with arsenopyrite habit changing from isolated disseminated acicular arsenopyrite (sample 58) to small sulphide replaced clasts (sample 59) to arsenopyrite veins and flooding (sample 60). Acicular arsenopyrite would here mainly seem to conform to foliation. Protolith seems to be very similar to previous unit with occasional rounded quartz clasts held in fine grained ash.	<1	5	3	4	4	4	2	2	0	1	1	3
C565-082	271.57	265.85	61, 62 and 63	Quartz-Ash Tuff	As alteration increases there is a gradual change towards a more aggressive, wormy texture. Embayed quartz is common with the protolith showing very strong sericite alteration.Quartz veins are embayed throughout the rock and have a mottled white-grey colour. Host rock shows extreme sericite alteration with host rock completely altered with the exception of small, usually rounded, ejector quartz clasts. Previous to the most intense areas of quartz there are thin, wormy arsenopyrite veins (sample 61). Surrounding the quartz is randomly orientated acicular arsenopyrite (sample 62). Quartz density increases throughout the unit cumulatiung in m-wide vein (sample 63) (toatally consumed by Seabridge).	<1	5	1	5	5	5	1	1	0	1	1	5
C565-082	265.85	260.32	64, 65 and 66	Lapilli Tuff	Abrupt change from quartz vein to well foliated, fine grained ash unit. Rounded quartz clasts are common throughout the unit. Clast size generally increases throughout the unit grading into elongate lithic fragments. Although alteration would appear to be consistent throughout the unit, surrounding coarser ejector clasts more acicular arsenopyrite, usaully confroming to foliation is noticed. This difference is shown by sample 64 and 65. Clasts are elongate and show an obvious and consistent deformation. Small quartz veins often cross cut the foliation. Carbonate alteration is now prevelant with spots and concordant ankerite veins. Patches of ankerite are common.	1	2	3	4	3	2	2	2	0			

Hole	From	To	Sample taken	Rock name	Description	Modal Clast size (mm)	Well sorted (1-5)	Foliation Intensity (0-5)	Sericite Alteration (0-5)	Silica Alteration (0-5)	Calcite Alteration (0-5)	Ankerite Alteration (0-5)	Chlorite Alteration (0-5)	Py (%)	Po (%)	Asp (%)
C565-006	59.97	43.78	43	Ash Tuff	Similar composition however foliation is less obvious (possibly finer grained with less elongate clasts causing less obvious foliation). There is a much stronger sericite bleaching with quartz veins of varying sizes common. Quartz veins do not seem to correspond and often cross cut foliation. Illustrated by sample 43. Acicular arsenopyrite is commonly found proximal to the quartz veins. Carbonate alteration is common throughout.	1	4	2	4	2	2	2	0	0.1	0.1	0.3
C565-006	43.78	30.53	44	Lapilli Tuff	Ejector fragments are much larger and much more common. There is a much larger degree of alteration with quartz veins more common and a dark red iron carbonate (oxide post drilling??) flooding the unit causing soft and broken core. Mineralisation is more abundant and arsenopyrite is especially apparent in small sub mm sulphide veins forming the matrix around undeformed clasts (sample 44). Ejector beta quartz fragments are common throughout the unit.	4	2	1	3	1	4	4	0	1	0.5	0.8
C565-006	30.53	21.71	45, 46 and 47	Ash Tuff	Return to sericite bleached ash tuff. Small ejector quartz fragments common with angular quartz. Small clasts are visible throughout and show well developed foliation. The smallest of clasts seem to have been replaced by fine grained sulphides (sample 45 and 46). There is moderate iron carbonate flooding with the core having a rusty red overprint. Grade would seem to be patchy throughout. Sample 47 shows example of non grade for comparison	<1	4	3	3	3	4	4	0	1	0.5	0.7
C565-006	21.71	15.05	48 and 49	Lapilli Tuff	Ejector clasts would seem larger but show consistent moderate foliation. Mineralisation would seem to be similar to 43-30 with clasts with fine grained sulphides as well as sulphide veins within the matrix (sample 48). Alteration would seem to be consistent with previous with potentially greater ankerite alteation and more common and abundant veining. There are patches of more intense mineralisation that flank thick 5cm quartz veins.	3	2	3	3	4	4	4	0	2	1	1.5
C565-006	15.05	11.1		Ash Tuff	Slow transition towards an ash tuff with clasts becoming less abundant and eventually absent. An iron carbonate staining is heavy towards the top of unit but gradually diminishes. Small concordant quartz veins are common however gradually decrease in abundance. Acicular arsenopyrite surrounds these veins. Foliation is moderate.	2	4	2	3	3	3	3	0	1	0.5	0.8
C565-050 (Part 1)	165.48	150.28	50 and 51	Felsic Flow	Angular (up to 5mm) feldspar and quartz phenocrysts seemily not part of bomb sized clasts composed mainly of silic material (quartz and feldspar). Occasional 5cm serectie bands throughout the unit. Alteration would seem to be minor. Angular crystals are held within a dark grey matrix with little imbrication or alignment. Towards the top of the unit there is a fining of the crystals and possible evidence of rip up clasts (sample 50). There are occasional parallel ankerite veins that give the unit a foliation. These are consistent with the direction of the slightly sericite bleached areas throughout. Decompression and expression of bedding is not visible.	N/A	N/A	1	2	2	2	3	0	0.1	0.1	0
C565-050 (Part 1)	150.28	137.15	52	Ash Tuff	Gradual transition from felsic flow to ash tuff. This begins with a mixed melange-like texture and the gradual increase in rip up clasts and an increase in density and decrease in size of felsic phenocrysts. Sericite texture and bleaching is more apparent. Gradually changes into a fine grained well foliated ash with common beta fragments and foliation. Small quartz veins are common with spotty ankerite alteration usually accompanying this. Mineralisation is generally very poor. With oxidised sulphides adjacent to the areas of greater altartion.	<1	5	3	3	1	2	3	0	0.1	0.1	0

Hole	From	To	Sample taken	Rock name	Description	Modal Clast size (mm)	Well sorted (1-5)	Foliation Intensity (0-5)	Sericite Alteration (0-5)	Silica Alteration (0-5)	Calcite Alteration (0-5)	Ankerite Alteration (0-5)	Chlorite Alteration (0-5)	Py (%)	Po (%)	Asp (%)
CL-090	325.01	319.12		Ash Tuff	Fine grained ash with intense serecite bleaching. Unit coarsens with ejector fragments becoming more and more common gradually heading towards a lapilli sized tuff. As clast size increases quartz veins become more common. There does not appear to be intense deformation with slight elongation of these clasts but no intense fragments. Small broken ankerite veins are common.	2	3	2	4	2	1	2	0	1	5	0.1
CL-090	319.12	314.8	38	Lapilli Tuff	Increase in abundance of clasts and flooding of silica. Mineralisation appears to be much greater. Unit does not seem to show heavy deformation. There appear to be multiple stages of silica generation indicated by sample 39. Heavily serectite bleaching consistent with previous unit. Foliation is fairly poor. There is good consistent mineralisation with acicular arsenopyrite common.	4	1	2	4	4	1	2	0	3	1	0.3
CS65-050 (Part 2)	114.78	106.67	39	Lapilli Tuff	Well foliated, serecite bleached unit. Quartz veins parallel to foliation are common. More intense areas have more complete silica flooding with boudinaged discordant quartz veins. Unit has moderate deformation textures. Thick quartz veins seem to have been common but core is missing. These accompany the areas showin the greatest degree of deformation and correlate with an increase in ejector clast size with lapilli fragments rather then fine grained ash. Mineralisation is good and especially common rimming the quartz veins.	1	5	3	4	4	2	2	0	1	2	0.3
CS65-050 (Part 2)	106.67	94.83	40	Ash Tuff	Smooth transition following quartz vein to fine grained, well foliated felsic ash unit. Foliation consistent and unifrom throughout with fine grained ash well sorted. Multiple examples of small concordant quartz veins with proximal mineralisation. Arsenopyrite mineralisation is often proximal to small quartz veins (illustrated by sample 40). Usually acicular however not abundant in appearance.	<1	5	4	4	3	2	2	0	2	1	0.5
CS65-050 (Part 2)	94.83	86.15	41	Lapilli Tuff	Alteration is similar however increase in lithic fragments throughout the whole unit. Foliation alteration is thought to be similar however more pronounced with clasts showing elongate textures. Carbonate alteration is more intense but is now largely oxidised (old core). Between clasts fine crystaline arsenopyrite seems to reflect paleofluid pathways. These are not nessasenily lined with silica. Mineralisation would seem to have increased in abundance within this unit (sample 41).	4	2	4	4	3	3	3	0	2	1	0.8
CS65-050 (Part 2)	86.15	62.48	42	Ash Tuff	Foliated ash tuff similar to 106-94. Patchy and occasional appearance of large quartz veins. Quartz veins appear black-white and are generally flanked by areas of weak to moderate pre-deformation ankerite. Small isolated lithoclasts appear elongate and there is a consistent and heavy foliation throughout. Mineralisation is evident throughout but does not appear to be omnipresent.	<1	5	5	3	3	2	4	0	1	0.4	0.1
CS65-006	70	59.97		Ash Tuff	Ash dominated unit with moderate foliation. There is moderate serecite bleaching and a consistnet appearance of moderate serecite bleaching. Samll sub cm sized ejector fragments are unifromly common throughout the unit and usaully elongate. There is moderate carbonate alteration with ankerite veins common.	1	4	4	2	1	0	3	0	0.2	0.2	0.1

Hole	From	To	Sample taken	Rock name	Description	Modal Clast size (mm)	Well sorted (1-5)	Foliation intensity (0-5)	Sericite Alteration (0-5)	Silica Alteration (0-5)	Calcite Alteration (0-5)	Ankerite Alteration (0-5)	Chlorite Alteration (0-5)	Py (%)	Po (%)	Asp (%)
CL-102	309.47	303	104 and 105	Lapilli Tuff	Increase in silica flooing of unit. This would seem to manifest in an overall overprint rather then quartz veins. The protolith remains similar to previous unit with small up to 4mm sized, angular clasts common throughout the unit. Blebs of arsenopyrite are common within the unit. Changes in aspect ration indicating clast deformation intensity does not seem to correlate with silica alteration. Small areas of greater chlorite alteration are often visible.	3	2	3	3	3	2	2	1	0.1	0.1	0.1
CL-102	303	288.12	106 and 107	Lapilli Tuff	Very consistent aletation and mineralisation (weak to moderate sericite and poor mineralisation) throughout. Consistent slightly elongate 0.5cm diameter ejector clasts occur througout. There are occasionally slightly more elongate clasts and these would seem to correlate with areas of greater brecciation. This would also seem to be ther coarsest clasts.	3	2	2	2	2	2	3	0	0.1	0.1	0.1
CL-102	288.12	282.62	108, 109, 110 and 111	Lapilli Tuff	Greater sericite intensity with a consistent overall bleaching. Foliated beds are often noticed where ash dominates the unit. There are slightly elongate clasts in areas domianted by sub 0.5cm sized lapilli fragments. Pervassive quartz veins often parallel to foliation however occasionally cross cutting and boudinaged. These would not seem to be associated with great mineralisation typically seen with this much silica. The most intense areas would seem to have accompanying arsenopyrite.	3	2	3	3	2	2	2	0	0.1	0.1	0.5
CL-102	282.62	275.61	112	Lapilli Tuff	Silica alteration is still apparent but becomes much more patchy. There is a decrease in the foliation intensity and an increase in the density of angular, 0.5cm sized ejector clasts. Small acicular arenopyrite clasts commonly accompany areas of greater sericite bleaching. These would appear to mostly overprint lapilli clasts that seem to have retained their proto-eliptical shape. These areas surround thin confromant quartz veins.	3	2	2	4	2	1	1	0	0.1	0.1	0.4
CL-102	275.61	267.34	113	Ash Tuff	Much more intense foliation and loss of lapilli clasts with the return of ash tuff. Coarser areas with elongate clasts would seem to be accompanied by greater flooding of silica and a greater density of quartz veins. Pervassive silica alteration would seem to overprint most of the unit. The unit has lost its more intense sericite bleaching. Much greater deformation throughout. Arsenopyrite is common throughout the unit and would seem to correlate with the coarser, more silica rich areas. There are small patches of carbonate alteration.	1	3	4	2	3	1	1	0	0.1	0.1	0.3
CL-102	267.34	261		Lapilli Tuff	Gradual coarsening of unit with lapilli clasts now visible. Unit has lost its alteration with sericite and silica impregnation mostly absent. There are small areas of carbonate alteration however these would not seem to correlate with mineralisation.	4	2	2	1	1	2	3	0	0.1	0.1	0.1

Hole	From	To	Sample taken	Rock name	Description	Modal Clast size (mm)	Well sorted (1-5)	Foliation intensity (0-5)	Sericite Alteration (0-5)	Silica Alteration (0-5)	Calcite Alteration (0-5)	Ankerite Alteration (0-5)	Chlorite Alteration (0-5)	Py (%)	Po (%)	Asp (%)
CL-118W1	884.38	874.5	141, 142 and 143	Lapilli Tuff	Loss of carbonate veining. Unit does however have a moderate and fairly consistent sericite bleaching throughout. Elongate ejecotr clasts are visible throughout. Arsenopyrite would seem to correlate with areas of greater sericite bleaching however in the less aletered, usaully ash rich areas pyrite stringers are visible. Foliation is poor and with cross cutting veins common, not always obvious. Serecite banding and alteration would seem to show consistent orientation.	2	2	2	3	3	3	2	2	0.3	0.3	0.5
CL-118W1	874.5	865.02	144, 145 and 146	Lapilli Tuff	More intense sericite bleaching throughout the unit. Size of ejector fragments have coarsened with bomb size clasts commnon. Sericite bleaching follows a prefered consistent orientation. Clasts would seem to have fairly good presearvation and usually appear angular and do not appear to show heavy deformation. The unit would appear to have minor silica flooding. Despite this mineralisation would seem to be poor with occasional pyrtie and pyrrhotite but minor, very fine crystaline arsenopyrite.	4	1	3	4	3	1	1	2	0.2	0.2	0.5
CL-118W1	865.02	851.64	147 and 148	Lapilli Tuff	Sericite alteration is less abundant with protolith showing much better preservation. Angular, ejector clasts are common thoughout and up to 6mm in size. Coarsest areas of clasts have small stringers of pyrite- these tend to concentrate around angular quartz clasts (sample 147). Quartz alteration and sericite alteration are poor throughout. There is moderate carbonate alteration with common small carbonate veins cross cutting the unit. Chlorite smears throughout the unit. Arsenopyrite is much less abundant.	3	1	2	2	2	4	3	3	0.5	0.5	0.1
CL-118W1	851.64	840.6	149	Lapilli Tuff	Tightening in porosity of unit. Very similar to previous with occasional bands of sericite. These develop in bands of foliations concordant with deformation. Clasts are typically more elongate then previous unit. Chlorite veins are seen in conjunction with the sericite. Mineralisation is poor.	1	2	3	3	2	4	2	3	0.5	0.5	0.1
CL-117	862	866.1	154	Ash Tuff	Ash tuff with foliation exposing bedding. Aleteration is poor with minor sericite throughout. There is moderate carbonate impregnation and minot occasional calcite veinletts. Mineralisation is poor. Small ejector clasts become more common throughout the unit. This correlates with an increase in pyrite mineralisation however this is a minor component of the whole unit.	<1	4	3	1	1	3	2	1	0.4	0.2	0.1
CL-117	866.1	844.66	155, 156, 157, 158, 159 and 160	Lapilli Tuff	Gradual increase in sericite alteration that would seem to accompany a slow coarsening in ejector fragments. Caused a heavy and consistent banding that has allowed for localised patches of high mineralisation. These accompany thin sulphide veins in the most agressivly altered areas. Veins are composed of acicular arsenopyrite that would seem to confrom to foliation orientation. Ejector clasts largely overprinted by protolith but usaully around 2-3mm in size, angular and consistant throughout unit. The unit has moderate, consistent silica flooding however quartz veins do not seem to be present. Calcite veins remain promenant. There are occasional chlorite smears throughout the unit.	3	3	4	5	3	3	2	2	0.4	0.4	0.8

Appendix B: Sample Catalogue

Assay number	Drill Hole	Depth of oldest end	Domain	Au (ppm)	Sampling reason	Thin Section Taken	Thin section core	Asp Mount
47086	CL-118W	774.49	4	3.098	Very high level of mineralisation with arsenopyrite dense throughout the sample. Look for difference in mineralisation between deformed and less deformed area. Style of mineralisation and habit of gold related to arsenopyrite			
47093	CL-118W	783.22	4	3.282	Change in foliation. See if grade is related to cross cutting and deformed calcite vein. Habbit of mineralisation following good grade in 21. Is there a change? Is the style of folation different?	X		
47094	CL-118W	784.35	4	5.998	Abrupt increase in mineralisation surrounding cross cutting ankerite veins. Test to see how vein is related to large clast in protolith and habit and generations of mineralisation.			
47095	CL-118W	786.29	4	0.039	Illustrating a gradual change in the system as foliation, sereite alteration, quartz veining and mineralisation increases from sample 18 to 19 to 20. More foliation and alteration then previous.	X		
47100	CL-118W	791.79	4	5.821	Illustrating a gradual change in the system as foliation, sereite alteration, quartz veining and mineralisation increases from sample 18 to 19 to 20	X		
47102	CL-118W	795.71	4	1.138	Beginning of mineralisation in domain 4. Previous to this similar protolith however very unaltered and less well developed foliation. Arsenopyrite seems to now be common and consitent and abundant proximal to quartz veins. Look for relationship between these.	X		
507579	CL-111	167.53	4	0.339	Looking at distal shut off of system. Very fine grained with oxidation bands. Test to see if these are pre deformation. How has system evolved- has it evolved through time or and seeing a gradual decrease in mineralisation			
507583	CL-111	171.1	4	0.078	Conglomerate looking rock with fairly major serecite alteration but no mineralisation. Designed to test whether mineralisation is congruous with alteration.			
507588	CL-111	178.76	4	1.904	Quartz vein. Look at sulphides and gold within to see habbit. Order and generations of crystallisation			
507589	CL-111	181.18	4	1.83	Cross cutting relationship with quartz vein. Look at stages of mineralisation. 10cm quartz vein 2cm above sample. Why has the quartz vein exploited this area and what are the effects?			
507590	CL-111	181.78	4	1.666	Sulphide vein within bleached serecite zone. Relate to distal areas for gold habbit. Seems oxidised. Carbonate alteration? Check habits of pyrite vs arsenopyrite for generations of sulphides			

Assay number	Drill Hole	Depth of oldest end	Domain	Au (ppm)	Sampling reason	Thin Section Taken	Thin section core	Asp Mount
501232	CL-090	354.74	4	0.539	Style of mineralisation above quartz veins. Is it the same system to previous? Do the cross cutting veins have anything to do with mineralisation?			
501237	CL-090	359.18	4	0.02	Quartz vein above domain 4. To be compared to other similar beds as evidence of potential marker bed?			
501241	CL-090	336.95	4	1.194	Example of non mineralsed foliated ash over domain four. Shows transition in terms of mineralisation and grade- to be compared to sample 27			
501257	CL-090	383.01	4	7.7	Deformation style and timing of foliated rock with quartz veins. Are veins related to mineralisation? Relationship between quartz and ankerite.			
501258	CL-090	384.94	4	9.301	Taken to examine strong silica alteration that does not seem to have foliation or to postdate deformation. Localised undeformed area showing silica flooding? Is there mineralisation?			
501262	CL-090	390.93	4	1.561	Shows relationship between deformation and mineralisation. Strong serecite rock with background acicular arsenopyrite. Deformed quartz vein with arsenopyrite rims.			
501266	CL-090	396.47	4	15.09	To look at evolution of quartz vein and determine whether quartz is syngenetic and look at its relationship with brrecciа- silica apron or metamorphic. Look for grade within breccia (with or without metamorphic signiture).			
47050	CL-118W	724.65	4	0.009	Example of non mineralised ash above domain 4.	X		
47071	CL-118W	753.68	4	7.271	Large quartz apron overlying ash tuff. Are clasts within rip up and do they contain grade- if so grade would have to predate deformation.	X	X	
47073	CL-118W	756.31	4	3.06	Start of mineralisation. Examine for increase in alteration and relate to mineralisation. Wavy arsenopyrite veins- habbit and genesis. Examine stage of quartz emplacement. Has the system restarted or are we looking at later stage fluid activation (from either epithermal or orogenic source?)	X		
47083	CL-118W	770.34	4	2.538	Taken to examine the change in deformation- much less with angular quartz clasts and relate to any change in grade or gold mineralisation style.			

Assay number	Drill Hole	Depth of oldest end	Domain	Au (ppm)	Sampling reason	Thin Section Taken	Thin section core	Asp Mount
	C565-006	30.35	4	#N/A	Comparison of arsenopyrite habbit to sample 45. Clast supported mineralisation style and similarities/differences			
	C565-006	22.49	4	#N/A	Example of proximal non grade. What has occurred in sample 46 and 45 that allows for grade? Why has it not occurred here?			
	C565-006	20.39	4	#N/A	Sulphide vein cross cutting and breaking up ankerite vein. Gives clue to timing relationship? Look for relationship throughout with arsenopyrite			
	C565-006	20.04	4	#N/A	More intense mineralisation similar style to 48. Look at what has changed to allow for this to occur- change in protolith or shear intensity?			
	C565-050	156.45	4	#N/A	Showing typical section of felsic flow. To be compared to 51 to show evolution of the system			
	C565-050	151.04	4	#N/A	Towards the top of the felsic flow. More sericite alteration and part of the transition towards more volitile ash			
	C565-050	138.06	4	#N/A	Transition into felsic ash. To be studied for mineralisation and compared to stratigraphically similar units. Look for evolution of system			
	C565-050	123.24	4	#N/A	Quartz taken within felsic ash. Non-concordant relationship within foliation and test to see if it is responsible for mineralisation. Comparison to 52 showing evolution of system			
	C565-050	120.82	4	#N/A	Similar to sample 53 however with mineralisation and proximity to quartz veins. Acicular arsenopyrite seems parallel to foliation and not the cross cutting quartz vein- timing of mineralisation.			
	C565-050	119.69	4	#N/A	Dense arsenopyrite within quartz vein- habbit of mineralisation and comparison to quartz along this and in other domains.			

Assay number	Drill Hole	Depth of oldest end	Domain	Au (ppm)	Sampling reason	Thin Section Taken	Thin section core	Asp Mount
	C565-050	120.3	4	#N/A	Wormy deformed quartz veins in highly mineralised zone. Look for temporal and spacial relationships and comparision to proximal 54 and 55 samples.			
	C565-050	115.65	4	#N/A	Quartz with sulphides. Comparison with other quartz. Taken from within the centre of the quartz and looks to be indicative of the highest grade within the sample			
	C565-082	273.1	4	#N/A	Showing transition in mineralisation comparible to sample 59 and 60. Look at habit of acicular arsenopyrite in well foliated rock and associated minerals and textures and compare to 59 and 60			
	C565-082	272.77	4	#N/A	Showing transition in mineralisation comparible to sample 58 and 60. Look at habit of acicular arsenopyrite and sulphide clasts in well foliated rock and associated minerals and textures and compare to 58 and 60. Check for orientation of asp compared to foliation			
	C565-082	272.17	4	#N/A	Showing transition in mineralisation comparible to sample 58 and 59. Look at habit of acicular arsenopyrite and sulphide clasts in well foliated rock and associated minerals and textures and compare to 58 and 59. Check for orientation of asp compared to foliation. Look at sulphide vein and relate to fluids temporally- which other mineral assembledge(s) are these genetically related to?			
	C565-082	273.5	4	#N/A	Increase in sericite alteration relative to sample 60. Arsenopyrite vein- timing and relationship to gold? Any relic protolith?			
	C565-082	268.64	4	#N/A	Increase in alteration and quartz from 61. What has caused the habit of the quartz veins? Deformation and which event is related to Au? Orientation of arsenopyrite			
	C565-082	267	4	#N/A	See if quartz is high grade. Relate this to other quartz veins and blanket quartz vein that typically overlies domain 4			
	C565-082	264.45	4	#N/A	To show evolution of grade and investigate extent of deformation in ash heavy areas. Comapre to 63, 65 and 66			
	C565-082	263.29	4	#N/A	Sulphide veins and acicular arsenopyrite formed now that unit has coarsened. Look for orientation of arsenopyrite and habit in relation to gold. Temportal and spaial relationship with quartz vein			

Assay number	Drill Hole	Depth of oldest end	Domain	Au (ppm)	Sampling reason	Thin Section Taken	Thin section core	Asp Mount
	C565-082	261.71	4	#N/A	Higher grade- what has changed to allow for more asp? Does it relate to coarsening of tuff. pre diagenetic gold?			
	C565-082	258.47	4	#N/A	Spotty carbonate alteration. Look at composition of protolith and relate to fluid pathways and mineralisation			
	C565-082	207.57	4	#N/A	Carbonate flooding and after effects- look to see change and ankerite relationship with arsenopyrite and gold			
	C565-082	255.45	4	#N/A	Highest grade? Is arsenopyrite replacing palaeoejector clasts. Comparision with previous samples for change in gold habit			
	C565-082	239.71	4	#N/A	Sampe of unit. Taken to compare to mineralised zones either side.			
	C565-082	232.6	4	#N/A	Sulphide vein (replaced quartz) look for genetic relationships and understand significance of foliation parallel arsenopyrite veins			
	C565-082	231.65	4	#N/A	Evolution of system from sample 71. Habit of quartz vein? Is the protolith getting coarser? Does this affect fluid/grade intensity?			
	C565-082	229.18	4	#N/A	Spotty carbonate towards the end of the unit. How has this changed from 71 and 72? Different fluid system or evolution of same fluid that has created earlier grade?			
	C565-082	256.91	4	#N/A	Beginning of intense alteration. Should be able to see clasts in protolith and relate to sample 73. Do these have any control over mineralisation?			
	C565-082	223.99	4	#N/A	Higher grade. Compare evolution of system to 74 and 76.			

Assay number	Drill Hole	Depth of oldest end	Domain	Au (ppm)	Sampling reason	Thin Section Taken	Thin section core	Asp Mount
505476	CL-088	337.27	4	3.664	Section overlying quartz vein but with limited arsenopyrite mineralisation. Can be related to later samples. Different generation of quartz? Does the sericite event corrrelate with mineralisation?			
505471	CL-088	332.04	4	2.46	Onset of carbonate alteration towards the bottom of the unit. Occasional mineralisation- relate mineralisation to carbonate fluids- number of generations of fluid?			
505470	CL-088	330.41	4	1.524	Quartz vein overlying hydrothermal brecciated unit. Look for evolution of the quartz vein and any relationship to mineralisation	X		
505468	CL-088	327.31	4	0.316	Further coarsening of unit. Is the coarser ejector fragments indicative of a more proximal environment. Clasts are common and deformed but not to a great extent. Fine crystals of arsenopyrite visible- relate deformation intensity to grade	X		
505466	CL-088	324.12	4	0.003	Beginning of silica alteration with fine crystaline arsenopyrite. Taken to look at development of mineralsiation			
505457	CL-088	314.58	4	0.287	Look at different habit of arsenopyrite and relate to gold and mineralisation process. Chlorites effect on arsenopyrite? Is silica alteration related to chlorite? How many fluid events?	X		
505447	CL-088	298.12	4	0.093	Typical alteration within unit. Look for timing of events and for cross cutting relationships			
505439	CL-088	287.32	4	0.001	Typical rock stratigraphically below domain 4. Rare example of mineralisation within this unit- within lithic clast. To compare mineralisaed annd non mineralised areas			
	C565-082	212.81	4	#N/A	Typical mineralisation above quartz vein. New volcanic system. Does fluid have a different chemical signiture? Different sulphide generations?			
	C565-082	217.12	4	#N/A	Quartz vein overlying domain 4. Test continuity against other veins along section as potential marker bed.			
	C565-082	219.04	4	#N/A	Top of mineralised zone just below quartz vein. Clasts appear heavily altered and mineralised. May be able to relate to epithermal system?			

Assay number	Drill Hole	Depth of oldest end	Domain	Au (ppm)	Sampling reason	Thin Section Taken	Thin section core	Asp Mount
505477	CL-088	338.31	4	1.559	Look at quartz veins vs sericite vs grade			
505478	CL-088	340.5	4	4.083	Beginning of wormy quartz veins. To be related to other similar textures along section. Lots of pyrite- look at generation vs asp and gold	X		X
505481	CL-088	344.03	4	8.042	Well foliated rock- compare grade to previous, less deformed areas. Boudinaged quartz veins. Pre foliation? Same generation as gold?	X		
505482	CL-088	346.5	4	3.686	Heavily silicified area. Look for habbit of gold in relation to arsenopyrite in relation to gold. Any other sulphides? How does the most intense mineralisation relate to other areas of grade? Different genetic event?	X		
505483	CL-088	346.93	4	2.753	Slight decrease in silica with elongate protolith now visible. How does this affect mineralisation? Is there any sign of the quartz being deformation related?	X		
505484	CL-088	349.44	4	0.057	Shows evolution of system. Look for habit and orientation of sulphide clasts and relate to gold genesis			
505491	CL-088	358.62	4	0.096	Bleached serectite unit- look at habit of sulphide within lithic clasts and pyrite mineralisation. Different fluid event?			
505496	CL-088	365.11	4	2.216	Relitively coarse clasts in heavily carbonate altered area with acicular arsenopyrite throughout the unit. Look to see if mineralisation is sepperated from deformation- any significance of orientation of crystals? Different type/generation of arsenopyrite and different correlation to gold?			
505496	CL-088	365.76	4	2.216	Proximal to sample 94 to show relationship between clast size, foliation and foliation. Arsenopyrite is less common but still abundant.			
505497	CL-088	366.56	4	0.134	Evolution above a bomb clast towards overlying ash. Heavily altered but not foliated. Any relationship to grade?			
505500	CL-088	369.67	4	0.056	Fine grained ash with good foliation. Look at pyrite- same generation as arsenopyrite and gold? Why does arsenopyrite not occur in this habit?			
505660	CL-088	385.18	4	5.543	Well presearved clast in heavily altered matrix. Any relationship to mineralisation? Why has that particular isolated clast been well presearved?			

Assay number	505661	512413	512411	512407	512410	512404	512402	512397	512393	512390	512388	512387
Drill Hole	CL-088	CL-102	CL-102	CL-102	CL-102	CL-102	CL-102	CL-102	CL-102	CL-102	CL-102	CL-102
Depth of oldest end	385.85	318.69	315.79	311.81	313.76	307.42	304.12	297.61	291.74	287.05	284.14	283.24
Domain	4	4	4	4	4	4	4	4	4	4	4	4
Au (ppm)	0.078	0.003	0.014	0.08	0.863	0.001	0.103	0.001	0.012	5.372	7.686	11.45
Sampling reason	Pyrite habit. Look at sulphides and different generations and relate to timing events. Evolution of arsenopyrite throughout the sample.	Apparently non-mineralised areas of lapilli tuff. Look to see if there is any mineralisation or why it has not occurred here. Well preserved protolith textures indicative to poor mineralisation?	Why has mineralisation occurred here? Related to clast size change? Different generations of fluid?	Mineralised area does not seem to relate to deformation (compared to sample 101). Correlate deformation fluid with mineralisation.	Shows proto-lithic clasts and relationship with surrounding deformation in sericite altered environment	Habit of mineralisation within silica flooded zone. Arsenopyrite is in blebs and non acicular . Is this part of a different style of mineralisation?	Interesting cross cutting quartz vein. Timing and emplacement relationship?	Fresh well preserved lapilli clasts within sericite latered matrix. Is the sericite pre deformation? Any relation to any mineralisation.	Interesting relationship with quartz vein. Look for timing relationships. Relationship with mineralising fluid?	Look at relationship between quartz veins, carboante veins and deformation within the unit.	Most intense area of silica alteration within the unit. Look at the relationship with with itensity of silica alteration and style and degree of mineralisation.	Wormy deformed quartz. Seems to be good mineralisation with acicular arsenopyrite common throughout- how is this related to mineralisation? Timing of events may be important? Look at relationship and see if this relates to more intense domain 4 deformation in other tones.
Thin Section Taken												
Thin section core												
Asp Mount												

Assay number	Drill Hole	Depth of oldest end	Domain	Au (ppm)	Sampling reason	Thin Section Taken	Thin section core	Asp Mount
SG66268	CL-061	68.69	3	27.093	Habit and style of mineralisation. Look at silica flooding and relationship with protolith. Why here?			
SG66260	CL-061	57.21	3	12.286	Why has this silica flooding occurred? Has this changed the habit of arsenopyrite? Is this a different generation of arsenopyrite and what is its relationship to gold?			x
SG66252	CL-061	47.95	3	6.538	Change in mineralisation style. What has caused this? Correlate habit of quartz veins to mineralisation. Acicular arsenopyrite? Orientation?			
SG66251	CL-061	45.44	3	11.414	Similar alteration style to previous but change in protolith texture. Has this affected mineralisation and any relationship and causative change between mineralisation and protolith.			
SG66241	CL-061	33.75	3	6.557	Effect of quartz vein and relationship with mineralisation. Difference with this quartz vein in relation to domain 4?			
SG66227	CL-061	18.09	3	4.141	Silica veining has increased in abundance since sample 114 and 115. Look to timing relationship of bedding and any change in density of mineralisation? Relate habit to domain 4			
SG66221	CL-061	10.19	3	6.818	Unit is full of acicular arsenopyrite- seems to be randomly orientated. Relate this to the amount of of deformation and fresh looking clasts			
SG66220	CL-061	8.78	3	4.474	Showing mineralisation in unfolated zone. Habit and timing of quartz veins and relationship with arsenopyrite and gold			
512380	CL-102	274.85	4	7.973	Deformation relate arsenopyrite? Halbt and orientation of mineralisation?			
512382	CL-102	276.58	4	1.892	Well preseanved volcanic textures with quatz veins and good mineralisation. May show epithermal gold genesis			
512387	CL-102	282.8	4	11.45	Brief area of silica flooding. How does this relate to sample 110? Mineralisation intesnity and habit?			

Assay number	Drill Hole	Depth of oldest end	Domain	Au (ppm)	Sampling reason	Thin Section Taken	Thin section core	Asp Mount
SG66273	CL-061	72.98	3	14.417	Good mineralisation with slightly coarser protolith. Has style of mineralisation changed? How has silica flooding been affected by mineralisation?			
SG66278	CL-061	79.55	3	0.757	Showing a change in mineralisation style as protolith changes in composition (specifically coarsness of ejector clasts). Would seem to show well preseared textures and limited folation in an larely unfoliated environment. Ash beds not showing deformation or epithermal mineralisation. Compare generation of arsenopyrite to domain 4.			
SG66281	CL-061	83.36	3	5.635	Showing a change in mineralisation style as protolith changes in composition (specifically coarsness of ejector clasts). Would seem to show well preseared textures and limited folation in an larely unfoliated environment. Ash beds not showing deformation or epithermal mineralisation. Compare generation of arsenopyrite to domain 4.			
SG66286	CL-061	89.3	3	3.958	Showing a change in mineralisation style as protolith changes in composition (specifically coarsness of ejector clasts). Would seem to show well preseared textures and limited folation in an larely unfoliated environment. Ash beds not showing deformation or epithermal mineralisation. Compare generation of arsenopyrite to domain 4.			
SG66289	CL-061	93.18	3	10.629	Showing a change in mineralisation style as protolith changes in composition (specifically coarsness of ejector clasts). Would seem to show well preseared textures and limited folation in an larely unfoliated environment. Ash beds not showing deformation or epithermal mineralisation. Compare generation of arsenopyrite to domain 4.			
507714	CL-113	58.11	3	8.629	Sulphides within clasts showing poor levels of deformation. Look for habit of sulphides and correlate deformation intensity with grade. A gradual loss in elongation noticed with age. How does this equate to mineralisation?		X	
507720	CL-113	64.91	3	16.86	Has arsenopyrite habit changed as a result of deformation or from clast size change? Two proximal areas of core with different degrees of deformation. Similar grade? Similar mineralising system?			
507720	CL-113	65.25	3	16.86	Has arsenopyrite habit changed as a result of deformation or from clast size change? Two proximal areas of core with different degrees of deformation. Similar grade? Similar mineralising system?			
507723	CL-113	69.57	3	0.061	Can relate to previous units. Loss of mineralisation? Look at change across the unit. What has caused this?			
507730	CL-113	79.4	3	0.002	What has caused drop in alteration and mineralisation? Foliation seems to be strong with good deformation. Is this consistent with previous?			
507738	CL-113	89.4	3	0.001	Deformed conglomerate. Aspect ratio of clasts compared to grade and sample 133 should be looked at.			

Assay number	Drill Hole	Depth of oldest end	Domain	Au (ppm)	Sampling reason	Thin Section Taken	Thin section core	Asp Mount
47162	CL-118W1	878.74	3	0.488	Stringer pyrite. Does orientation reflect fluid pathwy? Which generation is this sulphide part of? Why not arsenopyrite?	X		
47165	CL-118W1	882.58	3	0.248	Sericite bleached but well presearved lithic clasts with little deformation. Look for habit of arsenopyrite.	X		
47160	CL-118W1	887.5	3	0.961	Deformed carbonate vein within well mineralised zone. Minor localised patch of sericite bleaching surrounding this area. Look for relationships of carbonates.	X	X	
47174	CL-118W1	894.48	3	0.364	Greater foliation and acicular arsenopyrote. Relate to previous samples and correlate alteration with foliation and grade	X		
47182	CL-118W1	906	3	0.001	More deformed elongate clasts with similar mineralisation to sample 137. To be compared for effect (if any) or orogenic processes.	X		
47183	CL-118W1	906.76	3	0.001	Angular, seemingly well presearved clasts with good minerlisation. To be compared to slightly more elongate clasts in sample 138 in order to look for difference in mineralisation style and concentration	X		
507750	CL-113	105.68	3	0.009	Carbonate mineralisation with quartz crystals. Generation of carbonate timing? Any mineralisation?			
507743	CL-113	97.15	3	0.002	Comparison of ejector clasts to sample 133			
507741	CL-113	95.14	3	0.043	Comparison of ejector clasts to sample 133			
507739	CL-113	91.17	3	0.001	Well presearved non imbricated conglomerate looking angular clasts. Any tuffaceous bedding in clasts? Any evidence of palaeoplacer gold?			

Assay number	Drill Hole	Depth of oldest end	Domain	Au (ppm)	Sampling reason	Thin Section Taken	Thin section core	Asp Mount
505392	CL-088	224.67	3	0.004	Coarse angular clasts with good alteration and fine crystaline disseminated arsenopyrite clasts. Overlay with jerocite layer. Look for gold within jerocite			
505631	CL-088	195.58	3	7.642	Heavily altered sericite altered area. Broken looking quartz. There is strange cross cutting relationships worth looking at. Possible jarocite- any gold within this?	X		
505631	CL-088	195	3	7.642	Quartz veins within sericite above mineralised section of domain. Look for cross cutting relationship with sericite foliation			
47138	CL-118W1	844.94	3	0.63	Sericite alteration with chlorite. Correlate chlorite alteration with sericite and in timeline	X		
47147	CL-118W1	859.11	3	0.074	Most elongate clasts within the unit. More pyrite. Compare to sample 147.			
47149	CL-118W1	861.89	3	0.103	Pyrite within angular quartz clasts. Relate to sulphide timelines	X		
47154	CL-118W1	868.5	3	0.186	Larger clasts still with similar poor alteration and mineralisation as previous. Angular and shows little deformation.	X		
47153	CL-118W1	865.71	3	0.637	Why has good silica flooding caused limited mineralisation. Different generation of alteration? Multiple fluid systems?	X		
47163	CL-118W1	879.69	3	0.205	Good silica alteration and sericite. Coarse protolith but poor mineralisation. Why? Is pyrite mineralisation significant and does its presence impact gold?	X		
47160	CL-118W1	877.12	3	0.961	Cross cutting veins and genesis relationships? Arsenopyrite mineralisation and grade in comparsion to sample	X		

Assay number	Drill Hole	Depth of oldest end	Domain	Au (ppm)	Sampling reason	Thin Section Taken	Thin section core	Asp Mount
505397	CL-088	232.03	3	0.001	Angular clasts with limited arsenopyrite mineralisation. Relationship between mineralisation and angularity of clasts. Later stage alteration?			
514490	CL-117	876.58	3	0.019	Pyrite mineralisation in ash tuff. Relate and contrast arsenopyrite in coarser protolith in following samples			
514490	CL-117	875.96	3	0.019	First instance of sericite bleaching accompanied by carbonate vein and arsenopyrite mineralisation. How are these related? Related to a coarsening?			
514474	CL-117	853.05	3	5.752	Heavy sericite bleaching overprinted by very strong mineralisation. What has allowed for this? Habit of sulphides related to previous? Acicular orientation crucial?			
514473	CL-117	850.74	3	0.761	Very pale bleached carbonate altered unit. What effect has carbonate alteration had?			
514471	CL-117	849.53	3	0.663	Increase in pyrite mineralisation different sulphide generation? Related to loss in sericite bleaching? Any change in protolith here?			
514469	CL-117	847.25	3	1.666	Patchy alteration with sericite bands. Any correlation to sericite? Timing relationship of quartz-carboante veins showing later deformation			
514468	CL-117	845.53	3	3.591	Show relationship of pyrite and arsenopyrite. Same generation? Good arsenopyrite?		X	X
514466	CL-117	842.61	3	5.964	Much greater arsenopyrite- larger acicular arsenopyrite crystals. Different habit or generation ro previous? Mineralisation correlative with foliation?			X
514466	CL-117	841.75	3	5.964	Increase in folation changing mineralisation? Is orientation now consistent with folation? Change in arsenopyrite habit?			
514465	CL-117	840.13	3	1.74	Further increase in folation however now not with abundant mineralisation. Shows concordant ankerite. Different generation to previous?			
514461	CL-117	836.55	3	0.003	Look at chlorite and ankerite relationship and try to correlate to timeline.			

Assay number	Drill Hole	Depth of oldest end	Domain	Au (ppm)	Sampling reason	Thin Section Taken	Thin section core	Asp Mount
502541	CL-100	211.23	5	0.79	Distribution of sulphides- why replacing clasts? Elongate clasts relitive to grade? Why suddenly clast replacement?			
502540	CL-100	210.33	5	1.073	How has greater bleaching affected mineralisation? Context of deformation relatuve to proximal rocks? What has caused/allowed for bleaching?			
514363	CL-118	703.88	5	0.109	Very dense fc asp. Why not acicular? How has protolith changed from domains 3/4?	X		
514359	CL-118	698.75	5	4.903	Mineralisation adjacent to quartz vein. Relate pyrite to asp event. Evolution of sulphides with distance from qtz vein. Py vs Po?	X		
	CL-102	210.7	5	#N/A	Trying to show variation though domains. Non mineriliased areas howevr fc asp throughout			
507534	CL-111	105.8	5	0.031	High foliation but poor mineralisation with elongate clasts and fc arsenopyrite which does not seem to correlate compared to sample 170			
507533	CL-111	103.54	5	2.138	Tempory increase in carbonate alteration with acicular arsenopyrite associated. Has ankerite vein any association?			X
514434	CL-117	802.48	3	0.001	Look at similar protolith and relate extent of deformation to minerlaisation. Is foliation correlative? Why are some areas more deformed then others?			
514440	CL-117	807.2	3	0.001	Look at similar protolith and relate extent of deformation to minerlaisation. Is foliation correlative? Why are some areas more deformed then others?			
514441	CL-117	809.06	3	0.001	Look at similar protolith and relate extent of deformation to minerlaisation. Is foliation correlative? Why are some areas more deformed then others?			
514442	CL-117	810.44	3	0.001	What has caused loss of mineralisation? How has the volcanic system evolved and is this correlative?			
514459	CL-117	833.14	3	0.003	Example of drop in mineralisation- any change in protolith that has triggered this?			

Assay number	Drill Hole	Depth of oldest end	Domain	Au (ppm)	Sampling reason	Thin Section Taken	Thin section core	Asp Mount
502542	CL-100	212.26	5	2.676	Sulphide flooding of matrix- habbit and generation of sulphides. Is there an evolution of fluids from previous samples?			
505700	CL-088	440.06	5	1.387	Compare sulphide veins to other mineralisation in domain 5. Look at generations with relation to deformation and to quartz. Are there different generations of sulphides?			
505702	CL-088	444.35	5	0.009	Following unmineralised section similar quartz vein to sample 178 however different mineralisation style. Is different generation epithermal? Undeformed protolith but 'wavy' quartz vein			
505704	CL-088	447.06	5	6.856	How does ankerite fit into picture? Lots of pyrite how does this relate? Deformation structure relevent? Carbonate seems broken but protolith intact?	X	X	X
505708	CL-088	452.76	5	0.499	Heavily bleached and broken with occasional acicular arsenopyrite. To be compared with sample 182 with similar bleached but less aggressive textures and mineraliation. Why is there lots of pyrite?	X		
505709	CL-088	453.71	5	0.84	Bleached and elongate but lacking aggressive broken texture with mineralisation. 'null sample'. Evidence of fluid and is it different to asp fluid?	X		
505710	CL-088	455	5	0.029	Little elongation and deformation but good mineralisation? Similar look and system to domain 3? Why sudden switch compared to sample 182? Different generation?	X		
505711	CL-088	457.77	5	0.025	High level of deformation relative to previous sample- more consistent foliation and consistently orientated concordant to acicular arsenopyrite			
505712	CL-088	459	5	1.789	Different swirly quartz showing plastic deformation. Compare sulphide suites to previous. Lots of py- is this cogenetic with gold?	X		
505714	CL-088	461.77	5	2.093	Strange- unique? Deformation generation seem to be lots of stages with fluid. Brittle asp flowwing fault planes are randomly orientated	X		
505716	CL-088	462.5	5	1.325	Similar to previous deformation style however better mineralisation. Random asp orientation. Does deformation pick out softest rocks or cause sericitisation?			
505719	CL-088	466.68	5	0.007	Well presearved angular clasts. Conglomerate or lapilli tuff? What sulphide suites occur here?			

Assay number	Drill Hole	Depth of oldest end	Domain	Au (ppm)	Sampling reason	Thin Section Taken	Thin section core	Asp Mount
505718	CL-088	465.96	5	0.011	Well presearved angular phenocrysts overprinted with hydrothermal alteration. Disseminated vfc asp is common- not caused by deformation or are bomb clasts nire competant and do not uptake foliation?			
505721	CL-088	469.63	5	1.807	Well presearved angular looking clasts (not very elongate) with sericite and sulphide flooded matrix. Look for generations of py vs asp. Evolution with time or different hydrothermal system? What has allowed for 'sulphide veins' and do these correlate with gold? Are these similar to sulphide veins at Walsh? Why patchy in this domain?	X		
505721	CL-088	469.87	5	1.807	Well presearved angular looking clasts (not very elongate) with sericite and sulphide flooded matrix. Look for generations of py vs asp. Evolution with time or different hydrothermal system? What has allowed for 'sulphide veins' and do these correlate with gold? Are these similar to sulphide veins at Walsh? Why patchy in this domain?	X		
505721	CL-088	470.16	5	1.807	Well presearved angular looking clasts (not very elongate) with sericite and sulphide flooded matrix. Look for generations of py vs asp. Evolution with time or different hydrothermal system? What has allowed for 'sulphide veins' and do these correlate with gold? Are these similar to sulphide veins at Walsh? Why patchy in this domain?	X		
505721	CL-088	470.36	5	1.807	Evolution of Po and Py in diminishing concentration away from quartz vein. What has caused mica within the sample and is this related to mineralisation? Angular clasts related to epithermal or orogenic?	X		
505722	CL-088	471	5	0.151	Angular clasts with good asp mineralisation. Epithermal? Which generation of fluid? Acicular arsenopyrite? Compare with py in more proximal sample (193)			
505723	CL-088	473.14	5	1.125	Lots of different sulphide habbits. Look at change in protolith and relate to sulphides Angular clasts are primary and epithermal??			
505723	CL-088	473.35	5	1.125	Quartz vein adjacent to sample 195. Is mineralisation in footwall different to hangingwall and does this correspond to lithological change? Look for sulphide generations			
505725	CL-088	474.53	5	1.178	Section of large ejector bombs. Look at acicular clasts and relate to phenocrysts. Is habbit cogentic with previous samples?			
505725	CL-088	475	5	1.178	Randomly orientated acicular asp surrounded by fresh clasts and poor foliation. Showing epithermal system?			
505727	CL-088	477.48	5	0.701	Randomly orientated acicular asp surrounded by fresh clasts and poor foliation. Showing epithermal system?			
505727	CL-088	477.77	5	0.701	Randomly orientated acicular asp surrounded by fresh clasts and poor foliation. Showing epithermal system?			

Assay number	Drill Hole	Depth of oldest end	Domain	Au (ppm)	Sampling reason	Thin Section Taken	Thin section core	Asp Mount
505753	CL-088	514.25	5	4.718	Total mineralisation across angular clasts. Seems to be epithermal textures?	X		
505751	CL-088	511.06	5	1.432	Pyrite vs arsenopyrite? Habbit and genetic timing			
505750	CL-088	509.05	5	6.347	Quartz vein replacing bomb clasts? Angular ejector fragments readily visible within matrix and sulphides= epithermal?	X	X	
505749	CL-088	507.29	5	2.607	Moderate mineralisation with angular clasts. First stage of mineralisation- to a lesser extent then complete sulphide veins?	X		
505743	CL-088	500.52	5	4.246	Very strong mineralisation in sulphide veins. Can see protolith and extent of deformation	X		
505740	CL-088	495.24	5	4.317	Good mineralisation with well preserved phenocrysts. Show alteration in undeformed areas?	X	X	
505739	CL-088	493.98	5	2.335	Relationship with sericite, arsenopyrite and quartz. Any evidence of protolith?			
505738	CL-088	493.35	5	0.315	Onset of sericite bleaching and related grade- proximal with quartz veins			
505732	CL-088	485.5	5	0.072	Greatest quartz vein with wavy behavior and flooding of adjacent to matrix with sulphides. Well preserved adjacent phenocrysts- limited deformation?	X		
505728	CL-088	479.09	5	2.317	Increased foliation and high magnitude of mineralisation. Do these correlate?	X		
505729	CL-088	479.5	5	2.934	Preceeding sericite foliation seems to correlate with asp. Later stage asp quartz and ankerite has any affect?	X		
505728	CL-088	478.16	5	2.317	Now with deformation. Caused increase in grade?			

Assay number	Drill Hole	Depth of oldest end	Domain	Au (ppm)	Sampling reason	Thin Section Taken	Thin section core	Asp Mount
505755	CL-088	516.11	5	9.602	Great mineralisation similar to previous now with quartz vein to look at further evolution of high grade. Which generation and habbit of arsenopyrite?			
505759	CL-088	520.04	5	4.62	As before but with very strong quartz vs arsenopyrite	X		
505761	CL-088	523.53	5	0.811	In order to try to show evolution of the system now there is less mineralisation. Does this correlate with protolith?	X		
507965	CL-113	400.42	5	6.557	Seemingly deformed quartz veins surrounded by acicular arsepnyrite. Any deformation control related to quartz?			
507972	CL-113	409.35	5	10.3	Similar to previous sample but less alteration and protolith now visible. Angular clasts? Relate to other domain 5 holes			
507980	CL-113	418.9	5	14.42	Wormy deformed quartz veins. Post mineralisation deformation? Does mineralisation correspond to deformation or principal quartz vein orientation? Similar to previous samples? Can see protolith clasts- relate to level of deformation with aspect ratio			
507976	CL-113	413.51	5	26.8	High grade. Look at occurance			
507980	CL-113	420	5	14.42	Cloudy quartz- is habbit the same as previously seen wormy quartz? Same mineralisation system? Cognate fragments are visible do not seem to be deformed?			
507988	CL-113	432.4	5	7.646	Good mineralisation with arsenopyrite veins. Compare grades to other pods within both hole and domains.			
507989	CL-113	432.67	5	10.58	Adjacent to previous sample. Protolith with lithic clasts. Look at mineralisation			
507998	CL-113	444.82	5	6.73	Showing devolution of system. Good grade with acicular asp overprint angular clasts. Relate to others			
501167	CL-090	267.1	5	0.202	Blocky quartz vein overprinting carbonate altered cognate rock. Which sulphides are associated with quartz?			

Assay number	Drill Hole	Depth of oldest end	Domain	Au (ppm)	Sampling reason
501169	CL-090	270.15	S	2.176	Edge of massive quartz vein. Look at genetics of sulphide suites and interplays
501177	CL-090	280.66	S	0.622	Edge of massive quartz vein. Look at genetics of sulphide suites and interplays
501179	CL-090	284.18	S	2.828	Edge of massive quartz vein. Look at genetics of sulphide suites and interplays
501181	CL-090	287.39	S	2.959	Edge of massive quartz vein. Look at genetics of sulphide suites and interplays
501165	CL-090	265.99	S	1.121	Is loss of grade related to loss of elongation of clasts? Why has mineralisation stopped?
	CL-220	194.2	NC	#N/A	Unaltered fresh, lapilli angular tuffs. From N courageous
	CL-231	160.4	NC	#N/A	Unaltered fresh, lapilli angular tuffs. From N courageous
683338	CL-248	236.69	WL	#N/A	Relate habbit of asp to FAT
683341	CL-248	240	WL	#N/A	Relate habbit of asp to FAT
683344	CL-248	243.42	WL	#N/A	Relate habbit of asp to FAT
684008	CL-254	81.43	WL	#N/A	Example of good deformation related mineralisation
684476	CL-257	211.99	WL	#N/A	Intergrowth of garents and asp= deformation

Thin Section Taken	
Thin section core	
Asp Mount	x

683549			SG58171	690776	690775	**Assay number**
CL-250	CL-185	CL-183	CL-054	CL-234	CL-234	**Drill Hole**
194	160	32.87	125.88	161.89	161.11	**Depth of oldest end**
WL	BL	BL	?	WL	WL	**Domain**
#N/A	#N/A	#N/A	31.226	#N/A	#N/A	**Au (ppm)**

Sampling reason
High grade. Deformation related but with acicular arsenopyrite
High grade with quartz
Spectacular VG
Bulldog lake. Fresh lapilli tuff
Bulldog lake. Fresh lapilli tuff
VG in arsenopyrite vein at Walsh

Thin Section Taken

Thin section core

Asp Mount

Assay number	Drill Hole	Depth of oldest end	Domain	Au (ppm)	Sampling reason	Thin Section Taken	Thin section core	Asp Mount
507624	CL-111	228.34	4	0.001	Show the evolution of grade within system towards oxidised area. Poor serectie alteration and grade to be compared to later samples. Baseline	X		
507617	CL-111	218.4	4	0.07	Top of area felsic ash package with foliation and composition similar to previous. Serecite alteration stronger then previous and now accompanied by mineralisation. To be compared with sample 1. Showing evolution of alteration and mineralisation	X		
507613	CL-111	214.5	4	2.912	First good instance of grade within the system and occurs as as jerosite alteration increases. Small acicular arsenopyrite clasts accompanied by stringers of dense fine crystaline arsenopyrite. Compare to previous samples and look to see if gold is within jerosite.	X		
507613	CL-111	213.24	4	2.912	More instense carboante but seemingly less grade then sample 3. Taken to look at grade within carbonate and evolution of oxidation.	X		
507609	CL-111	210.36	4	1.171	Mottled quartz above and including jerocite alteration. To see if there is grade within quartz and relationship (rip up? Or deformation) between quartz and jerocite. Show relative timings.			
507609	CL-111	210.1	4	1.171	Same quartz vein as sample 5 but with more intense jerocite potentially showing rip up textures.			
507609	CL-111	209.44	4	1.171	Transition from quartz vein towards felsic ash. Look at gold distribution and timing of quartz vein. Has the system evolved? First instance of consistant acicular arsenopyrite.			
507604	CL-111	201.96	4	4.708	Taken to determine whether greater grade is attributed to coarser ejector clasts or attributed to change in deformation intensity. Compare to sample 7. Cross cutting quartz vein seems to postdate deformation but is surrounded by the greatest level of asp.			
507603	CL-111	200.38	4	1.116	Similar to 8 however much greater proportion of coarser clasts. Look to see if grade is related to clast size and how system has evolved with more vent proximal system.			
507597	CL-111	193.4	4	2.582	Quartz veins parellel to foliation. Timing of quartz and relationship to mineralisation. Timing of sulphide emplacement and look for generations. Pyrite vs arsenopyrite. Has the system become more distal (less obvious clasts) or are they just elongate with a stronger metamorphic overprint.			
507597	CL-111	192.87	4	2.582	Asp mineralisation (without?) quartz veins. In sulphide veins parallel to foliation. Timing? Multiple generations? How has the system evolved since sample 10?			
507593	CL-111	186.54	4	5.053	Highest grade in this hole. Taken to look at very fine sulphides within the hole. Seem to be within larger clasts. Replacing feldspar within porpyritic clasts. Habbit of good grade.			

Sample Number	Thin Section Description
141	Very fine crystaline ash matrix with occasional ejectors. Quartz does not show uniform extinction angle and a mica within the matrix would seem to be rare. Specific cracks would seem to have more aggressive alteration that exploits specific horizons. Within these horizons, pyrite dominates commonly with much finer arsenopyrite cross cutting. Arsenopyrite is randomly orientated. Largest pyrite crystals have liquid filling morphologies and seem to be devoid of arsenopyrite but commonly have small blebs of chalcopyrite towards the rims.
142	Pyrite and arsenopyrite in equilibrium. Concordant with foliation. Arsenopyrite is often elongated in direction of foliation. Very fine quartz dominated ash matrix. Impregnated with mica that defines the foliation. Clasts are often reliced and only visible by extinction. They appear to be lenticular and not completelty deformed.
147	Very fine ash matrix with occasional ejectors that seem mostly undeformed. Poor mineralisation with occasional pyrite and chalcopyrite.
151	Slightly coarser matrix with fairly consistent felsic ash with intermitant mica veins. These now are much more wavey and do not show consistent extinction. Coarser crystaline quartz-carbonate veins cross cut the sample and so not seem to have much of an affect on sulphide abundance. Sulphides seem rare within the sample and occasionally arsenopyrite appears in
207	Significantly finer quartz matrix that is fairly well sorted and consistent throughout the slide. Frequently peppered with larger ejectors showing a range of stages of metamorphic degradation. There does not seem to be strong mica overprint with a very fine nextwork of small quartz veinletts and consistent silcaeous yellow and grey cement. Sulphides are distributed fairly evenly thorughout and occur in randomly oriented acicular crystals within the matrix. In the more dense sulphide areas these crystals form rossettes. There would seem to be a lack of pyrite with occasional pyrite veins rimming ejectors and seemingly not related to the arsenopyrite mineralising event.
210	Very fine matrix now with much more intense silacious matrix. This would seem to be especially apparent proximal to a large, coarse quartz vein. Coarsewr ejectors typical of domain 5 seem to still be ubundant but now would seem to be overprinted with and largely obscured. This intense mienralisation does not necessarily exploit these ejectors. Very dense and abundant fine crystaline arsenopyrite forms in a thick linitation parallel and adjecent to the vein. Sulhpide habit would seem to be largely monomineralic- mainly cubic arsenopyrite and occasionally acicular and occasionally larger blebs. There are instances of non-crystaline pyrite which is usually overprinted with the arsenopyrite. Coarse quartz vein has occsional large
212	Very fine crystaline quartz matrix but with very poorly sorted undeformed ejectors. Mica seems to be very scarce with a weak silicic cement occasionally visible. There is moderate mineralisation with fairly consistent acicular arsenopyrite throughout the sample. Occasional quartz veins within the matrix and these seem to be at close proximity to the sulhpides which otherwise seem to occur periodically throughout the sample and bear little relationship to largely unprevelant alteration textures or the protolith. Sulphide crystals would seem to show a greater range in size with larger crystals often appearing much more cubic then smaller surrounding acicular crystals. They remain randomly orientated.

Sample Number	Thin Section Description
18	Lithic tuff with well sorted, consistent ejector fragments held in vfc quartz matrix. Ejector fragments are usually sub-angular, spherical to elongate quartz clasts with occasionally feldspar. Larger fragments mottled with mica. Mica pressure shaddows form around largest quartz clasts seemigly with little preference for elongation of clast. Often overprrinting and occasionally cros-cutting these micas are sulphides. Micas occur in sub-parallel veins around quartz clasts and parallel with main deformation orientation as defined by ejector elongation. Acicular arsenopyrite is preferentially aligned with these micas and most abundant within the veins as is pyrite clasts. Sulphides seem to be preferntially concentrated in certain veins. Asp is occasionally noticed to cross cut mica allignment- here 2 generations of sulhpides seem to show asp overprinting py. An aggressive sulphide-filled coarser biotite
19	Similar protolith to sample 18. Rounded quartz ejector fragments visible throughout. Fine crystaline quartz ash matrix occasionally presearved but usually overprinted by foliated mica. Mica foliations are in sub parallel veins. They are usaully slightly controted with occasional, straigher thinner veins bending around ejector fragments and preferentially with the most dense sulphide content. Within these veins 2 sulphide habbits with amorphous pyrite and cubic to acicular arsenopyrite. Thought to be co-genetic fluid with pyrite generally crystalising first shown by growth textures. Sulphides tend to rim and not overprint the ejector fragments. One thick mica vein bisects the section. This seems more aggressive with muscovite breaking up ejector fragments which now undertake a mottled appearance. This contains acicular arsenopyrite which is usually alligned with foliation direction. Sulphides still seem to preferentially form around ejector clasts very occasionally overprinting. Arsenopyrite here seems to clearly overprint a more abraded and mottled looking pyrite. These veins seem to
20	Very fine grained quartz ash appears very well sorted. Occasional ejector clasts that are rare and sub rounded. Elongated and preferentially altered paleoclasts seem to be elongate and preferentially hosting rare pyrite. Texture seems aqueously reworked. Weak to moderate sericite alteration with interstial muscovite within ash. Muscovite has consistently aligned cleavage generally parallel to the long axis of ejector clasts. Seemingly overprinted rusty carbonate is common and liniated concordant to foliation. Pyrite is uncommon and usually forms in liquid blebs. In one instance this is overprinted by overprinted by arsenopyrite and occasionaly chalcopyrite.
22	Very fine grained well sorted ash with occasional rounded ejector clasts. There is moderate and consistent foliation defined by parallel mica veins and elongate carbonate blebs. Uniform very fine crystaline mica is apparent throughout the sample with consistent cleavage defining foliation. Moderate spots of chlorite are abundant throughout the sample. Disseminated sulphide clasts are distributed throughout. These seem to occur in areas with less abundant carbonate. They also seem to occur along specific foliation horizons. Sulphides would seem
26	Fairly unifrom quartz vein with defined by coarse crystaline interlcoking crystals. These form networks around a much finer crystaline, quartz dominated sericitised ash. This is very fine crystaline with occasional localised ejectors. These seem to be broken up and altered. Sulphides are present but not common within the quartz veins but ubiquitous within the host rock. Sulhpides are dominated by acicular arsenopyrite and cubic arsenopyrite especially in the areas and often overprinting ejector clasts. Many host rock areas seem sulphide poor with small chalcopyrite clasts and an absence of arsenopyrite. Quartz veins often have single isolated arsenopyrite crystals.
139	Very fine felsic matrix. Foliation defined by mica is moderate but fairly ubiquitous. Ejectors are common. Mineralisation seems to be controlled by primary porosity with foliation parallel arsenopyrite occuring in the foliation areas with the most ejectors. This seems to overprint the primary volcanics.
140	Fine crystaline quartz matrix with more apparent foliation. This is defined by elongate ejector clasts that would seem to preferentially occur in areas with more abundant mica and sulphides. These micas would seem to define a foliation with acicular arsenopyrite conforming to this. A late quartz-carbonate vein that cuts the section does not seem to affect mineralisation or alteration. Sulphides seem to be primarily arsenopyrite and occur in a range of cubic to acicular crystal habbits. Coarser ejectors are a lot more common and do not necessarily exhibit foliation throughout the slide. Patches of the unit show greater cementation. Mica is confined to certain veins that preferentially have greater abundances of sulphides.These often cross cut deformed ejector clasts but frequently envelop them. There does not seem to be a relationship between the mineralisation and the degree of elongation

Appendix C: SIMS and EMP analysis

Point	Comment	Sample num	SiO2(Mass%)	Al2O3(Mass%	Na2O(Mass%	MgO(Mass%	F(Mass%)	TiO2(Mass%	CaO(Mass%)	FeO(Mass%)	MnO(Mass%	BaO(Mass%	Cl(Mass%)	K2O(Mass%)	Total(Mass%	Au	Domain
1	118-142_Musc_01	142	45.705	34.175	0.264	1.019	0.042	0.458	0.017	1.603	0.031	0.146	0.001	11.189	94.65	0.488	3
2	118-142_Musc_02	142	45.728	34.036	0.247	1.092	0.112	0.57	0.019	1.694	0.027	0.142	0.007	11.146	94.82	0.488	3
3	118-142_Musc_03	142	45.345	34.559	0.291	0.842	0.039	0.373	0.017	1.539	0.018	0.14	0.005	11.009	94.177	0.488	3
4	118-142_Musc_04	142	47.203	32.83	1.158	1.069	0.099	0.295	0.227	1.525	-0.008	0.073	0.008	10.287	94.766	0.488	3
5	118-142_Musc_05	142	45.722	34.445	0.268	0.95	0.068	0.465	0.02	1.538	0.025	0.144	0.007	11.244	94.896	0.488	3
6	118-142_Musc_06	142	45.887	34.142	0.326	1.016	-0.058	0.448	0.016	1.614	-0.003	0.115	0.012	10.992	94.507	0.488	3
7	118-142_Musc_07	142	44.974	35.459	0.405	0.551	0.081	0.163	0.036	1.559	0.025	0.122	0.005	10.671	94.051	0.488	3
8	118-142_Musc_08	142	46.851	33.449	0.637	1.117	-0.041	0.46	0.128	1.631	-0.002	0.09	0.008	10.722	95.05	0.488	3
9	118-142_Musc_09	142	46.137	34.507	0.28	0.899	-0.021	0.163	-0.005	1.623	-0.003	0.067	0.001	11.007	94.655	0.488	3
10	118-142_Musc_10	142	45.844	34.132	0.446	0.932	-0.038	0.407	0.063	1.552	0.021	0.116	0.016	10.849	94.34	0.488	3
11	088-192_Musc_01	192	45.885	33.554	0.378	1.266	0.11	0.847	0.003	1.347	0.033	0.106	0.01	11.013	94.552	0.488	3
12	088-192_Musc_02	192	45.824	34.658	0.449	1.019	0.08	0.195	0.009	1.31	0.008	0.133	-0.001	10.759	94.443	0.488	3
13	088-192_Musc_03	192	45.53	35.584	0.636	0.553	-0.025	0.18	0.014	1.424	0.002	0.065	0.001	10.402	94.366	0.488	3
14	088-192_Musc_04	192	45.906	34.766	0.411	0.758	-0.045	0.206	0.001	1.474	0.001	0.025	0.001	10.645	94.149	0.488	3
15	088-192_Musc_05	192	45.752	34.487	0.424	1.098	0.062	0.371	0.038	1.35	0.011	0.116	0.019	10.625	94.353	0.488	3
16	088-192_Musc_06	192	45.557	34.216	0.422	1.083	0.074	0.456	0.004	1.441	0.028	0.205	0.013	10.847	94.346	0.488	3
17	088-192_Musc_07	192	46.097	33.321	0.667	1.278	0.117	0.376	0.021	1.46	0.014	0.147	0.025	10.452	93.975	0.488	3
18	088-192_Musc_08	192	44.765	34.849	0.486	0.807	-0.103	0.322	0.006	1.66	0	0.112	0.011	10.484	93.199	0.488	3
19	088-192_Musc_09	192	44.444	35.123	0.513	0.833	-0.097	0.155	0.012	1.609	0.015	0.093	0.009	10.491	93	0.488	3
20	088-192_Musc_10	192	45.725	33.833	0.46	1.125	0	0.624	0.032	1.291	0.017	0.145	0.008	10.774	94.034	0.488	3
21	088-90A_Musc_01	90	45.374	35.517	0.601	0.736	0.049	0.326	0.034	0.974	0.014	0.144	0.03	10.402	94.201	0.488	3
22	088-90A_Musc_02	90	45.528	35.268	0.537	0.77	0.112	0.342	0.033	1.06	-0.006	0.118	0.014	10.524	94.3	0.488	3
23	088-90A_Musc_03	90	45.526	34.75	0.587	0.821	0.082	0.351	0.042	1.021	0.016	0.086	0.037	10.323	93.642	0.488	3
24	088-90A_Musc_04	90	45.864	35.696	0.651	0.744	0.072	0.242	0.064	1.028	0.009	0.085	0.022	10.494	94.971	0.488	3
25	088-90A_Musc_05	90	45.371	35.003	0.584	0.794	0.07	0.368	0.019	1.025	0.012	0.087	0.019	10.567	93.919	0.488	3
26	088-90A_Musc_06	90	45.416	35.237	0.583	0.691	0.031	0.267	0.019	0.991	0.005	0.073	0.01	10.359	93.682	0.488	3
27	088-90A_Musc_07	90	45.172	35.795	0.648	0.617	0.005	0.323	0.015	0.826	0.003	0.064	0.024	10.42	93.912	0.488	3
28	088-90A_Musc_08	90	45.627	35.178	0.54	0.754	-0.007	0.332	0.008	0.975	-0.011	0.071	0.015	10.589	94.071	0.488	3
29	088-90A_Musc_09	90	45.227	35.359	0.746	0.694	0.192	0.243	0.045	0.912	0.005	0.067	0.051	9.976	93.517	0.488	3
30	088-90A_Musc_10	90	44.964	35.615	0.566	0.592	0.109	0.258	0.021	0.902	0.005	0.081	0.007	10.602	93.722	0.488	3
31	252_Musc_01	252	44.364	34.402	0.287	0.719	-0.01	0.411	0.056	1.585	0.003	0.167	0.008	11.022	93.014	0.488	3
32	252_Musc_02	252	45.264	33.79	0.283	1.002	0.053	0.506	0.021	1.73	0.027	0.155	0.006	11.05	93.887	0.488	3
33	252_Musc_03	252	45.532	33.258	0.283	1.176	0.118	0.974	0.023	1.946	0.023	0.137	0.007	10.982	94.459	0.488	3
34	252_Musc_04	252	45.362	34.083	0.27	0.973	0.064	0.556	0.014	1.842	0.022	0.129	0.002	11.161	94.478	0.488	3
35	252_Musc_05	252	47.017	32.505	0.761	1.1	-0.022	0.335	0.627	1.667	0.018	0.208	0.007	10.07	94.293	0.488	3
36	252_Musc_06	252	45.191	33.149	0.264	1.157	0.03	0.658	0.018	1.969	-0.005	0.123	0.005	11.082	93.641	0.488	3
37	252_Musc_07	252	45.307	33.496	0.254	1.186	0.176	0.518	0.016	1.841	0.033	0.161	0	11.128	94.116	0.488	3
38	252_Musc_08	252	45.293	33.499	0.297	1.169	0.023	0.377	0.053	1.983	-0.001	0.112	0.007	10.845	93.657	0.488	3
39	252_Musc_09	252	45.261	33.982	0.272	1.054	0.115	0.484	0.014	1.927	0.032	0.111	0.004	11.112	94.358	0.488	3
40	252_Musc_10	252	44.728	34.354	0.284	0.877	-0.018	0.379	0.083	1.712	0.02	0.101	-0.003	11.089	93.606	0.488	3
41	118-143_Musc_01	143	44.95	33.715	0.293	1.191	0.06	0.255	0.083	1.758	-0.014	0.135	0.005	11.164	93.595	0.488	3
42	118-143_Musc_02	143	45.206	34.096	0.357	0.888	0.037	0.316	0.177	1.779	0.004	0.148	0.015	10.994	94.017	0.488	3
43	118-143_Musc_03	143	45.436	33.946	0.396	1.077	0.104	0.512	0.023	1.535	-0.01	0.084	0.025	10.797	93.925	0.488	3
44	118-143_Musc_04	143	46.221	33.718	0.565	1.045	-0.049	0.386	0.127	1.508	0.022	0.182	0.01	10.776	94.511	0.488	3
45	118-143_Musc_05	143	44.851	34.217	0.316	0.849	0.166	0.284	0.016	1.543	0.018	0.142	0.003	11.034	93.439	0.488	3
46	118-143_Musc_06	143	45.366	34.324	0.366	0.961	-0.023	0.341	0.003	1.55	0.004	0.093	0.007	10.786	93.778	0.488	3
47	118-143_Musc_07	143	45.151	33.169	0.414	1.121	0.054	0.63	0.141	1.539	0.01	0.174	0.035	10.368	92.806	0.488	3
48	118-143_Musc_08	143	45.057	33.911	0.294	0.981	0.05	0.428	0.02	1.707	0	0.141	0.007	11.049	93.645	0.488	3

Point	Comment	Sample num	SiO2(Mass%)	Al2O3(Mass%	Na2O(Mass%	MgO(Mass%	F(Mass%)	TiO2(Mass%	CaO(Mass%)	FeO(Mass%)	MnO(Mass%	BaO(Mass%)	Cl(Mass%)	K2O(Mass%)	Total(Mass%	Au	Domain	
49	118-143_Musc_09	143	44.927	34.201	0.289	0.921	-0.013	0.373	0.009	1.573	0.01	0.094	0.004	11.088	93.476	0.961		3
50	118-143_Musc_10	143	44.856	34.179	0.324	0.932	-0.034	0.404	0.053	1.524	-0.009	0.181	0.01	10.896	93.316	0.961		3
51	118-146_Musc_01	146	44.904	33.81	0.397	0.963	-0.044	0.46	0.068	1.531	0.004	0.128	0.038	10.975	93.234	0.186		3
52	118-146_Musc_02	146	45.286	34.401	0.303	0.858	0.009	0.345	0.027	1.591	0.032	0.123	0.016	10.948	93.939	0.186		3
53	118-146_Musc_03	146	45.628	34.228	0.336	0.99	0.032	0.383	0.037	1.547	0.003	0.094	0.013	10.763	94.054	0.186		3
54	118-146_Musc_04	146	45.403	34.085	0.306	1.015	0.139	0.513	0.012	1.485	0.013	0.139	0.019	10.979	94.108	0.186		3
55	118-146_Musc_05	146	44.883	35.024	0.345	0.718	0.109	0.147	0.023	1.576	0.001	0.159	0.006	10.959	93.95	0.186		3
56	118-146_Musc_06	146	45.539	33.581	0.278	1.231	0.052	0.229	0.056	1.68	0.018	0.184	0.01	11.122	93.98	0.186		3
57	118-146_Musc_07	146	45.316	34.24	0.279	0.959	0.049	0.518	0.013	1.429	0.007	0.1	0.014	11.047	93.971	0.186		3
58	118-146_Musc_08	146	45.036	34.135	0.401	0.95	0.027	0.326	0.052	1.569	-0.005	0.16	0.045	10.595	93.291	0.186		3
59	118-146_Musc_09	146	45.263	34.147	0.297	0.878	0.003	0.539	0.014	1.327	-0.014	0.099	0.013	11.011	93.577	0.186		3
60	118-146_Musc_10	146	45.301	34.295	0.316	0.791	-0.034	0.573	0.004	1.399	0.017	0.153	0.002	10.981	93.798	0.186		3
61	088-214_Musc_01	214	44.954	34.921	0.474	0.675	0.034	0.326	-0.003	1.252	0.009	0.148	0.009	10.687	93.486	4.62		5
62	088-214_Musc_02	214	45.172	35.875	0.348	0.643	-0.021	0.223	0.013	1.262	0.008	0.069	0.003	10.798	94.393	4.62		5
63	088-214_Musc_03	214	44.681	35.31	0.399	0.625	-0.019	0.172	0.01	1.203	0.015	0.128	0.009	10.942	93.475	4.62		5
64	088-214_Musc_04	214	45.336	33.804	0.409	1.073	0.037	0.451	0.03	1.288	0.003	0.165	0.018	10.694	93.308	4.62		5
65	088-214_Musc_05	214	44.824	35.243	0.505	0.657	-0.036	0.106	0.023	1.19	0.019	0.116	0.001	10.626	93.274	4.62		5
66	088-214_Musc_06	214	45.751	35.22	0.409	0.771	0.086	0.082	0.007	0.923	0.005	0.071	0.002	10.907	94.234	4.62		5
67	088-214_Musc_07	214	45.141	35.831	0.502	0.551	0.055	0.228	0.032	1.116	-0.001	0.103	0.002	10.34	93.9	4.62		5
68	088-214_Musc_08	214	45.078	35.533	0.389	0.601	-0.014	0.189	0.003	1.17	-0.014	0.124	0.001	10.863	93.923	4.62		5
69	088-214_Musc_09	214	45.195	35.918	0.431	0.621	-0.044	0.151	0.015	1.119	0.018	0.083	-0.003	10.647	94.151	4.62		5
70	088-214_Musc_10	214	44.938	35.514	0.481	0.623	-0.098	0.131	0.02	1.163	-0.015	0.101	0.015	10.549	93.422	4.62		5
71	251_Musc_01	251	45.069	33.757	0.34	0.763	0.001	0.251	0.022	2.299	-0.028	0.216	-0.005	10.597	93.282	0.01	B	
72	251_Musc_02	251	44.993	33.947	0.383	0.803	-0.121	0.282	0.022	2.473	0.003	0.111	0.004	10.844	93.744	0.01	B	
73	251_Musc_03	251	45.278	33.357	0.285	0.899	-0.092	0.398	0.011	2.45	-0.001	0.195	0.004	10.938	93.722	0.01	B	
74	251_Musc_04	251	45.062	33.345	0.29	1.057	0.018	0.053	0.03	2.479	0.02	0.165	0.005	10.799	93.323	0.01	B	
75	251_Musc_05	251	45.029	33.336	0.273	0.9	0.079	0.393	0.025	2.542	0.004	0.202	0.002	10.851	93.636	0.01	B	
76	251_Musc_06	251	45.254	33.849	0.311	0.68	-0.06	0.188	0.012	2.021	-0.001	-0.006	0.001	10.878	93.127	0.01	B	
77	251_Musc_07	251	44.689	35.779	0.337	0.34	0.028	0.172	0.003	1.55	0.019	0.138	-0.001	10.913	93.967	0.01	B	
78	251_Musc_08	251	45.974	33.557	0.313	0.826	0.016	0.12	0.004	1.966	0.001	0.1	-0.001	10.883	93.759	0.01	B	
79	251_Musc_09	251	44.603	33.311	0.279	0.914	0.079	0.354	0.009	2.793	-0.008	0.076	0	10.895	93.305	0.01	B	
80	251_Musc_10	251	45.02	33.236	0.285	1.122	-0.055	0.029	0.019	2.437	0.025	0.093	0.006	10.75	92.967	0.01	B	

Name	Domain	Hole	As(Mass%)	Zn(Mass%)	Fe(Mass%)	S(Mass%)	Sb(Mass%)	Cu(Mass%)	Te(Mass%)	Ni(Mass%)	Au(Mass%)	Pb(Mass%)	Total(Mass%)
088-180_ASP5_001	5	CL-088	40.213	-0.128	33.922	22.028	0.11	0	-0.016	0.004	-0.086	0.063	96.11
088-180_ASP5_002	5	CL-088	43.223	-0.145	33.744	21.114	0.055	-0.007	0.024	-0.001	0.014	0.056	98.077
088-180_ASP5_004	5	CL-088	38.481	-0.102	27.677	16.715	0.108	-0.004	-0.015	0.009	0.041	0.128	83.038
088-180_ASP5_005	5	CL-088	41.049	-0.13	33.942	22.176	0.258	0	-0.041	0.005	0.022	0.066	97.347
088-180_ASP5_006	5	CL-088	43.536	-0.162	34.154	20.542	0.287	-0.007	-0.041	-0.004	-0.078	0.07	98.297
088-180_ASP5_008	5	CL-088	42.903	-0.136	33.999	21.663	0.12	-0.01	-0.031	0.005	0.007	0.074	98.594
088-180_ASP6_001	5	CL-088	43.878	-0.113	33.734	20.623	0.021	-0.01	-0.019	0.034	0.288	0.054	98.49
088-180_ASP6_002	5	CL-088	42.743	-0.117	34.496	20.873	0.089	-0.002	-0.019	0.009	0.21	0.07	98.352
088-180_ASP6_003	5	CL-088	43.507	-0.106	34.958	21.231	0.057	-0.016	-0.019	0.003	0.012	0.052	99.679
088-180_ASP6_004	5	CL-088	43.039	-0.155	34.243	21.037	0.01	-0.003	-0.012	0.007	0.202	0.067	98.435
088-180_ASP6_005	5	CL-088	42.804	-0.123	33.987	21.163	0.027	-0.008	-0.029	-0.001	0.169	0.053	98.042
088-180_ASP6_006	5	CL-088	43.361	-0.119	34.315	20.491	0.024	-0.006	-0.016	0.008	0.322	0.069	98.449
088-140_ASP3_001	3	CL-088	45.216	-0.11	34.871	19.675	0.021	-0.007	-0.023	0.032	-0.018	0.063	99.72
088-140_ASP3_002	3	CL-088	42.171	-0.119	35.544	22.043	0.016	-0.002	-0.019	0.007	-0.031	0.045	99.655
088-140_ASP3_003	3	CL-088	39.287	-0.132	35.849	24.044	0.227	-0.004	-0.038	0.009	-0.064	0.063	99.241
088-140_ASP3_004	3	CL-088	44	-0.132	35.169	20.861	0.046	-0.007	-0.022	0.017	-0.01	0.067	99.989
088-140_ASP3_005	3	CL-088	41.951	-0.143	35.267	22.362	0.029	-0.011	-0.022	0.001	-0.02	0.052	99.466
088-140_ASP3_006	3	CL-088	45.33	-0.117	34.009	19.737	-0.002	-0.01	0.017	0.002	0.01	0.056	99.032
088-140_ASP3_007	3	CL-088	38.164	-0.158	36.318	24.706	0.483	-0.003	-0.059	0.007	-0.062	0.065	99.461
088-140_ASP3_008	3	CL-088	41.924	-0.149	35.59	22.288	0.021	-0.005	-0.018	0	0.028	0.056	99.735
088-140_ASP3_009	3	CL-088	38.49	-0.11	36.321	24.673	0.403	-0.01	-0.068	0.013	-0.068	0.072	99.716
088-140_ASP3_010	3	CL-088	39.234	-0.14	36.489	24.103	0.481	-0.017	-0.061	-0.002	-0.016	0.1	100.171
088-140_ASP3_011	3	CL-088	42.319	-0.101	35.696	22.188	0.033	-0.007	-0.022	-0.009	-0.074	0.078	100.101
088-140_ASP3_012	3	CL-088	39.219	-0.127	36.196	24.25	0.525	-0.008	-0.056	0.008	-0.015	0.073	100.065
088-140_ASP3_013	3	CL-088	40.557	-0.143	35.552	23.282	0.079	-0.015	-0.026	-0.001	-0.022	0.052	99.315
088-140_ASP3_014	3	CL-088	39.008	-0.143	35.795	24.068	0.046	-0.009	-0.017	0.001	0.001	0.066	98.816
088-140_ASP2_001	3	CL-088	39.369	-0.105	36.338	24.187	0.274	-0.009	-0.044	0.002	-0.001	0.072	100.083
088-140_ASP2_002	3	CL-088	42.155	-0.124	35.381	22.496	0.018	-0.006	-0.016	0.004	-0.022	0.052	99.938
088-140_ASP2_003	3	CL-088	38.906	-0.157	36.395	24.384	0.38	-0.004	-0.057	0.002	-0.02	0.054	99.883
088-140_ASP2_004	3	CL-088	44.673	-0.131	35.14	20.218	0.04	-0.01	-0.015	0.016	-0.056	0.08	99.955
088-140_ASP2_005	3	CL-088	42.159	-0.145	35.614	22.2	0.061	-0.008	-0.028	-0.004	0.038	0.064	99.951
088-140_ASP2_006	3	CL-088	38.422	-0.14	35.924	24.604	0.57	-0.001	-0.084	0.005	-0.028	0.109	99.381
088-140_ASP2_007	3	CL-088	40.58	-0.116	34.865	23.237	0.063	-0.009	-0.036	0.001	0.007	0.072	98.664
088-140_ASP2_008	3	CL-088	38.937	-0.104	35.663	24.291	0.209	-0.012	-0.047	0.001	-0.057	0.077	98.958
088-140_ASP2_009	3	CL-088	38.967	-0.145	36.141	24.179	0.207	-0.01	-0.025	0.003	-0.022	0.077	99.372
088-140_ASP1_001	3	CL-088	38.432	-0.142	34.793	24.242	0.514	-0.003	-0.071	-0.001	-0.052	0.06	97.772
088-140_ASP1_002	3	CL-088	40.673	-0.149	35.788	23.046	0.133	-0.012	-0.029	-0.005	-0.01	0.071	99.506
088-140_ASP1_003	3	CL-088	41.714	-0.165	35.224	22.309	0.018	-0.008	-0.009	-0.005	-0.048	0.055	99.085
088-140_ASP1_004	3	CL-088	42.078	-0.14	34.424	21.627	0.017	0.003	-0.009	-0.003	-0.009	0.058	98.046
088-140_ASP1_005	3	CL-088	41.361	-0.132	34.533	22.458	0.014	-0.005	-0.012	-0.004	-0.063	0.093	98.243
088-140_ASP1_006	3	CL-088	39.803	-0.133	35.87	24.054	0.238	-0.009	-0.045	-0.002	-0.042	0.06	99.794
088-140_ASP1_007	3	CL-088	38.907	-0.154	35.244	24.095	0.051	-0.002	-0.013	-0.001	-0.047	0.094	98.174
118-26_ASP8_001	4	CL-118	44.2	-0.1	34.654	20.414	0.016	-0.014	0.017	0.004	-0.031	0.062	99.222
118-26_ASP8_002	4	CL-118	40.091	-0.102	34.067	22.949	0.064	-0.005	-0.02	0.002	-0.075	0.086	97.057

Name	Domain	Hole	As(Mass%)	Zn(Mass%)	Fe(Mass%)	S(Mass%)	Sb(Mass%)	Cu(Mass%)	Te(Mass%)	Ni(Mass%)	Au(Mass%)	Pb(Mass%)	Total(Mass%)
118-26_ASP8_003	4	CL-118	41.395	-0.143	35.117	22.699	0.072	-0.006	-0.021	-0.005	-0.046	0.062	99.124
118-26_ASP8_004	4	CL-118	42.243	-0.181	35.301	21.876	0.022	-0.012	-0.01	-0.001	-0.065	0.057	99.23
118-26_ASP8_005	4	CL-118	43.351	-0.159	34.663	20.995	0.001	-0.008	-0.011	-0.003	0.098	0.082	99.009
118-26_ASP8_006	4	CL-118	40.462	-0.114	35.544	23.323	0.02	-0.006	-0.021	0	-0.034	0.084	99.258
118-26_ASP8_007	4	CL-118	39.561	-0.141	34.711	23.352	0.093	-0.012	-0.025	0.004	-0.073	0.054	97.524
118-26_ASP8_008	4	CL-118	39.214	-0.169	34.407	24.087	0.053	-0.012	-0.026	-0.008	-0.024	0.073	97.595
118-26_ASP8_009	4	CL-118	42.956	-0.135	34.495	21.502	0.018	-0.01	-0.014	-0.002	-0.047	0.057	98.82
118-26_ASP8_010	4	CL-118	41.283	-0.155	35.45	22.622	0.005	-0.006	-0.02	-0.002	-0.041	0.073	99.209
118-26_ASP7_001	4	CL-118	41.838	-0.146	35.453	22.343	0.009	-0.009	-0.026	-0.002	-0.053	0.061	99.468
118-26_ASP7_002	4	CL-118	42.951	-0.144	35.201	21.567	0.015	-0.007	-0.02	-0.005	-0.021	0.076	99.613
118-26_ASP7_003	4	CL-118	43.646	-0.108	34.182	21.003	0.012	-0.001	-0.016	-0.006	-0.034	0.061	98.739
118-26_ASP7_004	4	CL-118	43.191	-0.124	34.925	21.237	0.002	-0.002	0.018	-0.002	-0.047	0.054	99.252
118-26_ASP7_005	4	CL-118	44.052	-0.145	34.419	20.841	0.018	-0.019	-0.006	-0.003	0.044	0.07	99.271
118-26_ASP7_006	4	CL-118	39.616	-0.155	35.555	23.595	0.351	-0.007	-0.041	-0.004	-0.045	0.069	98.934
118-19_arsenopyrite	4	CL-118	41.952	-0.13	35.295	22.11	0.018	-0.001	-0.007	0.003	-0.066	0.067	99.241
118-19_arsenopyrite	4	CL-118	44.577	-0.141	34.658	20.011	0.019	-0.003	-0.013	0.009	-0.054	0.066	99.129
088-210A_arsenopyı	5	CL-088	43.183	-0.13	34.33	20.84	0.032	-0.01	-0.016	-0.015	-0.043	0.067	98.238
088-210A_arsenopyı	5	CL-088	39.123	-0.138	34.934	23.555	0.402	-0.007	-0.037	-0.004	-0.03	0.074	97.872
088-210A_ASP10_0(	5	CL-088	43.116	-0.118	34.025	20.983	0.028	0	-0.012	-0.009	-0.098	0.044	97.959
088-210A_ASP10_0(	5	CL-088	38.906	-0.119	35.602	23.761	0.272	-0.007	-0.044	-0.006	-0.03	0.069	98.404
088-210A_ASP10_0(	5	CL-088	41.009	-0.128	34.168	22.109	0.02	-0.004	-0.005	-0.002	-0.05	0.076	97.193
088-210A_ASP10_0(	5	CL-088	39.68	-0.128	35.473	23.316	0.064	-0.011	-0.01	-0.011	-0.054	0.064	98.383
088-210A_ASP10_0(	5	CL-088	38.134	-0.099	35.049	24.098	0.163	-0.001	-0.018	-0.006	-0.037	0.073	97.356
088-210A_ASP10_0(	5	CL-088	44.953	-0.144	34.197	20.614	0.009	-0.006	-0.01	-0.012	-0.014	0.043	99.63
088-210A_ASP10_0(	5	CL-088	39.585	-0.142	35.606	24.411	0.06	-0.003	-0.024	-0.007	-0.033	0.073	99.526
088-210A_ASP10_0(	5	CL-088	41.574	-0.113	35.193	22.734	0.078	-0.012	-0.005	-0.004	-0.044	0.067	99.468
088-210A_ASP11_0(	5	CL-088	43.496	-0.171	34.386	21.368	-0.002	-0.004	-0.003	-0.006	0.048	0.078	99.19
088-210A_ASP11_0(	5	CL-088	41.959	-0.095	32.596	20.704	0.008	-0.007	0.279	-0.007	-0.006	0.068	95.499
088-89_ASP9_001	4	CL-088	42.801	-0.158	34.822	21.724	-0.007	-0.008	-0.016	0.002	0.015	0.066	99.241
088-89_ASP9_002	4	CL-088	44.509	-0.161	34.452	20.511	0.006	-0.014	-0.025	-0.003	-0.065	0.082	99.292
088-89_ASP9_003	4	CL-088	43.102	-0.127	35.183	21.635	-0.005	-0.01	-0.013	0	-0.039	0.073	99.799
088-89_ASP9_004	4	CL-088	43.278	-0.123	35.369	21.908	0.012	-0.01	-0.004	0.005	-0.038	0.059	100.456
088-89_ASP9_005	4	CL-088	45.111	-0.146	34.822	20.601	0.01	-0.005	-0.016	0.019	-0.045	0.087	100.438
088-89_ASP9_006	4	CL-088	42.112	-0.101	35.667	22.43	0.012	-0.004	-0.012	0	-0.059	0.061	100.106
088-207A_ASP16_0(	5	CL-088	40.553	-0.1	34.975	22.232	0.014	-0.003	-0.009	-0.006	-0.06	0.06	97.656
088-207A_ASP16_0(	5	CL-088	38.146	-0.151	35.829	24.279	0.288	-0.01	-0.05	0.006	-0.059	0.064	98.342
088-207A_ASP16_0(	5	CL-088	41.647	-0.125	35.316	22.075	0.029	-0.007	-0.03	-0.002	-0.052	0.076	98.927
088-207A_ASP16_0(	5	CL-088	44.158	-0.101	35.077	20.645	0.01	-0.004	-0.03	0.001	-0.019	0.066	99.803
088-207A_ASP16_0(	5	CL-088	40.676	-0.112	35.655	22.812	0.098	-0.004	-0.008	-0.001	-0.016	0.19	99.29
088-207A_ASP17_0(	5	CL-088	38.601	-0.133	35.966	24.355	0.34	-0.01	-0.055	0.007	-0.031	0.088	99.128
088-207A_ASP17_0(	5	CL-088	43.569	-0.145	33.983	20.111	0.013	-0.001	-0.019	0.024	-0.062	0.065	97.538
088-207A_ASP17_0(	5	CL-088	40.938	-0.123	35.532	22.713	0.009	-0.009	-0.014	-0.003	-0.015	0.049	99.077
088-207A_ASP17_0(	5	CL-088	38.897	-0.11	36.064	24.318	0.384	-0.007	-0.054	0.011	-0.028	0.079	99.554
088-207A_ASP17_0(	5	CL-088	41.237	-0.122	35.082	22.745	0.02	-0.008	-0.017	0.004	-0.006	0.057	98.992

Name	Domain	Hole	As(Mass%)	Zn(Mass%)	Fe(Mass%)	S(Mass%)	Sb(Mass%)	Cu(Mass%)	Te(Mass%)	Ni(Mass%)	Au(Mass%)	Pb(Mass%)	Total(Mass%)
118-19_ASP14_001	4	CL-118	42.255	-0.129	35.461	21.901	0.009	-0.006	-0.013	0.001	-0.049	0.049	99.479
118-19_ASP14_002	4	CL-118	42.204	-0.152	35.372	22.191	0.023	-0.008	-0.027	0.005	-0.05	0.07	99.628
118-19_ASP14_003	4	CL-118	40.422	-0.136	35.214	22.289	0.053	-0.009	-0.02	0.008	-0.036	3.057	100.842
118-19_ASP14_004	4	CL-118	42.633	-0.105	35.829	21.922	0.02	0	-0.022	-0.001	-0.028	0.08	100.328
118-19_ASP14_005	4	CL-118	41.554	-0.109	35.565	22.34	0.013	-0.001	-0.006	-0.001	-0.056	0.051	99.35
118-19_ASP14_006	4	CL-118	42.383	-0.111	35.427	21.888	0.017	-0.004	-0.021	-0.003	-0.071	0.063	99.568
118-19_ASP14_007	4	CL-118	41.646	-0.118	35.403	22.829	0.063	0.003	-0.024	0.01	-0.033	0.068	99.847
118-19_ASP15_001	4	CL-118	42.251	-0.12	35.464	22.025	0.015	-0.006	-0.006	0.006	-0.061	0.076	99.644
118-19_ASP15_002	4	CL-118	42.361	-0.121	35.264	21.827	0.042	-0.009	-0.021	0.009	-0.058	0.05	99.344
118-19_ASP15_003	4	CL-118	43.017	-0.144	35.151	21.229	0.006	-0.008	0.021	0.004	-0.023	0.07	99.323
118-19_ASP15_004	4	CL-118	45.569	-0.122	34.586	19.636	0.005	-0.009	-0.022	0.008	0.005	0.081	99.737
118-19_ASP15_005	4	CL-118	42.457	-0.136	35.663	22.102	0.015	-0.007	-0.011	0.01	-0.068	0.063	100.088
118-19_ASP15_006	4	CL-118	42.256	-0.134	34.102	20.725	0.038	-0.009	-0.025	0.005	-0.04	0.074	96.992
118-19_ASP15_007	4	CL-118	41.419	-0.161	35.262	22.479	0.031	-0.004	-0.016	0.008	-0.059	0.064	99.023
118-19_ASP15_008	4	CL-118	42.781	-0.104	35.364	21.683	0.017	-0.011	-0.026	0.01	0.094	0.075	99.883
088-210A_around_e	5	CL-088	41.796	-0.156	35.358	22.298	0.075	-0.005	-0.022	-0.016	-0.032	0.065	99.361
088-210A_around_e	5	CL-088	41.221	-0.119	35.834	22.651	0.136	-0.012	-0.027	-0.002	0.044	0.081	99.807

Point	Sb(Mass%)	Ag(Mass%)	Au(Mass%)	Te(Mass%)	Pb(Mass%)	Cu(Mass%)	Ni(Mass%)	Zn(Mass%)	Fe(Mass%)	S(Mass%)	As(Mass%)
1	0.029	-0.001	0.007	0.004	0.08	0.001	0.003	-0.004	34.281	21.648	42.616
1	0.018	-0.001	0.049	0.001	0.095	-0.007	0.004	-0.005	34.304	21.177	42.363
2	0.363	-0.001	-0.001	-0.008	0.089	-0.001	0.008	0	34.408	22.454	40.858
2	0.023	-0.009	0.014	0.001	0.066	0	0.006	-0.006	34.144	21.089	42.54
3	0.032	-0.007	0.008	-0.001	0.071	0.002	0.008	-0.006	34.407	21.162	42.904
3	0.03	-0.005	0.077	0	0.064	0.003	0.015	-0.002	33.969	20.891	43.453
4	0.021	0	0.001	-0.005	0.065	-0.004	0.008	0.001	34.348	21.868	42.198
4	0.028	-0.008	0.089	0.004	0.08	0.003	0.007	-0.002	34.109	21.07	43.015
5	0.006	-0.005	0.022	0.006	0.073	-0.01	0.01	-0.005	34.234	21.379	42.049
5	0.02	-0.001	0.011	0	0.079	0.002	0.006	-0.005	34.075	21.409	42.713
6	0.015	-0.007	0.02	0.002	0.081	-0.001	0.006	-0.004	34.4	21.629	42.192
6	0.01	-0.006	0.01	-0.002	0.06	-0.001	0.01	-0.006	34.687	21.703	42.309
7	0.31	-0.011	0.013	-0.004	0.098	-0.003	0.004	-0.006	35.155	24.171	38.656
7	0.033	0.002	0.032	-0.001	0.086	-0.002	0.001	0	34.267	20.808	43.644
8	0.007	-0.003	0.036	0	0.097	-0.004	0.005	-0.007	34.178	21.949	41.852
8	0.027	-0.016	0.042	0.003	0.086	-0.003	0.002	-0.006	34.198	21.256	42.869
9	0.01	-0.007	-0.002	-0.004	0.082	0	0.002	-0.004	33.952	21.226	42.757
9	0.035	0.002	0.137	-0.001	0.068	0	0.02	-0.013	34.059	21.204	42.895
10	0.027	-0.006	0.006	0.002	0.077	-0.005	0.004	-0.003	34.672	23.036	40.385
10	0.045	-0.006	0.18	-0.002	0.065	-0.009	0.019	-0.005	33.955	21.16	42.222
11	-0.008	-0.002	0.004	0.007	0.116	-0.004	0.031	-0.001	59.026	39.155	0.057
11	0.012	-0.01	0.056	0.001	0.074	0	0.003	-0.005	34.085	21.036	42.554
12	0.007	-0.001	0.002	-0.011	0.12	-0.003	0.042	0.001	58.357	38.832	0.023
12	0.032	-0.017	0.032	-0.006	0.079	-0.006	0.016	-0.006	34.585	21.343	42.798
13	0.132	0.007	0.015	-0.007	0.077	-0.004	0.004	-0.002	34.199	21.533	42.344
13	0.028	-0.004	0.036	-0.002	0.072	-0.006	0.047	0.002	34.177	20.827	43.261
14	0.023	-0.003	0.108	-0.143	0.066	0.006	0.002	-0.008	33.672	21.281	42.072
14	-0.001	-0.013	0.013	-0.002	0.158	0.001	-0.003	-0.002	44.939	53.412	0.044
15	-0.004	-0.004	0.008	-0.001	0.116	-0.004	0.006	-0.011	58.182	38.718	0
15	0.043	-0.002	0.074	-0.007	0.085	-0.009	0.009	-0.01	34.235	21.238	42.609
16	0.064	-0.005	0.02	0.004	0.086	-0.006	0.003	-0.007	34.249	21.652	41.893
16	0.371	0.004	0.054	-0.008	0.074	-0.006	0.224	-0.012	33.893	22.209	40.763

Point	Sb(Mass%)	Ag(Mass%)	Au(Mass%)	Te(Mass%)	Pb(Mass%)	Cu(Mass%)	Ni(Mass%)	Zn(Mass%)	Fe(Mass%)	S(Mass%)	As(Mass%)
17	0.023	0	0.01	0	0.064	-0.002	0.007	-0.011	34.288	21.823	41.48
17	0.017	-0.008	0.007	-0.002	0.072	-0.001	0.005	-0.011	34.497	21.609	41.882
18	0.011	-0.003	0.008	0.002	0.079	-0.005	0.003	-0.005	34.455	21.865	41.557
18	0.079	0.004	0.015	0.004	0.083	0.004	0.002	-0.002	34.562	22.147	41.91
19	0.044	0	0	0.004	0.073	0	0.004	-0.008	34.244	20.905	42.96
19	0.004	0	0.034	0.003	0.073	0	0.001	-0.008	34.314	20.96	43.299
20	0.022	-0.011	0.016	-0.001	0.075	-0.003	0.02	-0.005	34.481	21.834	41.647
20	0.026	-0.011	0.104	0	0.079	-0.001	0.012	0.002	34.304	21.103	43.297
21	0.021	-0.005	0.001	0	0.07	-0.004	0.253	-0.007	33.173	20.342	44.131
21	0.006	-0.007	0.006	-0.001	0.055	0.001	0.002	-0.01	34.826	21.564	42.529
22	0.029	-0.021	0.002	-0.007	0.066	-0.004	0.005	-0.007	34.264	21.179	42.233
22	0.013	0.001	0.003	-0.008	0.079	0.002	0.002	-0.007	34.582	21.398	42.155
23	0.004	-0.012	0.004	0.002	0.064	-0.006	0.005	-0.004	34.354	21.82	42.026
24	0.022	0.001	0.002	0	0.073	-0.003	0.009	-0.01	34.574	21.557	42.226
24	0.066	-0.009	0.02	-0.002	0.073	0	0.17	0	33.697	21.785	41.443
25	0.026	0.006	0.013	-0.012	0.062	-0.004	0.006	0	34.04	20.96	43.097
25	-0.006	-0.013	-0.004	0.002	0.124	-0.003	0.006	-0.007	57.316	39.524	0
26	0.294	-0.009	0.006	-0.013	0.072	-0.002	0.011	-0.004	34.922	23.423	39.506
26	0.007	-0.001	0.068	0	0.066	0.005	0.008	-0.001	34.077	22.684	41.214
27	0.458	-0.004	0.012	-0.007	0.088	-0.001	0.01	0.001	34.975	23.287	38.953
27	0.005	-0.011	0.012	-0.002	0.084	0.006	0.014	-0.013	34.278	22.352	40.972
28	-0.005	0.013	-0.003	-0.003	0.096	33.117	0.003	0.017	28.943	34.388	0.014
28	0.017	0	0.026	-0.005	0.075	-0.008	-0.001	0.002	34.459	22.222	41.745
29	0.025	-0.005	0.006	-0.002	0.083	-0.004	0.007	-0.008	34.322	21.858	42.1
29	-0.004	-0.004	0.05	0.003	0.069	-0.002	0.002	0	33.912	20.886	43.097
30	0.011	0.001	0.001	-0.01	0.077	-0.004	0.017	-0.005	34.281	21.426	42.056
30	0.017	0.002	0.025	-0.014	0.078	-0.004	0.006	-0.008	34.431	22.145	41.876
31	0.082	-0.005	0.023	-0.005	0.073	-0.007	0.008	-0.006	33.885	21.332	41.994
31	0.007	0.001	0.012	-0.001	0.065	0.018	0.002	-0.004	34.385	21.805	41.65
32	0.191	-0.014	0.001	-0.004	0.068	-0.001	0.018	-0.006	34.492	22.493	41.13
32	0.038	0.012	-0.001	-0.004	0.137	0.358	0.021	-0.004	45.32	31.366	16.625
33	0.036	-0.007	0.004	-0.001	0.088	-0.005	0.015	-0.006	34.566	22.889	40.768

Point	Sb(Mass%)	Ag(Mass%)	Au(Mass%)	Te(Mass%)	Pb(Mass%)	Cu(Mass%)	Ni(Mass%)	Zn(Mass%)	Fe(Mass%)	S(Mass%)	As(Mass%)
33	-0.006	-0.006	0.027	0.006	0.076	0.005	0.003	-0.006	33.871	20.89	43.539
34	0.042	-0.013	0.009	-0.002	0.07	-0.001	0.002	-0.015	35.008	22.347	42.388
34	0.006	-0.004	0.007	0.001	0.068	-0.003	0.014	-0.007	33.724	21.666	42.601
35	0.013	0.003	-0.001	0.008	0.073	-0.005	0.005	-0.014	34.435	21.656	42.971
35	0.161	0.004	0.013	-0.005	0.085	0	0.016	-0.012	35.146	24.231	39.581
36	0.009	-0.001	0.024	-0.001	0.066	-0.003	0.003	-0.007	34.349	21.487	42.629
36	0.015	-0.007	0.038	-0.006	0.068	0.001	0.01	-0.01	34.504	21.917	42.135
37	0.009	-0.008	-0.001	0.002	0.07	-0.001	0.002	-0.005	34.712	21.921	41.54
37	0.002	0	0.041	-0.003	0.072	-0.004	0.005	-0.006	34.106	21.153	44.199
38	0.068	0.014	0.014	-0.004	0.085	-0.006	0.026	-0.008	34.303	21.853	42.48
38	0.009	0.005	0.006	-0.001	0.087	-0.004	0.013	-0.008	34.422	22.355	41.281
39	0.017	-0.005	0.052	-0.004	0.088	-0.004	0.008	-0.005	34.742	22.462	41.913
39	0.016	-0.006	0.014	-0.002	0.075	-0.007	0.007	-0.01	34.637	22.112	42.212
40	0.235	-0.008	0.023	-0.004	0.072	-0.003	0.002	-0.005	34.646	22.117	41.3
40	0.011	-0.008	0.025	-0.002	0.065	0	0	-0.003	34.468	22.312	41.288
41	0.075	-0.017	0.01	-0.003	0.084	-0.003	0	-0.009	34.509	22.788	40.292
41	-0.002	-0.006	0.033	-0.005	0.069	-0.001	0.026	-0.006	34.094	21.551	42.812
42	0.242	-0.003	0.008	-0.005	0.085	-0.004	0.004	-0.008	34.865	22.818	40.677
42	0.01	-0.001	0.016	0.004	0.07	-0.004	0.031	-0.001	33.98	21.501	42.515
43	0.137	0.001	0.003	0.005	0.066	0	0.003	-0.007	34.635	22.484	41.319
43	0.003	-0.019	0.012	0.001	0.082	-0.004	0.005	-0.008	34.29	21.718	42.937
44	0.027	0.001	0.018	0.002	0.078	-0.001	0.003	-0.015	34.528	22.192	42.031
44	0.007	0.002	0.013	-0.002	0.069	0.002	0.004	0	33.97	21.051	42.994
45	0.025	-0.003	0.012	-0.005	0.076	-0.002	0.001	-0.01	34.352	21.543	41.85
45	0.023	0.001	0.023	0	0.078	-0.008	0.01	-0.006	34.554	21.903	42.166
46	-0.006	-0.009	0.02	0.003	0.076	-0.005	0.016	-0.004	33.797	21.002	43.679
47	-0.006	-0.002	0.002	0.002	0.061	0	0.009	-0.003	34.528	22.44	42.049
48	0.007	0	0.02	0	0.072	-0.006	0.005	-0.007	34.127	21.401	42.981
49	0.042	0	0.035	0.003	0.084	0	0.018	-0.002	33.882	20.814	44.202
50	0.053	-0.003	0.019	-0.003	0.054	-0.002	0.006	-0.008	34.3	21.449	43.471
52	0.52	-0.01	0.031	-0.011	0.084	0.002	0.026	-0.002	34.985	24.075	39.131
53	0.039	-0.002	0.021	0.003	0.058	-0.004	0.011	-0.004	33.834	21.057	43.277

Point	Sb(Mass%)	Ag(Mass%)	Au(Mass%)	Te(Mass%)	Pb(Mass%)	Cu(Mass%)	Ni(Mass%)	Zn(Mass%)	Fe(Mass%)	S(Mass%)	As(Mass%)
54	0.008	0	0.015	0.001	0.073	-0.005	0.01	-0.005	34.554	22.406	41.396
55	0.695	-0.005	0.014	-0.018	0.08	-0.009	0.023	-0.002	34.181	22.446	40.629
56	-0.004	-0.005	0.013	-0.003	0.072	-0.002	0.02	-0.001	33.93	20.381	43.983
57	0.02	-0.014	0.015	-0.002	0.079	0.014	0.021	-0.008	33.459	19.389	43.371
58	0.069	0.003	0.044	-0.001	0.089	0.001	0.045	-0.008	33.922	20.501	43.536
59	0.25	-0.001	0.034	-0.002	0.092	-0.003	0.038	-0.002	34.287	22.256	41.393
60	0.21	0.004	0.034	-0.005	0.072	0.003	0.023	-0.011	34.156	21.667	42.183
61	0.006	0.002	0.088	-0.005	0.09	0.002	0.017	0.002	32.587	20.806	43.162
63	0.001	-0.002	-0.002	0.001	0.086	0.003	0.049	-0.009	33.995	20.273	43.9
64	0.006	-0.009	0.011	0.001	0.089	0.012	0.091	0	34.554	21.5	42.543
65	0.005	-0.004	0.005	0.002	0.081	-0.01	0.154	-0.006	33.443	19.117	45.842
66	-0.001	0.006	0.016	0.004	0.08	0.001	0.063	-0.007	34.693	21.799	42.339
67	0.006	-0.012	0.027	0.003	0.061	0.001	0.054	-0.002	33.852	20.945	43.228
68	-0.002	0.003	0.001	0.004	0.078	0.004	0.09	-0.012	34.309	21.429	43.304
69	0.002	-0.007	0.012	0.008	0.094	0.003	0.088	-0.01	34.255	21.523	43.028
70	-0.004	-0.009	-0.008	0.002	0.076	-0.003	0.066	-0.005	34.362	21.68	43.034
71	-0.009	-0.009	0.014	-0.004	0.072	0.002	0.069	0	34.254	21.631	42.367
72	0.004	0.007	0.024	0	0.084	0.002	0.447	-0.01	32.318	18.688	46.138
74	0.029	-0.002	0.024	0.002	0.077	-0.003	0.003	-0.009	34.143	21.627	41.686
75	0.026	-0.001	0.022	-0.002	0.064	0.003	0.02	-0.001	34.283	21.999	42.303
76	0.019	-0.003	0.024	0.007	0.085	-0.001	0.173	-0.002	34.203	21.45	42.458
77	0.178	-0.002	0.011	-0.005	0.074	-0.004	0.007	-0.005	35.07	22.949	41.267
78	0.012	0.003	-0.001	0.001	0.069	-0.003	0.008	-0.008	34.54	21.482	42.911
79	0.017	-0.003	0.003	0.004	0.083	0	0.029	-0.002	33.925	21.359	43.598
80	0.016	-0.016	0.019	0.004	0.055	0	0.018	-0.003	33.877	21.27	42.856
81	0.31	-0.005	0.024	-0.009	0.083	-0.005	0.012	-0.004	34.702	22.534	41.303
82	0.02	0.006	0.015	-0.002	0.077	-0.007	0.006	-0.004	34.277	21.892	42.971

Point	Total(Mass%)	Au ppm	Sb counts	Comments	Width	Height	Width:Heig	Habbit	Apy type	Core Au ppı	Rim Au ppn
1	98.664	0.95	99.64	0	1.06	5	4.716981	C	B	0	0
1	97.998	244.48	131	core	1.23	2.54	2.065041	C	B	244.48	405.3
2	98.169	0.73	259	0	1.39	4.21	3.028777	P	C	0	0
2	97.868								B		
3	98.58	20.79	132.6	0	2.17	2.81	1.294931	C	B	0	0
3	98.495								C		
4	98.501	5.13	96.7	0	1.79	2.09	1.167598	C	A	0	0
4	98.395								C		
5	97.759	3.95	227.5	0	0.47	8	17.02128	C	A	0	0
5	98.309								A		
6	98.333								B		
6	98.774								A		
7	98.383	315.17	235.6	0	0.31	1.52	4.903226	C	C	0	0
7	98.87								B		
8	98.11	214.01	121.7	0	0.25	0.85	3.4	C	C	0	0
8	98.458								B		
9	98.012	6.03	195.2	0	0.67	1.86	2.776119	C		0	0
9	98.406	2345.19	68.5	core	1.33	3.93	2.954887	C	A	2345.19	2462.81
10	98.195	142.89	148.5	0	0.96	2.39	2.489583	C		0	0
10	97.624								A		
11	98.381								P		
11	97.806	1491.65	438.2	0	0.33	3.95	11.9697	C	A	0	0
12	97.369								P		
12	98.85	192.24	88.5	core	1.07	2.16	2.018692	C	C	192.24	182.28
13	98.298	255.49	276.3	0	2.62	3.03	1.156489	A	C	255.49	229.37
13	98.438								C		
14	97.076								C		
14	98.546								P		
15	97.006								P		
15	98.265	1654.42	207.9	core	0.77	3.24	4.207792	C	B	1654.42	2418.16
16	97.953	1.6	58.9	core	1.48	3.72	2.513514	C	B	1.6	20.89
16	97.566								B		

Point	Total(Mass%)	Au ppm	Sb counts	Comments	Width	Height	Width:Heig	Habbit	Apy type	Core Au ppi	Rim Au ppn
17	97.682								B		
17	98.067	18.27	112.7	core	1.1	5.25	4.772727	C	B	18.27	66.22
18	97.967	22.21	133.9	core	0.96	3.39	3.53125	C	B	22.21	19.04
18	98.808								B		
19	98.226								B		
19	98.68	916.8	96.3	core	1.1	5.21	4.736364	C	A	916.8	1108.81
20	98.075	18.78	100.2	core	2.28	4.71	2.065789	C	B	18.78	20
20	98.915								A		
21	97.975								B		
21	98.971	236.06	357.1	core	0.79	2.74	3.468354	C	B	236.06	97.43
22	97.739	3.23	101.2	core	1.58	6.53	4.132911	C	B	3.23	0.69
22	98.22								B		
23	98.257								B		
24	98.451								B		
24	97.243	113.23	175.2	0	1.29	3	2.325581	P	C	0	0
25	98.194								B		
25	96.939								P		
26	98.206	38.65	232.8	0	0.64	2.85	4.453125	C		0	0
26	98.127								A		
27	97.772	13.9	288.1	0	0.62	2.22	3.580645	C		0	0
27	97.697								A		
28	96.58								P		
28	98.532								B		
29	98.382	1.46	64.8	0	0.8	0.93	1.1625	C	B	0	0
29	98.009								B		
30	97.851	8.52	232.2	0	0.44	5.32	12.09091	C	A	0	0
30	98.554	14.37	108.8	0	1.74	1.89	1.086207	P	C	0	0
31	97.374								C		
31	97.94	14.3	125.6	0	1.68	1.93	1.14881	P	C	0	0
32	98.368								A		
32	93.868								P		
33	98.347								A		

Point	Total(Mass%)	Au ppm	Sb counts	Comments	Width	Height	Width:Heig	Habbit	Apy type	Core Au ppm	Rim Au ppm
33	98.399	19.08	76 core		1.66	5.46	3.289157 C	B		19.08	210.98
34	99.835	61.51	880.1	0	0.22	3.42	15.54545 C	A		0	0
34	98.073							B			
35	99.144	7.86	361	0	0.7	0.83	1.185714 C	A		0	0
35	99.22	93.69	395.6 core		1.92	5.2	2.708333 C	B		93.69	333.34
36	98.555	17.31	125.3 core		1.28	4.64	3.625 C	B		17.31	45.65
36	98.665							B			
37	98.241							B			
37	99.565	312.03	41 core		1.88	3.46	1.840426 C	B		312.03	133.6
38	98.825	54.64	173 core		1.64	4	2.439024 C	B		54.64	112.35
38	98.165							B			
39	99.264							B			
39	99.048	104.59	168.6 core		0.84	3.89	4.630952 C	A		104.59	24.06
40	98.375	9.82	458.9	0	1.13	3.33	2.946903 P	C		0	0
40	98.156							A			
41	97.726	4.68	116	0	1.72	2.1	1.22093 R	C		0	0
41	98.565	34.63	135 core		0.92	2.36	2.565217 P	C		34.63	91.66
42	98.679	29.58	372.2	0	0.62	0.71	1.145161 C	B		0	0
42	98.121							C			
43	98.646	39.17	188.2	0	0.58	0.88	1.517241 P	B		0	0
43	99.017	2.69	66.9 core		1.86	4.21	2.263441 C	B		2.69	86.9
44	98.864	6.63	233	0	0.39	3.19	8.179487 C	A		0	0
44	98.11							B			
45	97.839	28	94.45	0	1.16	1.19	1.025862 C	A		0	0
45	98.744	189.37	164.5 core		1.07	3.6	3.364486 C	A		189.37	108.27
46	98.569							A			
47	99.08	0.45	173.5 core		1.29	1.8	1.395349 P	C		0.45	43.62
48	98.6							C			
49	99.078	167.35	225.4 core		1.32	1.39	1.05303 C	B		167.35	136.03
50	99.336							B			
52	98.831							B			
53	98.29							B			

Point	Total(Mass%)	Au ppm	Sb counts	Comments	Width	Height	Width:Heig	Habbit	Apy type	Core Au ppi	Rim Au ppn
54	98.453	0.72	154.6	0	1.12	1.76	1.571429	C	A	0	0
55	98.034	101.24	1282	0	0.71	4.22	5.943662	C	A	0	0
56	98.384								C		
57	96.344								C		
58	98.201	447.95	314.5	0	0.26	0.67	2.576923	R	B	0	0
59	98.342	320.08	254.2	0	0.24	0.73	3.041667	R	B	0	0
60	98.336	534.77	256.4	0	0.12	0.54	4.5	R	B	0	0
61	96.757	1167.42	1285	0	0.35	2.62	7.485714	C	A	0	0
63	98.295								W		
64	98.798								W		
65	98.629								W		
66	98.993								W		
67	98.163								W		
68	99.208								W		
69	98.996								W		
70	99.191								W		
71	98.387								W		
72	97.702								W		
74	97.577	95.34	144.4	0	1	1.07	1.07	C	B	0	0
75	98.716	8.27	333.3	0	1.2	1.38	1.15	C	B	0	0
76	98.413	119.11	266.1	0	1.07	5.01	4.682243	C	B	0	0
77	99.54								A		
78	99.014								A		
79	99.013								B		
80	98.096								B		
81	98.945								B		
82	99.251								B		

Point	Core Sb cou	Rim Sb cou	Average Au	Max Au ppr	Average Sb	Max Sb cou	Au core-rim	Sb core-rim	Domain
1	0	0	0.95	0.95	99.64	99.64	0	0	3
1	131	299.9	244.48	405.3	131	299.9	-160.82	-168.9	3
2	0	0	0.73	0.73	259	259	0	0	3
2									
3	0	0	20.79	20.79	132.6	132.6	0	0	3
3									
4	0	0	5.13	5.13	96.7	96.7	0	0	3
4									
5	0	0	3.95	3.95	227.5	227.5	0	0	3
5									
6									
6									
7	0	0	315.17	315.17	235.6	235.6	0	0	3
7									
8	0	0	214.01	214.01	121.7	121.7	0	0	3
8									
9	0	0	6.03	6.03	195.2	195.2	0	0	3
9	68.5	98.1	2345.19	2462.81	68.5	98.1	-117.62	-29.6	3
10	0	0	142.89	142.89	148.5	148.5	0	0	3
10									
11									
11	0	0	1491.65	1491.65	438.2	438.2	0	0	3
12									
12	88.5	281	192.24	192.24	88.5	281	9.96	-192.5	3
13	276.3	144.4	255.49	255.49	276.3	276.3	26.12	131.9	3
13									
14									
14									
15									
15	207.9	305.9	1654.42	2418.16	207.9	305.9	-763.74	-98	3
16	58.9	318.3	1.6	20.89	58.9	318.3	-19.29	-259.4	3
16									

Point	Core Sb cou	Rim Sb cou	Average Au	Max Au ppr	Average Sb	Max Sb cou	Au core-rim	Sb core-rim	Domain
17									
17	112.7	272	18.27	66.22	112.7	272	-47.95	-159.3	3
18	133.9	362.4	22.21	22.21	133.9	362.4	3.17	-228.5	3
18									
19									
19	96.3	247.2	916.8	1108.81	96.3	247.2	-192.01	-150.9	3
20	100.2	162.9	18.78	20	100.2	162.9	-1.22	-62.7	3
20									
21									
21	357.1	329.5	236.06	236.06	357.1	357.1	138.63	27.6	3
22	101.2	108.4	3.23	3.23	101.2	108.4	2.54	-7.2	3
22									
23									
24									
24	0	0	113.23	113.23	175.2	175.2	0	0	4
25									
25									
26	0	0	38.65	38.65	232.8	232.8	0	0	5
26									
27	0	0	13.9	13.9	288.1	288.1	0	0	5
27									
28									
28									
29	0	0	1.46	1.46	64.8	64.8	0	0	5
29									
30	0	0	8.52	8.52	232.2	232.2	0	0	5
30	0	0	14.37	14.37	108.8	108.8	0	0	4
31									
31	0	0	14.3	14.3	125.6	125.6	0	0	4
32									
32									
33									

Point	Core Sb cou	Rim Sb coui	Average Au	Max Au ppr	Average Sb	Max Sb cou	Au core-rim	Sb core-rim	Domain
33	76	88.4	19.08	210.98	76	88.4	-191.9	-12.4	4
34	0	0	61.51	61.51	880.1	880.1	0	0	5
34									
35	0	0	7.86	7.86	361	361	0	0	5
35	395.6	84.6	93.69	333.34	395.6	395.6	-239.65	311	4
36	125.3	540.6	31.48	45.65	332.95	540.6	-28.34	-415.3	5
36									
37									
37	41	36	312.03	312.03	41	41	178.43	5	4
38	173	740.8	54.64	112.35	456.9	740.8	-57.71	-567.8	5
38									
39									
39	168.6	146	104.59	104.59	168.6	168.6	80.53	22.6	4
40	0	0	9.82	9.82	458.9	458.9	0	0	5
40									
41	0	0	4.68	4.68	116	116	0	0	5
41	135	127.5	34.63	91.66	135	135	-57.03	7.5	4
42	0	0	29.58	29.58	372.2	372.2	0	0	5
42									
43	0	0	39.17	39.17	188.2	188.2	0	0	5
43	66.9	54.9	2.69	86.9	66.9	66.9	-84.21	12	4
44	0	0	6.63	6.63	233	233	0	0	5
44									
45	0	0	28	28	94.45	94.45	0	0	5
45	164.5	61.2	189.37	189.37	164.5	164.5	81.1	103.3	4
46									
47	173.5	206.3	0.45	43.62	173.5	206.3	-43.17	-32.8	4
48									
49	225.4	169.7	167.35	167.35	225.4	225.4	31.32	55.7	4
50									
52									
53									

Point	Core Sb cou	Rim Sb cou	Average Au	Max Au ppr	Average Sb	Max Sb cou	Au core-rim	Sb core-rim	Domain
54	0	0	0.72	0.72	154.6	154.6	0	0	5
55	0	0	101.24	101.24	1282	1282	0	0	5
56									
57									
58	0	0	447.95	447.95	314.5	314.5	0	0	5
59	0	0	320.08	320.08	254.2	254.2	0	0	5
60	0	0	534.77	534.77	256.4	256.4	0	0	5
61	0	0	1167.42	1167.42	1285	1285	0	0	5
63									
64									
65									
66									
67									
68									
69									
70									
71									
72									
74	0	0	95.34	95.34	144.4	144.4	0	0	3
75	0	0	8.27	8.27	333.3	333.3	0	0	3
76	0	0	119.11	119.11	266.1	266.1	0	0	3
77									
78									
79									
80									
81									
82									

Appendix D: Terraspec Data

Sample name	Mineral	Confidence	2200nm	1410 NM	2194 NM	2200nm	2210 NM	2330 NM	Domain	Au GMPT
088-180.asd	Muscovite	1	2198.54	1410.33	2198.54	2198.54	0	0	5	6.856
088-181.asd	Muscovite	0.515	2199.12	1409.65	2199.12	2199.12	0	2327.57	5	0.499
088-182.asd	Muscovite	1	2199.35	1409.94	2199.35	2199.35	0	0	5	0.84
088-183.asd	Muscovite	1	2199.26	1409.95	2199.26	2199.26	0	0	5	0.029
088-185.asd	Muscovite	0.812	2197.71	1409.76	2197.71	2197.71	0	0	5	1.789
088-190.asd	Muscovite	0.68	2201.78	1409.99	2201.78	2201.78	2201.4	0	5	1.807
088-191.asd	Muscovite	1	2200.77	1410.05	2200.77	2200.77	2200.85	0	5	1.807
088-191B.asd	Muscovite	0.806	2202.13	1410.57	2202.08	2202.13	2202.15	0	5	1.807
088-192.asd	Muscovite	1	2201.75	1410.26	2201.67	2201.75	2201.68	0	5	1.807
088-202.asd	Muscovite	1	2203.73	1410.43	0	2203.73	2203.73	0	5	2.934
088-203.asd	Chlorite-FeMg	0.552	2205.72	1408	0	2205.72	2205.72	0	5	2.317
088-204.asd	Chlorite-FeMg	0.627	2204.56	1408.11	2203.62	2204.56	2204.56	2337.78	5	0.072
088-207A.asd	Muscovite	1	2203.32	1410.23	2203.15	2203.32	2203.32	0	5	4.317
088-207B.asd	Muscovite	0.667	2203.16	1410.19	2203.35	2203.16	2203.16	0	5	4.317
088-207C.asd	Muscovite	0.622	2205.16	1410.2	0	2205.16	2205.16	0	5	4.317
088-208.asd	Muscovite	1	2200.17	1410.28	2200.17	2200.17	2200.51	0	5	4.246
088-209.asd	Muscovite	0.582	2202.14	1409.53	2202.2	2202.14	2202.14	0	5	2.607
088-210A.asd	Muscovite	1	2203.35	1410.27	2202.91	2203.35	2203.25	0	5	6.347
088-210B.asd	Chlorite-FeMg	0.773	2206.43	1406.15	0	2206.43	2206.43	0	5	6.347
088-212.asd	Chlorite-FeMg	0.613	2205.09	1408.38	0	2205.09	2205.09	0	5	4.718
088-81.asd	Muscovite	0.556	2200.16	1408.64	2200.16	2200.16	0	0	4	0.287
088-83.asd	Chlorite-FeMg	0.571	2202.42	1409.65	2202.48	2202.42	2202.42	0	4	0.316
088-84.asd	Muscovite	0.702	2200.93	1409.86	2200.93	2200.93	2200.68	0	4	1.524
088-85.asd	Chlorite-FeMg	0.578	2201.46	1408.59	2201.46	2201.46	2201.42	0	4	2.46
088-88B.asd	Muscovite	1	2200.53	1410.06	2200.53	2200.53	2200.3	0	4	4.083
088-90A.asd	Muscovite	1	2198.3	1409.86	2198.3	2198.3	0	0	4	3.686
088-90B.asd	Muscovite	1	2197.06	1409.93	2197.06	2197.06	0	2338.39	4	3.686
118-137.asd	Muscovite	1	2205.93	1410.68	0	2205.93	2205.93	0	3	0.001
118-138.asd	Muscovite	1	2203.71	1410.33	0	2203.71	2203.71	0	3	0.001

Sample name	Mineral	Confidence	2200nm	1410 NM	2194 NM	2200nm	2210 NM	2330 NM	Domain	Au GMPT
118-139.asd	Chlorite-FeMg	0.528	2202.99	1405.57	2202.54	2202.99	2202.99	2337.22	3	0.364
118-140.asd	Chlorite-FeMg	0.556	2206.5	1407.85	0	2206.5	2206.5	0	3	0.961
118-141.asd	Chlorite-FeMg	0.63	2205.61	1408.36	0	2205.61	2205.61	0	3	0.248
118-142.asd	Muscovite	0.597	2202.78	1408.79	2203.55	2202.78	2202.78	0	3	0.488
118-144.asd	Muscovite	1	2201.86	1409.62	2201.86	2201.86	2201.78	2337.14	3	0.205
118-145.asd	Muscovite	0.566	2200.98	1408.92	2200.98	2200.98	2200.01	0	3	0.637
118-146.asd	Muscovite	1	2202.48	1410.56	2202.38	2202.48	2202.47	0	3	0.186
118-147.asd	Muscovite	1	2201.79	1410.29	2201.85	2201.79	2201.88	0	3	0.103
118-149.asd	Chlorite-FeMg	0.559	2203.67	1409.88	0	2203.67	2203.67	0	3	0.63
118-17.asd	Muscovite	1	2202.57	1409.53	2202.44	2202.57	2202.56	0	4	0.339
118-173.asd	Chlorite-FeMg	0.601	2207.52	1410.03	0	2207.52	2207.52	2336.54	5	4.903
118-174.asd	Chlorite-FeMg	0.753	2200.21	1403.02	2200.21	2200.21	2200.1	0	5	0.109
118-19.asd	Muscovite	1	2200.72	1410.45	2200.72	2200.72	0	0	4	5.821
118-20.asd	Muscovite	0.526	2203.18	1409.75	2203.03	2203.18	2203.18	0	4	0.039
118-22.asd	Muscovite	0.724	2200.89	1410.06	2200.89	2200.89	2201.11	0	4	3.282
118-25.asd	Muscovite	0.517	2205.47	1409.55	2203.67	2205.47	2205.47	2337.76	4	3.06
118-26.asd	Muscovite	0.78	2204	1410.64	0	2204	2204	2337.21	4	7.271
118-27.asd	Muscovite	1	2198.36	1408.97	2198.36	2198.36	0	0	4	0.009
MA10.asd	Muscovite	1	2198.73	1409.93	2198.73	2198.73	0	0	4	2.582
MA100.asd	Chlorite-FeMg	0.691	2199.61	1404.83	2199.61	2199.61	0	0	4	0.003
MA101.asd	Muscovite	0.603	2199.88	1409.78	2199.88	2199.88	0	0	4	0.014
MA102.asd	Muscovite	0.622	2199.88	1408.64	2199.88	2199.88	2200.25	0	4	0.08
MA103.asd	Muscovite	1	2199.66	1409.98	2199.66	2199.66	0	0	4	0.863
MA104.asd	Chlorite-FeMg	0.781	2207.1	1401.09	0	2207.1	2207.1	0	4	0.001
MA107.asd	Muscovite	0.645	2199.68	1408.94	2199.68	2199.68	0	2339.88	4	0.012
MA108.asd	Muscovite	0.662	2200.39	1409.57	2200.39	2200.39	2200.05	0	4	5.372
MA11.asd	Muscovite	1	2200.12	1409.62	2200.12	2200.12	0	0	4	2.582
MA110.asd	Muscovite	0.685	2201.08	1409.67	2201.08	2201.08	2202.81	2337.79	4	11.45
MA111.asd	Muscovite	1	2200.9	1408.96	2200.9	2200.9	2201.14	0	4	11.45

Sample name	Mineral	Confidence	2200nm	1410 NM	2194 NM	2200nm	2210 NM	2330 NM	Domain	Au GMPT
MA112.asd	Muscovite	1	2200.43	1410.21	2200.43	2200.43	2200.67	0	4	1.892
MA113.asd	Muscovite	0.676	2200.07	1409.86	2200.07	2200.07	0	0	4	7.973
MA114.asd	Muscovite	1	2198.37	1409.7	2198.37	2198.37	0	0	3	4.474
MA115.asd	Muscovite	1	2199.38	1409.75	2199.38	2199.38	0	0	3	6.818
MA115B.asd	Muscovite	1	2198.69	1409.73	2198.69	2198.69	0	0	3	6.818
MA116.asd	Ankerite	0.745	2202.97	1411.19	2203.07	2202.97	2202.97	2325.41	3	4.141
MA116B.asd	Muscovite	1	2199.04	1409.76	2199.04	2199.04	0	0	3	4.141
MA117.asd	Muscovite	1	2199.02	1409.73	2199.02	2199.02	0	0	3	6.557
MA119.asd	Muscovite	1	2198.35	1409.77	2198.35	2198.35	0	0	3	6.538
MA12.asd	Muscovite	1	2198.86	1409.87	2198.86	2198.86	0	0	4	5.053
MA120.asd	Muscovite	1	2198.42	1409.63	2198.42	2198.42	0	0	3	12.286
MA121.asd	Muscovite	1	2198.42	1409.62	2198.42	2198.42	0	0	3	27.093
MA122.asd	Muscovite	1	2198.32	1409.73	2198.32	2198.32	0	0	3	14.417
MA123.asd	Muscovite	1	2199.07	1409.84	2199.07	2199.07	0	0	3	0.757
MA124.asd	Muscovite	1	2198.59	1409.64	2198.59	2198.59	0	0	3	5.635
MA124B.asd	Muscovite	1	2198.41	1409.7	2198.41	2198.41	0	0	3	5.635
MA126.asd	Muscovite	1	2198.53	1409.69	2198.53	2198.53	0	0	3	10.629
MA128.asd	Muscovite	1	2198.1	1409.7	2198.1	2198.1	0	0	3	16.86
MA129.asd	Muscovite	1	2198.28	1409.64	2198.28	2198.28	0	0	3	16.86
MA13.asd	Muscovite	1	2199.21	1409.93	2199.21	2199.21	0	0	4	1.666
MA130.asd	Muscovite	0.812	2198.89	1409.97	2198.89	2198.89	0	2339.45	3	0.061
MA132.asd	Muscovite	0.572	2199.02	1409.58	2199.02	2199.02	0	0	3	0.001
MA133.asd	Muscovite	0.505	2198.99	1410.01	2198.99	2198.99	0	0	3	0.001
MA134.asd	Chlorite-FeMg	0.522	2199.11	1409.68	2199.11	2199.11	0	0	3	0.043
MA135.asd	Chlorite-FeMg	0.611	2199.21	1409.8	2199.21	2199.21	0	0	3	0.002
MA136.asd	Muscovite	1	2198.9	1409.87	2198.9	2198.9	0	0	3	0.009
MA14.asd	Muscovite	1	2198.85	1409.72	2198.85	2198.85	0	0	4	1.83
MA148.asd	Muscovite	1	2202.92	1410.1	2203.47	2202.92	2202.92	0	3	0.074
MA15.asd	Aspectral	1	2203.33	1412.02	2202.77	2203.33	2203.33	2324.33	4	1.904

Sample name	Mineral	Confidence	2200nm	1410 NM	2194 NM	2200nm	2210 NM	2330 NM	Domain	Au GMPT
MA150.asd	Muscovite	0.571	2200.09	1409.83	2200.09	2200.09	0	2332.91	3	7.642
MA151.asd	Muscovite	0.578	2199.26	1409.69	2199.26	2199.26	0	0	3	7.642
MA152.asd	Chlorite-FeMg	0.6	2199.95	1408.64	2199.95	2199.95	2200.1	0	3	0.004
MA153.asd	Muscovite	0.655	2200.56	1410.18	2200.56	2200.56	2200.57	0	3	0.001
MA154.asd	Muscovite	1	2200.32	1410.35	2200.32	2200.32	0	0	3	0.019
MA154B.asd	Muscovite	1	2200.59	1410.38	2200.59	2200.59	2200.13	0	3	0.019
MA155.asd	Muscovite	1	2201.66	1410.49	2201.66	2201.66	2201.48	0	3	0.019
MA155B.asd	Muscovite	1	2201.72	1410.59	2201.72	2201.72	2201.5	0	3	0.019
MA156.asd	Muscovite	1	2200.44	1410.41	2200.44	2200.44	0	0	3	5.752
MA156B.asd	Muscovite	1	2201.54	1410.49	2201.5	2201.54	2201.48	0	3	5.752
MA157.asd	Muscovite	0.725	2202.93	1410.26	2202.82	2202.93	2202.93	2335.73	3	0.761
MA158.asd	Muscovite	1	2201.48	1410.11	2201.48	2201.48	0	0	3	0.663
MA158B.asd	Muscovite	1	2202.67	1410.27	2202.64	2202.67	2202.67	0	3	0.663
MA159.asd	Muscovite	0.58	2206.11	1410.53	2203.66	2206.11	2206.11	2337.25	3	1.666
MA16.asd	Chlorite-FeMg	0.701	2202.12	1409.64	2202.48	2202.12	2202.12	0	4	0.078
MA160.asd	Muscovite	1	2201.64	1409.93	2201.64	2201.64	2201.63	0	3	3.591
MA161.asd	Muscovite	0.704	2203.05	1409.9	2202.81	2203.05	2203.05	0	3	5.964
MA162.asd	Muscovite	1	2203.51	1410.23	2203.09	2203.51	2203.51	0	3	5.964
MA163.asd	Chlorite-FeMg	0.62	2206.94	1409.94	0	2206.94	2206.94	0	3	1.74
MA164.asd	Chlorite-Fe	0.636	2202.97	1410.41	0	2202.97	2202.97	0	3	0.003
MA165.asd	Muscovite	0.586	2200.77	1410.17	2200.77	2200.77	2200.27	0	3	0.003
MA166.asd	Muscovite	1	2200.28	1410.48	2200.28	2200.28	2200.05	0	3	0.001
MA167.asd	Chlorite-FeMg	0.788	2200.81	1408.61	2200.81	2200.81	0	0	3	0.001
MA168.asd	Chlorite-FeMg	0.692	2201.75	1407.38	2201.71	2201.75	2201.79	0	3	0.001
MA169.asd	Biotite	0.589	2201.89	0	2201.99	2201.89	2201.89	0	3	0.001
MA171.asd	Muscovite	1	2198.33	1409.78	2198.33	2198.33	0	0	5	0.031
MA172.asd	Muscovite	1	2198.72	1409.86	2198.72	2198.72	0	0	5	#N/A
MA173.asd	Muscovite	1	2199.9	1410	2199.9	2199.9	0	0	5	4.903
MA174.asd	Chlorite-FeMg	0.672	2206.47	1407.87	0	2206.47	2206.47	0	5	0.109

Sample name	Mineral	Confidence	2200nm	1410 NM	2194 NM	2200nm	2210 NM	2330 NM	Domain	Au GMPT
MA175.asd	Muscovite	1	2198.99	1409.79	2198.99	2198.99	0	0	5	1.073
MA176.asd	Muscovite	1	2198.91	1409.83	2198.91	2198.91	0	0	5	0.79
MA177.asd	Chlorite-FeMg	0.525	2197.16	1410.08	2197.16	2197.16	0	2337.96	5	2.676
MA178.asd	Chlorite-FeMg	0.506	2200.71	1409.46	2200.71	2200.71	2200.76	0	5	1.387
MA178B.asd	Chlorite-FeMg	0.619	2200.58	1408.5	2200.58	2200.58	0	0	5	1.387
MA179.asd	Muscovite	1	2198.1	1409.8	2198.1	2198.1	0	0	5	0.009
MA180.asd	Muscovite	0.6	2199.06	1409.59	2199.06	2199.06	0	0	5	6.856
MA184.asd	Muscovite	1	2200.02	1410.09	2200.02	2200.02	0	0	5	0.025
MA184B.asd	Muscovite	1	2200.29	1410.01	2200.29	2200.29	2200.46	0	5	0.025
MA189.asd	Muscovite	1	2200.12	1410.13	2200.12	2200.12	0	0	5	0.011
MA194.asd	Muscovite	1	2201.1	1410.45	2201.1	2201.1	2201.01	0	5	0.151
MA195.asd	Muscovite	1	2202.38	1410.05	2202.39	2202.38	2202.34	0	5	1.125
MA196.asd	Chlorite-FeMg	0.57	2199.68	1403.72	2199.68	2199.68	0	0	5	1.125
MA197.asd	Muscovite	1	2202.06	1410.58	2201.96	2202.06	2201.94	0	5	1.178
MA198.asd	Muscovite	1	2202.14	1410.16	2201.94	2202.14	2202.06	0	5	1.178
MA199.asd	Muscovite	1	2203.04	1410.6	2203.44	2203.04	2203.04	0	5	0.701
MA2.asd	Muscovite	0.566	2199.43	1409.43	2199.43	2199.43	0	0	4	0.07
MA200.asd	Muscovite	0.646	2201.24	1409.74	2201.24	2201.24	0	0	5	0.701
MA201.asd	Muscovite	1	2203.55	1410.62	0	2203.55	2203.55	0	5	2.317
MA203.asd	Muscovite	0.507	2203.61	1408.93	2202.86	2203.61	2203.61	0	5	2.317
MA204.asd	Muscovite	1	2204.78	1410.46	2202.43	2204.78	2204.78	0	5	0.072
MA205.asd	Muscovite	1	2203.86	1410.5	2203.75	2203.86	2203.86	0	5	0.315
MA206.asd	Muscovite	1	2202.94	1410.63	2202.95	2202.94	2202.94	0	5	2.335
MA208.asd	Muscovite	1	2201.84	1410.2	2201.77	2201.84	2201.81	0	5	4.246
MA213.asd	Muscovite	0.523	2202.24	1409.22	2202.32	2202.24	2202.24	0	5	9.602
MA215.asd	Muscovite	1	2200.04	1409.63	2200.04	2200.04	0	0	5	0.811
MA215B.asd	Muscovite	0.511	2200.02	1408.17	2200.02	2200.02	2200.03	0	5	0.811
MA217.asd	Muscovite	1	2201.29	1410.13	2201.29	2201.29	2200.34	0	5	10.3
MA218.asd	Muscovite	1	2204.89	1409.96	0	2204.89	2204.89	0	5	14.42

Sample name	Mineral	Confidence	2200nm	1410 NM	2194 NM	2200nm	2210 NM	2330 NM	Domain		Au GMPT
MA219.asd	Muscovite	1	2201.11	1410.05	2201.11	2201.11	2200.64	0		5	26.8
MA219B.asd	Muscovite	1	2203.56	1409.8	0	2203.56	2203.56	2336.57		5	26.8
MA220.asd	Muscovite	1	2201.92	1410.4	2201.84	2201.92	2201.87	0		5	14.42
MA221.asd	Chlorite-FeMg	0.576	2201.23	1409.13	2201.23	2201.23	2201.17	0		5	7.646
MA222.asd	Muscovite	1	2200.85	1410.35	2200.85	2200.85	2201.03	0		5	10.58
MA223.asd	Muscovite	0.597	2200.85	1409.89	2200.85	2200.85	2200.86	0		5	6.73
MA224.asd	Aspectral	1	2208.41	1416.77	2189.85	2208.41	2210.6	2321.99		5	0.202
MA225.asd	Tourmaline-Fe	1	2207.33	1415.3	2203.67	2207.33	2207.34	2332.49		5	2.176
MA226.asd	Chlorite-FeMg	0.525	2200.28	1409.03	2200.28	2200.28	2200.98	0		5	0.622
MA227.asd	Muscovite	1	2199.5	1409.94	2199.5	2199.5	0	0		5	2.828
MA228.asd	Muscovite	0.663	2199.66	1409.78	2199.66	2199.66	2200.13	0		5	2.959
MA229.asd	Muscovite	0.589	2198.7	1409.71	2198.7	2198.7	0	0		5	1.121
MA231.asd	Paragonite	0.558	2192.98	1408.37	2192.99	2192.98	0	2336.11	NC		#N/A
MA233.asd	Muscovite	0.554	2200.77	1409.97	2200.77	2200.77	2202.97	2339.52	WL		#N/A
MA239.asd	Paragonite	0.566	2195.12	1408.98	2195.12	2195.12	0	2338.23	#N/A		#N/A
MA246.asd	Chlorite-FeMg	0.603	2204.03	1407.71	2203.92	2204.03	2204.03	2337.43	WL		#N/A
MA247.asd	Chlorite-Fe	1	2204.81	1411.42	0	2204.81	2204.81	0	WL		#N/A
MA250.asd	Aspectral	1	2195.99	1402.43	2195.99	2195.99	2201.63	2325.18	?		31.226
MA251.asd	Muscovite	1	2199.97	1410.41	2199.97	2199.97	0	0	BL		#N/A
MA252.asd	Muscovite	0.518	2202.58	1409.81	2202.4	2202.58	2202.57	0	BL		#N/A
MA253.asd	Chlorite-FeMg	0.61	2203.12	1406.97	2202.75	2203.12	2203.12	0	WL		#N/A
MA28.asd	Muscovite	1	2200.31	1409.94	2200.31	2200.31	2200.21	0		4	15.09
MA30.asd	Chlorite-FeMg	0.535	2201.41	1409.01	2201.53	2201.41	2201.72	0		4	9.301
MA31.asd	Muscovite	1	2199.76	1410.02	2199.76	2199.76	2200.31	0		4	7.7
MA32.asd	Muscovite	0.603	2201.51	1410.47	2201.51	2201.51	2201.34	0		4	1.194
MA33.asd	Aspectral	1	2201.95	1417.69	2201.88	2201.95	2202.09	2322.03		4	0.02
MA34.asd	Muscovite	0.566	2199.3	1409.89	2199.3	2199.3	2200.04	0		4	0.539
MA35.asd	Muscovite	1	2200.21	1410.11	2200.21	2200.21	2200.24	0		4	4.272
MA38.asd	Muscovite	1	2199.85	1409.77	2199.85	2199.85	2200.39	0		4	3.761

Sample name	Mineral	Confidence	2200nm	1410 NM	2194 NM	2200nm	2210 NM	2330 NM	Domain	Au GMPT
MA39.asd	Muscovite	1	2198.38	1409.78	2198.38	2198.38	0	0	4	#N/A
MA40.asd	Muscovite	1	2198.37	1409.73	2198.37	2198.37	0	0	4	#N/A
MA41.asd	Muscovite	1	2198.99	1409.78	2198.99	2198.99	0	0	4	#N/A
MA42.asd	Muscovite	1	2198.47	1409.73	2198.47	2198.47	0	0	4	#N/A
MA43.asd	Muscovite	1	2198.61	1409.9	2198.61	2198.61	0	0	4	#N/A
MA44.asd	Muscovite	0.591	2199.13	1410.07	2199.13	2199.13	0	0	4	#N/A
MA45.asd	Muscovite	1	2198.37	1409.71	2198.37	2198.37	0	0	4	#N/A
MA46.asd	Muscovite	1	2198.3	1409.7	2198.3	2198.3	0	0	4	#N/A
MA47.asd	Muscovite	1	2199.02	1410.09	2199.02	2199.02	0	0	4	#N/A
MA48.asd	Muscovite	1	2199.37	1410.1	2199.37	2199.37	0	0	4	#N/A
MA49.asd	Dolomite	1	2206.47	1411.87	2200.73	2206.47	2206.47	2322.39	4	#N/A
MA5.asd	Aspectral	1	2201.65	1419.35	2201.65	2201.65	2201.8	2325.02	4	1.171
MA50.asd	Chlorite-FeMg	0.548	2205.18	1408.39	2202.65	2205.18	2205.18	0	4	#N/A
MA51.asd	Muscovite	0.586	2200.98	1409.93	2200.98	2200.98	2200.98	0	4	#N/A
MA51B.asd	Muscovite	0.508	2201.86	1409.72	2201.86	2201.86	2201.79	0	4	#N/A
MA52.asd	Muscovite	0.547	2201.98	1409.25	2201.98	2201.98	2201.99	0	4	#N/A
MA53.asd	Muscovite	0.656	2201.76	1409.89	2201.77	2201.76	2201.76	0	4	#N/A
MA54.asd	Muscovite	1	2198.54	1409.88	2198.54	2198.54	0	0	4	#N/A
MA56.asd	Muscovite	1	2198.79	1409.71	2198.79	2198.79	0	0	4	#N/A
MA57.asd	Tourmaline-Fe	1	2206.41	1405.2	0	2206.41	2206.41	0	4	#N/A
MA58.asd	Muscovite	1	2200.28	1409.57	2200.28	2200.28	2200.48	0	4	#N/A
MA58B.asd	Muscovite	1	2199.51	1409.88	2199.51	2199.51	2200.21	0	4	#N/A
MA59.asd	Muscovite	1	2200.28	1410.09	2200.28	2200.28	2200.31	0	4	#N/A
MA6.asd	Muscovite	0.702	2199.78	1409.98	2199.78	2199.78	0	0	4	1.171
MA61.asd	Muscovite	1	2200.27	1409.83	2200.27	2200.27	2201.01	0	4	#N/A
MA63.asd	Aspectral	1	2192.96	0	2192.96	2192.96	0	2333.11	4	#N/A
MA64.asd	Muscovite	0.715	2199.56	1409.76	2199.56	2199.56	0	0	4	#N/A
MA65.asd	Muscovite	0.716	2199.81	1409.81	2199.81	2199.81	0	0	4	#N/A
MA66.asd	Muscovite	1	2198.12	1410.05	2198.12	2198.12	0	2336.14	4	#N/A

Sample name	Mineral	Confidence	2200nm	1410 NM	2194 NM	2200nm	2210 NM	2330 NM	Domain	Au GMPT
MA67.asd	Muscovite	0.637	2199.51	1409.7	2199.51	2199.51	0	0	4	#N/A
MA68.asd	Chlorite-FeMg	0.52	2199.78	1409.2	2199.78	2199.78	2200.92	2337.66	4	#N/A
MA68B.asd	Chlorite-FeMg	0.53	2201.92	1410.19	2201.92	2201.92	2201.89	2339.85	4	#N/A
MA69.asd	Muscovite	0.567	2199.17	1409.49	2199.17	2199.17	0	0	4	#N/A
MA7.asd	Muscovite	0.539	2199.67	1409.43	2199.67	2199.67	0	0	4	1.171
MA70.asd	Muscovite	1	2199.38	1409.58	2199.38	2199.38	0	0	4	#N/A
MA71.asd	Muscovite	1	2198.91	1410.21	2198.91	2198.91	2200.03	0	4	#N/A
MA72.asd	Muscovite	1	2199.86	1410.18	2199.86	2199.86	0	2336.49	4	#N/A
MA73.asd	Muscovite	1	2200.14	1410.02	2200.14	2200.14	2200.29	0	4	#N/A
MA74.asd	Muscovite	1	2199.6	1410	2199.6	2199.6	2200.33	0	4	#N/A
MA75.asd	Muscovite	0.789	2201.45	1410.01	2201.44	2201.45	2201.69	2338.74	4	#N/A
MA76.asd	Muscovite	0.665	2199.66	1409.78	2199.66	2199.66	2200.73	0	4	#N/A
MA77.asd	Aspectral	1	2193.36	1418.91	2193.36	2193.36	2201.29	2323.53	4	#N/A
MA8.asd	Muscovite	1	2200.66	1409.84	2200.66	2200.66	0	0	4	4.708
MA82.asd	Muscovite	1	2200.02	1409.69	2200.02	2200.02	0	0	4	0.003
MA83.asd	Muscovite	0.575	2200.18	1409.37	2200.18	2200.18	0	0	4	0.316
MA84.asd	Muscovite	0.575	2200.02	1409.66	2200.02	2200.02	0	0	4	1.524
MA86.asd	Muscovite	1	2201.09	1410.1	2201.09	2201.09	2200.64	0	4	3.664
MA87.asd	Muscovite	1	2200.5	1410.17	2200.5	2200.5	2200.26	0	4	1.559
MA88.asd	Chlorite-FeMg	0.512	2201.35	1403.87	2201.43	2201.35	2201.48	2338.33	4	4.083
MA9.asd	Muscovite	1	2200.09	1410.11	2200.09	2200.09	0	0	4	1.116
MA92.asd	Muscovite	1	2199.78	1409.96	2199.78	2199.78	0	0	4	0.057
MA93.asd	Chlorite-Fe	1	0	1411.65	2203.49	0	0	0	4	0.096
MA96.asd	Muscovite	0.652	2199.69	1409.94	2199.69	2199.69	0	0	4	0.134
MA97.asd	Chlorite-FeMg	0.542	2200.44	1408.4	2200.44	2200.44	2201.05	0	4	0.056
MA9B.asd	Muscovite	0.686	2200.07	1409.03	2200.07	2200.07	0	0	4	1.116

Sample name	AS_PPM	S_PCT	AG_GPMT	AL_PCT	CU_PPM	PB_PPM	SB_PPM	BA_PPM	CA_PCT	FE_PCT
088-180.asd	6108	0.68	1.2	1.57	23	3	8	37	1.93	2.78
088-181.asd	2755	0.68	0.7	1.22	14	1.5	1.5	23	2.77	2.25
088-182.asd	957	0.89	0.7	0.87	21	1.5	1.5	17	2.43	2.13
088-183.asd	502	0.29	0.15	0.86	12	3	1.5	21	2.29	1.34
088-185.asd	4440	0.74	0.7	0.59	15	5	8	18	0.99	1.35
088-190.asd	3245	0.73	1	0.66	10	141	1.5	22	1.11	1.72
088-191.asd	3245	0.73	1	0.66	10	141	1.5	22	1.11	1.72
088-191B.asd	3245	0.73	1	0.66	10	141	1.5	22	1.11	1.72
088-192.asd	3245	0.73	1	0.66	10	141	1.5	22	1.11	1.72
088-202.asd	6210	0.72	1	1.16	13	12	5	56	1.65	2.42
088-203.asd	5446	0.87	1.3	1.02	15	9	3	39	1.16	2.38
088-204.asd	305	0.27	0.15	1.28	14	4	1.5	58	1.36	2.49
088-207A.asd	6426	0.55	0.3	0.66	12	6	4	25	1.62	1.4
088-207B.asd	6426	0.55	0.3	0.66	12	6	4	25	1.62	1.4
088-207C.asd	6426	0.55	0.3	0.66	12	6	4	25	1.62	1.4
088-208.asd	8228	0.97	0.4	0.76	10	3	6	26	1.59	2.14
088-209.asd	4810	0.58	0.5	1.38	17	17	3	30	2.06	2.38
088-210A.asd	10001	1.12	0.5	0.8	7	5	8	18	2.11	2.68
088-210B.asd	10001	1.12	0.5	0.8	7	5	8	18	2.11	2.68
088-212.asd	10001	1.49	0.9	0.78	16	3	6	22	1.84	3.29
088-81.asd	779	0.06	0.15	0.99	8	1.5	1.5	46	1.27	1.33
088-83.asd	205	0.35	0.6	1.18	20	1.5	1.5	26	1.37	2.28
088-84.asd	3474	0.48	0.4	0.37	13	1.5	5	12	0.87	1.17
088-85.asd	6989	0.94	1.3	0.84	19	1.5	12	17	2.38	2.18
088-88B.asd	7171	1.04	3.6	0.45	5	7	5	13	0.9	1.82
088-90A.asd	5582	0.45	0.9	0.37	3	1.5	1.5	12	0.61	1.03
088-90B.asd	5582	0.45	0.9	0.37	3	1.5	1.5	12	0.61	1.03
118-137.asd	11	0.025	0.15	0.9	9	4	1.5	63	1.52	1.48
118-138.asd	20	0.025	0.15	1.29	10	5	1.5	68	2.07	2.14

Sample name	AS_PPM	S_PCT	AG_GPMT	AL_PCT	CU_PPM	PB_PPM	SB_PPM	BA_PPM	CA_PCT	FE_PCT
118-139.asd	1010	0.23	0.15	1.2	13	20	1.5	47	1.5	1.94
118-140.asd	4287	1	0.5	0.74	12	8	5	30	2.2	2.36
118-141.asd	2130	0.63	0.15	1.08	11	1.5	5	40	1.31	2.28
118-142.asd	2146	0.44	0.15	0.78	8	7	1.5	32	2.1	1.57
118-144.asd	948	0.38	0.15	1	14	1.5	1.5	37	2.42	1.86
118-145.asd	2855	0.47	0.15	0.87	12	4	1.5	37	1.9	1.8
118-146.asd	965	0.41	0.15	0.78	8	4	1.5	31	2.04	1.53
118-147.asd	11	0.24	0.15	1.09	11	9	1.5	50	1.61	1.92
118-149.asd	1218	0.43	0.15	1.19	17	1.5	3	36	2.13	2.3
118-17.asd	0	0	0	0	0	0	0	0	0	0
118-173.asd	6751	0.86	1.1	0.81	74	8	1.5	15	2.11	1.81
118-174.asd	413	0.1	0.6	1.5	13	1.5	1.5	54	1.56	1.98
118-19.asd	8477	1.19	1.1	0.93	25	6	6	22	2.39	2.5
118-20.asd	213	0.14	0.4	1.12	12	1.5	1.5	37	1.9	1.58
118-22.asd	4822	0.64	0.6	0.82	8	3	5	25	1.67	1.74
118-25.asd	6744	0.85	1.7	1.1	14	1.5	4	17	1.55	2.26
118-26.asd	7018	0.54	2.2	0.47	52	5	3	10	0.45	1.3
118-27.asd	144	0.025	0.6	1.18	12	1.5	1.5	46	1.12	1.61
MA10.asd	0	0	0	0	0	0	0	0	0	0
MA100.asd	0	0	0	0	0	0	0	0	0	0
MA101.asd	0	0	0	0	0	0	0	0	0	0
MA102.asd	0	0	0	0	0	0	0	0	0	0
MA103.asd	0	0	0	0	0	0	0	0	0	0
MA104.asd	0	0	0	0	0	0	0	0	0	0
MA107.asd	0	0	0	0	0	0	0	0	0	0
MA108.asd	0	0	0	0	0	0	0	0	0	0
MA11.asd	0	0	0	0	0	0	0	0	0	0
MA110.asd	0	0	0	0	0	0	0	0	0	0
MA111.asd	0	0	0	0	0	0	0	0	0	0

Sample name	AS_PPM	S_PCT	AG_GPMT	AL_PCT	CU_PPM	PB_PPM	SB_PPM	BA_PPM	CA_PCT	FE_PCT	
MA112.asd	0	0	0	0	0	0	0	0	0	0	0
MA113.asd	0	0	0	0	0	0	0	0	0	0	0
MA114.asd	0	0	0	0	0	0	0	0	0	0	0
MA115.asd	0	0	0	0	0	0	0	0	0	0	0
MA115B.asd	0	0	0	0	0	0	0	0	0	0	0
MA116.asd	0	0	0	0	0	0	0	0	0	0	0
MA116B.asd	0	0	0	0	0	0	0	0	0	0	0
MA117.asd	0	0	0	0	0	0	0	0	0	0	0
MA119.asd	0	0	0	0	0	0	0	0	0	0	0
MA12.asd	0	0	0	0	0	0	0	0	0	0	0
MA120.asd	0	0	0	0	0	0	0	0	0	0	0
MA121.asd	0	0	0	0	0	0	0	0	0	0	0
MA122.asd	0	0	0	0	0	0	0	0	0	0	0
MA123.asd	0	0	0	0	0	0	0	0	0	0	0
MA124.asd	0	0	0	0	0	0	0	0	0	0	0
MA124B.asd	0	0	0	0	0	0	0	0	0	0	0
MA126.asd	0	0	0	0	0	0	0	0	0	0	0
MA128.asd	0	0	0	0	0	0	0	0	0	0	0
MA129.asd	0	0	0	0	0	0	0	0	0	0	0
MA13.asd	0	0	0	0	0	0	0	0	0	0	0
MA130.asd	0	0	0	0	0	0	0	0	0	0	0
MA132.asd	0	0	0	0	0	0	0	0	0	0	0
MA133.asd	0	0	0	0	0	0	0	0	0	0	0
MA134.asd	0	0	0	0	0	0	0	0	0	0	0
MA135.asd	0	0	0	0	0	0	0	0	0	0	0
MA136.asd	0	0	0	0	0	0	0	0	0	0	0
MA14.asd	0	0	0	0	0	0	0	0	0	0	0
MA148.asd	418	0.19	0.15	0.9	10	7	1.5	42	2.02	1.57	
MA15.asd	0	0	0	0	0	0	0	0	0	0	0

Sample name	AS_PPM	S_PCT	AG_GPMT	AL_PCT	CU_PPM	PB_PPM	SB_PPM	BA_PPM	CA_PCT	FE_PCT
MA150.asd	6885	0.74	0.4	0.73	14	1.5	7	17	2.42	1.85
MA151.asd	6885	0.74	0.4	0.73	14	1.5	7	17	2.42	1.85
MA152.asd	14	0.15	0.15	1	31	5	1.5	42	1.22	1.88
MA153.asd	5	0.025	0.15	0.76	9	1.5	1.5	38	1.48	1.33
MA154.asd	33	0.025	0.15	1.12	11	1.5	1.5	40	0.9	1.52
MA154B.asd	33	0.025	0.15	1.12	11	1.5	1.5	40	0.9	1.52
MA155.asd	33	0.025	0.15	1.12	11	1.5	1.5	40	0.9	1.52
MA155B.asd	33	0.025	0.15	1.12	11	1.5	1.5	40	0.9	1.52
MA156.asd	9229	1.05	0.4	0.61	8	5	1.5	22	2.8	2.23
MA156B.asd	9229	1.05	0.4	0.61	8	5	1.5	22	2.8	2.23
MA157.asd	1963	0.63	0.15	0.7	9	7	1.5	23	2.46	1.58
MA158.asd	2184	0.79	0.15	0.87	11	8	1.5	28	2.08	2.07
MA158B.asd	2184	0.79	0.15	0.87	11	8	1.5	28	2.08	2.07
MA159.asd	4677	1.01	0.3	0.63	9	9	1.5	21	1.97	1.93
MA16.asd	0	0	0	0	0	0	0	0	0	0
MA160.asd	4782	0.8	0.15	0.83	11	4	1.5	32	1.96	2.08
MA161.asd	8633	0.78	0.4	0.8	8	4	5	36	1.99	2.08
MA162.asd	8633	0.78	0.4	0.8	8	4	5	36	1.99	2.08
MA163.asd	2345	0.4	0.15	1.1	9	5	1.5	43	1.84	1.8
MA164.asd	7	0.025	0.3	1.4	9	1.5	1.5	65	2.27	2.42
MA165.asd	1	0.025	0.15	1.23	11	1.5	1.5	81	1.96	2.05
MA166.asd	1	0.025	0.3	1.46	8	1.5	1.5	68	2.85	2.41
MA167.asd	3	0.025	0.15	1.55	9	1.5	1.5	75	4.41	2.53
MA168.asd	2	0.025	0.3	1.23	11	1.5	1.5	91	2.5	1.98
MA169.asd	3	0.025	0.15	1.11	7	1.5	1.5	57	6.67	1.81
MA171.asd	0	0	0	0	0	0	0	0	0	0
MA172.asd	#N/A	#N/A	#N/A	#N/A	#N/A	#N/A	#N/A	#N/A	#N/A	#N/A
MA173.asd	6751	0.86	1.1	0.81	74	8	1.5	15	2.11	1.81
MA174.asd	413	0.1	0.6	1.5	13	1.5	1.5	54	1.56	1.98

Sample name	AS_PPM	S_PCT	AG_GPMT	AL_PCT	CU_PPM	PB_PPM	SB_PPM	BA_PPM	CA_PCT	FE_PCT
MA175.asd	0	0	0	0	0	0	0	0	0	0
MA176.asd	0	0	0	0	0	0	0	0	0	0
MA177.asd	0	0	0	0	0	0	0	0	0	0
MA178.asd	2044	0.4	0.7	1.43	19	14	1.5	38	2.33	2.28
MA178B.asd	2044	0.4	0.7	1.43	19	14	1.5	38	2.33	2.28
MA179.asd	71	0.08	0.8	1.82	18	10	1.5	59	2.14	2.72
MA180.asd	6108	0.68	1.2	1.57	23	3	8	37	1.93	2.78
MA184.asd	900	0.16	0.4	0.83	6	11	1.5	21	1.76	1.1
MA184B.asd	900	0.16	0.4	0.83	6	11	1.5	21	1.76	1.1
MA189.asd	70	0.025	0.5	0.88	8	1.5	1.5	37	2.39	1.21
MA194.asd	560	0.27	0.6	1.23	16	25	1.5	48	1.64	2.09
MA195.asd	3150	0.54	0.6	1.07	20	5	1.5	41	1.53	2.3
MA196.asd	3150	0.54	0.6	1.07	20	5	1.5	41	1.53	2.3
MA197.asd	2417	0.51	0.6	1.01	17	5	1.5	37	1.74	2.07
MA198.asd	2417	0.51	0.6	1.01	17	5	1.5	37	1.74	2.07
MA199.asd	1329	0.18	1.1	0.91	7	5	1.5	29	1.41	1.42
MA2.asd	0	0	0	0	0	0	0	0	0	0
MA200.asd	1329	0.18	1.1	0.91	7	5	1.5	29	1.41	1.42
MA201.asd	5446	0.87	1.3	1.02	15	9	3	39	1.16	2.38
MA203.asd	5446	0.87	1.3	1.02	15	9	3	39	1.16	2.38
MA204.asd	305	0.27	0.15	1.28	14	4	1.5	58	1.36	2.49
MA205.asd	1050	0.15	0.15	0.81	11	1.5	1.5	61	1.26	1.3
MA206.asd	3824	0.65	0.6	0.62	8	1.5	1.5	23	1.34	1.39
MA208.asd	8228	0.97	0.4	0.76	10	3	6	26	1.59	2.14
MA213.asd	10001	1.68	1.1	1.05	13	4	14	31	1.99	4.08
MA215.asd	2017	0.6	0.15	1.02	19	1.5	1.5	31	2.64	2.03
MA215B.asd	2017	0.6	0.15	1.02	19	1.5	1.5	31	2.64	2.03
MA217.asd	0	0	0	0	0	0	0	0	0	0
MA218.asd	0	0	0	0	0	0	0	0	0	0

Sample name	AS_PPM	S_PCT	AG_GPMT	AL_PCT	CU_PPM	PB_PPM	SB_PPM	BA_PPM	CA_PCT	FE_PCT	
MA219.asd	0	0	0	0	0	0	0	0	0	0	0
MA219B.asd	0	0	0	0	0	0	0	0	0	0	0
MA220.asd	0	0	0	0	0	0	0	0	0	0	0
MA221.asd	0	0	0	0	0	0	0	0	0	0	0
MA222.asd	0	0	0	0	0	0	0	0	0	0	0
MA223.asd	0	0	0	0	0	0	0	0	0	0	0
MA224.asd	0	0	0	0	0	0	0	0	0	0	0
MA225.asd	0	0	0	0	0	0	0	0	0	0	0
MA226.asd	0	0	0	0	0	0	0	0	0	0	0
MA227.asd	0	0	0	0	0	0	0	0	0	0	0
MA228.asd	0	0	0	0	0	0	0	0	0	0	0
MA229.asd	0	0	0	0	0	0	0	0	0	0	0
MA231.asd	#N/A	#N/A	#N/A	#N/A	#N/A	#N/A	#N/A	#N/A	#N/A	#N/A	
MA233.asd	#N/A	#N/A	#N/A	#N/A	#N/A	#N/A	#N/A	#N/A	#N/A	#N/A	
MA239.asd	#N/A	#N/A	#N/A	#N/A	#N/A	#N/A	#N/A	#N/A	#N/A	#N/A	
MA246.asd	#N/A	#N/A	#N/A	#N/A	#N/A	#N/A	#N/A	#N/A	#N/A	#N/A	
MA247.asd	#N/A	#N/A	#N/A	#N/A	#N/A	#N/A	#N/A	#N/A	#N/A	#N/A	
MA250.asd	0	0	0	0	0	0	0	0	0	0	0
MA251.asd	#N/A	#N/A	#N/A	#N/A	#N/A	#N/A	#N/A	#N/A	#N/A	#N/A	
MA252.asd	#N/A	#N/A	#N/A	#N/A	#N/A	#N/A	#N/A	#N/A	#N/A	#N/A	
MA253.asd	#N/A	#N/A	#N/A	#N/A	#N/A	#N/A	#N/A	#N/A	#N/A	#N/A	
MA28.asd	0	0	0	0	0	0	0	0	0	0	0
MA30.asd	0	0	0	0	0	0	0	0	0	0	0
MA31.asd	0	0	0	0	0	0	0	0	0	0	0
MA32.asd	0	0	0	0	0	0	0	0	0	0	0
MA33.asd	0	0	0	0	0	0	0	0	0	0	0
MA34.asd	0	0	0	0	0	0	0	0	0	0	0
MA35.asd	0	0	0	0	0	0	0	0	0	0	0
MA38.asd	0	0	0	0	0	0	0	0	0	0	0

Sample name	AS_PPM	S_PCT	AG_GPMT	AL_PCT	CU_PPM	PB_PPM	SB_PPM	BA_PPM	CA_PCT	FE_PCT
MA39.asd	#N/A	#N/A	#N/A	#N/A	#N/A	#N/A	#N/A	#N/A	#N/A	#N/A
MA40.asd	#N/A	#N/A	#N/A	#N/A	#N/A	#N/A	#N/A	#N/A	#N/A	#N/A
MA41.asd	#N/A	#N/A	#N/A	#N/A	#N/A	#N/A	#N/A	#N/A	#N/A	#N/A
MA42.asd	#N/A	#N/A	#N/A	#N/A	#N/A	#N/A	#N/A	#N/A	#N/A	#N/A
MA43.asd	#N/A	#N/A	#N/A	#N/A	#N/A	#N/A	#N/A	#N/A	#N/A	#N/A
MA44.asd	#N/A	#N/A	#N/A	#N/A	#N/A	#N/A	#N/A	#N/A	#N/A	#N/A
MA45.asd	#N/A	#N/A	#N/A	#N/A	#N/A	#N/A	#N/A	#N/A	#N/A	#N/A
MA46.asd	#N/A	#N/A	#N/A	#N/A	#N/A	#N/A	#N/A	#N/A	#N/A	#N/A
MA47.asd	#N/A	#N/A	#N/A	#N/A	#N/A	#N/A	#N/A	#N/A	#N/A	#N/A
MA48.asd	#N/A	#N/A	#N/A	#N/A	#N/A	#N/A	#N/A	#N/A	#N/A	#N/A
MA49.asd	#N/A	#N/A	#N/A	#N/A	#N/A	#N/A	#N/A	#N/A	#N/A	#N/A
MA5.asd	0	0	0	0	0	0	0	0	0	0
MA50.asd	#N/A	#N/A	#N/A	#N/A	#N/A	#N/A	#N/A	#N/A	#N/A	#N/A
MA51.asd	#N/A	#N/A	#N/A	#N/A	#N/A	#N/A	#N/A	#N/A	#N/A	#N/A
MA51B.asd	#N/A	#N/A	#N/A	#N/A	#N/A	#N/A	#N/A	#N/A	#N/A	#N/A
MA52.asd	#N/A	#N/A	#N/A	#N/A	#N/A	#N/A	#N/A	#N/A	#N/A	#N/A
MA53.asd	#N/A	#N/A	#N/A	#N/A	#N/A	#N/A	#N/A	#N/A	#N/A	#N/A
MA54.asd	#N/A	#N/A	#N/A	#N/A	#N/A	#N/A	#N/A	#N/A	#N/A	#N/A
MA56.asd	#N/A	#N/A	#N/A	#N/A	#N/A	#N/A	#N/A	#N/A	#N/A	#N/A
MA57.asd	#N/A	#N/A	#N/A	#N/A	#N/A	#N/A	#N/A	#N/A	#N/A	#N/A
MA58.asd	#N/A	#N/A	#N/A	#N/A	#N/A	#N/A	#N/A	#N/A	#N/A	#N/A
MA58B.asd	#N/A	#N/A	#N/A	#N/A	#N/A	#N/A	#N/A	#N/A	#N/A	#N/A
MA59.asd	#N/A	#N/A	#N/A	#N/A	#N/A	#N/A	#N/A	#N/A	#N/A	#N/A
MA6.asd	0	0	0	0	0	0	0	0	0	0
MA61.asd	#N/A	#N/A	#N/A	#N/A	#N/A	#N/A	#N/A	#N/A	#N/A	#N/A
MA63.asd	#N/A	#N/A	#N/A	#N/A	#N/A	#N/A	#N/A	#N/A	#N/A	#N/A
MA64.asd	#N/A	#N/A	#N/A	#N/A	#N/A	#N/A	#N/A	#N/A	#N/A	#N/A
MA65.asd	#N/A	#N/A	#N/A	#N/A	#N/A	#N/A	#N/A	#N/A	#N/A	#N/A
MA66.asd	#N/A	#N/A	#N/A	#N/A	#N/A	#N/A	#N/A	#N/A	#N/A	#N/A

Sample name	AS_PPM	S_PCT	AG_GPMT	AL_PCT	CU_PPM	PB_PPM	SB_PPM	BA_PPM	CA_PCT	FE_PCT
MA67.asd	#N/A	#N/A	#N/A	#N/A	#N/A	#N/A	#N/A	#N/A	#N/A	#N/A
MA68.asd	#N/A	#N/A	#N/A	#N/A	#N/A	#N/A	#N/A	#N/A	#N/A	#N/A
MA68B.asd	#N/A	#N/A	#N/A	#N/A	#N/A	#N/A	#N/A	#N/A	#N/A	#N/A
MA69.asd	#N/A	#N/A	#N/A	#N/A	#N/A	#N/A	#N/A	#N/A	#N/A	#N/A
MA7.asd	0	0	0	0	0	0	0	0	0	0
MA70.asd	#N/A	#N/A	#N/A	#N/A	#N/A	#N/A	#N/A	#N/A	#N/A	#N/A
MA71.asd	#N/A	#N/A	#N/A	#N/A	#N/A	#N/A	#N/A	#N/A	#N/A	#N/A
MA72.asd	#N/A	#N/A	#N/A	#N/A	#N/A	#N/A	#N/A	#N/A	#N/A	#N/A
MA73.asd	#N/A	#N/A	#N/A	#N/A	#N/A	#N/A	#N/A	#N/A	#N/A	#N/A
MA74.asd	#N/A	#N/A	#N/A	#N/A	#N/A	#N/A	#N/A	#N/A	#N/A	#N/A
MA75.asd	#N/A	#N/A	#N/A	#N/A	#N/A	#N/A	#N/A	#N/A	#N/A	#N/A
MA76.asd	#N/A	#N/A	#N/A	#N/A	#N/A	#N/A	#N/A	#N/A	#N/A	#N/A
MA77.asd	#N/A	#N/A	#N/A	#N/A	#N/A	#N/A	#N/A	#N/A	#N/A	#N/A
MA8.asd	0	0	0	0	0	0	0	0	0	0
MA82.asd	137	0.025	0.4	1.1	11	1.5	1.5	46	1.43	1.72
MA83.asd	205	0.35	0.6	1.18	20	1.5	1.5	26	1.37	2.28
MA84.asd	3474	0.48	0.4	0.37	13	1.5	5	12	0.87	1.17
MA86.asd	4235	0.62	2.7	0.81	13	5	4	17	1.64	1.81
MA87.asd	4817	0.89	2.2	0.89	14	6	3	20	1.6	1.97
MA88.asd	7171	1.04	3.6	0.45	5	7	5	13	0.9	1.82
MA9.asd	0	0	0	0	0	0	0	0	0	0
MA92.asd	59	0.33	0.15	1.17	16	4	1.5	22	1.7	1.79
MA93.asd	132	0.38	1	1.29	24	3	1.5	27	2.01	2.48
MA96.asd	70	0.28	0.15	0.91	9	1.5	1.5	22	2.02	1.48
MA97.asd	20	0.18	0.15	1.72	10	1.5	1.5	35	2.42	2.79
MA9B.asd	0	0	0	0	0	0	0	0	0	0

Appendix E: In situ isotopes

δ^{34}S VCDT	Au ppm	Thin Section	Domain	File name	Sulphide type	Width:Height	Apy type
0.1	8.4	T1	5	T1S1_Arpsy1	Apy	1.1300813	B
1.9	399.88	T1	5	T1S1_Arpsy2	Apy	1.1300813	B
-0.7	9.52	T1	5	T1S1_Arpsy3	Apy	1.00892857	B
2.1	19.47	T1	5	T1S1_Arpsy4	Apy	1.66393443	B
1.9	60.06	T2	4	T2S1 Arspy1	Apy	8.7826087	A
2.5	178.90	T2	4	T2S1 Arspy2	Apy	8.7826087	A
-0.4	241.93	T2	4	T2S2 Arspy1	Apy	0.2371134	B
1.5	45.33	T2	4	T2S2 Arspy2	Apy	0.2371134	B
0.9	188.33	T2	4	T2S2 Arspy3	Apy	1.71232877	C
1.1		T2	4	T2S2 Arspy4	Apy		B
2.3	1513.58	T3	5	T3S1 Arspy1	Apy	5.4	A
4.1	1529.78	T3	5	T3S1 Arspy2	Apy	5.4	A
2.8	776.00	T3	5	T3S2 Arspy1	Apy	6.25	A
3.1	724.70	T3	5	T3S2 Arspy2	Apy	6.25	A
1.3		T3	5	T3S2 Arspy3	Apy		B
2.9	1165.43	T3	5	T3S3 "Arspy1"	Apy	1.93478261	C
5.0	127.88	T3	5	T3S3 Arspy2	Apy	3.11764706	B
0.4	7.34	T4	5	T4S1 Arspy1	Apy	4.39285714	B
1.6	5.96	T4	5	T4S1 Arspy2	Apy	1.13	B
1.9	4.86	T4	5	T4S3 Arspy2	Apy	0	C
0.6	74.52	T4	5	T4S3 Arspy3	Apy	3.91603053	C
4.1	228.06	T5	3	T5S1 Arspy1	Apy	15.1219512	A
1.7	340.01	T5	3	T5S1 Arspy2	Apy	15.1219512	A
0.0	485.06	T5	3	T5S2 Arspy1	Apy	1.78	B
-0.1	353.97	T5	3	T5S2 Arspy2	Apy	1.78	B
1.6		T5	3	T5S2 Arspy3	Apy		B
2.3	170.47	T5	3	T5S2 Arspy4	Apy	1.18987342	B
2.6	3.64	T2	4	T2S3 Py1	Py		P
2.3	1.87	T2	4	T2S3 Py2	Py		P
3.0		T3	5	T3S3 Py1	Py		P
2.0	22.04	T4	5	T4S2 Py1	Py		P
2.3	1.58	T4	5	T4S2 Py2	Py		P
2.4	1.21	T1	5	T1S2 Py1	Py		P
3.0	0.60	T1	5	T1S2 Py2	Py		P

Curriculum Vitae

Name: Marcus Adam
marcus.adam4@gmail.com

Post-secondary Education and Degrees:

University of Leeds,
Leeds, United Kingdom
BSc. Geological Sciences **(**2009-2012)

The University of Western Ontario
London, Ontario, Canada
2013-2016 MSc

Related Work Experience

Geologist
Seabridge Gold Inc.
2012- present (as of publication date)

Teaching Assistant
University of Western Ontario
2013-2015